



The
University
Of
Sheffield.

Microbubble mediated sequential saccharification, inactivation, and aerobic fermentation with *in situ* selective product removal

By:

Ali R. Mulakhudair

A Thesis submitted in partial fulfilment of the requirements for the degree of Doctor of Philosophy (PhD)

The University of Sheffield
Faculty of Engineering
Department of Chemical and Biological Engineering

Submission Date:

December -2017

The candidate confirms that the work submitted is his own, except where work that has formed as part of a co-authorship is included in the declaration section. The contribution of the candidate and the other authors to this work has been explicitly indicated overleaf.

Dedication

To my Family, who dedicated and offered unconditional support and love through my study and to my wonderful Mother in particular: Thameena Ibrahim for her advice, which inspired commitment, and focuses till today

ABSTRACT

Microbubble mediated technologies are employed for pretreatment steps due to the characteristics of the gas-liquid interface. Traditionally, pretreatment processes are energy intensive operations and use hazardous chemicals such as sulfuric acid and hydrochloric acid, which need to be removed from the pretreatment slurry before feeding it to the fermentation process. Alternative approaches to microbubbles for pretreatment, however, have significant challenges. For example, conventional bubbles are several orders of magnitude larger than the bubble exit pore and therefore have less direct contact with the biomass or delivery the ozone efficiently to the pretreatment slurry. Consequently, these concerns have been addressed in this research, and microbubble-microbe synergy and Ozonolysis-microbe synergy for biomass pretreatment with the developing of microbubbles driven systems, were used to facilitate microbubble generation suitable for pretreatment processes.

The first approach was achieved by exploiting the synergy between microbubble-microbe to pretreat lignocellulosic biomass and glucose was the target product. The effects of microbubbles, microbe and the synergy between them on morphology, functional groups and glucose yield were investigated. It was found that free radicals around the gas-liquid interface of the microbubble can readily attack and degrade lignocellulosic biomass, rendering it more amenable to digestion. The combination of microbubbles and *Pseudomonas putida*—a robust delignification and cellulolytic microbe, further improved biomass degradation and consequently, increased glucose production from wheat straw in comparison to solo pretreatment of the biomass with microbubbles and *Pseudomonas putida* respectively. In addition, it was found that the highest glucose achieved was 0.27 mg/ml.

The second was conducted by exploiting ozonolysis-microbe synergy to pretreat lignocellulosic biomass and glucose was also the target product. The effects of ozonation at various pHs and ozone concentrations, biological pretreatment by *Pseudomonas putida* and the synergy between them on morphology, functional groups and glucose yield were explored. Ozone is a strong oxidative agent that reacts with lignin by attacking the carbon-carbon double bonds, while *P. putida* preferentially hydrolyses the exposed cellulolytic parts of the biomass to simple sugars. It was found that both lignin and cellulose contents were reduced under this pretreatment with relatively high glucose recovery. The highest glucose concentration reached was 1.1 mg/ml after 24 hr ozonation at 8.86 mg/L ozone and pH 3 with 50 % reduction in the biological pretreatment duration but crucially, increasing microbial biomass.

Using the synergetic approach for the biomass pretreatment is promising approach but leaves the pretreatment slurry contaminated with the cellulolytic microbe, *Pseudomonas putida*, which needs to be inactivated or removed before feeding the pretreatment slurry into the fermenter. The ability of carbon dioxide enriched microbubbles to inactivate *Pseudomonas putida* was subsequently investigated. Many drawbacks of the traditional sterilization methods were avoided by using carbon dioxide enriched microbubbles, such as high energy consumption and using toxic and corrosive reagents. It was found that 2-Log reduction in the bacterial population after 90 min was achieved using carbon dioxide enriched microbubbles. Further reductions were achieved by adding additives such as ethanol and acetic acid and the highest reduction performed was 3.5 Log with 10 % ethanol, while a 2.5-Log reduction was achieved with 0.5 % acetic acid. These reductions in the bacterial population were concurrent with changing cells shape from rod cells to coccus shape with cell damage such as lesions and cells death.

Subsequently, aerobic fermentation with glucose as a carbon source proceeded with *Zymomonas mobilis* ZM4 as the microbial fermentation agent. Acetaldehyde has drawn the attention in this research because it is an important chemical, and it can be used in many processes such as plastic manufacturing and fuels production such as ethanol and butanol. Several attempts to produce acetaldehyde from *Zymomonas mobilis* or genetically modified microbes contained some genes from *Zymomonas* are reported, but the inhibition of microbial growth by the accumulated acetaldehyde was the main challenge to keep its continuous production. This challenge has been addressed in this study and microbubbles generated by fluidic oscillation were used to remove both acetaldehyde and carbon dioxide from the fermentation broth. Additionally, the oxygenation concurrent with the stripping process by microbubbles efficiently maintained the oxygen concentration in the fermentation broth above the critical oxygen concentration, leading to stable aerobic conditions. The results show that 45 % yield of ethanol and 1 % yield of acetaldehyde with 110 % yield of microbial biomass in comparison with 70 %, 0.5 % and 90 % yield for ethanol, acetaldehyde, and biomass respectively in the initially sparged group were achieved. Also, acetaldehyde was removed from the fermentation broth with 99 % efficiency.

Acetaldehyde production in the fermentation was enhanced by selecting the mutant cells with attenuated or modified alcohol dehydrogenase activity using increasing concentrations of allyl alcohol. The results show that 17-fold increase was achieved in the mutant strain in comparison with the wild strain. In addition, the mutant strain produced 90 % less ethanol than the wild

strain. Also, the acetaldehyde removal efficiency was 88.5 % in comparison with 42 % efficiency achieved with the fine bubbles (bigger bubbles). Additionally, biomass yield produced by the mutant strain was less by a half than the yield produced by the wild strain.

To enhance the biomass yield of the mutant strain, different techniques were used to grow this bacterium aerobically, but maintaining sufficient oxygen concentration was challenging in the bacterial propagation stage. Oxygen is the limiting factor in the aerobically grown bacterial cultures, but similarly, the impact of mixing can be critical. The results show that the oxygen uptake rate and mass transfer coefficient are substantially increased using microbubbles technology and there were 41-fold and 150-fold increase in the oxygen uptake rate and mass transfer coefficient respectively in the microbubbles-dosed culture in comparison with the shaking flask culture. This technology can also achieve a proper mixing. Regarding the biomass yield, the mutant strain of *Zymomonas mobilis* shows an increased yield using the shaking flask (around 100 % and 133 % increases) in comparison with other (microbubbles-dosed and stationary respectively) techniques, while the wild strain produces more biomass in the microbubble-based technique (around 50 % and 100 %) than other (shaking flask and stationary respectively) techniques. In addition, a propagation unit was designed and simulated to grow the mutant strain aerobically in the propagation stage before using this grown biomass as an inoculum to the fermentation process. Fundamentally, the results obtained in this study are achieved in a laminar flow with several orders of magnitude lower energy density than conventional benchmarks, which are a highly turbulent flow.

Declaration

Chapter 4: Reproduces a manuscript published in Biomass and Bioenergy.

Mulakhudair, A.R., Hanotu, J. and Zimmerman, W., (2016) Exploiting microbubble-microbe synergy for biomass processing: Application in lignocellulosic biomass pretreatment. *Biomass and Bioenergy*, 93, 187-193.

The experimental work, data collection and data analysis were carried out by ARM as well as the design and setup for the biomass pretreatment. Writing and production of Figures/ tables/ photos were also completed by ARM. Ammonium sulfate precipitation experiments were done at Molecular Biology and Biotechnology Department, the University of Sheffield with the aid from Dr. Svetlana Sedolnikova. LC-MS/MS analysis of cellulolytic proteins experiments were done at the biOMICS Facility at the university of Sheffield.

Chapter 5: Reproduces a manuscript submitted to Biomass and Bioenergy.

Mulakhudair, A.R., Hanotu, J. and Zimmerman, W., (2017), Exploiting ozonolysis-microbe synergy for biomass processing: lignocellulosic biomass pretreatment. *Biomass and Bioenergy*, 105, 147-154.

The experimental work, data collection and data analysis were carried out by ARM as well as the design and setup for the biomass pretreatment. Writing and production of Figures/ tables/ photos were also completed by ARM. Other help with the data analysis, interpretations, scientific discussions and comments on the manuscript were with the aid of Dr. James Hanotu.

Chapter 6: Reproduces two manuscripts, one is published in Journal of Chemical Technology and Biotechnology and the other one is in preparation for submission.

Mulakhudair, A.R., Al-Mashhadani, Mahmood, Hanotu, J. and Zimmerman, W., (2017) Inactivation combined with cell lysis of *Pseudomonas putida* using a low-pressure carbon dioxide microbubble technology, *Journal of Chemical Technology and Biotechnology*, DOI: 10.1002/jctb.5299doi:

Mulakhudair, A.R., Al-Mashhadani, Mahmood, Hanotu, J. and Zimmerman, W., (2017), Reducing the survivor ratio of *Pseudomonas putida* combined with cell lysis using CO₂ enriched microbubbles and acetic acid as an additive, In preparation for submission.

The experimental work, data collection and data analysis were carried out by ARM as well as the design and setup for the inactivation process. Writing and production of Figures/ tables/ photos were also completed by ARM. Other help with the data analysis, interpretations, developing equations, scientific discussions and comments on the manuscript is credited to Dr. Mahmood Mashhadani and Dr. James Hanotu.

Chapter 7: Reproduces an abstract submitted to ChemEngDayUK 2017 in Birmingham, UK.

Mulakhudair, A.R. and Zimmerman, W., (2017) Fermentation integrated with *in situ* separation of bio-products using microbubble technology (Submitted to ChemEngDayUK and it was accepted for both poster presentation and oral presentation).

The experimental work, data collection, data analysis, interpretations, developing equations and scientific discussions were carried out by ARM as well as the design and setup for the fermentation process. Gas chromatography calibration and samples analysis was carried out with the aid of Mr. Andrew Fairburn from Groundwater Protection and Restoration Group at the university of Sheffield.

Chapter 8: Contains experiments that is considering for commercialisation and an abstract has been submitted to for Biotech France 2017 and it has been accepted.

The experimental work, data collection, data analysis, interpretations and scientific discussions were carried out by ARM as well as the design and setup for the fermentation process. The fermentation process using synthetic medium in both aerobic and anaerobic conditions were conducted with the aid of Mr. Bastian Saputra, who was shadowing the author through his master study.

Chapter 9: Reproduces a manuscript in preparation for submission:

Mulakhudair, A.R., Al-Mashhadan, Mahmood and Zimmerman, W., (in preparation). Intensification of Bacterial growth using microbubble technology: Bacterial Propagation.

The experimental work, data collection, data analysis, interpretations and scientific discussions were carried out by ARM as well as the design and setup of the fermentation process. Mass and flow modelling were carried out and discussed with the aid of Dr. Mahmood Mashhadani, from the University of Baghdad, Iraq, but all the experiments, design, setup and data analysis of the experiments that fed to the modelling, were conducted by ARM.

“The role of the infinitely small is infinitely large”

(Louis Pasteur)

Acknowledgement

I am profoundly grateful to my family and all my relatives for their regular care. To all my friends and colleagues past and present, for their helpful suggestions during my time in Sheffield and to all members of the Prof. Zimmerman's group.

To my supervisor, Prof William Zimmerman, his kind support, guidance and leadership that helped encourage and facilitate personal and professional development. I am profoundly grateful to him for his role in my academic development.

I would like to thank the Iraqi Ministry of Higher Education and Scientific Research for the doctoral Scholarship and the University of Babylon for the nomination.

To the CBE Technical team for their constant help with equipment fabrication, general technical support in the laboratory and logistics issues during my study years. I would also like to thank the entire Chemical and Biological Engineering Department staff for their assistance and kindness with my profound gratitude to the University of Sheffield for allowing me to finish my study.

Ali

Scientific contributions

Publication list

- Mulakhudair, A.R., Hanotu, J. and Zimmerman, W., (2016) Exploiting microbubble-microbe synergy for biomass processing: Application in lignocellulosic biomass pretreatment. *Biomass and Bioenergy*, 93, 187-193.
- Mulakhudair, A.R., Al-Mashhadan, Mahmood, Hanotu, J. and Zimmerman, W., (2017) Inactivation combined with cell lysis of *Pseudomonas putida* using a low-pressure carbon dioxide microbubble technology, *Journal of Chemical Technology and Biotechnology*, DOI: 10.1002/jctb.5299.
- Mulakhudair, A.R., Hanotu, J. and Zimmerman, W., (2017), Exploiting ozonolysis-microbe synergy for biomass processing: lignocellulosic biomass pretreatment. *Biomass and Bioenergy*, ,105, 147-154.

Published abstracts

- 1- 'Exploiting microbubble-microbe synergy for biomass processing : Lignocellulosic biomass pretreatment by ozonolysis' USBES, 2016.
- 2- Using low-pressure carbon dioxide enriched microbubbles as an inactivation tool to the microbial cells' RSC, PCIG, 2016.
- 3- 'Aerobic fermentation integrated with *in situ* separation of bio-products using microbubble technology", 28th Birmingham, ChemEngDay 2017.
- 4- 'Aerobic fermentation integrated with *in situ* separation of bio-products using microbubble technology and mutant strain of *Zymomonas mobilis*", 28th-30th June Paris, France 2017.

Presented Posters:

- 1- '*Pseudomonas putida* KT2240 as a promising delignification agent', 17th-18th September 2015 – CBMnet Meeting Sheffield.
- 2- '*Pseudomonas putida* KT2440 as a promising biological pretreatment agent', Grantham Centre for Sustainable Futures - Sustainable Futures Symposium 2016.
- 3- 'Exploiting microbubble application for lignocellulosic biomass pretreatment (Wheat straw)'
- 4- 'Enhancement of Oxygen delivery to the fermentation system of *Zymomonas mobilis* ZM4 by periodical microbubbles sparging strategy' 18th January 2016.
- 5- 'Aerobic fermentation integrated with *in situ* separation of bio-products using microbubble technology", 27-28th Birmingham, ChemEngDay 2017.
- 6- 'Exploiting Microbubble-microbe Synergy For Biomass Processing: Lignocellulosic Biomass Pretreatment By Ozonolysis', Esbes 11-14 September 2016, Dublin, Ireland.
- 7- "Lignocellulosic biomass processing: Potential of using Microbubble-mediated Pre-treatment", 5th-7th Cheshire, LBNetwork 2nd conference.

Nomenclature

Symbol	Description	Unit
k	Sterilisation constant	(hr ⁻¹)
ϕ_l	Liquid volume fraction	(m ³ / m ³)
M_w	The molecular weight of the gas bubble	(kg)
Re_b	Reynolds number	(dimensionless)
d_b	Bubble diameter	(m)
m_{gl}	Mass transfer rate	(kg/m ³ /s).
u_g	The velocity of the gas	(m/s)
u_l	The velocity of the liquid phase	(m/s)
u_{slip}	Relative velocity	(dimensionless)
η_l	Dynamic viscosity of the liquid phase	(Pa.s)
ρ_g	The density of gas phase	(kg/m ³)
ΔG	Gibbs free energy	(kJ mole ⁻¹)
ΔG_0	Gibbs free energy at standard conditions	(kJ mole ⁻¹)
ΔH	Changing in Enthalpy	(kJ)
ΔS	Changing in Entropy	(J K ⁻¹)
ΔH	The height difference between two cylinders	(m)
Δp	Liquid height	(m)
a	Interfacial surface area	(m ²)
C_G	Equilibrium Concentration of dissolved gas	(mole m ⁻³)
c_i	The concentration of species i	(mol/L)
C_L	Concentration of dissolved gas in bulk liquid	(mole m ⁻³)
C_s	Organic compound concentration	(mM)
d	maximum inner flask diameter	(m)
D	Diffusion coefficient	(m ² /s)
d_0	Shaking diameter	(m)
D_c	The diameter of the collection tube	(m)
g	Gravitational acceleration	(m s ⁻²)
H_{hs}	Height of collected gas	(m)
K_{a1}	Carbon dioxide dissociation constant	(mol dm ⁻³)
K_{a2}	Carbonic acid dissociation constant	(mol dm ⁻³)
K_{eq}	Equilibrium constant	(M)
K_h	Water equilibrium dissociation constant	(mol dm ⁻³)
K_{La}	Overall mass transfer coefficient	(hr ⁻¹ or min ⁻¹)
K_{sa}	Stripping rate constant	(hr ⁻¹)
n	Shaking frequency	(1/s)
NA	Mass transfer fluxes	(mole sec ⁻¹)
OD	Optical density	(A)
P	Hydrostatic pressure	(Pa)
ρ	Density of the fluid	(kg m ⁻³)
P_{O_2}	Oxygen partial pressure	(bar)
Q	Volumetric flow rate of Gas	(l/min)
r	Microbubble radius	(m)
R	Universal gas constant	(J mole ⁻¹ K ⁻¹)

r	Specific oxygen uptake rate	mmol. g (dry weight) ⁻¹ .hr ⁻¹
R_P	Production rate	(mM hr ⁻¹)
R_s	Stripping rate	(mM hr ⁻¹)
s	The interface area of bubble	(m ²)
t	Time	min
T	Absolute temperature	(K)
T	The temperature of the gas	(K)
U_{stokes}	Terminal velocity of the gas bubbles	(m s ⁻¹)
v	The volume of bubble	(m ³)
v	Kinematic viscosity	(m ² /s)
V_g	The volume of the collected gas	(m ³)
V_L	Filling volume	(m ³)
X	Biomass concentration	g (dry weight)/L
X₀	The initial concentration	(mM)
X_r	The residual concentration	(mM)
y	Glucose concentration	(mg/ml)
y₀	Initial Glucose concentration	(mg/ml)
μ	Specific growth rate	(hr ⁻¹)
μ_l	Viscosity of liquid	(kg m ⁻¹ s ⁻¹)
C_d	Viscous drag coefficient	(dimensionless)
P	Pressure	(Pa)
R	Ideal gas constant	(J/mol/K)
τ	Time constant	hr

Table of Contents

Dedication.....	III
ABSTRACT	IV
Declaration.....	VII
Acknowledgement	X
Scientific contributions.....	XI
Nomenclature.....	XII
Table of Contents	XIV
List of Figures.....	XXI
List of tables	XXXI
Chapter 1	1
General Introduction and Project Objectives.....	1
1.1 Introduction	1
1.2 Research Hypotheses	4
1.3 Research Objectives	5
1.4 General benefits of the current project	8
1.5 Thesis Organisation	9
Chapter 2	12
Literature Review	12
2.1 Pretreatment methods of lignocellulosic biomass	12
2.1.1 Mechanical pretreatment.....	14
2.1.2 Physicochemical pretreatment.....	14
2.1.3 Chemical Pretreatment	15
2.1.4 Biological Pretreatment.....	16
2.1.4.1 Cellulases applications	16
2.1.4.2 Control the cellulases' secretion.....	17
A- Endoglucanases (EC.3.2.1.4, 1,4-B-D-glucan-4-glucanohydrolases).....	18
B- Exocellobiohydrolases (EC.3.2.1.91, 1, 4-B-D-glucan-glucohydrolases)	18
C- β -glucosidases (EC. 4.2.1.21, β -D-glucoside – glucohydrolase)	18
2.1.4.3 Characteristics of <i>Pseudomonas putida</i> as a cellulolytic agent.....	18
2.2 Inactivation of microbial culture using carbon dioxide.....	20
2.2.1 Inactivation processes	20
2.2.2 Carbon dioxide mechanisms of action	21
2.2.2.1 Step one: Solubility of CO ₂ in the exterior liquid phase	21
2.2.2.2 Step two: Modification of cell membrane	22

2.2.2.3 Step three: Decreasing the intercellular pH.....	22
2.2.2.4 Step four: Inactivation of vital enzymes and inhibition of cellular metabolisms due to low internal pH.....	23
2.2.2.5 Step five: Direct inhibitory effect of CO ₂ and HCO ₃ ⁻ on metabolism.....	23
2.2.2.6 Step six: Unbalancing the internal electrolytes	23
2.2.2.7 Step seven: Removal of vital moieties from cell membrane.....	23
2.3 Characteristics of <i>Zymomonas mobilis</i> in acetaldehyde and ethanol production	24
2.3.1 Entner-Doudoroff (ED) pathway	24
2.3.2 Putative energy dissipation mechanisms and carbon dioxide accumulation.....	27
2.3.2.1 Putative energy dissipation mechanisms.....	27
2.3.2.2 Carbon dioxide accumulation.....	28
2.4 Acetaldehyde	29
2.5 Classification of Low-molecular-weight fermentation products.....	32
2.5.1 Product formation directly coupled with the energy generation	32
2.5.2 Product formation indirectly coupled with the energy generation	32
2.5.3 Product formation not coupled with the energy generation	32
2.6 Acetaldehyde as a precursor for fuels production	32
2.7 Recovery of final products from the fermentation broth by gas stripping	33
2.8 Acetaldehyde separation instead of ethanol distillation	34
2.9 Microbubble technology.....	36
2.9.1 Properties of microbubbles.....	36
2.10 Thin film theory of mass transfer	40
2.11 Airlift loop bioreactors (ALB).....	42
2.11.1 ALB base	42
2.11.2 ALB riser	43
2.11.3 ALB downcomer	43
2.11.4 Gas separator	43
2.11.5 Draught tube	44
2.12 Effects of the chemical activity on acetaldehyde and CO ₂ production.....	44
Chapter 3	47
Materials and Methods	47
3.1 Introduction	47
3.2 Pretreatment of lignocellulosic biomass.....	47
3.2.1 Microbubble-microbe synergetic approach	47
3.2.1.1 Biomass and growth media preparation.....	47

3.2.1.2 Experimental Procedures.....	48
3.2.1.3 Testing the cellulolytic activity of <i>Pseudomonas putida</i>	49
A. Qualitative measurement of cellulolytic activity.....	49
B. Quantitative measurement of cellulolytic activity.....	50
1. Determination of protein concentrations.....	50
2. Enzymes activities.....	50
3. SDS-PAGE.....	51
4. Ammonium sulfate precipitation.....	51
3.2.2 Ozonolysis-microbe synergetic approach.....	52
3.2.2.1 Material and culture medium preparation.....	52
3.2.2.2 Ozone generation and quantification.....	52
3.2.3 Analytical methods.....	53
3.2.3.1 Determination of glucose concentration.....	53
3.2.3.2 Scanning Electron Microscope (SEM).....	53
3.2.3.3 Fourier transform infrared spectroscopy- Attenuated Total Reflectance (FTIR-ATR)	54
3.3 Inactivation with CO ₂ -enriched microbubbles.....	54
3.3.1 Material and culture medium preparation.....	54
3.3.2 Determination of carbon dioxide concentration.....	55
3.3.3 Morphological examination of the bacterial cells.....	57
3.3.3.1 Combined microscopy.....	57
3.3.3.2 Scanning electron microscopy.....	58
3.4 Fermentation integrated with <i>in situ</i> separation of bioproducts.....	58
3.4.1 Material preparation.....	58
3.4.2 Experimental procedures.....	58
3.4.3 Vapour collectors.....	60
3.4.4 Gas collector.....	63
3.4.5 Analytical methods.....	65
3.4.5.1 measurement of glucose concentration.....	65
3.4.5.2 Biomass calibration curve.....	65
3.4.5.3 Detection of acetaldehyde production using acid fuchsin.....	65
3.4.5.4 Selection of overproducing strains using allyl alcohol.....	66
3.4.5.5 Measuring the relative alcohol dehydrogenase activity.....	66
3.4.5.6 Sampling.....	67
3.4.5.7 Product yield calculations.....	67
3.5 Bacterial Propagation.....	69

3.5.1 Experimental procedures.....	69
3.5.2 Determination of K_{La}	69
Chapter 4	73
Exploiting microbubble-microbe synergy for biomass processing: Application in Lignocellulosic biomass pretreatment	73
Overview	73
4.1 Pseudomonas Putida growth on culture medium	73
4.2 Morphological changes on wheat straw	75
4.3 Changes in the functional groups of the biomass	79
4.4 Pseudomonas cellulolytic activities on Petri dishes	82
4.5 Proteomics of cellulases enzymes	84
4.5.1 Crude enzymes activities.....	84
4.5.2 Partial purification and precipitation of cellulases enzymes using ammonium sulfate salt	85
4.5.3 LC-MS/MS analysis of cellulolytic proteins.....	91
4.6 Conclusions	92
Chapter 5	93
Exploiting ozonolysis-microbe synergy for biomass processing: Application in lignocellulosic biomass pretreatment.....	93
Overview	93
5.1 Measuring the ozone concentrations	93
5.2 Effect of pH and ozone on the functional groups.....	94
5.3 Effect of pH and ozone on the morphological characteristics.....	96
5.4 Effect of ozone exposure time on lignocellulosic biomass	99
5.5 Bubble analysis.....	105
5.6 Comparison of traditional methods with the microbubble-mediated technologies developed in the current study for lignocellulosic biomass pretreatment.....	106
5.7 Conclusions	107
Chapter 6	109
Inactivation combined with cell lysis of Pseudomonas putida using a low-pressure carbon dioxide microbubble technology	109
Overview	109
6.1 Inactivation of Pseudomonas putida using CO ₂ microbubbles with and without the additives .	109
6.2 CO ₂ concentrations during CO ₂ -enriched microbubbles sparging with and without the additives	116
6.3 Morphological changes on Pseudomonas putida cells using CO ₂ microbubbles with and without the additives	118
6.4 Conclusions	122

Chapter 7 124

Aerobic fermentation integrated with in situ separation of bio-products using microbubble technology and wild type <i>Zymomonas mobilis</i> ZM4 strain.....	124
Overview	124
7.1 Acetaldehyde accumulation and its inhibitory effect	125
7.2 Combined accumulation of both acetaldehyde and carbon dioxide with their inhibitory effects.....	128
7.3 Oxygen requirement of the fermentation system	130
7.3.1 Initial sparging strategy	131
7.3.2 Continuous sparging strategy	132
7.3.3 Periodical sparging strategy	133
7.3.4 Specific oxygen uptake rate patterns.....	137
7.4 Central metabolic routes.....	140
7.5 Fermentation products (Acetaldehyde, ethanol, and carbon dioxide).....	143
7.6 In situ removal of some fermentation products.....	144
7.7 Bubble analysis.....	149
7.8 Reducing the cleaning requirements in the airlift loop bioreactor using microbubble technology	152
7.9 Maintenance of asepsis conditions	154
7.10 Conclusions	157

Chapter 8 159

Aerobic fermentation integrated with in situ separation of bio-products using microbubble technology and a mutant type <i>Zymomonas mobilis</i> ZM4 strain	159
Overview	159
8.1 Selection of acetaldehyde over-producing mutant strain using allyl alcohol.....	160
8.2 Differentiation of the overproduced strain with the use of acid fuchsin	164
8.3 Central metabolic routes.....	165
8.4 Fermentation products (Acetaldehyde, ethanol, and carbon dioxide).....	167
8.5 In situ removal of some fermentation products.....	171
8.6 Changing the glucose concentration to optimize the fermentation process	173
8.7 Separation of acetaldehyde-water mixture using air-microbubbles generated by fluidic oscillation	179
8.8 Testing the performance of the mutant strain in a synthetic medium	183
A. 20g/L glucose concentration	183
B. 40g/L glucose concentration.....	188
8.9 Testing the performance of the mutant strain under anaerobic conditions.....	192

8.9.1 Synthetic medium.....	193
8.9.2 Complex medium.....	195
8.10 Conclusions	198
Chapter 9	200
Intensification of the Zymomonas mutant strain growth using various cultivating techniques:	
Bacterial Propagation	200
Overview	200
9.1 Dissolved oxygen (DO) level	200
A- Stationary cultures.....	200
B- Shaking flasks cultures.....	201
C- Microbubble-sparged cultures.....	202
9.2 Biomass concentration.....	206
9.3 Design and simulation of a propagation unit for Zymomonas mobilis	209
9.3.1 Computational modelling.....	210
9.3.2 Computational geometry	211
9.3.3 Governing equations	211
9.3.4 Boundary conditions	213
9.3.5 Numerical method.....	213
9.3.6 Flow modeling of the propagation unit	213
9.3.7 Mass transfer modelling of the proposed propagation unit.....	216
9.4 Effect of the inoculum size on the fermentation process	219
9.5 Conclusions.....	223
Chapter 10	224
Conclusions and Future Perspective.....	224
10.1 General Conclusions.....	224
10.2 Future works and perspective	229
10.2.1 Lignocellulosic biomass pretreatment.....	229
10.2.2 Inactivation of the microbial pretreatment agent	231
10.2.3 Fermentation integrated with in situ separation by microbubble technology	231
B- Deletion of Alcohol dehydrogenase gene(s)	231
A- Over expression of NADH dehydrogenase (ndh)	231
C- Enhance the diffusibility of acetaldehyde through the cytoplasmic membrane.....	232
Chapter 11	233
References	233

Appendices	I
Appendix A: Cultural media compositions	I
M9 broth medium composition	I
Carboxymethyl cellulose Medium (CMC Medium) composition.....	I
Wheat straw Medium (WS Medium) composition	I
Lignin Medium (L Medium) composition	I
4 % sucrose standard medium (4SSM) composition.....	I
Acid fuchsin agar composition.....	II
The fermentation medium (FM) composition	II
Pre-inoculum medium composition	II
Second stage inoculum medium composition	II
Storage medium composition.....	II
RM medium	III
The synthetic medium (SM) composition	III
Appendix B: Measurement of ozone concentration using Potassium iodide method	IV
Appendix C: Preparing Zymomonas mobilis biomass standard curve	V
Appendix D: Preparing glucose standard curve	VI
Appendix E: Identification of the fermentation products using GC/MS.....	VII
Appendix F: Quantification of acetaldehyde and Ethanol in the fermentation broth and condensatesVII	
Appendix G: Quantification of Ethanol in the fermentation broth under anaerobic conditions	VIII
Appendix H: LC-MS/MS Analysis	IX

List of Figures

Figure 1.1: General flow chart of the current project	10
Figure 1.2: Stages of the current project with the potential uses of the final product.....	11
Figure 2.1: The typical arrangement of lignocellulosic biomass components, showing cellulose, hemicellulose and lignin fractions (Adapted from Mussatto and Teixeira, 2010).....	13
Figure 2.2: The main action of various pretreatment methods, whereby both lignin and hemicellulose as well as reducing the cellulose crystallization and polymerisation are the main targets of these pretreatment methods (Adapted from Hsu et al. 1980).....	14
Figure 2.3: Enzymatic degradation of cellulose by cellulolytic enzymes, involving cellobiohydrolases (CBH), endoglucanases (EG), type1 and type 2 PMOs (PMO1 and PMO2, respectively). Cellobiose dehydrogenase (CDH) is a potential electron donor for PMOs. EGs and PMOs cleave internally cellulose chains releasing chain ends that are targeted by CBHs. CBHs generate cellobiose or oxidized cellobiose that are subsequently hydrolyzed by β -glucosidase (Adapted from Dimarogona 2012).....	18
Figure 2.4: Actions of carbon dioxide on bacteria, besides the different steps of the inactivation mechanism—are① a phospholipid bilayer, ② integral membrane proteins, ③ a plasma membrane H ⁺ -ATPase, and ④intracellular substances (Adapted from Garcia-Gonazalez et al., 2007).....	21
Figure 2.5: Entner-Doudoroff pathway combined with Krebs cycle, enzymes missing from <i>Z. mobilis</i> are represented by red dotted arrow (Adapted from Seo et al., 2005).....	26
Figure 2.6: The competition between the respiratory electron transport chain and alcohol dehydrogenase on reducing equivalent NAD (P)H (Adapted from Kalnenieks et al., 2000).	27
Figure 2.7: The putative energy-spilling pathways in <i>Zymomonas mobilis</i> (Adapted from Kalnenieks, 2006).....	29
Figure 2.8: Structural formula of acetaldehyde (Adapted from WHO, 1999).	30
Figure 2.9: A comparison of the vapor pressure curves of acetaldehyde in water and ethanol in water at 30°C (Adapted from d’avila and Silva, 1970, but redrawn using Aspen Plus software V8.4).	35
Figure 2.10: Benefits of microbubble technology. A) Benefit of dividing a volume ratio into smaller volumes produces additional surface area. (B)(C) Relationship between surface area and transfer rate with bubble size is a square of bubble size and cubic with its volume.	37
Figure 2.11: The rise velocity of microbubble (Adapted from Levich, 1962 cited in Zimmerman et al., 2008).	38
Figure 2.12: Microbubble profile after $t=0.0001.5$ s with radius $R=100$ μ m. The arrows are the induced, steady state velocity field from bubble rising, imposed as the velocity field. The contours are concentration curves, with 20 contours rising from 0.002(inner) to 0.0032(outer) molar concentration (Adapted from Zimmerman et al., 2013).	39
Figure 2.13: The fluidic oscillator. A) Stack of laser cut Perspex plate with its amplifier. B) Feedback loop connects to two control terminals to generate oscillation. C) History of flow rate for fluidic oscillator connected to a nozzle bank with 600 μ m pore size. The oscillation frequency is ranged from 1-100 Hz, which is depending on the length of feedback loop (Adapted from Zimmerman et al., 2008).	40

Figure 2.14: Interfacial dynamics of mass transfer for gas exchange (Adapted from Moo-Young and Blanch, 1981).....	41
Figure 2.15: General oxygen transport path to microorganisms (Adapted from Moo-Young and Blanch, 1981).	42
Figure 2.16: Diagram of airlift bioreactor with draught tube supplied from the outlets of fluidic oscillator, the microbubbles are rising in the riser region and dissociated at the gas separator, thereafter the liquid is circulated in the downcomer region (Adapted from Zimmerman et al., 2009).	44
Figure 3.1: Schematic representation of the experimental set-up. Compressed air (1 bar) at 100 ml/min flow rate is fed into the oscillator, and there are two outputs from the fluidic oscillator. While, one feeds the microbubbles diffuser, the other is bleed-off. The overall volume is 1.5 L and the working volume of the pretreatment column is 1 L.	49
Figure 3.2: Experiment set up. Gas from the fluidic oscillator passes through the fluidic oscillator to the ozone generator. The gas emerges as microbubble-rich ozone. The overall volume is 0.15 L and the working volume of the pretreatment column is 0.1L.	53
Figure 3.3: Experiment set up. Carbon dioxide gas from the gas cylinder passes through the fluidic oscillator to feed the microbubbles diffuser. The gas emerges as microbubble-rich carbon dioxide at 100 ml/min flow rate and the working volume of the inactivation column is 1L.....	55
Figure 3.4: Experiment set up. Air from the fluidic oscillator passes through the fluidic oscillator to feed the microbubbles diffuser. there are two outputs from the fluidic oscillator with two bleeding on both sides to control the oscillatory flow.	59
Figure 3.5: Experimental design of the fermentation process using wild strain of <i>Zymomonas mobilis</i> ZM4. The initially sparged group is referred to as control group.	60
Figure 3.6: Schematic flow diagram of the fermenter connected with both trapping system and gas collector.....	61
Figure 3.7: (A) Schematic flow diagram of the fermenter connected with both condensation system and gas collector. (B) A picture of the final set up used in this study.	62
Figure 3.8: The used gas collector which is connected to the vapor collector.....	64
Figure 3.9: The conversion of allyl alcohol to toxic acryldehyde by alcohol dehydrogenase (Adapted from Rando, 1974)	66
Figure 3.10: Pictures for the airtight vials used to storage the withdrawal samples.	67
Figure 3.11: Schematic representation of the Airlift Loop Bioreactor. Microfiltered air was supplied through the sparger for bubble generation. The ALB is also fitted with pH, DO, thermocouple sensor. This reactor was incorporated in the microbiological incubator to regulate the temperature	72
Figure 4.1: Plot of the growth pattern of <i>Pseudomonas putida</i> KT2440 on three different culture media. (A) growth pattern on Carboxymethyl cellulose medium (CMC), Lignin medium (LM)and Wheat straw medium (WM).(B) Specific growth rates on the three different media. Error bars are representative of the standard error of triplicate results	74
Figure 4.2: Morphological changes on wheat straw after different pretreatment conditions. Images (A) and (B) are the untreated wheat straw; (C) and (D) are wheat straw after pretreatment with microbubble; (E) and (F) are the wheat straw after biological pretreatment with <i>Pseudomonas putida</i> ; (G) and (H) are the wheat straw after the combined pretreatment with both microbubbles and the biological organisms.....	76

- Figure 4.3:** Plot of glucose concentration with time during pretreatment of lignocellulosic biomass. (A) Microbubble pretreatment. (Bi) Biological pretreatment of straw (BTS) (Bii) Combined pretreatment of straw (CTS) –microbubble and biological method. Increased glucose yield was reordered for combined pretreatment method. Error bars depict the standard deviations. 78
- Figure 4.4:** Microbubble size distribution plot. Sub-100 μm bubbles were largely produced. Second visible peak exists as a result of slight production damage on the microporous sparger 79
- Figure 4.5:** (A) FTIR-ATR spectrum of biomass after pretreatment with microbubbles (MTS) (B) FTIR-ATR spectrum of biomass after pretreatment with a bacterium (BTS). A more pronounced difference in the mid part of the absorbance spectrum, showing the effect of *Pseudomonas putida* on lignocellulosic biomass pretreatment. UTS is untreated samples. 82
- Figure 4.6:** Cellulolytic activities of *Pseudomonas putida* on two media. A and B represent the cellulolytic activity on CMC after 3 and 4 days respectively. C and D represent cellulolytic activity on WSM after 3 and 4 days respectively 83
- Figure 4.7:** SDS-PAGE of *Pseudomonas putida* KT 2440 cultural filtrates showing the produced proteins. The black-coded bands represents the bands used in the In-gel digestion and analysed with LC-MS/MS, while the red-code band shows the identified protein, which has molecular weight around 96 kDa. 85
- Figure 4.8:** SDS-PAGE for proteins after fractionation with ammonium sulfate. 88
- Figure 4.9:** Enzymes activities of cellulases on different media. (A) CMC medium (B) Wheat straw medium 89
- Figure 4.10:** Specific enzymes activities on different cellulose contained media (A) CMC (B) wheat straw 90
- Figure 5.1:** FTIR-ATR spectrum of lignocellulosic biomass after MMO and MMO-M pretreatments. (A) MMO at pH 3 and 6.67 mg/L ozone concentration and MMO-M at pH 3 and 6.67 mg/L ozone concentration (B) MMO at pH 3 and 8.86 mg/L ozone concentration and MMO-M at pH 3 and 8.86 mg/L ozone concentration (C) MMO at pH 7 and 6.67 mg/L ozone concentration and MMO-M at pH 7 and 6.67 mg/L ozone concentration. (D) MMO at pH 7 and 8.86 mg/L ozone concentration and MMO-M at pH 7 and 8.87 mg/L ozone concentration. The readings are representative of triplicate results. 96
- Figure 5.2:** Morphological changes on wheat straw after MMO and MMO-M pretreatments for 2 h. (A) Untreated wheat straw. (B) MMO at pH 7 and 6.67 mg/L ozone concentration. (C) MMO-M at pH 7 and 6.67 mg/L ozone concentration. (D) MMO at pH 7 and 8.86 mg/L ozone concentration. (E) MMO-M at pH 7 and 8.86 mg/L ozone concentration. (F) MMO at pH 3 and 6.67 mg/L ozone concentration. (G) MMO-M at pH 3 and 6.67 mg/L ozone concentration. (H) MMO at pH 3 and 8.86 mg/L ozone concentration. (I) MMO-M at pH 3 and 8.86 mg/L ozone concentration. 97
- Figure 5.3:** FTIR-ATR spectrum of biomass after MMO and MMO-M pretreatment for 6 h at pH 3 and ozone concentration of 8.87 mg/L. Spectra have been normalised at 710-1100 cm^{-1} and 1500-1600 cm^{-1} . The readings are representative of triplicate results. 99
- Figure 5.4:** Graph of glucose production after 6 h pretreatment. (A) MMO pretreatment (B) MMO-M pretreatment. Glucose at day fourth in the biological pretreatment was not reported due to its low concentration. The readings are representative of triplicate results. 100

Figure 5.5: FTIR-ATR spectrum of lignocellulosic biomass after MMO and MMO-M pretreatment for 12 h at pH 3 and ozone concentration of 8.87 mg/L. Spectra have been normalised at 710-1100 cm ⁻¹ and 1500-1600 cm ⁻¹ . The readings are representative of triplicate results.	101
Figure 5.6: Graph of glucose production after 12 h pretreatment. (A) MMO pretreatment (B) MMO-M pretreatment. Glucose at day fourth of the biological pretreatment was not reported due to its low concentration. The readings are representative of triplicate results.	102
Figure 5.7: FTIR-ATR spectrum of lignocellulosic biomass after MMO and MMO-M pretreatment for 24 h at pH 3 and ozone concentration of 8.87 mg/L. Spectra have been normalised at 710-1100 cm ⁻¹ and 1500-1600 cm ⁻¹ . The readings are representative of triplicate results.	103
Figure 5.8: Graph of glucose production after 24 h pretreatment. (A) MMO pretreatment (B) MMO-M pretreatment. The readings are representative of triplicate results.....	104
Figure 5.9: Microbubble size distribution plot.....	106
Figure 6.1: Survivor ratio of <i>Pseudomonas putida</i> after treatment with. (A) CO ₂ microbubbles. (B) CO ₂ microbubbles plus 2% (v/v) ethanol. (C) CO ₂ microbubbles plus 5% (v/v) ethanol. (D) CO ₂ microbubbles plus 10% (v/v) ethanol. (E) CO ₂ microbubbles plus 0.5% (v/v) acetic acid. Error bars depict standard deviation.....	111
Figure 6.2: Temperature profile during CO ₂ enriched microbubbles inactivation process, highlighting the range of temperatures used in the current study. Error bars depict standard deviation.	112
Figure 6.3: CO ₂ concentrations with different pHs observed during sparging. (A) CO ₂ microbubbles. (B) CO ₂ microbubbles plus 2% ethanol. (C) CO ₂ microbubbles plus 5% ethanol. (D) CO ₂ microbubbles plus 10% ethanol. (E) CO ₂ microbubbles plus 0.5% acetic acid. Readings are representative of triplicate results.	117
Figure 6.4: Numerical changes after treatment with CO ₂ microbubbles on 1000X. (A) Bacterial smears before sparging CO ₂ . (B) Bacterial smear after treating with CO ₂ -enriched microbubbles for 90 min.	119
Figure 6.5: Figure 7: Morphological changes after treatment with microbubble CO ₂ and 2% ethanol using Scanning electron Microscopy. (A) <i>Pseudomonas</i> cells before the inactivation process (B) <i>Pseudomonas</i> cells after the inactivation process.....	121
Figure 7.1: (A) Effect of added acetaldehyde on exponential cell growth of <i>Zymomonas mobilis</i> ZM4 after 2 hours. The red arrow shows the time of the acetaldehyde addition (B) Specific growth rate of <i>Zymomonas mobilis</i> ZM4 after adding various concentrations of acetaldehyde. Error bars depict standard deviation.....	125
Figure 7.2: The morphological changes on <i>Zymomonas mobilis</i> ZM4 cells after acetaldehyde addition. (A) The control group without acetaldehyde addition. (B) the morphological changes on the cells after adding 0.5 % of acetaldehyde. (C) the morphological changes on the cells after adding 1.0 % of acetaldehyde.	126
Figure 7.3: Mechanism of acetaldehyde toxicity (Adapted from Bolstad, 2003).	127
Figure 7.4: (A) Effect of added acetaldehyde on exponential cell growth of <i>Zymomonas mobilis</i> ZM4 after 4 hours. The red arrow shows the time of the acetaldehyde addition. (B) Specific growth rate of <i>Zymomonas mobilis</i> ZM4 after addition various concentrations of acetaldehyde at hour fourth. Error bars depict standard deviation.....	128

- Figure 7.5:** The morphological changes on *Zymomonas mobilis* ZM4 cells after carbon dioxide and acetaldehyde accumulation. (A) The control group before carbon dioxide and acetaldehyde accumulation. (B) The morphological changes on the cells after carbon dioxide accumulation by sparging carbon dioxide for 20 mins at 0.3 l/min.(C) The morphological changes on the cells after addition of 0.5% of acetaldehyde after 2 hrs and carbon dioxide accumulation for 20 mins. (D) The morphological changes in the cells after addition of 1% of acetaldehyde after 2 hrs and carbon dioxide accumulation for 20 mins. 129
- Figure 7.6:** (A) The dissolved oxygen concentration against time during the fermentation process of *Zymomonas mobilis* ZM4 using the initial sparging strategy. (B) Typical plot of initial *KLa* estimation under initial sparging strategy, where the slope of straight line indicates mass transfer coefficient *KLa* (min^{-1}). The readings are representative of triplicate results. 132
- Figure 7.7:** The dissolved oxygen concentration against time during the fermentation process of *Zymomonas mobilis* ZM4 using the continuous sparging strategy, whereby the concentration of the dissolved oxygen is kept far from the critical oxygen concentration. The readings are representative of triplicate results. 133
- Figure 7.8:** A model of periodical oxygen dosing and consuming in *Zymomonas* fermentation culture. Two periods were identified during the aeration. The first period was at the beginning of the fermentation process, while at the second period, fermentation process has already begun, and the cultured started consuming oxygen, and many gaseous products have been produced. The readings are representative of triplicate results. 135
- Figure 7.9:** Graphic determination of Volumetric oxygen transfer coefficient for *Zymomonas mobilis* ZM4 culture (for 0.3 L min^{-1} dosing). (A) During the first period (8 mins). (B) During the second period (16.5 mins). The readings are representative of triplicate results. 136
- Figure 7.10:** (A) A model of periodical oxygen dosing and consuming in *Zymomonas* fermentation culture. (B) Comparison between the growth pattern of *Zymomonas mobilis* under initial and periodical sparging strategies, highlighting the importance of keeping aerobic conditions. Error bars depict standard deviation. 137
- Figure 7.11:** *Zymomonas* growth pattern during periodical sparging strategy (Flow rate 0.3 L min^{-1}) labelled with the specific oxygen uptake rate (q_{O_2}) $\text{mmol.g(dry weight)}^{-1}.\text{hr}^{-1}$. The oxygen uptake rate hits its highest in the exponential phase, while it is gradually decreased in both stationary and death phases. The readings are representative of triplicate results. 139
- Figure 7.12:** Glucose consumption pattern in *Zymomonas mobilis*. (A) Glucose concentration against time. (B) Glucose consumption rate in both initially and periodically sparged groups, whereby Initially sparged culture consumed more glucose than that the periodically sparged group under anaerobic conditions. Error bars depict standard deviation. 140
- Figure 7.13:** Proposed scenarios of the products shifting in *Z. mobilis*. (A) Under the aerobic conditions (Higher than the critical oxygen level). (B) Under anaerobic conditions (Lower than the critical oxygen level) (Adapted from Ishikawa et al., 1990). 142
- Figure 7.14:** Acetaldehyde and Ethanol production during the fermentation course. (A) Ethanol production (B) Acetaldehyde production. Error bars depict standard deviation. 143
- Figure 7.15:** Accumulated fermentation products, considering both the produced and stripped products from the fermentation broth. (A) Total produced ethanol. (B) Total produced

acetaldehyde. Error bars depict standard deviation. * The mean difference is significant at the 0.05 level.	144
Figure 7.16: Stripping process of acetaldehyde from the fermentation broth using air microbubbles. (A) Fluctuation of acetaldehyde concentrations within the fermentation broth after stripping it with microbubble. (B) Variation of acetaldehyde concentrations with each sparging cycle and calculation of stripping rate constant KSa . Error bars depict standard deviation.	147
Figure 7.17: Cumulated collected carbon dioxide at the end of the fermentation process (27 hrs), which was collected using the gas collection system. The readings are representative of triplicate results. * The mean difference is significant at the 0.05 level.....	148
Figure 7.18: Bioproducts percent yields. (A) Ethanol and acetaldehyde yields. (B) Biomass yield.....	149
Figure 7.19: Bubble analysis. (A) bubble size measurement set up. (B) Bubble size distribution used in the current study, where the microbubbles with 400-600 μm were dominant than other sizes. The readings are representative of triplicate results.....	150
Figure 7.20: A comparison between an oscillated flow and a continuous flow in water at the same flow rate 0.3 L/min. (A) Oscillated flow fed by the fluidic oscillator generated microbubbles with uniform spacing between them. (B) Continuous flow generated fine bubbles, which tend to coalesce, producing even bigger bubbles (Adapted from Al-Mashhadani, 2013).....	151
Figure 7.21: Snapshots of gas concentration (Kg/m^3) at two bubble diameters (400 μm and 600 μm) after steady state (Adapted from AL-Mashhadani et al., 2015)	152
Figure 7.22: Snapshots of the internal walls of the bioreactor. (A) Under initial sparging strategy, where the internal walls have bacterial biofilms, giving them the dirty appearance. (B) Under periodical sparging strategy, where the internal walls were clean without any bacterial biofilms.....	154
Figure 7.23: Microscopic pictures for the bacterial culture at the beginning of and after finishing the fermentation process for both Wild and 200 mM allyl alcohol selected strain (In the next chapter). (A) Wild strain culture at the beginning of the fermentation process. (B) Wild strain culture after finishing the fermentation process. (C) 200 mM allyl alcohol selected strain at the beginning of the fermentation process (Next chapter). (D) 200 mM allyl alcohol selected strain after finishing the fermentation process (Next chapter).	156
Figure 8.1: A sequential scheme using increasing allyl alcohol levels for the selection of <i>Z. mobilis</i> ZM4 mutant type with decreased or modified alcohol dehydrogenase activity. 161	161
Figure 8.2: (A) Acetaldehyde and ethanol production against used allyl alcohol concentration (Adapted from Wecker and Zall, 1987). (B) Shifting of wild type <i>Zymomonas</i> population to a population with attenuated or modified alcohol dehydrogenase activity in the mutant strain.	162
Figure 8.3: The acetaldehyde/ acid fuchsin colony reaction. (A) <i>Zymomonas mobilis</i> wild strain, where limited amounts of acetaldehyde are produced to give the pink colour. (B) <i>Zymomonas mobilis</i> mutant strain, where increased amounts of acetaldehyde are produced to give the red colour.....	164
Figure 8.4: Alcohol dehydrogenase relative activity in mutant type in comparison with the wild type, showing around 77 % reduction in the activity in mutant type compared to the wild type.....	165

- Figure 8.5:** Glucose consumption pattern in *Zymomonas mobilis* ZM4 mutant strain. (A) Glucose concentration with time, whereby more glucose consumption was recorded under the anaerobic growth. (B) Glucose consumption rate in both initially and periodically sparged groups. Error bars depict standard deviations..... 167
- Figure 8.6:** Comparison between the growth patterns of *Zymomonas mobilis* mutant strain in the initially sparged group and periodically sparged group with the wild strain of *Z. mobilis* ZM4. Error bars depict standard deviation..... 167
- Figure 8.7:** Acetaldehyde and Ethanol production during the fermentation process. (A) Acetaldehyde production with time, whereby acetaldehyde produced preferentially in the periodical sparged group. (B) Ethanol production with time, whereby ethanol produced preferentially in the initially sparged group. Error bars depict standard deviation..... 169
- Figure 8.8:** Accumulated fermentation products. (A) Produced acetaldehyde. (B) Produced Ethanol. Error bars depict standard deviation. * The mean difference is significant at the 0.05 level. 169
- Figure 8.9:** Accumulated produced carbon dioxide, whereby the amount of the produced carbon dioxide in the periodically sparged group was significantly higher than its counterpart in the initially sparged group. Error bars depict standard deviation. *The mean difference is significant at the 0.05 level..... 171
- Figure 8.10:** Stripping process of acetaldehyde from the fermentation broth using air microbubbles. (A) Fluctuation of acetaldehyde concentrations within the fermentation broth after each sparging course. (B) Variation of acetaldehyde concentrations with each sparging cycle and calculation of stripping rate constant (K_{sa}). Error bars are representative of triplicate results. 171
- Figure 8.11:** Bioproducts percent yields of mutant strain in comparison with the wild strain. (A) Ethanol and acetaldehyde yields. (B) Biomass yield..... 172
- Figure 8.12:** Glucose consumption pattern in *Zymomonas mobilis* ZM4 mutant strain grown on 20 g/l glucose supplied medium. (A) Glucose concentration with time. (B) Glucose consumption rate in both initially and periodically sparged groups. Error bars depict standard deviation. 174
- Figure 8.13:** Comparison between the growth patterns of *Zymomonas mobilis* mutant strain in both initially and periodically sparged groups grown on fermentation medium supplied with 20 g/L glucose. Error bars depict standard deviation..... 175
- Figure 8.14:** Accumulated fermentation products. (A) Produced acetaldehyde. (B) Produced Ethanol. (C) Produced carbon dioxide. Error bars depict standard deviation. * The mean difference is significant at the 0.05 level..... 175
- Figure 8.15:** Acetaldehyde and Ethanol production during the fermentation process. (A) Acetaldehyde production with time. (B) Ethanol production with time. Error bars depict standard deviation. 176
- Figure 8.16:** Stripping process of acetaldehyde from the fermentation broth using air microbubbles. (A) Fluctuation of acetaldehyde concentrations within the fermentation broth after each sparging cycle. (B) Variation of acetaldehyde concentrations with each sparging cycle and calculation of stripping rate constant (K_{sa}). Error bars depict standard deviation. 177
- Figure 8.17:** Bioproducts yields. (A) Ethanol and acetaldehyde yields. (B) Biomass yield. 178

Figure 8.18: A comparison between the acetaldehyde results obtained in the current study with previous promising studies, whereby acetaldehyde is both produced and stripped out from the fermentation broth.	179
Figure 8.19: Stripping process of acetaldehyde from the acetaldehyde-water mixture using air microbubbles. (A) Calculation of stripping rate constant (K_{sa}) during sparging course. (B) Decreasing of acetaldehyde concentrations within the mixture after sparging course. Error bars depict standard deviation.	180
Figure 8.20: Stripping process of acetaldehyde from the acetaldehyde-water mixture using the continuous flow. (A) Calculation of stripping rate constant (K_{sa}) during sparging course. (B) Decreasing of acetaldehyde concentrations within the mixture after each sparging course. Error bars are representative of triplicate results.	182
Figure 8.21: Growth pattern of <i>Zymomonas mobilis</i> mutant strain in the synthetic medium under periodically sparging strategy supplied with 20 g/L glucose. Error bars are representative of the triplicate results.....	184
Figure 8.22: Glucose consumption pattern in <i>Zymomonas mobilis</i> ZM4 mutant strain grown in the synthetic medium supplied with 20 g/l glucose. (A) Glucose concentration with time. (B) Glucose consumption rate with time. Error bars depict standard deviation.	184
Figure 8.23: Ethanol production during the fermentation in the defined mineral salts medium supplied with 20 g/L, where the highest ethanol concentration was at hour thirty and thereafter, the concentration decreased due to the stripping process as well as ethyl acetate formation. Error bars depict standard deviation.	185
Figure 8.24: Proposed mechanism for ethyl acetate formation from both acetyl-coA and ethanol.	186
Figure 8.25: Ethyl acetate production corresponding with ethanol production. (A) Ethanol production during the fermentation process. (B) Ethyl acetate production during the fermentation process. Error bars depict standard deviation.	187
Figure 8.26: (A) Effect of added ethyl acetate on exponential cell growth of <i>Zymomonas mobilis</i> mutant strain after 2 hours, where the inhibitory effect of ethyl acetate is proportional to its concentration. (B) Specific growth rate of <i>Zymomonas mobilis</i> mutant strain after adding various concentrations of ethyl acetate. Readings are representative of triplicate results.	188
Figure 8.27: Growth pattern of <i>Zymomonas mobilis</i> mutant strain in the synthetic medium under periodically sparging group supplied with 40 g/L glucose. Error bars depict standard deviation.	189
Figure 8.28: Glucose consumption pattern in <i>Zymomonas mobilis</i> ZM4 mutant strain grown on 40 g/l glucose supplied the synthetic medium. (A) Glucose concentration with time. (B) Glucose consumption rate with time. Error bars depict standard deviation.....	190
Figure 8.29: Ethanol production during the fermentation in the defined mineral salts medium supplied with 40 g/L. Error bars depict standard deviation.	191
Figure 8.30: Ethyl acetate production corresponding with ethanol production. (A) Ethanol production during the fermentation process. (B) Ethyl acetate production during the fermentation process. Error bars depict standard deviation.	191
Figure 8.31: The dissolved oxygen profile in the fermentation broth during the sparging with nitrogen-enriched microbubble, showing the anaerobic conditions were maintained throughout the fermentation process. Points are representative of triplicate results.....	193

Figure 9.1: The profile of dissolved oxygen levels against time during stationary culture, whereby the concentration of dissolved oxygen dropped below the critical oxygen concentration after 40 mins. Error bars depict standard deviation.....	201
Figure 9.2: The profile of dissolved oxygen level against time during shaking flask culture, where the concentration of dissolved oxygen dropped below the critical oxygen level after 200 mins. Error bars depict standard deviation.....	202
Figure 9.3: The profile of dissolved oxygen level against time during microbubbles-sparged culture, where the concentration of dissolved oxygen dropped below the critical oxygen level after 30 mins. Error bars depict standard deviation.....	203
Figure 9.4: A model of periodical sparging strategy for the oxygenation process of the mutant strain of <i>Zymomonas</i> culture using microbubble technology, which describes the time needed to turn the air supply on and the time required to leave the culture before the next sparging course. Error bars depict standard deviation	204
Figure 9.5: Calculation of the mass transfer coefficient and the equilibrium concentration. Error bars depict standard deviation.	205
Figure 9.6: Mass transfer rate against time at different flowrates. Rate of oxygen transfer increased directly with the increase in flowrate (Q). (A) Q= 0.1 L/min ; $KLa = 25.2 \text{ hr}^{-1}$. (B) Q= 0.3 L/min ; $KLa = 29.4 \text{ hr}^{-1}$. (C) Q= 0.5 L/min; $KLa = 33.6 \text{ hr}^{-1}$	206
Figure 9.7: (A) The biomass concentration of the mutant strain of <i>Zymomonas mobilis</i> against time, where a variation in the growth patterns seen in different cultivation systems. (B) specific growth rates of the mutant strain within various cultivation systems. Error bars depict standard deviation.....	207
Figure 9.8: (A) The biomass concentration of the wild strain of <i>Zymomonas mobilis</i> ZM4 against time, whereby the wild type shows its highest growth in the microbubble-dosed system. (B) Specific growth rates within various cultivation systems. Error bars depict standard deviation.	208
Figure 9.9: Illustration and drawing of the propagation unit. (A) The fully assembled propagation unit. (B) Computational domain and mesh for the investigated propagation unit (Mesh-independent solutions were obtained with 7171 tetrahedral elements).....	210
Figure 9.10: 2D axisymmetric domain used along with the meshing of the propagation region within the unit.....	210
Figure 9.11: Snapshots of gas fraction at different flowrates after steady state with 150 μm bubble diameter, where a small fraction of the gas can be seen in the downer corner of the 0.1 L/min flowrate with no eddy currents. (A) At 0.1 L/min (B) At 0.3 L/min (C) At 0.5 L/min.	215
Figure 9.12: The gas fraction in a cross section of riser region at three different flowrates, 0.1, 0.3 and 0.5 L/min, where the gas fraction is proportionate to the air flowrate.	216
Figure 9.13: Oxygen concentration profiles in the propagation unit at flowrate 0.1 L/min, where is a gradual increase in the oxygen concentration in both regions. (A) in the riser region (B) in the downcomer region.	217
Figure 9.14: Snapshots of oxygen concentration at different times after steady state with 150 μm bubble diameter and 0.1 L/min.	218
Figure 9.15: Biomass synthesis trends at different inoculum concentrations. Using high inoculum size generated low biomass with limited ethanol, while low and middle inoculum sizes generated elevated concentration of biomass as well as ethanol and acetaldehyde. Error bars depict standard deviations.	220

Figure 9.16: Ethanol and acetaldehyde production at high inoculum concentration, whereby it can be seen that only limited amount of ethanol produced in the fermentation broth without acetaldehyde. Error bars depict standard deviations.221

Figure 9.17: Ethanol and acetaldehyde productions at low inoculum concentration. Error bars depict standard deviation.....222

Figure 9.18: Ethanol and acetaldehyde productions at medium inoculum concentration. Error bars depict standard deviation.222

List of tables

Table 2.1: Chemical and Physical properties of acetaldehyde (Adapted from EPA, 1987). ...	30
Table 3.1: Shows the chemical reactions with their correspondent reaction rate constants used to integrate the carbon dioxide concentration equations in the current study	57
Table 4.1: Cellulolytic activities of <i>Pseudomonas putida</i> on Petri dishes	83
Table 4.2: Initial protein concentrations and concentrated protein concentrations with corresponding cellulases activities. Results are representative of triplicate readings. ...	85
Table 4.3: Enzyme activity of various cellulolytic enzymes during different steps of ammonium sulfate fractionation. The results are representative of triplicate readings. ...	87
Table 5.1: Ozone concentrations with flow rate	94
Table 5.2: Glucose production at varying ozone and pH levels under both MMO and MMO-M pretreatments.....	99
Table 5.3: Glucose production and accumulative produced glucose at the end of MMO and MMO-M of various prolonged exposure times.....	104
Table 5.4: Energy calculation of pre-treatment processes	107
Table 7.1: The oxygen mass transfer coefficient (for 0.3 L min ⁻¹ dosing) with equilibrium concentrations and sparging time (mins) calculated during the experimental sets.	135
Table 8.1: The oxygen mass transfer coefficient (for 0.3 L min ⁻¹ dosing flow rate) with equilibrium concentrations and sparging time (mins) calculated during the experimental sets with <i>Zymomonas mobilis</i> mutant strain.....	163
Table 8.2: Cell biomass concentration (OD), glucose concentration and ethanol concentration of the fermentation process with 20 g/L and 40 g/L glucose under anaerobic conditions. The reading are representative of triplicate results	194
Table 8.3: Cell biomass concentration (OD), glucose concentration and ethanol concentration of the fermentation process with 20 g/L and 40 g/L glucose supplied in complex medium under anaerobic conditions. The readings are representative of triplicate results.	196
Table 9.1: A summary of the objectives, predictions and earning outcomes of flow and mass modelling developed in the current study	219

Chapter 1

General Introduction and Project Objectives

1.1 Introduction

Increasing global demand for energy and population increases have been causing many problems for the environment, resulting from increased use of fossil fuels, significant rainforest deforestation and expanding industrial operations. These factors are leading to the depletion of natural resources as well as producing various forms of toxic emission, which have many harmful effects on biota. These effects are in some cases short term, such as respiratory diseases like asthma, and are in some cases long term, such as mutations and genetic abnormalities (Commonwealth of Massachusetts, 2015). These emissions have also caused a crisis for the whole of Earth's ecosystem, a symptom of which is climate change. However, until now there is still no effective approach to reducing these emissions (Schrag, 2007).

Seeking renewable fuels, which are from environmentally friendly sources, represents a priority for many researchers. Those researchers have been exploring many methodologies and technologies to generate energy in a way that causes less harm and might meet international requirements. One of the most encouraging sources of renewable energy is the biomass. McKendry (2002) defined "biomass" as any organic material that can be derived from plants. Plants convert solar energy into chemical energy using photosynthesis, which is stored in their tissues as chemical bonds. However, in nature, lignin, cellulose, and lignocellulose are the dominant sources of biomass (Pérez et al., 2002).

Lignocellulosic biomass has drawn much attention as a natural and a renewable resource in developed societies, and this biomass is produced as a waste from many agricultural activities (Pérez et al., 2002). A lignocellulosic biomass might include a variety of materials such as sugarcane, bagasse, wheat, rice and barley straws as well as sawdust, poplar trees and switchgrass. Annually, lignocellulosic biomass accumulates in large quantities, and because its chemical composition is based on carbohydrates, it can be utilised to produce many highly valued products such as enzymes, alcohols, food additives and organic acids (Mussatto and Teixeira, 2010). Therefore, besides the problems caused by the accumulation of these wastes in the environment, these resources represent a worthy energy source that could replace fossil fuels.

Lignocellulosic biomass has three principal components, which are cellulose, hemicellulose, and lignin, and depending on the feedstock source lignocellulosic biomass has a different percentage of these three elements. Typically, it is made up of around 30-50 % of cellulose, 15-35 % hemicellulose and 10-20 % lignin (Pettersen, 1984 cited in Limayem and Ricke, 2012).

Commonly, there are two major routes for energy recovery from biomass, which are the thermochemical route and the biological route. The thermochemical route can be achieved by several methodologies such as air-steam gasification, direct combustion, liquefaction, pyrolysis, supercritical water extraction and ozonolysis (Balat et al., 2009). Some of these methods, however, are energy consuming and use a variety of chemicals, which are toxic, hazardous and corrosive and thus require a reactor (pretreatment vessel) to tolerate these harsh conditions, which are often very expensive. The biological route uses microbial-based methods such as a fermentation, biological water-gas shift reaction and biological pretreatment (Saxena, et al., 2009) but most biological methods use commercial enzymes, which are very costly and might represent a substantial part of operational expense for any industrial process.

In order to improve the traditional pretreatment techniques, further work is necessary to understand the key physicochemical and biochemical mechanisms underpinning these techniques and to explore options to improve glucose yield. One option is to use the microbubble-microbe biomass processing technique, which offers many benefits including a decrease in capital and production cost in comparison with traditional techniques, which utilise a substantial amount of chemicals and enzymes as well as high temperature and pressure. Dosing ozone-enriched microbubbles is an alternative option, which has been proven as an efficient technique to degrade the lignin polymer, and also helps to oxidise carbohydrates concurrently. Crucially, however, it also improves *Pseudomonas putida* growth and consequently the production of enzymes, as the latter plays an influential role in glucose production.

After finishing pretreatment, the inactivation of pretreatment slurries is conventionally achieved by autoclaving for 15 minutes at 121°C and 1-1.5 bar. Autoclaving different slurries requires different operational conditions, such as increasing the autoclaving duration or doing the autoclaving in stages, as there is only a limited capacity for each autoclave. This will increase costs and it might take a long time to achieve the sterilisation process (McNeil and Harvey, 2008). Therefore, an alternative inactivation (sterilisation) technique needs to be sought to avoid some or all of the drawbacks mentioned above. Using carbon dioxide-enriched microbubbles

is a relatively cheap option that works at ambient temperatures, and crucially it uses carbon dioxide, which is a byproduct gas produced by many bioprocesses as a waste gas. Also, carbon dioxide-enriched microbubbles can be applied *in situ* and thus can be performed simultaneously with pretreatment in the same pretreatment vessel.

The inactivated pretreatment slurry can be then fed to the fermenter in order to conduct the fermentation process. Bacterial fermentation can be divided into two main categories, which are aerobic and anaerobic fermentation, depending on the final electron acceptor. Oxygen is the final electron acceptor in aerobically-grown microbes, whereas either organic or inorganic compounds act as a final electron acceptor (such as the sulfate compounds) in anaerobically-grown microbes (Müller, 2001). Depending on the required product, microorganisms can grow either aerobically or anaerobically; however, some microorganisms can grow under both conditions (facultative anaerobic microbes).

Zymomonas mobilis has long been known as the best ethanol producer, and it is widely used to produce a high quantity of ethanol in anaerobic conditions, offering many advantages over other ethanol producers such as *Saccharomyces cerevisiae*. While many researchers have mentioned that this bacterium produces considerable quantities of ethanol under anaerobic conditions, others have noticed that this bacterium can produce an amount of acetaldehyde with a lower quantity of ethanol in aerobic conditions (Wecker, 1987).

Acetaldehyde is a substrate used in various industries such as plastic manufacturing and production of synthetic dyes, and is used as pyridine and pyridine bases, for butanol and as a food additive. Also, it is used to produce ethanol using Ni-based catalysts (Neramittagapong et al., 2008). These uses make acetaldehyde an extremely valuable product at a price near £57.90 per liter according to the sigma-Aldrich website (07-03-2017). However, many researchers have noticed its toxicity to the microbial culture, causing severe inhibition of *Zymomonas* growth when it accumulates in the culture medium.

Removing the final products (acetaldehyde and carbon dioxide) from the culture medium reduces the chemical activity in the liquid of these gaseous products with a negative value change in Gibbs free energy. For this reason, the biological reactions become thermodynamically favourable and provide momentum for the formation of more product. Indeed, removing acetaldehyde and carbon dioxide means removing the stresses that inhibit and prevent proper microbial functions. Theoretically, acetaldehyde can be removed at room

temperature using microbubble technology as this chemical has a boiling point of about 20.8°C, which is surpassed during the fermentation, which requires 30°C. The gaseous carbon dioxide can be removed from the fermentation broth using the same technology. Ethanol, however, tends to preferentially accumulate in the fermentation broth.

1.2 Research Hypotheses

The current project explores the use of a novel microbubble technology in lignocellulosic biomass pretreatment, the inactivation of microorganisms using carbon dioxide, and simultaneous fermentation and separation of bio-products from the fermentation broth of *Zymomonas mobilis*. The fluidic oscillator invented by Zimmerman and co-workers helps to generate micron-sized bubbles with low energy requirements. Reducing the time given to grow the generated bubbles from the pores of a diffuser prevents them from growing any bigger than micron size.

The ability of collapsing microbubbles to enhance lignocellulosic biomass pretreatment is investigated through lignocellulosic biomass pretreatment processes. The increase in surface charge of a collapsing microbubble (ζ potential) supports the hypothesis that significant increase in ions concentrations around a shrinking gas-liquid interface provides a mechanism for free radical generation (Takahashi et al. 2007). When in contact with a solid body (particles), the charges are readily deposited and effectively attack the surface, consequently degrading the particle's physical structure. Ranger et al. (1999) found that generated hydroxyl radicals resulted in extracting a hydrogen atom from the methyl groups or the carbon in the middle structure of lignin. The extent of surface damage can vary depending on the bubble's surface charge magnitude, the particle size and the carrier gas. Dosing charge-laden microbubbles with ozone can play a crucial role in the catalysis and cleavage of cellulose and hemicellulose and, inadvertently, facilitate the release of sugar from the biomass.

Ozone-enriched microbubbles are used to enhance the standard microbubble pretreatment process. Ozone is a strong oxidative agent, and it reacts with lignin by attacking the carbon-carbon double bonds, and free radicals are generated from the reaction of ozone with an aromatic lignin unit. While ozone acts selectively on the carbon double bonds, free radicals act non-selectively and they react with both the lignin and carbohydrates within the biomass. Therefore, ozone can substantially reduce lignin content and increase biomass digestibility with many advantages over other pretreatment methods, such as producing almost no toxic compounds, being usable at room temperature and with standard pressure (Lee et al., 2010).

Traditional methods apply ozone with less attention to mass transfer optimality, resulting in low efficiency and high operating cost. However, the slow velocity of rising microbubbles and high surface-to-volume ratio allow efficient mass transfer to be achieved during the process (Kuvshinov et al., 2014). Direct ozone dosing is the most efficient way to deal with such a highly reactive and short-lived chemical. Both pretreatment methods are followed by a biological pretreatment with the cellulolytic bacterium *Pseudomonas putida*, which preferentially hydrolyses the exposed cellulolytic parts of the biomass to simple sugars.

The ability of carbon dioxide-enriched microbubbles to inactivate microbes and decrease the energy consumed with high microbial reductions are also investigated in the current study. The efficacy of this process depends on the diffusion coefficient of carbon dioxide, which can be controlled by contact time and interfacial area. Microbubbles can significantly improve the efficiency of dosage due to their high surface area-to-volume ratio and their low-rise velocity, ensuring maximum gas-liquid contact time. This substantially cuts down on the operating time.

Integration of the microbubble generation system into the fermentation vessel and testing the performance of this technology in its ability to remove some bioproducts from the fermentation broth are also explored in the current study. In addition, the collection of the stripped products and the behavior of microbial culture after this removal are considered. A fluidic oscillator is used to generate microbubbles from a ceramic diffuser at the bottom of the bioreactors.

Based on the fascinating characteristics of microbubbles, this project investigates the ability of rising bubbles to remove some products from the fermentation medium through a mass transfer process, as the injected air bubbles are dry and have almost zero concentration of these products in them. The rising microbubbles are also expected to remove some heat, which is generated from metabolic activities of microorganisms, and thus might help to control the temperature within the system.

1.3 Research Objectives

Four main objectives are considered in the current study:

- (1) To use microbubble-mediated technologies in the pretreatment of lignocellulosic biomass in synergy with the cellulolytic bacterium *Pseudomonas Putida*.
- (2) To inactivate the cellulolytic bacterium with carbon dioxide-enriched microbubbles.

- (3) To oxygenate the microbial culture and strip out some fermentation products from the fermentation medium by integrating the microbubble generation system into the bioreactor.
- (4) To intensify the bacterial growth during the propagation stage.

These objectives achieve an ultimate goal, which is simultaneous saccharification and fermentation integrated with *in situ* separation of some fermentation products (See Figure 1.1). Traditionally, these processes are conducted as stages, where the lignocellulosic biomass hydrolysis is followed by fermentation and then product recovery. The simultaneous process is a promising strategy for effective bioproducts production from lignocellulosic biomass because of the resulting reduction in utilities, which would reduce the investment cost and simplification of the operation but crucially, the avoidance of the process inhibition by the final products such as acetaldehyde and carbon dioxide and thereby increasing the process rate and products yield. Typically, the collected products can be used in numerous processes especially in fuels production such as ethanol and butanol, and the carbon dioxide can be recycled to use in the inactivation process as well as for algal growth.

These objectives can be achieved by the following:

- Investigation and characterisation of cellulolytic activity of *Pseudomonas putida* KT 2440 as well as monitoring growth patterns on different culture media. This bacterium can then be used to hydrolysis the cellulose content of the biomass to produce sugar, glucose.
- Designing and using a new prototype system to pretreat lignocellulosic biomass and investigate the potential effects of the generated microbubbles on lignocellulosic biomass. This is executed by examining the biomass before and after the pretreatment and testing it with FTIR-ATR and SEM in addition to measuring glucose concentration.
- Carrying out microbubble-mediated ozonolysis as a step forward in the pretreatment of lignocellulosic biomass. Ozone is a highly reactive nonlinear triatomic molecule towards compounds containing double bonds and functional groups with high electron densities. Consequently, lignin is most likely to be oxidised in this process as it has a high content of double bonds. *Pseudomonas putida* is used in all pretreatment experiments as a source of cellulolytic activity, which used as an alternative to the expensive commercial enzymes.

All above three points are testing the first objective in the current study, which is using microbubble-mediated technologies in the pretreatment of lignocellulosic biomass in synergy with the cellulolytic bacterium *Pseudomonas Putida*. This objective is explored in chapter 4 and 5 and green-coded in Figure 1.1.

- Using carbon dioxide-enriched microbubbles in the inactivation process. Because practical and economic aspects are crucial in the processes of producing highly valued products and biofuels, it is critical to consider the inactivation process of pretreatment and fermentation slurries. The fermentation process (downstream process) is prone to contamination by this adventitious agent (*Pseudomonas Putida*), which has a huge impact on the biological process as this bacterium might introduce product variability and can cause loss of potency due to degradation or modification of product by microbial enzymes, changes in impurity profiles, and an increase in the levels of bacterial endotoxins. In addition, it can result in lengthy shutdown periods and delays in fermentation operations that in turn, may sometimes result in shortages of products formation.

The primary action of this inactivation process trigs the disturbance or damages the balance of the biological system of cells. This process can be enhanced by using added solutions such as mixed ethanol and acetic acid, which increases the solubility of carbon dioxide as well as working on different sites within the biological system.

This point targets to test the second objective in the current study, which is using carbon dioxide-enriched microbubbles as an inactivation process. This objective is explored in chapter 6 and brown-coded in Figure 1.1.

- Oxygenating the fermentation process as well as the stripping of some bioproducts from the fermentation broth of *Zymomonas mobilis* using air microbubbles generated by a fluidic oscillator. The provision of enough oxygen is crucial for keeping the aerobic fermentation process going, but similarly removing acetaldehyde and carbon dioxide might help to prevent the detrimental effect of these products on microbial cells, whilst increasing productivity from the microbial culture.

To enhance the acetaldehyde productivity, mutant strain with attenuated or modified alcohol dehydrogenase activity can be selected using allyl alcohol but unfortunately, this strain has low biomass yield and therefore has limited acetaldehyde production as this product is directly associated with the biomass synthesis.

This point targets to test the third objective, which is to oxygenate the microbial culture and strip out some fermentation products from the fermentation medium by integrating the microbubble generation system into the bioreactor. These objectives are explored in chapter 7 and 8 and blue-coded in Figure 1.1.

- Enhancing the biomass yield of the allyl alcohol selected strain. Generally, the wild strain of *Zymomonas mobilis* shows a relatively low biomass yield in comparison with other fermentative microorganisms under anaerobic conditions, but it shows an increased growth yield during the exponential phase of the aerobic growth. However, the selected strain of allyl alcohol, shows an even lower biomass yield and since the acetaldehyde production is directly associated with biomass synthesis, the biomass yield of the mutant strain needs to be enhanced. To enhance the biomass yield of the allyl alcohol selected strain, a microbubble-driven system can be used to grow this bacterium aerobically. Microbubbles are more efficient in mass transfer than larger bubbles due to their high surface area-to-volume ratio. It is also more efficient than traditional cultivating techniques, leading to the maintenance of sufficient oxygen concentration during the bacterial propagation stage.

This point targets to test the fourth objective, which is intensifying the bacterial growth during the propagation stage by integrating the microbubble generation system into the propagation unit. This objective is explored in chapter 9 and black-coded in Figure 1.1.

1.4 General benefits of the current project

The processes of pretreatment, inactivation, propagation and fermentation are clean processes with very low pollution levels. In fact, the pretreatment process uses lignocellulosic biomass as a substrate; therefore, it contributes to the recycling of energy in the ecosystem. Wheat straw is cheap biomass, and it might reduce the total operational cost of the fermentation process. Microbubbles might decrease the total cost of the pretreatment process, and could help to avoid the formation of inhibitory compounds from the biomass and lead to increased productivity of the whole process (Arrows 1, 2 and 3 in Figure 1.2).

The inactivation process is a relatively new, non-thermal method. It uses the byproduct of the downstream process, the fermentation process, to inactivate the *Pseudomonas* culture. Also, it can be applied *in situ*, which might shorten the number of stages to connect to the upstream stage, the pretreatment process, with the downstream process, the fermentation process. Carbon

dioxide-enriched microbubbles might substantially reduce the amount of consumed energy compared with thermal methods such as autoclaving (Arrow 4 in Figure 1.2).

Stripping of acetaldehyde and carbon dioxide contributes significantly to increasing the productivity of the fermentation process. It is worth mentioning that this process might also contribute to an increase in productivity of other fuels, since acetaldehyde represents a precursor for fuel production, especially for ethanol and butanol, and hence this might help to meet the global demand for these fuels (Arrows 6, 7, 8 and 9 in Figure 1.2).

Ethyl acetate can also be produced during the growth in the synthetic medium. Ethyl acetate is one of the most important volatile industrial compounds as it is used as a chemical solvent and in the synthesis of biodiesels, paints, adhesives, herbicides and resins. Its annual production volume reached around 3.5 million tons in 2015, which corresponds to a \$3.7 billion global market (Kruis et al., 2017).

Additionally, the results from the propagation study are crucial for bacterial-based industries such as the biofuel, food, pharmaceutical industries, for which microbial biomass growth is a premium (Arrows 5 and 10 in Figure 1.2).

Furthermore, this project will provide useful information about the operational conditions of both the fermentation and stripping processes, which can be used to scale up the benchmark process to larger industrial plants.

1.5 Thesis Organisation

This thesis is organised in the following way:

- (1) The first chapter gives a general introduction and the project objectives.
- (2) The second chapter gives some general background and literature reviews on the basic topics covered in this study.
- (3) The third chapter gives details about the study's materials and experimental methods.
- (4) The fourth chapter shows the obtained results from the exploiting of microbubble-microbe synergy for biomass pretreatment, along with its discussion.
- (5) The fifth chapter shows the obtained results and discussion of the exploiting of ozonolysis-microbe synergy for biomass pretreatment.
- (6) The sixth chapter shows the obtained results and discussion of the inactivation combined with cell lysis of *Pseudomonas putida* at low pressure using carbon dioxide-enriched microbubbles.

- (7) The seventh chapter shows the obtained results and discussion of the fermentation process using wild type strain integrated with the *in-situ* stripping of the fermentation products using microbubble technology.
- (8) The eighth chapter shows the obtained results and discussion of the fermentation process integrated with *in situ* stripping using a mutant *Zymomonas* strain selected with allyl alcohol.
- (9) The ninth chapter shows the obtained results and discussion of the intensification of the bacterial growth of *Zymomonas mobilis*, both wild-type and mutant-type, using microbubbles driven system and compared with traditional methods.
- (10) The tenth chapter provides references relevant to this study.

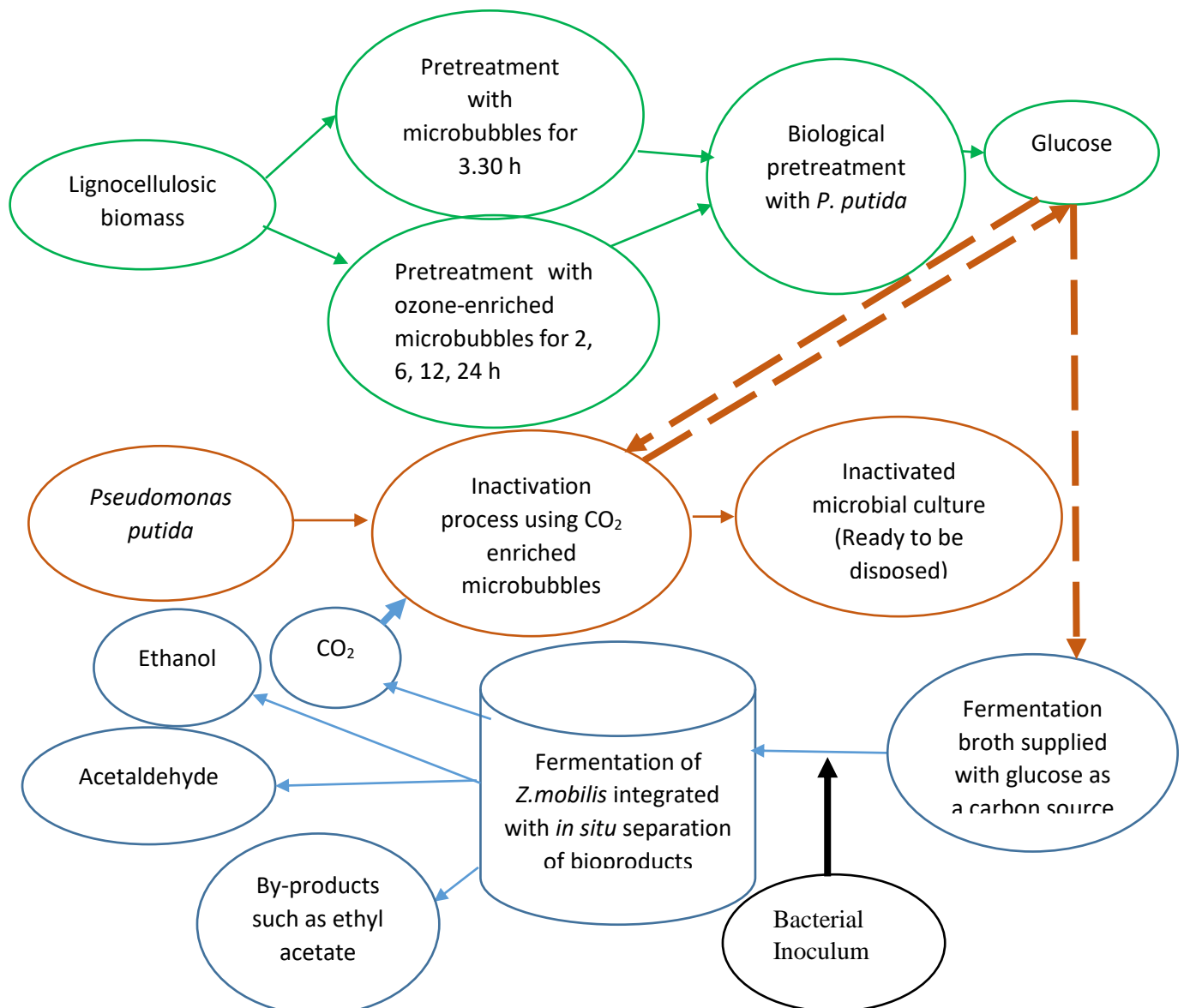


Figure 1.1: General flow chart of the current project.

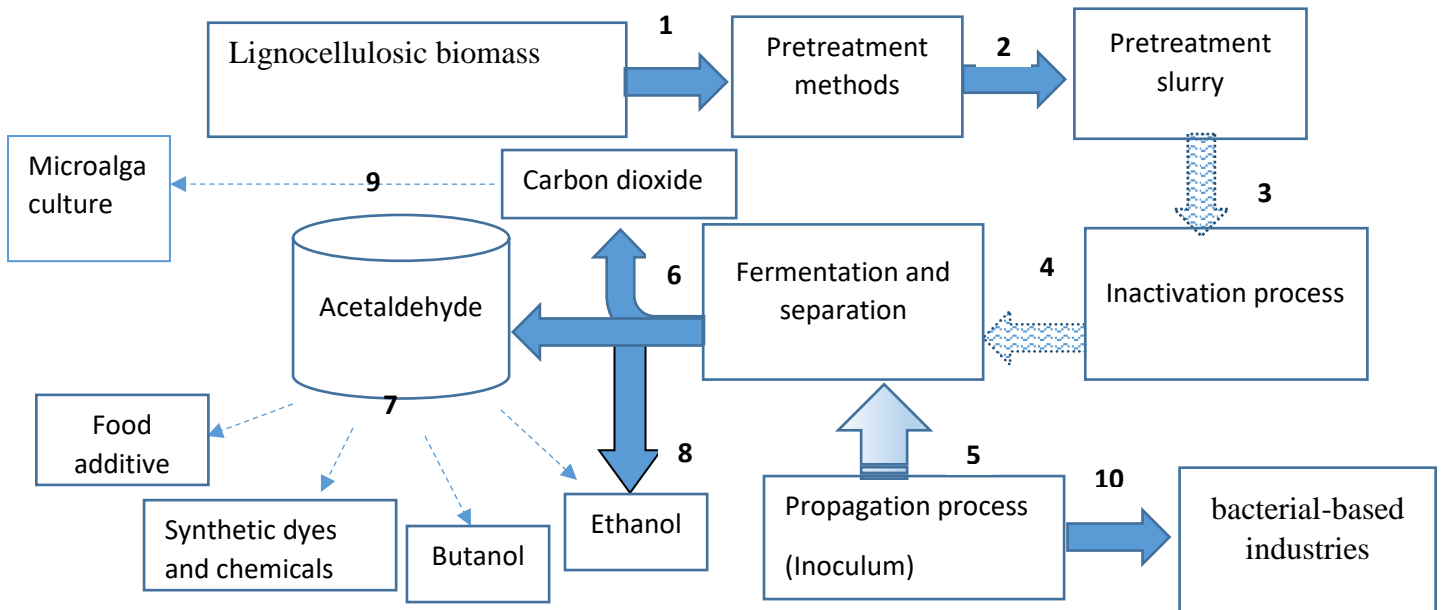


Figure 1.2: Stages of the current project with the potential uses of the final products.

Chapter 2

Literature Review

This chapter provides a critical assessment of relevant literature on the structure and pretreatment of lignocellulosic biomass, inactivation of microorganisms and fermentation processes using *Zymomonas mobilis*.

Firstly, various pretreatment methods of lignocellulosic biomass are critically evaluated and the concept and importance of these methods are considered. The evaluation starts with non-bubble based techniques such as mechanical, physiochemical, chemical and biological pretreatment methods, and then moves on to highlight the benefits of the application of microbubbles as part of a bubble-based technique. Using biological pretreatment methods to pretreat lignocellulosic biomass will leave the pretreatment slurry contaminated with cellulolytic microbes and, before using the sugary content in the pretreatment slurry, the slurry needs to be inactivated.

Next, various inactivation methods are critically evaluated and the proposed mechanisms of action of carbon dioxide are reported in some detail.

The characteristics of *Zymomonas mobilis* as a fermentive microorganism used in the current study to conduct the fermentation process and its metabolic pathway are described, where particular attention is drawn to acetaldehyde as a target product. Acetaldehyde separation techniques are critically evaluated. The benefits of using gas stripping are discussed. Microbubble characteristics are given and discussed with emphasis on their advantages in both oxygenation and stripping off. The generation of microbubbles with the fluidic oscillator and an overview of the working mechanism of the novel device are given, on which the research work is centred.

An important part of the literature review considers the fundamentals of the airlift loop bioreactor and the advantages of using this type of reactor to conduct the fermentation process.

The last section presents an overview of the effects of chemical activity of both acetaldehyde and carbon dioxide on the fermentation process.

2.1 Pretreatment methods of lignocellulosic biomass

Many pretreatment methodologies have aimed to make cellulose more accessible for cellulase enzymes which eventually can break down cellulose (and probably hemicellulose) to its basic unit, glucose (Kumar et al., 2009). Typically, the main purpose of pretreatment is to break down

the shield formed by lignin and hemicellulose and to disrupt the crystalline structure and reduce the degree of cellulose polymerisation (Zheng et al., 2009).

Lignin is the most complicated component in lignocellulosic materials, and it covers this biomass and prevents access of cellulase enzymes to hydrolyse cellulose. On the other hand, cellulose forms a backbone that is surrounded by hemicellulose and lignin (Mussatto and Teixeira, 2010). Figure 2.1 shows the main components of lignocellulosic biomass with the typical arrangement of these elements (Mussatto and Teixeira, 2010).

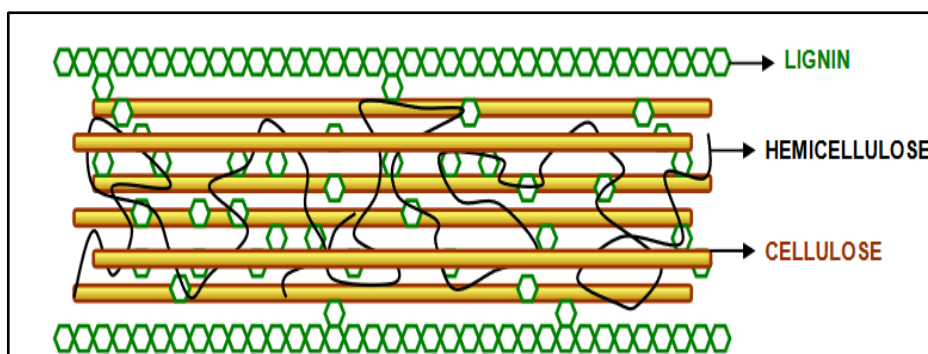


Figure 2.1: The typical arrangement of lignocellulosic biomass components, showing cellulose, hemicellulose and lignin fractions (Adapted from Mussatto and Teixeira, 2010).

Yang et al. (2011) reported that the degree of cellulose polymerisation represents a recalcitrance for hydrolysing of lignocellulosic biomass. In contrast, Ioelovich and Morag (2011) observed that the degree of polymerisation has a minor effect on cellulolytic activities when commercial cellulases were used to study these activities. On the other hand, Yang et al. (2011) claimed that the amorphous cellulose is easier to hydrolyse by cellulase enzymes in comparison with crystalline cellulose, in which glucose chains are connected to each other by hydrogen bonds. Furthermore, Hall et al. (2010) found that cellulose crystallinity plays a crucial role in determining the hydrolysis rate of this molecule, where an increase in the cellulases' initial rate was noticed alongside a decrease of the degree of cellulose crystallinity.

Pretreatment methods can be categorised into mechanical (such as milling and grinding), physicochemical (steam pretreatment/autohydrolysis, wet oxidation and hydrothermolysis), chemical (alkali, dilute acids and ozonolysis), biological (cellulolytic microorganisms and commercial enzymes) and electrical (negative and positive currents), or a combination of these methods (Kumar et al., 2009). Hsu et al. (1980) showed the main action of different pretreatment methods on lignocellulosic biomass (Figure 2.2).

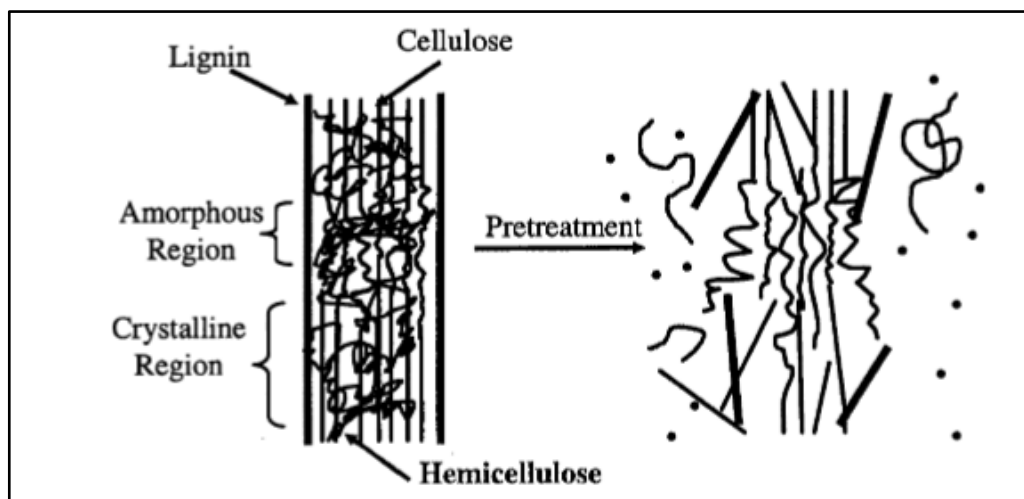


Figure 2.2: The main action of various pretreatment methods, whereby both lignin and hemicellulose as well as reducing the cellulose crystallization and polymerisation are the main targets of these pretreatment methods (Adapted from Hsu et al. 1980).

2.1.1 Mechanical pretreatment

Lignocellulosic biomass can be mechanically pretreated using chipping, milling and grinding, and the main purposes of this pretreatment are to reduce biomass size to small particles, decrease cellulose crystallinity and increase the surface area of the produced particles to improve their digestibility. Different types of apparatuses are used to achieve this goal, such as vibrating ball milling, ordinary ball milling and mortar and pestle. A mortar and pestle was used in the current project to accomplish the above goals (Kumar et al., 2009).

2.1.2 Physicochemical pretreatment

Lignocellulosic biomass can be physicochemically pretreated using steam explosion and Ammonia Fiber Explosion (AFEX). In the former method, biomass is treated with saturated steam at high pressure, and then this pressure is released to produce sudden decomposition of the biomass. This method is combined with using high temperatures starting at 160-260°C for several seconds to few minutes, which ends with a biomass explosion. Also, this method increases hemicellulose hydrolysis and lignin transformation to its fundamental units and cellulose hydrolysis. However, the steam explosion has many limiting factors, such as a residence time, temperature, particle size, water content and generation of inhibitors (Gnansounou and Dauriat, 2005).

AFEX represents another well-known physicochemical pretreatment method. In this method, lignocellulosic biomass is exposed to liquid ammonia at a high temperature and pressure for a

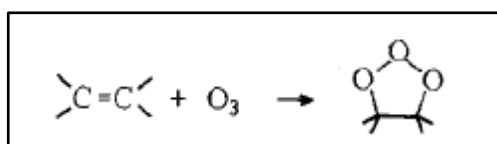
particular period, and the pressure is suddenly dropped to cause a biomass explosion. Typically, liquid ammonia doses are 1-2kg per kg of biomass at 90°C (Teymouri et al., 2004).

2.1.3 Chemical Pretreatment

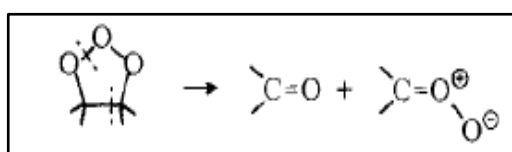
Chemically, lignocellulosic biomass can be pretreated using ozone, which can substantially reduce lignin content and increase biomass digestibility. This method has many advantages over other pretreatment methods, such as producing almost no toxic compounds. In addition, ozonolysis is carried out at room temperature with standard pressure, and ozone can then quickly decompose using a catalytic bed (Lee et al., 2010). In contrast, there are some disadvantages related with this process, such as expensive, as this process requires a massive amount of ozone to achieve this goal due to the technical limitation of the ozonation process (Kumar et al., 2009).

Recently, Kuvshinov et al. (2014) reported an improved technology to enhance ozonolysis. This technology depends mainly on direct injection of ozone into a pretreatment reactor using microbubble technology. It was found that the efficacy of this technology depends on the diffusion coefficient of ozone, which relies on contact time with and interfacial area of the microbubbles, the carriers. Phorbol-12-myristate-13-acetate (TPA) was treated with ozonolysis, and the detoxification of this chemical was achieved in 30 minutes with 26ppm of dissolved ozone, and oil with highly nutritious value was produced as a final product (Kuvshinov et al., 2014).

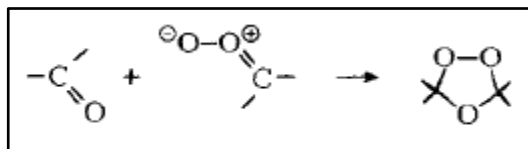
Criegee (1975) described the mechanism of ozonolysis, and how the carbon double bond was the primary target of this cleavage mechanism. This mechanism has three steps to complete the cleavage of double bonds by ozone. In the first reaction, the carbon double bond is reacting with the ozone, forming primary ozonide according to the following reaction (Criegee, 1975):



The primary ozonide is decomposed into two compounds in the second reaction, which are carbonyl compound and carbonyl oxide:



In the third reaction, carbonyl oxide is added to the carbonyl compound (addition reaction).



According to the above reactions, carbon double bond is the principal goal for ozonolysis, and it is cleaved to produce double bond free compounds.

Acid hydrolysis represents another chemical pretreatment method, which has been widely used to treat lignocellulosic materials. Acids such as HCl and H₂SO₄ have been extensively used for this purpose, resulting in an increase in enzymatic hydrolysis activities. However, these acids are toxic, hazardous and corrosive, and they require a withstandable reactor to tolerate these harsh conditions, and that makes the pretreatment method very expensive. These acids should be recovered from the pretreatment slurry after finishing hydrolysis (Sun and Cheng, 2002). On the other hand, diluted acids have been used as an alternative method for concentrated acids. Typically, diluted HCl and H₂SO₄ are used below 4% to treat lignocellulosic biomass as an effective and inexpensive method, and there are many other advantages of this method such as removing hemicellulose from lignocellulosic biomass and enhancing the digestibility of cellulose by cellulases (Sun and Cheng, 2002).

2.1.4 Biological Pretreatment

Biologically, lignocellulosic materials can be hydrolysed into fermentable sugars, which can be utilised as substrates for fermentation processes. While chemical and physicochemical methods require specific instrument design and have high energy requirements, the biological method uses various types of microorganisms to achieve this purpose. This method is environmentally friendly and does not need a high amount of energy. In addition to lignin and hemicellulose degradation, this method is very efficient in cellulolytic activity (Kumar et al., 2009).

2.1.4.1 Cellulases applications

Cellulolytic enzymes have drawn much attention as they can be used in the textile industry for improving fabric quality, and to improve the nutritional quality and digestibility of animal feed. These enzymes have also been utilised in the paper and detergent industries for several decades (Sukumaran et al., 2005). Recently, the fossil fuels shortage causes an increasing need for an alternative source of renewable energy, and lignocellulosic biomasses represent one promising sources of bioenergy. The cellulosic part of this biomass can be converted biologically to its fundamental unit, glucose, using cellulases. The production of these enzymes and using them in different technologies has reached a stage where these enzymes become a vital element in these processes (Xia and Cen, 1999). For example, Belghith et al. (2001) used cellulases from

Penicillium occitanis in the bio-stoning of denim as an alternative to pumice stones, which are traditionally used in the textile industry. The enzymes act on cellulose fibers to release the indigo dye used to colour these fabrics, which consequently produces an etiolated view of the denim. However, On the other hand, pure enzymes are expensive, and they might take a major part of the capital costs (Sukumaran et al., 2005).

Cellulolytic microorganisms can degrade cellulosic materials and convert them to glucose and other fermentable sugars, which can be used as a microbial substrate or fermentation substrate to produce a variety of products such as biofuels (Deshpande et al., 1986). While there are many cellulolytic microorganisms that have been described previously, none of them is effective enough alone to hydrolyse various components of lignocellulosic biomass. Currently, the strategy used in the production of biofuels from lignocellulosic feedstock is a multi-stage strategy including pretreatment of this biomass to extract lignin and hemicellulose, and residual cellulose is then converted to fermentable sugar at mild temperatures, which is eventually used by microorganisms to produce alcohols as final products (Rani et al., 1997). Much research has focused on the isolation of new cellulase systems and the optimisation of process conditions. *Trichoderma reesei* has been used to achieve this process in many bioethanol production plants, as it showed highly efficient cellulolytic activity (Sukumaran et al., 2005). To increase the efficiency of biofuels production, serious attempts have been made to identify efficient cellulolytic systems, and the current study puts the spotlight on the cellulolytic activity of *Pseudomonas putida* KT2440.

2.1.4.2 Control the cellulases' secretion

Cellulolytic microbes are carbohydrate degrader microorganisms, which cannot use proteins or lipids as energy sources for their growth and propagation (Lynd et al., 2002). Various microbiological groups have shown cellulolytic activities, notably bacteria such as *Cellulomonas* and *Cytophaga*, while fungi tend to have a wide range of carbohydrate utilisation (Poulsen and Petersen, 1988; Rajoka and Malik, 1997). The ability to secrete large quantities of extracellular proteins is distinguishable among some fungi such as *Trichoderma reesei*, though this ability is less available in bacteria (Sukumaran et al., 2005).

The cellulolytic systems can be divided into secreted and cell-associated enzymes according to their mode of action and structural properties (Henrissat et al., 1998; Crout and Vic, 1998). There are three major groups of enzymes:

A- Endoglucanases (EC.3.2.1.4, 1,4-B-D-glucan-4-gluconohydrolases)

This group of enzymes attacks cellulose chains at random sites and produces smaller chains. In addition, this group might release glucose and cellobiose, and create sites for the activity of the next group, exocellobiohydrolases (Ibrahim and El-diwany, 2007).

B- Exocellobiohydrolases (EC.3.2.1.91, 1, 4-B-D-glucan-glucohydrolases)

This group of enzymes attacks the non-reducing ends of cellulose chains and releases cellobiose as the main product of their activity (Ibrahim and El-diwany, 2007).

C- β -glucosidases (EC. 4.2.1.21, β -D-glucoside – glucohydrolase)

This group represents the last group of the cellulolytic system, and it cleaves cellobiose into two glucose molecules, the final product in cellulolytic activity (Bravo et al., 2002). Figure 2.3 shows the mode of action of the three major groups of cellulases activities.

Cellulase production is a growth-associated activity associated with increase in the biomass. During submerged fermentation, many factors can influence cellulase production, such as the type and concentration of the inducer, carbon sources, nitrogen sources and the mode of culture, i.e. batch, fed-batch, or continuous cultures.

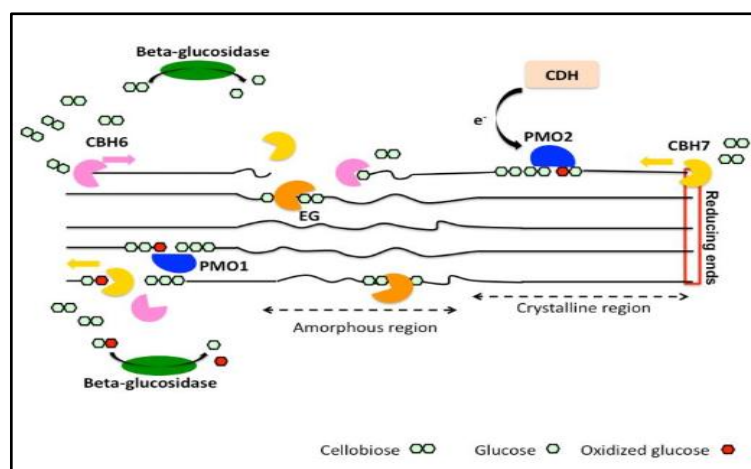


Figure 2.3: Enzymatic degradation of cellulose by cellulolytic enzymes, involving cellobiohydrolases (CBH), endoglucanases (EG), type1 and type 2 PMOs (PMO1 and PMO2, respectively). Cellobiose dehydrogenase (CDH) is a potential electron donor for PMOs. EGs and PMOs cleave internally cellulose chains releasing chain ends that are targeted by CBHs. CBHs generate cellobiose or oxidized cellobiose that are subsequently hydrolyzed by β -glucosidase (Adapted from Dimarogona 2012).

2.1.4.3 Characteristics of *Pseudomonas putida* as a cellulolytic agent

Pseudomonas putida is a gram-negative, rod-shaped, aerobic bacterium. It shows significant metabolic diversity. It is adapted to different environments such as soils, aquatic systems, and the rhizosphere (Timmis, 2002). Dos Santos et al. (2004) described *Pseudomonas putida* as a

well-studied species in this genus, and its biological features have been intensively explored along with its underlying mechanisms. This bacterium has shown rapid growth behaviour and many fantastic features such as robustness. Amenability for genetic modifications makes this bacterium serve as a model microorganism for research on soil bacteria and the many processes that depend on the interaction between bacteria and soil (Timmis, 2002).

Regarding cellulolytic activities, Fagade and Bamigboye (2012) studied the effects of cultural conditions on cellulase activities of different bacterial strains such as *Pseudomonas putida*, *Bacillus subtilis*, *Bacillus licheniformis I* and *Bacillus licheniformis II*, which had been isolated from corn cobs. *Pseudomonas putida* exhibited moderate cellulase activities at 28°C and 40°C, where high cellulase activity was observed at 32°C. While highest cellulase activity was observed at pH7, the lowest cellulase activity was noticed at pH4 and pH5.5. Fagade and Bamigboye (2012) also examined cellulases activities with different nitrogen sources, and the highest cellulase activity was observed with yeast extract and NaNO₃ as a nitrogen source, while moderate activities were observed with peptone, urea and NH₄Cl. Dabhi et al. (2014) used bacterial consortia to hydrolyse banana waste and to produce cellulase enzymes. Four bacteria were used to produce these consortia: *Cellulomonas cartae*, *Pseudomonas fluorescence*, *Pseudomonas putida* and *Bacillus megaterium*. Finally, *Pseudomonas putida* was found to have all the cellulase enzymes required to hydrolyse lignocellulosic biomass (Dabhi et al., 2014).

The cellulolytic enzymes of *Pseudomonas putida* have been tested. For example, filter paperase, carboxymethyl cellulase and β -D-glycosidase were tested, and the enzymatic activities were 0.3 U/ml, 0.2 U/ml and 0.02 U/ml after 25 days for β -D-glycosidase, CMCase and FPase respectively (Dabhi et al., 2014).

Indeed, this microbe is a potent candidate for biological pretreatment of lignocellulosic biomass, and it has all of the important features to achieve this process. This bacterium is very efficient in phenol degradation, and because the fundamental unit of lignin is phenol propionic unit, *Pseudomonas putida* is likely to overcome this barrier.

After using *Pseudomonas putida* in the biological pretreatment of lignocellulosic biomass, the pretreatment slurry should then be inactivated prior feeding it to the fermentation process. Various inactivation processes are critically evaluated and given in the below section.

2.2 Inactivation of microbial culture using carbon dioxide

2.2.1 Inactivation processes

Inactivation (disinfection) is a process of reduction of some contaminating organisms to a level that cannot cause infection. Conventionally, disinfection methods can be divided into two main categories, which are thermal and non-thermal methods. Thermal methods are used to sterilise various materials such as food, medical devices and water. However, many biomaterials are heat-sensitive materials, and they can be destroyed by heat such as removal of flavour, denaturation of proteins compounds, changing in physical, mechanical and optical characteristics of these materials (Nair, 1995). Steam sterilisation represents one of the most common techniques in this category, which has a reasonable operational cost and effectiveness, however, due to the drawbacks mentioned above, it is not suitable for many bioprocesses (Dillow et al., 1999).

Consequently, there is increasing demand for non-thermal inactivation methods, such as ethylene oxide, γ -irradiation and supercritical carbon dioxide. Ethylene oxide can be applied to heat-labile materials as an efficient sterilisation technique, but this chemical is toxic, flammable and carcinogenic, and it may cause hemolysis, and undesirable chemical changes in the treated biomaterials (Dillow et al., 1999). On the other hand, γ -irradiation is suitable for heat sensitive materials as well, but it can cause harmful mechanical changes within biomaterials. In addition, the infrastructure of these biomaterials can also be affected, and its chains might be broken down by this radiation (Premnath et al., 1996). While ethylene oxide and γ -irradiation might have destructive effects on treated biomaterials, inactivation with carbon dioxide does not have many of these limitations.

Recently, CO₂ has been used to preserve food as a non-thermal process as it can inactivate a wide range of microorganisms such as yeast and bacteria. The primary action of inactivation is triggered by disturbance of or damage to the balance of the biological system of cells (Hong and Pyun, 2001). There are many proposed targets for CO₂ activities, which are discussed below.

Previously, it was observed that CO₂ has a very high tendency to dissolve in water, and this tendency becomes even greater with hydrophobic solutions such as ethanol and acetone. The CO₂ solubility coefficient is approximately 1 at 15°C, and that means at 15°C, 1ml of CO₂ dissolved in 1 ml of water, and this solubility decreases with increasing temperature (Slaughter, 1989).

The survivor ratio can be calculated using the following equation, which described by (Spilimbergo and Bertucco, 2003):

$$\text{Log} \frac{N}{N_0} = k \cdot t \cdot 2.303 \quad (\text{Eq. 2.1})$$

Where k is the sterilisation rate constant (h^{-1}), and t is the time.

2.2.2 Carbon dioxide mechanisms of action

Carbon dioxide can inactivate microorganisms via various potential mechanisms, which have been reviewed by Garcia-Gonzalez et al., (2007). These mechanisms are arranged as steps to illustrate them and to explain their bacteriostatic actions. Figure 2.4 shows the potential mechanisms of carbon dioxide actions.

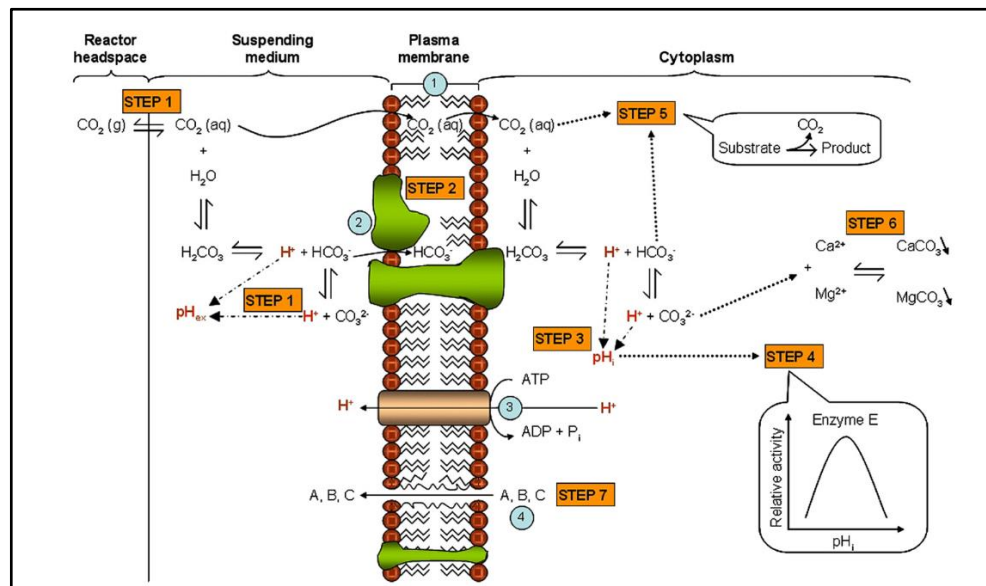


Figure 2.4: Actions of carbon dioxide on bacteria, besides the different steps of the inactivation mechanism—are ① a phospholipid bilayer, ② integral membrane proteins, ③ a plasma membrane H⁺-ATPase, and ④ intracellular substances (Adapted from Garcia-Gonzalez et al., 2007)

2.2.2.1 Step one: Solubility of CO₂ in the exterior liquid phase

CO₂ can dissolve in foodstuff and culture broths with high water content, after which it can be dissociated to form carbonic acid (H₂CO₃). This acid is dissociated into three other compounds, which are bicarbonate (HCO₃⁻), carbonate (CO₃²⁻) and ionic species hydrogen (H⁺) (Garcia-Gonzalez et al., 2007).

The formation of carbonic acid and liberation of H⁺ ionic species can lower extracellular pH (pH_{ex}) in the broth cultures, which may inhibit microbial growth (Valley and Rettger, 1927; Hutkins and Nannen, 1993). Decreasing extracellular pH may also reduce microbial resistance

to an inactivation process due to increasing energy consumption by proton motive force to maintain the pH balance within microorganisms (Hutkins and Nannen, 1993; Hong and Pyun, 1999). However, decreasing the pH of extracellular liquid cannot be the primary reason for the lethal effect of CO₂, as the observed effect is greater than effects of other acids that have been typically used to increase medium acidity, such as HCl and H₃PO₄. In addition, these acids do not show a tendency to penetrate microbial cells, while CO₂ seems to enter microbial cells quickly (King and Mabbitt, 1982; Debs-Louka et al., 1999; Ho-mu et al., 1993).

2.2.2.2 Step two: Modification of cell membrane

It has been noticed that CO₂ diffuses through the cell membrane of microorganisms, and it can accumulate in the phospholipid layer of this membrane. This accumulation leads to an increase in the fluidity of the plasma membrane and causes an anesthesia effect on microbial cells (Isenschmid et al., 1995). Spilimbergo et al. (2002) noticed that CO₂ is dissolved in the phospholipid layer to a very great extent.

In addition, a decrease in the water permeability of the membrane was observed as an additional effect of treatment with CO₂ (Glinka and Reinhold, 1972, cited in Jones and Greenfield, 1982). It was suggested that the formation of bicarbonate might change charged phospholipids head groups and integrated proteins with the plasma membrane, and this leads to alter the density of surface charges and optimal loss functions of the membrane (Garcia-Gonzalez et al., 2007).

2.2.2.3 Step three: Decreasing the intercellular pH

Increasing membrane permeability allows pressured CO₂ to easily cross the cell membrane and accumulate within the cytoplasm. Initially, penetrated CO₂ and HCO₃⁻ are controlled by the internal buffer within cell cytoplasm as there are many mechanisms to control and regulate pH within the cell such as cytoplasmic buffering, proton symport systems, production of acids and bases, and proton pumps (Booth, 1985). Membrane-bound H⁺-ATPase system might play the most important role in maintaining an almost constant internal pH. In this system, protons are expelled outside the cells against both pH gradient and electrochemical gradient, and both of these gradients are known as a motive proton force (Hutkins and Nannen, 1993). Under normal conditions, the cells can neutralise penetrated CO₂ and keep the internal pH within a standard range, however, with increasing the dissolved CO₂, the cells cannot expel all generated protons, and the internal pH will start to decrease. Subsequently, a cell's viability can seriously be harmed if the internal pH severely decreases if there is a large difference between the internal and external pH ($\Delta\text{pH}=\text{pHi}-\text{pHex}$) (Hutkins and Nannen, 1993).

2.2.2.4 Step four: Inactivation of vital enzymes and inhibition of cellular metabolisms due to low internal pH

Lowering the internal pH can affect a range of enzymes and proteins in the cytosol. Typically, these enzymes optimally work under optimum pH, while their activities are declined and impaired with decreased internal pH. Similarly, decreasing the internal pH can inhibit many metabolic systems such as glycolysis, amino acid, and peptide transport temporarily or permanently, leading to the inactivation of key enzymes (Hutkins and Nannen, 1993).

Hong and Pyun (2001) studied the membrane damage and enzyme inactivation in *Lactobacillus plantarum* after treating it with pressured CO₂. It was found that *Lactobacillus* cells suffer from irreversible changes in their cellular membrane, reducing glycolytic activities and inactivating constituent enzymes.

2.2.2.5 Step five: Direct inhibitory effect of CO₂ and HCO₃⁻ on metabolism

There are many factors that regulate enzymes' reactions. As mentioned above, the intracellular pH represents one factor, as do the concentration of substrates, products, and cofactor, which regulate the enzymes' activities. Jones and Greenfield (1982) found that many enzymes can be regulated (stimulated or inhibited) by bicarbonate anion as these enzymes have anion-sensitive sites in their structures. However, dissolved CO₂ does not seem to have this function.

2.2.2.6 Step six: Unbalancing the internal electrolytes

Inorganic electrolytes have many roles inside microbial cells, such as maintaining an osmotic balance between cells and its surrounding environment, and they contribute in the stabilisation of the cell membrane and proteins. The applied CO₂ can accumulate inside the cytoplasm of bacterial cells, where bicarbonate converts to carbonate. Carbonate can react with some of the inorganic electrolytes (such as Mg⁺² and Ca⁺²), causing precipitation of these electrolytes. The precipitation of these electrolytes have harmful effects on volumes of cells, as these electrolytes contribute to the osmotic relationship of cells with their surroundings (Lin et al., 1993). In addition, carbonate can react with some of the proteins, which have magnesium and calcium binding to their structures, and this would precipitate these proteins after binding CO₃⁻² to their binding sites (Gangola and Rosen, 1987).

2.2.2.7 Step seven: Removal of vital moieties from cell membrane

Lin et al. (1992) have shown that the accumulation of pressured CO₂ within the cells has a high extracting power for vital constituents from cells and cells membranes. It was found that dissolved CO₂ tends to build up to a critical level within cells, leading to the removal of some internal moieties such as phospholipid bilayers, and this will disturb the structure of the

cytoplasmic membrane (Lin et al., 1992). Furthermore, the rapid release of the applied pressure can enhance the movement of these internal constituents to the outer environment (Lin et al., 1993).

As will be shown later on in this chapter, microbubbles have many fantastic characteristics such as a high surface area-to-volume ratio, slow rising velocity and high solubility in water, and they can be used to increase the solubility of CO₂. Recently, Ying (2013) used CO₂-enriched microbubbles to grow microalgae, and it was found that using 5% CO₂ can enhance the mass transfer coefficient of CO₂ (K_{La}) by 30-100% with different flow rates. Additionally, Al-Mashhadani (2013) has shown pH responses during bubbling CO₂ into water, where it was found that after 6 minutes the pH value dropped from 7 to 4.5 in a 8.3L reactor full of water. These two studies show the potential of using CO₂-enriched microbubbles in the inactivation process of *P.putida*.

The inactivated pretreatment slurry can be then fed to the fermenter in order to conduct the fermentation process. The bacterial fermentation in the current study is conducted using *Zymomonas mobilis* as a fermentative microbe and the metabolic features of *Zymomonas mobilis* is reviewed in the next section.

2.3 Characteristics of *Zymomonas mobilis* in acetaldehyde and ethanol production

2.3.1 Entner-Doudoroff (ED) pathway

Zymomonas mobilis has long been used in equatorial regions to produce various sorts of alcoholic beverages. It uses the Entner-Doudoroff (ED) pathway to metabolise sugars (mainly glucose) to produce ethanol. This pathway (Figure 2.5) produces one mole of ATP for each mole of glucose being metabolised (Seo et al., 2005). Microorganisms have developed various glucose-consuming pathways as a part of the metabolism diversity, such as the Entner-Doudoroff (ED), Embden-Meyerhof-Parnas (EMP) and phosphoketolase pathways. However, it has been argued that using any particular glucose metabolism pathway represents a bargain between the energy yield and the amount of proteins needed to catalyse the flux of the pathway (Flamholz et al., 2013). These glycolytic pathways are varied in the sequencing of their reactions and the amount of ATP produced from each mole of glucose being metabolised, which might range from 0 to 3 in many cases (Bar-Even et al., 2012). The typical scenario is the same in all these pathways, where glucose is phosphorylated and then dissected into two molecules of three-carbon atoms, pyruvate. These triplet molecules are eventually metabolised to produce ethanol.

Although it seems that the EMP pathway provides twice as much ATP as the ED pathway, the latter pathway has many advantages over using the classical EMP pathway. For example, microorganisms that are lacking the ED pathway cannot grow on the gluconate and ultimately cannot colonise many environments, such as a mammalian large intestine. Hence, the ED pathway represents an advantage for these microbes in such environments (Sweeney et al., 1996). In addition, the ED pathway has more exergonic reactions than the EMP pathway, and that makes it thermodynamically favourable (Flamholz et al., 2013; Noor et al., 2012).

Additionally, the EMP pathway has several more folds of enzymatic proteins than the ED pathway and many of them are thermodynamic bottlenecks, such as 6 biphosphate aldolase, while the ED pathway has several times fewer enzymes, and it avoids thermodynamic bottlenecks (which is thermodynamically unfavourable) by missing these reactions (Flamholz et al., 2013; Beard and Qian, 2007). The importance of the former feature is using very exergonic reactions (which is thermodynamically favourable), whereas the latter feature means that microorganisms avoid adverse effects of high enzymatic expressions, which could increase the misfolding probabilities of these enzymes (Drummond and Wilke, 2008) or the toxic activities of enzymes is being promiscuous (Eames and Kortemme, 2012). Moreover, these pathways differ in their requirements for cofactors such as NAD⁺ and NADP⁺ (Conway, 1992).

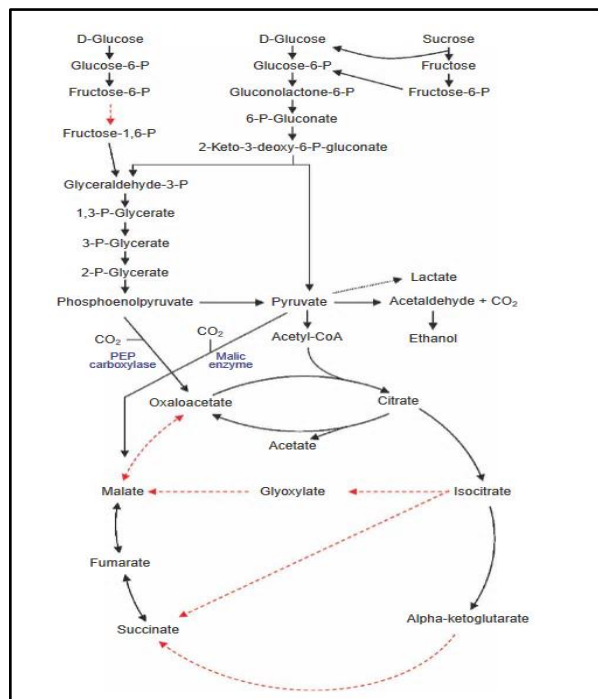


Figure 2.5: Entner-Doudoroff pathway combined with Krebs cycle, enzymes missing from *Z. mobilis* are represented by red dotted arrow (Adapted from Seo et al., 2005).

There are many advantages of using *Z. mobilis* in the fermentation processes. These include: i) large and specific uptake rates of glucose and ethanol production; ii) High ethanol productivity, which is close to theoretical productivity with relatively little amount of biomass formation; iii) Tolerance to high ethanol concentration, which may reach 16 % (v/v); and iv) Feasibility for genetic manipulation (Rogers et al., 1979). While the wild strain of *Z. mobilis* can use only a narrow range of sugars (such as glucose, fructose, and sucrose) as a sole carbon source, recombinant strains have been developed to utilise pentose sugars such as xylose and arabinose as well as hexoses sugars (Deanda et al., 1996).

Interestingly, *Z. mobilis* has a respiratory electron transport chain, and it shows an increased growth yield during the exponential phase of the aerobic growth. Concurrently, ethanol productivity decreases and other products start to be accumulated, which are reduced metabolites such as acetaldehyde and acetate (Seo et al., 2005). This chain competes with the alcohol dehydrogenase reaction, as both reactions use reducing equivalents NAD (P) H as a cofactor (Kalnenieks et al., 2000). Figure 2.6 shows the competition between respiratory electron transport chain and alcohol dehydrogenases.

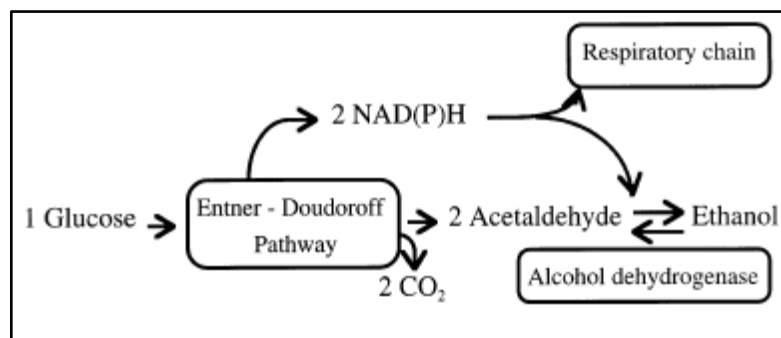


Figure 2.6: The competition between the respiratory electron transport chain and alcohol dehydrogenase on reducing equivalent NAD (P)H (Adapted from Kalnenieks et al., 2000).

While the respiratory chain consumption of NAD (P) H, limits the reduction of acetaldehyde to ethanol, the inhibition of the respiration chain leads to less acetaldehyde to be accumulated. The presence of the respiration chain in this bacterium leads to less NADH being available for the alcohol dehydrogenase reaction, which is responsible for converting acetaldehyde to ethanol and thus acetaldehyde accumulates. The accumulation of acetaldehyde might inhibit the bacterium growth.

2.3.2 Putative energy dissipation mechanisms and carbon dioxide accumulation

2.3.2.1 Putative energy dissipation mechanisms

There are many ATP-hydrolysing activities in *Zymomonas mobilis* such as acid and alkaline phosphatases, a periplasmic 5'-nucleotidase and ATPase. However, ATPase has the highest contribution of the hydrolysis of the intracellular pool of ATP (Kalnenieks, 2006). ATPase hydrolysis activity contributes to about 20% of the total intracellular ATP hydrolysis according to the calculation based on the proton-pumping ATPase activity in the membrane preparations (Reyes and Scopes, 1991; Zikmanis et al., 1999). The membrane F₀-F₁ ATPase enzyme is the most likely candidate for recycling the excess ATP in the *Zymomonas mobilis* (Lazdunshi and Belaich, 1972; Reyes and Scopes, 1991; Kalnenieks, 2006).

Other energy-consuming activities, such as kinase's and phosphatase's futile cycles, are less likely to be significantly involved in the energy-consuming reactions (Jones and Doelle, 1991). Lazdunshi and Belaich (1972) showed that ATPase enzyme exhibits two functions, which are a high-affinity system and a low-affinity system. While the high-affinity system is responsible for pumping the protons across the cytoplasmic membrane, the low-affinity system works as an ATPase only. Indeed, using a F₀-F₁ inhibitor such as dicyclohexylcarbodiimide (DCCD) supported the key role of membrane-ATPase in the cellular energy dissipation in *Zymomonas mobilis*. The increase in growth yield on glucose was achieved when 0.5mM DCCD used during

the growing of *Zymomonas* cells (Kalnenieks et al., 1987, cited in Kalnenieks, 2006). Russell and Strobel (1990) also reported the same effect of DCCD in *Streptococcus bovis*, when the F₀-F₁ ATPase was completely inhibited by this inhibitor. It should be noted that this enzyme plays a major role in the energy-spilling reaction under plenty of glucose (Cook and Russell, 1994). H⁺-ATPase, however, does not dissipate the energy itself but instead converts it to the form of transmembrane proton-motive force (ΔP) and thus the energy-dissipation problem is converted to an ΔP dissipation problem, which is a futile transmembrane proton cycle.

2.3.2.2 Carbon dioxide accumulation

Carbon dioxide is the second major end-product of *Zymomonas mobilis* catabolism. Several papers were published in the 1980s (e.g. Nipkow et al., 1985 and Veeramulla and Agrawal, 1986) on CO₂'s effect on the fermentative performance of *Zymomonas mobilis*. This bacterium is one of the most accelerated producers of CO₂ in the microbial world. Seemingly, the major portion of this gas leaves the *Zymomonas* cell by passive diffusion as a neutral gas molecule (Kalnenieks, 2006). Forster et al. (1988) found that the lipid bilayer of the cell membrane does not represent a serious diffusion barrier for CO₂ when erythrocytes were used as a model for CO₂ permeability. Concurrently, some of the generated CO₂ in the cytoplasm of bacterial cells might go through a hydration reaction catalysed by carbonic anhydrase. The produced carbonic acid is subsequently dissociated into a proton and bicarbonate anion (Merlin et al., 2003). Considering the equilibrium constants of the dissociation reactions (Merlin et al., 2003; Mills and Urey, 1940) and using 6.4 as an intracellular pH, it can be estimated that around 10% of CO₂ can be present as a bicarbonate anion in *Zymomonas mobilis* culture under equilibrium conditions (Kalnenieks, 2006).

Exporting these bicarbonate anions outside the cell represents an efficient Δp (transmembrane proton-motive force) dissipation pathway, equivalent to importing mechanism of protons; a unit negative charge might be translocated into the extracellular medium due to this pathway (Figure 2.7). This translocation would decrease the $\Delta\Psi$ (the transmembrane electric potential) by leaving a proton behind in the cytoplasm, and this eventually leads to a diminishing of the transmembrane pH gradient (Kalnenieks, 2006).

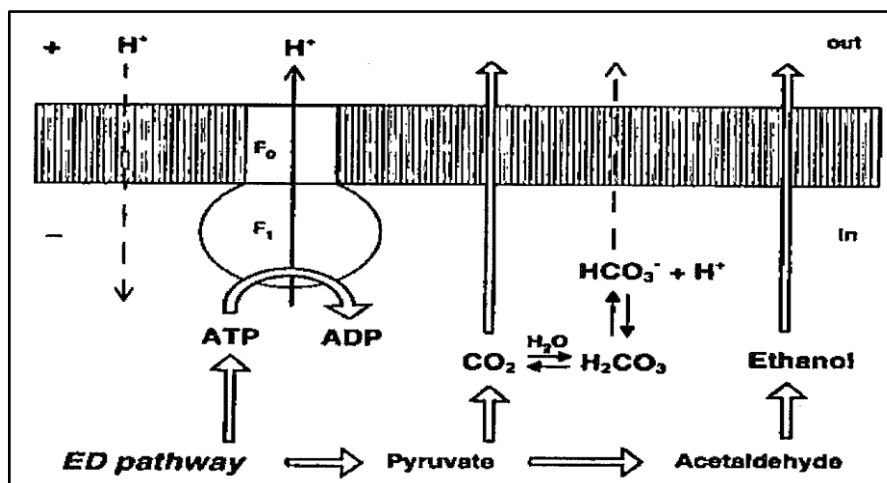


Figure 2.7: The putative energy-spilling pathways in *Zymomonas mobilis* (Adapted from Kalnenieks, 2006).

Kalnenieks (2006) speculated that these pathways can work in *Zymomonas mobilis* as long as some conditions are met. These conditions are:

1. A high intracellular concentrations of carbon dioxide;
2. Equilibrium between the intracellular pools of carbon dioxide and bicarbonate;
3. Enough membrane permeability of bicarbonate anions;
4. An alkaline transmembrane gradient of pH.

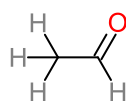
The first and the last conditions have been fulfilled (Kalnenieks, 2006), while the second and the third conditions need to be further explored.

Carbonic anhydrase is a crucial enzyme for an efficient conversion of the carbon dioxide to bicarbonate anions (Merlin et al., 2003). The gene of this enzyme had already been identified in the genome of *Zymomonas mobilis* by Seo et al. (2005). However, no evidence for carbonic anhydrase activity in *Zymomonas mobilis* has been published so far. The permeability of the lipid bilayer for charged species is substantially lower than the neutral molecules; therefore, a specific transport system must be acted upon the bicarbonate ions to generate a computable depolarising effect (Kalnenieks, 2006).

2.4 Acetaldehyde

Acetaldehyde is a colourless, clear liquid with an acrid and fruity smell. It is extremely flammable, and its vapour will explode if it is exposed to outside factors such as a flame or heat. This chemical has the molecular formula C_2H_4O (Eckert et al., 2012). Acetaldehyde is also

called ethanal, and it has a structural formula shown in Figure 2.8 and chemical and physical properties shown in Table 2.1.



Acetaldehyde molecule

Figure 2.8: Structural formula of acetaldehyde (Adapted from WHO, 1999).

Table 2.2.1: Chemical and Physical properties of acetaldehyde (Adapted from EPA, 1987).

Properties	Value
Molecular weight	44.06 g/mole
Melting point	-123.5°C (-190.3°F)
Boiling point	20.16°C (68.3°F)
Density at 18°C (64.4°F)	0.783 g/ml
Vapor pressure at 20°C (68°F)	0.97 atm.
Flash point (closed cup)	-38.0°C (-36.4°F)
Solubility in water at 25°C	infinite
Conversion at 25°C (77°F) and 760 mm Hg	1 ppm = 1.8 mg/m ³

Ethanal naturally exists in many food and beverages such as fruit, vegetables, dairy products and bread, but its concentrations vary. It was found that its concentration ranges between 0.2-230ppm, 0.2-400ppm, 0.001-76ppm and 4.2-9.9ppm in the above products, respectively (TNO, 1996; Cantox Health Science International, 2003, cited in Food Safety Commission, 2005). Acetaldehyde is miscible with water and some other solvents such as benzene, gasoline and acetone (Department of Health and Human Services, 2014).

Acetaldehyde has many industrial uses, and it has been suggested that the industrial production of acetaldehyde in large quantities is crucial to meet the industrial demands. For instance, acetaldehyde is used as an intermediate to produce products such as acetic acid, acetic anhydride, pyridine derivatives, plastic, butanol, dyes like aniline dye, and even synthetic rubber and pesticides (American Conference of Governmental Industrial Hygienists, 1991; United States National Library of Medicine, 1998, cited in WHO, 1999). In addition, acetaldehyde is produced naturally by many processes such as combustion and the photo-

oxidation of hydrocarbons, but it is emitted to the atmosphere. Because it is an intermediate in the metabolism of ethanol and sugars, it could be found in small quantities in the human blood and alcoholic beverages (Jira et al., 1985; Hagemeyer, 1991, cited in WHO, 1999). Additionally, ethanal is added to some types of food and beverages as a flavouring agent or an additive. For example, it is added to some baked foodstuffs, desserts and candy, and is utilised to add a flavour to the dairy products and fruit juices (WHO, 1999).

Acetaldehyde was previously produced from different microorganisms for industrial purposes. For example, Romano et al. (1994) produced this chemical from *S.cerevisiae* in a synthetic medium and grape must, and it was found that acetaldehyde concentrations ranged from a few mg/L to 60 mg/L at 30°C. It was concluded that its production is strain-dependent, and that there was no significant difference between those two media (Romano et al., 1994). Zhu (2011) studied the acetaldehyde production from *E.coli* K12 MG1655 after the genetic modification to produce a new strain (ZH88), and it was found that this bacterium could produce 4.91 ± 0.29 mM of acetaldehyde after cloning acetaldehyde dehydrogenase and acetyl-CoA reductase genes from *Salmonella enterica*.

Wecker and Zall (1987), however, used *Zymomonas mobilis* ZM4 to produce acetaldehyde, when *Zymomonas mobilis* was selected using 100mM of allyl alcohol to produce a mutant strain, which can produce an elevated concentration of acetaldehyde. The highest concentration of acetaldehyde produced was 92mM in an aerated flask as an accumulated concentration (Wecker and Zall, 1987). In addition, Ishikawa and Tanaka (1992) compared the acetaldehyde production from *Zymomonas mobilis* in plugged flasks with its production in aerated flasks after considering the volatilisation rate constant (K_v) and the initial oxygen transfer coefficient (K_{La}). The authors found that the aerated flasks had more potential to produce acetaldehyde in large quantities than plugged flasks, and it was observed that cell growth of *Zymomonas mobilis* was strongly inhibited by acetaldehyde, and that makes acetaldehyde production very difficult in plugged flasks (Ishikawa and Tanaka, 1992). The jar fermenter was developed to scale up the acetaldehyde production from the aerated flasks, and it was used to produce about 150mM of acetaldehyde (Ishikawa et al., 1990).

Growing *Zymomonas mobilis* under aerobic conditions has many physiological advantages over anaerobic conditions, including enhancing biomass growth and producing less reduced metabolites such as acetaldehyde. The produced acetaldehyde at the early stages of aerobic growth, however, provides a competitive growth strategy against other microorganisms, which

might exist in its environment (Kalnenieks et al., 2000). However, the production of inhibitory substances such as acetaldehyde can reduce the rapid growth of *Zymomonas*, and can also inhibit a wide range of microorganisms. This inhibitory effect for other bacteria was well-studied in conjugation experiments (Pappas et al., 1997). Initially, it was thought that the inhibition of other bacteria was due to colicin production from this bacterium (Dos Santos et al., 2004; De Souza et al., 2011). However, it has been found that this bacterium has two competitive strategies to inhibit the growth of other bacteria. The first strategy is in anaerobic conditions in which *Zymomonas* has very high ethanol-specific production rates, as well as a high ethanol tolerance exceeding that of many other microorganisms. The second strategy is to use aerobic conditions in which *Zymomonas* shows high respiration rates with self-inhibition as a result of acetaldehyde production (Kalnenieks et al., 2000).

2.5 Classification of Low-molecular-weight fermentation products

The fermentation products can be classified according to the relationship between product synthesis and energy generation in the cell (Doran, 2013).

2.5.1 Product formation directly coupled with the energy generation

In this class, products are formed directly as end or by-products of the energy generation and synthesised using ATP production pathways. The classical examples for this category are ethanol, acetic acid, acetone, acetaldehyde, and butanol. Growth is normally the principal energy requiring process of the microbial cells and thus; these products will be formed whenever there is growth within the fermentation process.

2.5.2 Product formation indirectly coupled with the energy generation

This class is partly associated with the energy generation, but it requires further energy for synthesis these products. Examples of this category are amino acids, nucleotides, and citric acid.

2.5.3 Product formation not coupled with the energy generation

Formation of these products involves reactions, which are far from the energy generation pathways. Examples of this group are antibiotics such as Penicillin, Streptomycin, and vitamins. In addition, the production of these metabolites is complicatedly related with the growth as the growth and product synthesis are dissociated (Doran, 2013).

2.6 Acetaldehyde as a precursor for fuels production

Interestingly, acetaldehyde can also use as a potential substrate for fuels production. Mainly, there are two different ways to use this compound in fuels production, which are the chemical

and the biological methods. These methods have been used to produce ethanol and butanol from this compound. For example, Eram and Ma (2013) used the biological method to produce ethanol, and it was mentioned that aldehydes generally and acetaldehyde specifically can be reduced to ethanol by alcohol dehydrogenases and these enzymes have been widely characterised from various mesophilic, thermophilic and hyperthermophilic microorganisms. Neale et al. (1986) had purified two alcohol dehydrogenase enzymes in *Zymomonas mobilis*, which are responsible for converting acetaldehyde to ethanol and vice versa. Therefore, it is fair to say that many microorganisms use acetaldehyde as a substrate to produce ethanol inside their biological systems. However, the structure of these enzymes and cofactors are varied between microorganisms.

Regarding the chemical methods, Dowson and Wass (2012) patented a novel method to convert ethanol to butanol using acetaldehyde as an intermediate. This method has two main stages. In the first stage, ethanol is dehydrogenated into acetaldehyde by a catalyst, which generates hydrogen as a by-product. The second stage includes a selective aldol condensation of two acetaldehyde molecules, which were generated in the first stage into one crotonaldehyde (but-2-enal) molecule. The latter molecule is hydrogenated by hydrogen created in the first stage to yield butanol as a final product. Using acetaldehyde as a substrate can lead to avoiding the first stage, which is the endergonic stage (non-spontaneous and thermodynamically unfavourable).

2.7 Recovery of final products from the fermentation broth by gas stripping

Many methods have been developed for *in situ* recovery of a product from the fermentation broth. These methods, such as adsorption, liquid-liquid extraction, pervaporation, and reverse osmosis, can remove products from the fermentation broths *in situ*, but they have common problems of intensive energy consumption and low efficiency in product recovery with high concentrations of products and some of them use membranes, which might be fouled and need regular replacement (Xue et al., 2013). To remove the accumulated products (mainly acetaldehyde and carbon dioxide) from the fermentation broth, various separations processes can be used; however, the attention in the current study is drawn towards the gas stripping technique using microbubbles.

Gas stripping is a promising alternative technique and is used in the current study. It involves sparging a gas through a bioreactor by using a sparger or perforated plates. Sparged gas can generate bubbles with different sizes, which rise and break to cause the removal of volatiles from the culture medium to the headspace. Alternatively, it can be defined as a physical

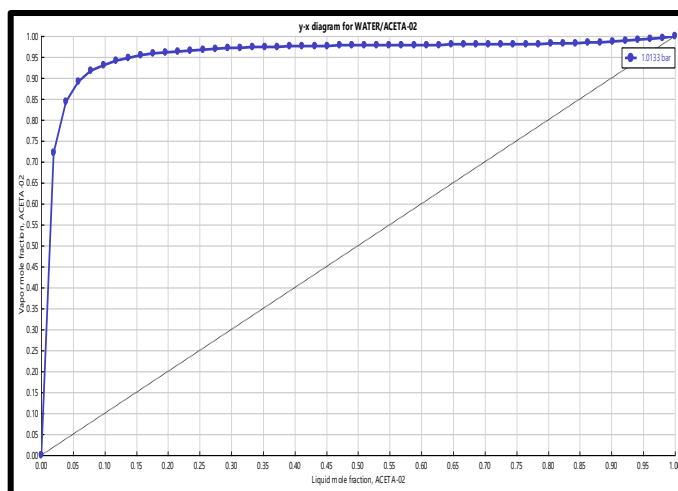
separation process, whereby one or more ingredients could be evacuated from the liquid phase to the gas phase (Yamane et al., 2013). Interestingly, there are many advantages of using this technique to remove a fermentation product as it is an easy technique, does not need an expensive instrument, and does not harm microorganisms within the bioreactor. In gas stripping, there are many gasses that can be used depending on the purpose of the process. This process does not discharge culture nutrients and other reactions intermediates (Qureshi and Blaschek, 2001; Inokuma et al., 2010).

While using gas stripping can reduce the final product inhibition due to the product accumulation, it allows the use of concentrated sugar solutions in the bioreactor, which can cause microbial inhibition under normal fermentation processes (Ezeji et al., 2005). This technique has been used to remove some fermentation products such as isopropanol and butanol, which cause a reduction in production yields and inhibition of the microbial growth. However, most studies have focused on using gas stripping to remove butanol from the culture medium, and they used a sparger or perforated plates to produce coarse bubbles, which are less efficient than microbubble in gas stripping (Zimmerman et al., 2013).

2.8 Acetaldehyde separation instead of ethanol distillation

Pure acetaldehyde has a boiling point of around 20.8°C, while ethanol boils at 78.5°C (Doran, 2013). At temperatures for mesophilic fermentations (~30°C), acetaldehyde is more readily stripped out from the fermentation culture than ethanol. Figure 2.9(A and B) shows the vapour-liquid equilibrium data for both acetaldehyde in water and ethanol in water at 30°C (D'Avila and Silva, 1970). It can be seen from this figure that at 30°C a mole fraction of 0.025 (5.8 %) of acetaldehyde was in the liquid solution, while there was a mole fraction of approximately 0.70 (85 %) in the vapour phase. This can be compared favourably with ethanol, where a mole fraction of 0.025 (6.2 %) of ethanol exists in the liquid phase, while a mole fraction of about 0.22 (42 %) ethanol exists in the vapour phase. In addition to the advantage of being more volatile than ethanol, acetaldehyde does not form an azeotrope with water (Wecker, 1987).

(A)



(B)

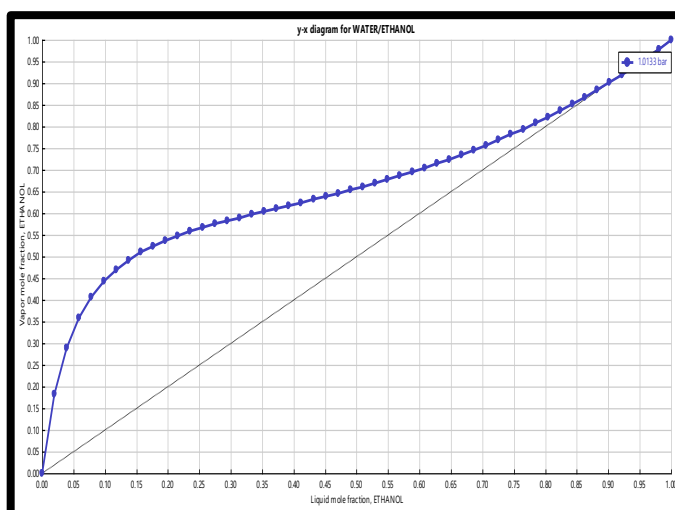


Figure 2.9: A comparison of the vapor pressure curves of acetaldehyde in water and ethanol in water at 30°C (Adapted from d'Avila and Silva, 1970, but redrawn using Aspen Plus software V8.4).

On the other hand, the cost analysis of ethanol production shows that the major energy cost of ethanol production by biological methods is the separation and purification of the ethanol from the fermentation medium (Wecker, 1987). Indeed, it was estimated that ethanol distillation accounts for 63% of the total energy cost of ethanol production, which includes feedstock receiving, sterilisation, mixing and processing of feeds, fermentation, distillation, by-product recovery, and general plant management (Kalter, 1981). This estimation was based on a continuous-processing ethanol-producing plant that produced 27.5 million gallons of ethanol

per year, where both corn and cheese whey were used as feedstock, and ethanol concentration was around 4.5% previous distillation. Katzen (1978) had assessed the ethanol production from corn economically, and the distillation process accounted for 8.8% of the total operating cost for a plant producing 50 million gallons of ethanol per year. These two studies used full stream stripping and vacuum distillation. Typically, the cost of distillation depends on the energy source used and the location. For example, in Brazil, sugar cane bagasse is used at only the cost of collecting it from nearby plantations, and generally, it is a waste with only limited alternative utility. The distillation cost per litre of ethanol decreases with the increase of ethanol concentration in the broth, but increases the product concentration result in the product inhibition and extends the fermentation times (Hacking, 1986).

In contrast, using some continuous separation techniques can decrease the production cost of fermentation products. These techniques, such as solvent extraction, selective membranes and flash vapourisation, treat the recycling stream from the fermenter and selectively remove the products from the fermentation stream, and allow the use of higher sugar concentrations without inhibiting the microbial culture by accumulating the final products. Also, using high sugar concentrations means mitigating the operational costs of the plant, centrifugation and feed sterilisation (Maiorella et al., 1984). As product separation costs are lowered, waste recovery system will, in turn, become more economically feasible.

A design project study was done in 2015 at the University of Sheffield under the supervision of Professor William Zimmerman and in cooperative with Vivergo Fuels Ltd, suggested that the incorporation of hot-microbubble technology into the fermentation process to produce ethanol has the potential to make the fermentation process 80% more productive. Also, this technology can increase the produced ethanol by about 70%.

2.9 Microbubble technology

A microbubble is a very fine bubble with a diameter of microns but below one millimetre. These bubbles have certain properties that make them attractive to use for various applications (Takahashi, 2005).

2.9.1 Properties of microbubbles

Microbubbles have a high surface area-to-volume ratio with high internal pressure, as the internal pressure increases inversely proportionately to its radius (Zimmerman et al., 2009). All interfacial transport phenomena such as heat, mass, and momentum transfers rely on the surface

area-to-volume ratio. As a spheroidal object, this ratio increases inversely proportionately to its radius (Figure 2.10):

$$\frac{s}{v} = \frac{4\pi r^2}{\left(\frac{4}{3}\right)\pi r^3} = \frac{3}{r} \quad (\text{Eq. 2.2})$$

Where s is the interface area, v is the volume, and r is the radius of the bubble.

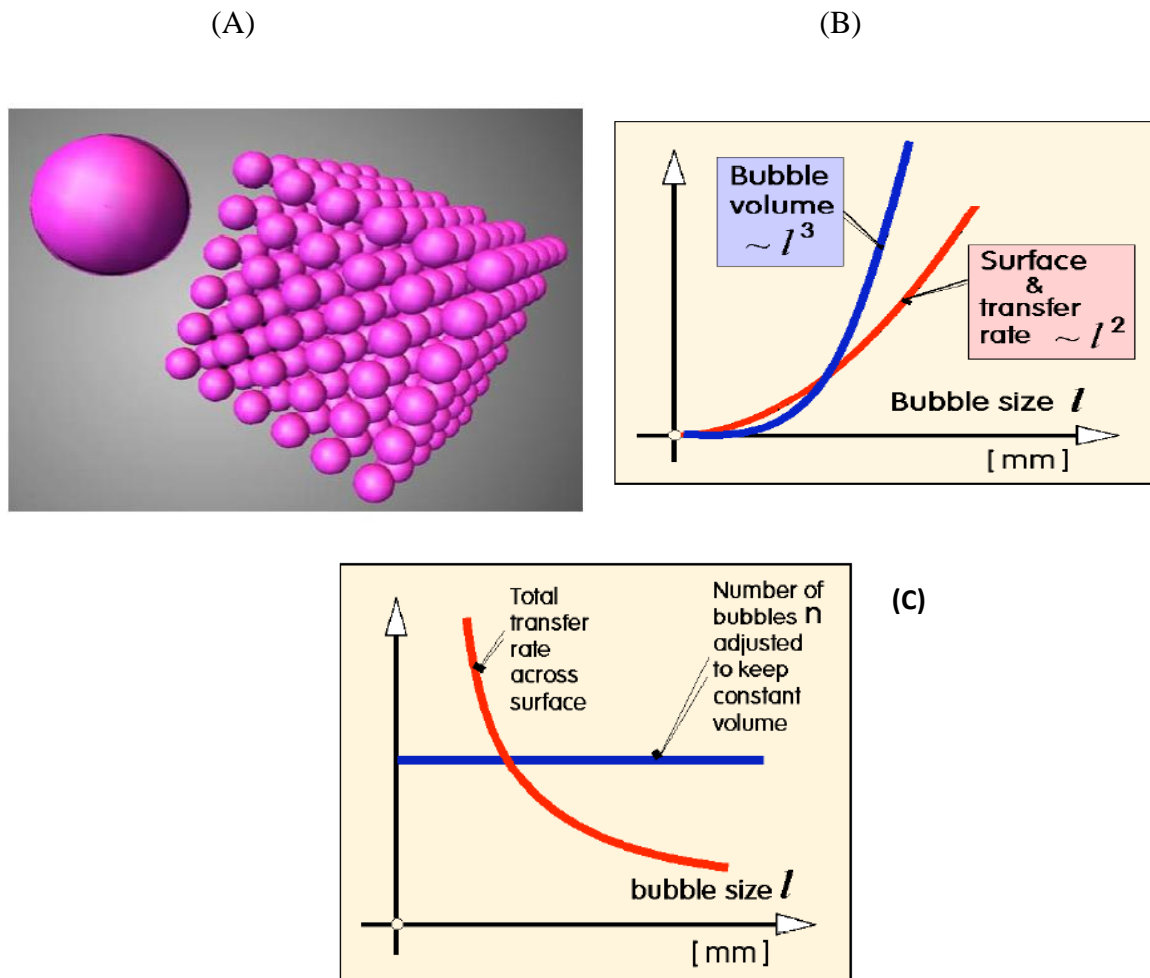


Figure 2.10: Benefits of microbubble technology. A) Benefit of dividing a volume ratio into smaller volumes produces additional surface area. (B)(C) Relationship between surface area and transfer rate with bubble size is a square of bubble size and cubic with its volume.

In addition, the residence time of a microbubble in a viscous liquid can be anticipated via using Stokes' law for rising velocity:

$$U_{\text{stokes}} = \frac{2}{9} \frac{g \Delta \rho d^2}{\mu l} \quad (\text{Eq. 2.3})$$

Where U is the rising velocity, g is the gravitational acceleration, Δp is the liquid height and μl is the liquid viscosity.

According to Stokes' law, it is clear that the residence time of a microbubble is remarkably longer than a fine bubble for the same height of liquid (Figure 2.11).

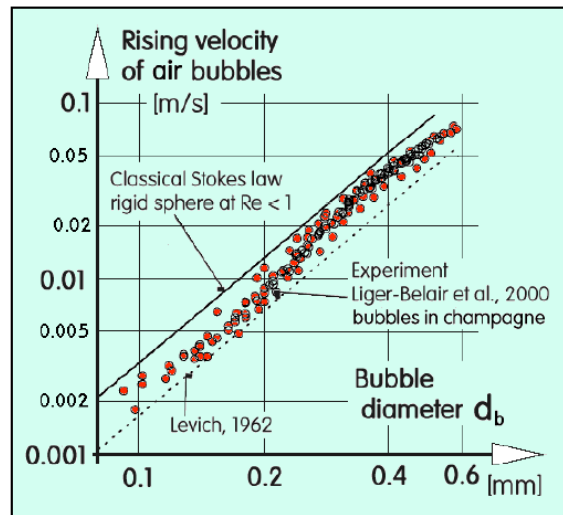


Figure 2.11: The rise velocity of microbubble (Adapted from Levich, 1962 cited in Zimmerman et al., 2008).

Using microbubbles allows a high gas dissolve rate because the surface area and internal pressure in these bubbles increase with the decrease of the radius. Also, the smaller bubble rises slower than the larger bubble. The latter feature allows an increased amount of gas to be exchanged between the microbubble and the surrounding area (Zimmerman et al., 2009). In addition, the inside of a microbubble is uniformly mixed at a much earlier residence time than for a fine or coarse bubble, and the time to achieve this mixing is sufficiently fast to enable the microbubble to reach equilibrium after a very short residence time (in the order of 10^{-3} s) with a diameter of $100\mu\text{m}$ (Zimmerman et al., 2013). Figure 2.12 shows the internal mixing within a microbubble with a diameter of $100\mu\text{m}$.

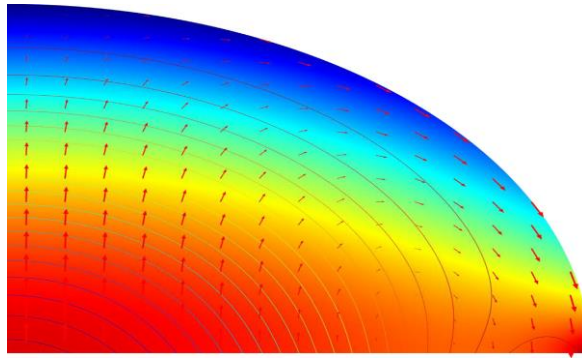
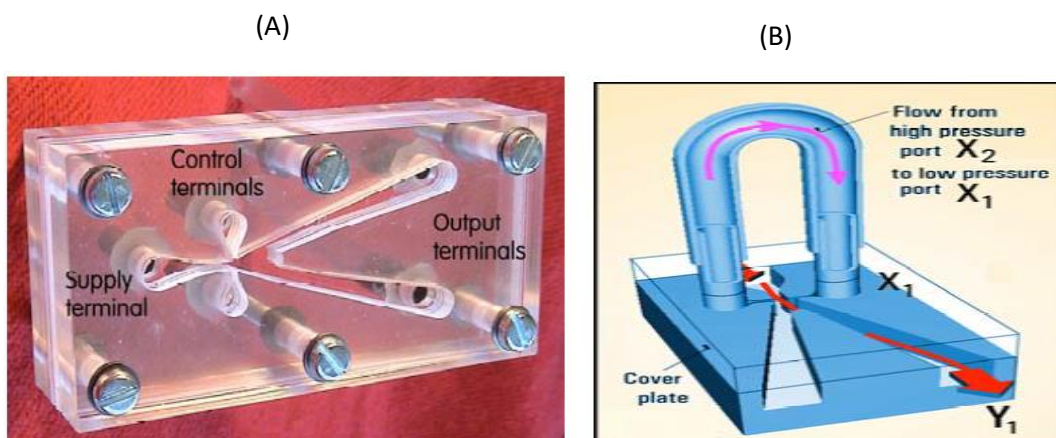


Figure 2.12: Microbubble profile after $t=0.0001.5$ s with radius $R=100$ μm . The arrows are the induced, steady state velocity field from bubble rising, imposed as the velocity field. The contours are concentration curves, with 20 contours rising from 0.002(inner) to 0.0032(outer) molar concentration (Adapted from Zimmerman et al., 2013).

A fluidic oscillator was used in this study to generate microbubbles. Tesař and Zimmerman had invented in 2006 the fluidic oscillator as a novel method to generate microbubble. The fluidic oscillator was used in this study to generate microbubbles. In this method, air is oscillated by switching to one of the two output channels based on the Coanda effect and by providing it with a feedback loop. The generation of microbubbles by fluidic oscillator has many advantages, such as formation well-spaced and uniform clouds of microbubbles (Tesař et al., 2006). Additionally, microbubbles from fluidic oscillator can achieve up to 8-fold oxygen transfer coefficient rate than without it (Hu, 2006, cited in Zimmerman et al., 2009). In addition, this method can achieve high hold-ups, which is resulted from slow rising time and low coalescence rate, with low energy consumption and dissipation (Varma, 2007, cited in Zimmerman et al., 2009). Figure 2.13 shows the design of fluidic oscillator with its main parts.



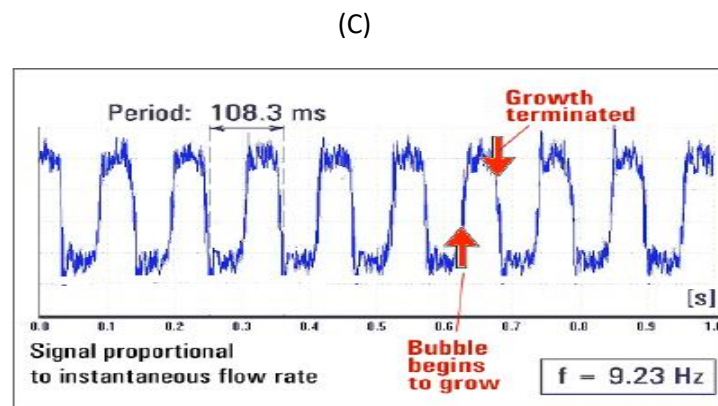


Figure 2.13: The fluidic oscillator. A) Stack of laser cut Perspex plate with its amplifier. B) Feedback loop connects to two control terminals to generate oscillation. C) History of flow rate for fluidic oscillator connected to a nozzle bank with 600 μm pore size. The oscillation frequency is ranged from 1-100 Hz, which is depending on the length of feedback loop (Adapted from Zimmerman et al., 2008).

2.10 Thin film theory of mass transfer

Bailey and Ollis (1986) comprehensively described gas-liquid thin film theory. It has been found that mass transfer rate is proportional to driving force, which is the difference in concentrations at the interface and interfacial area. The mass transfer flux can be calculated from following the mathematical relationship:

$$N_A = K_{La} (C_L - C_G) \quad (\text{Eq. 2.4})$$

Where N_A is mass transfer flux, and K_{La} is mass transfer coefficient. C_L is the concentration of dissolved gas in the bulk liquid phase, and C_G is the concentration that is in equilibrium with initial bubble gas concentration. The latter concentration is sometimes called the equilibrium concentration. The mass transfer flux is shown in Figure 2.14.

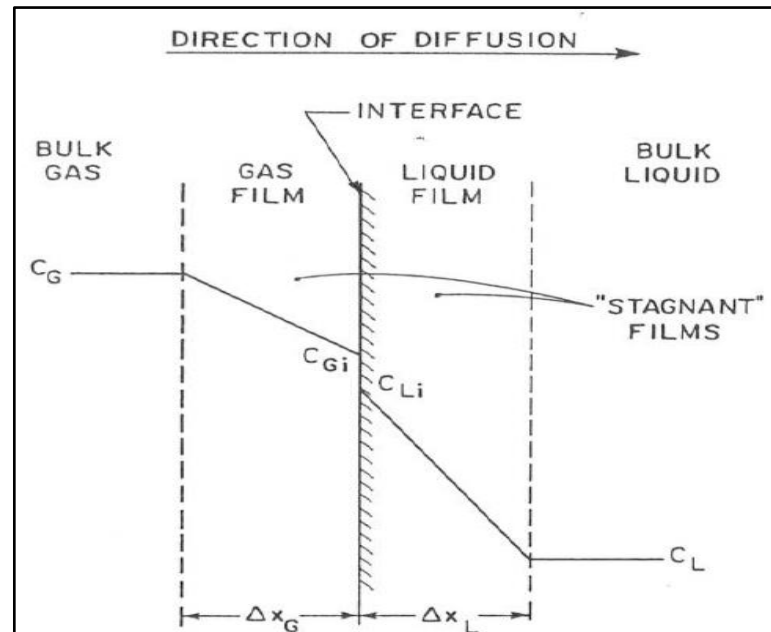


Figure 2.14: Interfacial dynamics of mass transfer for gas exchange (Adapted from Moo-Young and Blanch, 1981).

Moo-Young and Blanch (1981) described the potential constraints of oxygen transfer to the culture medium and then to microbial cells. It was reported that there are eight resistances to the oxygen transfer, which are:

1. In a gas film inside the bubble
2. At the gas-liquid interface
3. In a liquid film at gas-liquid interface
4. In the bulk liquid
5. In a liquid film surrounding cell
6. At the cell-liquid interface
7. At the internal cell resistance
8. At the sites of biochemical reactions.

However, not all of the above resistances are significant, and some of these resistances are insignificant and can be ignored. For example, the resistance of liquid film that surrounds singled cells and dispersed mycelia can be ignored because the difference in density between microbial cells and suspended liquid is quite small, meaning that there is a stagnant liquid film surrounding microbial cells. The above eight resistances are shown in Figure 2.15.

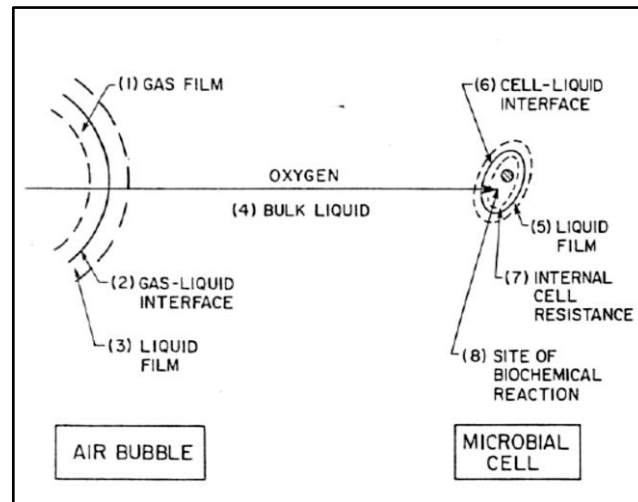


Figure 2.15: General oxygen transport path to microorganisms (Adapted from Moo-Young and Blanch, 1981).

In this study, an airlift loop bioreactor (the fermenter) is connected to a fluidic oscillator to produce microbubbles, where a grooved nozzle bank distribution system is a substitute for the traditional base. In the following section, the fundamentals of airlift loop bioreactors are considered.

2.11 Airlift loop bioreactors (ALB)

Williams (2002) defines a bioreactor as a system in which biological conversion occurs. It has been reported that the biological conversion can be achieved by whole cells such as microbial, animal and plant cells or by enzymes or other biological metabolites (Williams, 2002). An airlift loop bioreactor (ALB) is pneumatically agitated system device, which has been characterised by fluid circulation in a particular pattern through canals built mainly to achieve this purpose (Merchuk and Siegel, 1988). One of several mixing procedures can be used is the closed stirred tank, which can achieve a better performance in degradation processes compared with the ALB. However, when the energy requirements of the process are weighed against the yielded energy from produced biofuel, the process becomes economically unfavourable. Therefore, reduction of consumed energy for mixing purposes with in situ stripping off the fermentation products represents a major challenge to the development of biological processes (Al mashhadani, 2013). This reactor consists of an ALB base, internal draught tube, riser, downcomer and gas separator (Fatemeh et al., 2012). The properties of these parts are described below:

2.11.1 ALB base

Several studies have involved the ALB base area, the most promising of which was contributed by Merchuk and Gluz (1999), which showed that the base of an ALB has only a minor effect

on ALB performance (Merchuk and Gluz, 1999, cited in Zimmerman et al., 2009). In the current study, the ALB is connected to a fluidic oscillator to produce microbubbles, where a grooved nozzle bank distribution system substituted the traditional base in ALB. It should be noted that there must be a sufficient clear space between ALB base and draught tube, which allows moving liquid from the downcomer area to the riser area without considerable friction losses.

2.11.2 ALB riser

The riser is the phase transfer part of the airlift loop bioreactor, where mass transfer between gas-liquid and liquid-microbial cells is the most predominant feature (Zimmerman et al., 2009). In addition, this area has greater gas hold-up than downcomer region. The high gas hold-up, which is the result of the bubbly flow, is responsible for the difference in densities of liquid in both regions, causing liquid circulation in this reactor (Chisti et al., 1995). Using microbubbles can increase the mass transfer flux in comparison with traditional distribution methods. Accordingly, using microbubbles with an airlift loop bioreactor will increase mass transfer within the bioreactor. If nutrients are introduced as a gas phase, such as oxygen for aerobic cultivation, then a higher mass transfer rate might lead to enhance the growth of the microbial culture (Terasaka et al., 2011).

2.11.3 ALB downcomer

The downcomer region of airlift bioreactor has less gas hold-up than the riser, and this difference between two regions is the driving force for liquid circulation and mixing activity inside this reactor (Xu and Yu, 2008). This region has been described as a less dynamic region in the airlift bioreactor, and its composition depends mainly on the riser region with a large bulk of liquid in this region with less gas-hold-up (Zimmerman et al., 2009).

2.11.4 Gas separator

This region is at the top of the ALB, and connects the riser and the downcomer. It allows recirculation of liquid and disentangling of gas between those sections (Merchuk and Siegel, 1988). The gas separator is the most sensitive area of the ALB and the occupation time of liquid in this area depends primarily on the design of bioreactor and operation conditions, which determine gas hold-up in both the riser and the downcomer (Zimmerman et al., 2009). Merchuk and Siegel (1988) described that when the gas separator is more effective in disengaging the gas phase, there are fewer bubbles recirculating into the downcomer, which eventually leads to increased liquid velocity because of the difference in liquid densities between the riser and the downcomer.

2.11.5 Draught tube

Draught tubes are used in different kinds of bioreactors, which have been utilised to achieve the industrial production of enzymes, biomass and antibiotics. This tube is used to improve circulation of reactor components, and thereby enhance the performance of processes (Rayi and Ananthula, 2014). In Addition, Tekić, et al. (2014) reported many advantages of using a draught tube in airlift bioreactors, such as reducing turbulence inside the reactor and providing a clear circulation pattern for the liquid inside ALBs. The draught tube increases mixing time in the ALB in comparison to conventional bioreactors (Tekić et al., 2014). Additionally, Yakubu-Gumery (2010) reported that the draught tube has an effect on mixing time and hydrodynamics, which includes liquid circulation, the velocity with gas hold-up, and shear rate with different geometries. Figure 2.16 shows the general geometry of the airlift loop bioreactor used in the current study.

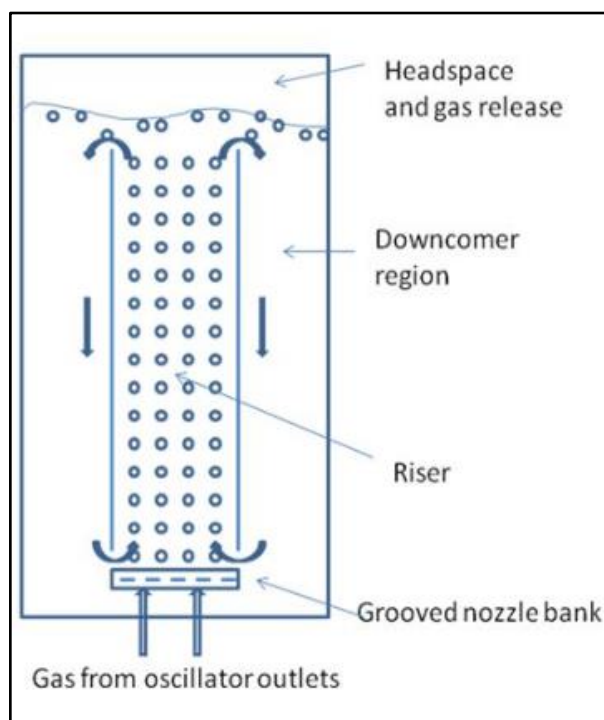


Figure 2.16: Diagram of airlift bioreactor with draught tube supplied from the outlets of fluidic oscillator, the microbubbles are rising in the riser region and dissociated at the gas separator, thereafter the liquid is circulated in the downcomer region (Adapted from Zimmerman et al., 2009).

2.12 Effects of the chemical activity on acetaldehyde and CO₂ production

Gibbs free energy (G) has been used to describe the spontaneity of a process. Gibbs free energy or free energy can be defined as the part of the total energy of a system that is available to do useful work (Devlin, 2002). This energy can be described by the following equation:

$$\Delta G = \Delta H - T \Delta S \quad (\text{Eq. 2.5})$$

Where ΔG is the changing in Gibbs free energy, ΔH is the changing in enthalpy or heat content, T is the absolute temperature and ΔS is the change in entropy.

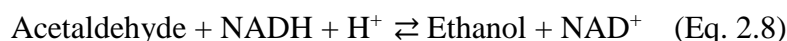
Typically, biological systems tend to work toward a status with a maximum entropy because a system cannot reach equilibrium with its surroundings without this kind of randomness or disorder. The sign and value of ΔG do not refer to the speed of reaction, but to the direction of the reaction. On the other hand, the equilibrium constant of this reaction is related to the change in free energy for that reaction, and it can be described as follows:

$$K_{eq} = [\text{products}]/[\text{reactants}] \quad (\text{Eq. 2.6})$$

It is suggested that living systems (such as microbial and animal cells) do not work under the standard conditions when pH equals 0 and concentrations of products and reactants is at 1M. It has therefore been proposed that the change in free energy at any concentration of substrates and reactants can be calculated by the following equation:

$$\Delta G = \Delta G^\circ + RT \ln [\text{products}]/[\text{reactants}] \quad (\text{Eq. 2.7})$$

Burton (1974) measured the equilibrium constant of ethanol oxidation reaction. He found that it is as low as $6.92 \times 10^{-12} \text{M}$, whereby ΔG° is equal to 63.7 KJ/mol (15.23 Kcal/mol) at 25°C. Ethanol oxidation reaction can be shown as follows:



Accordingly, the change in free energy of this reaction at the equilibrium can be calculated as follows:

$$\Delta G = 63.7 + 0.0083 * 298 * \ln (6.92 * 10^{-12})$$

$$\Delta G = 63.7 + 63.7$$

$$\Delta G = 0 \text{ KJ mol}^{-1}$$

The above reaction happens spontaneously when the products (acetaldehyde) are removed, and is shown to be thermodynamically favourable as the final ΔG would have a negative sign.

Gary (2004) mathematically described the relationship between Gibbs free energy and vapour pressure of reactants and products. This relationship is described as follows:



$$\Delta G = \Delta G^\circ + RT \ln \frac{[pC]^c \times [pD]^d}{[pA]^a \times [pB]^b} \quad (\text{Eq. 2.10})$$

Where:

- ΔG is the Gibbs free energy change
- ΔG° is the standard Gibbs free energy
- R is the universal gas constant
- T is the temperature of reaction
- pA, pB, pC and pD are partial pressures of reactants and products respectively
- a,b,c and d are the coefficients in the balanced chemical equation.

Clearly, low partial pressure of products contributes to Gibbs free energy change with a negative sign ($-\Delta G$), whereas the high partial pressure of products contributes to Gibbs free energy change with a positive sign ($+\Delta G$). $-\Delta G$ means that the bioreaction is spontaneous, and it is thermodynamically favourable and it is called exergonic reaction. $+\Delta G$, however, means that the bioreaction is unspontaneous and thermodynamically unfavourable, which is called an endergonic reaction (Gary, 2004).

Unspontaneous reactions can be dealt by two approaches. One approach includes adding enough energy to convert endergonic reactions to exergonic reactions, which are spontaneous reactions. The other approach is to reduce the partial pressure of products, which eventually leads to converting unspontaneous reactions to spontaneous ones. The mathematical relationship between Gibbs free energy and partial pressure has been intensively examined in widespread applications. However, most data have come from biological processes, in particularly the production process of bio-hydrogen (Almashhadani, 2013).

The simultaneous production and separation of acetaldehyde in an airlift loop bioreactor using microbubble technology, however, is a novel strategy used to grow *Zymomonas mobilis*. It promises to achieve a high acetaldehyde productivity by increasing the oxygen transfer coefficient and removing the produced acetaldehyde. In addition, the produced carbon dioxide can be removed by microbubble technology, and this might drive the reaction further towards becoming exergonic according to Le Chatelier's principle.

Chapter 3

Materials and Methods

3.1 Introduction

This project aims to develop a fluidic oscillator-powered microbubble generating system that can use lignocellulosic biomass as a substrate for the fermentation process with *in situ* separation after inactivation the pretreatment slurry with carbon dioxide enriched microbubbles. Also, it aims to develop a propagation unit that can be used to intensify the bacterial growth. All these processes are mass transfer limited processes and using microbubbles enhances the overall efficiency. In this chapter, details of the materials and methods used are presented and described. The size of microbubbles is considered in all processes. This chapter is divided into four main parts. The first presents the equipment and methods employed in the pretreatment of lignocellulosic biomass using both microbubble-microbe synergetic approach and ozonolysis-microbe synergetic approach. In the second part, the materials and methods used in inactivation of *Pseudomonas* culture and in assessing the performance after adding additives such as (ethanol and acetic acid) are outlined. In the third part, the materials and methods used in the fermentation process of *Zymomonas mobilis* both the wild type and the mutant type under aerobic and anaerobic conditions are described in detail. The fourth part presents the materials and methods used in the bacterial propagation.

3.2 Pretreatment of lignocellulosic biomass

3.2.1 Microbubble-microbe synergetic approach

3.2.1.1 Biomass and growth media preparation

All the chemicals and reagents used in the current project were bought with ~ 98-99.9% purity from Sigma-Aldrich, UK unless different supplier has been mentioned and of them used in the media preparations were suitable for microbiological cultures.

This study used wheat straw as a lignocellulosic biomass owing to its high cellulose and hemicellulose content, 29-35% and 26-32% respectively, with low lignin percent (16-21%) (McKendry, 2002) and availability.

Wheat straw was prepared for pretreatment by mechanically reducing biomass particle size to ≤ 1 mm using pestle and mortar and then sieved (Sigma-Aldrich, UK). The biomass was then washed using distilled water and oven-dried at 80°C for 24 hrs. Wheat straw solution (1% w/v) was prepared with distilled water, and the pH was set at 3, using concentrated HCl (Sigma-Aldrich, UK). The growth medium with a composition of: 1 % wheat straw, 0.5 % yeast extract,

0.02% magnesium sulphate and 0.02% ammonium phosphate dibasic was prepared according to Abdul-Kadhim and Jarallah, (2013). The medium was sterilized by autoclaving at 121°C for 15 minutes and 1 bar pressure before cultivating with 10 % (v/v) of 18 hr grown *Pseudomonas putida* KT2440.

3.2.1.2 Experimental Procedures

The experimentation was divided into four (4) groups to study the effects of each pretreatment. The first group was a control group consisting with biomass in liquid at pH 3. The second group was pretreatment with microbubbles. In this case, wheat straw was treated for more than 3 hrs at pH 3, by sparging with fluidic oscillator generated microbubbles. The time of pretreatment, 3.30 hrs, was selected after preliminary studies had revealed no additional glucose was produced after 4 hours. The third group was the combined pretreatment in which wheat straw was pre-treated with microbubbles for 3.30 hours and then, the pre-treatment continued with the application of *Pseudomonas putida* for an additional four (4) days. Conversely, the fourth group entailed pretreatment with only *Pseudomonas putida*.

After pH adjustment of the wheat straw solution to 3, this solution was introduced into the pretreatment column, which was connected to the fluidic oscillator (Zimmerman et al., 2008). Figure 3.1 shows the experimental rig, which consists of a fluidic oscillator, a micro-porous diffuser, and a pretreatment column. On the other hand, the biological pretreatment was achieved using *Pseudomonas putida* KT2440 in a 500 ml Erlenmeyer flask at 30°C. All experiments were conducted at room temperature (~25 °C), and untreated biomass was used as a control group to compare with other treated biomass. Samples were assayed daily by centrifuging for 15 minutes at 13000 xg and then filtered with a syringe filter unit (Whatman® Anotop® 25 Plus syringe filter, pore size 0.2 µm, Sigma- Aldrich) to measure glucose concentration using glucose assay kit (Sigma-Aldrich).

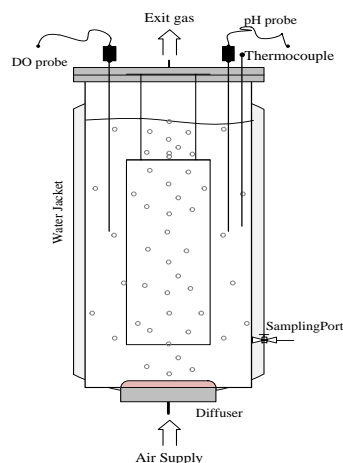


Figure 3.1: Schematic representation of the experimental set-up. Compressed air (1 bar) at 100 ml/min flow rate is fed into the oscillator, and there are two outputs from the fluidic oscillator. While, one feeds the microbubbles diffuser, the other is bleed-off. The overall volume is 1.5 L and the working volume of the pretreatment column is 1 L.

It should be mentioned that after biological pretreatment, samples were washed with normal saline for several times to remove bacterial cells, and then they dried in an oven at 80°C for 24 hrs before examining with SEM and FTIR-ATR.

3.2.1.3 Testing the cellulolytic activity of *Pseudomonas putida*

Pseudomonas putida is grown on M9 medium to test its ability to use Carboxymethyl cellulose (CMC) as a sole carbon and energy source. After growing on this medium, the bacterium then moved to Wheat straw medium (WS medium) to detect its ability to hydrolysis and use wheat straw as a carbon source. Moving the bacterium from WS medium to lignin medium (L medium) is to detect its ability to use lignin as a complex carbon source.

Bacteria growing on different media were monitored using optical densities at 600 nm using spectrophotometer (DTSTM-1700, 1900 NIR) for all other culture media on an hourly basis (Douka et al., 1999).

A. Qualitative measurement of cellulolytic activity

Cellulolytic activity of *Pseudomonas putida* was measured on both CMC and WS agar media and Lugol solution was used to cover the agar media, and it left for 10-15 minutes (Abdul-kadhim and Jarallah, 2013). After that, pictures were taken to the hydrolysis zones (clear zones), and measured using ImageJ software (V1.48), and the results were recorded.

B. Quantitative measurement of cellulolytic activity

1. Determination of protein concentrations

Bradford protein assay was used to measure protein concentrations within both CMC and WS media, and these concentrations can give valuable information about secreted enzymes. This assay was used according to the protocol provided by instruction manual of Bio-Rad Laboratories, Inc. In this test, 20 µl of samples were mixed with 1 ml of Bradford quick start reagent, which has a Coomassie Brilliant Blue G 250 dye. This dye binds to proteins and forms a stable protonated blue complex, which its absorbance and quantity can be measured at 595 nm. The protein concentration can be calculated using the following equation:

$$\text{Protein concentration (mg/ ml)} = \frac{OD\ 595nm \times 15}{\text{Volume of protein sample } (\mu\text{l})} \quad (\text{Eq. 3.1})$$

2. Enzymes activities

Endoglucanase activity (Carboxymethyl cellulase activity, CMCCase) was measured according to Ghose, (1987). Concentrations of reducing sugar (glucose) were measured using glucose assay kit (Sigma-Aldrich, UK). One enzyme unit is defined as the amount of enzyme required to release 1 µmol of reducing sugar per min during the incubation time. 0.1 ml of enzyme solution was added to 0.9 ml of substrate (CMC 0.5 %) in 50 mM citrate buffer pH 4.8, and this mixture was incubated for 30 minutes at 50°C. The amount of reducing sugar was calculated after finishing the incubation time.

Filter paper assay was used to measure Exocellobiohydrolase (FPase) activity of *Pseudomonas putida* according to Gilna and Khaleel, (2011). The concentrations of reducing sugar were also measured using glucose assay kit (Sigma-Aldrich, UK). One enzyme unit is defined as the amount of enzymes required to release 1 µmol of glucose per min during the incubation time. 50 mg of filter paper (Whatman, NO.1) were mixed with 1 ml of each enzyme solution and 1 ml of 50 mM citrate buffer pH 4.8, and this mixture was incubated for 2 hours at 50°C. After finishing the incubation time, the amount of released glucose was calculated.

β- glucosidase activity of *Pseudomonas putida* was measured according to Dashtban et al., (2010). The concentrations of released sugar were measured using glucose assay kit (Sigma-Aldrich, UK). One enzymes unit is defined as the amount of enzyme required to release 1 µmol of glucose per min during the incubation time. 0.9 ml of (5mM) of cellobiose was incubated with 0.1 ml of enzyme solution for 10 minutes at 50°C . After 10 minutes, the concentration of glucose was calculated.

It is worth noting that enzyme solution was prepared by centrifuging culture media for 15 minutes at 13000 xg with a refrigerated centrifuge (Thermo Scientific, Multifuge 1S-R), and then filtrated it with syringe filtrated unit (Whatman® Anotop® 25 Plus syringe filter, pore size 0.2 µm, Sigma- Aldrich, UK).

3. SDS-PAGE

Sodium dodecyl sulfate (SDS) - Polyacrylamide gel electrophoresis (PAGE) preparations were performed using SDS-PAGE TM Novex 4-12% Bis-Tris Gel System with 17 slots (Invitrogen, Carlsbad CA) according to the company's instructions. Protein samples were concentrated to reach approximately 1 mg/ml using Amicon Ultra centrifugal filter 10,000 NMWL, 5 ml (Merck Millipore, UK). 10 – 20 µl of each sample were taken and loaded on a native gel in each well. These samples were mixed with 4X SDS-PAGE TM loading buffer (Invitrogen, Carlsbad CA) at a volume ratio 3:1. While, anode buffer was formed by diluting 20X SDS-PAGE TM running buffer (Invitrogen, Carlsbad CA), the cathode buffer was made by mixing running buffer with cathode additive (Coomassie Blue G-250 dye, Invitrogen, Carlsbad CA). It is worth mentioning that all these steps were achieved according to the company's instructions. Finally, the electrophoresis was run at 200 volts for 36 minutes using XCell SureLock™ Mini-Cell (Invitrogen), and the gel was stained using instant blue stain (Coomassie stain, Expedeon). The same protocol was applied for various protein fractions after fractionating these proteins with ammonium sulfate. SDS-PAGE assay was done at Molecular Biology and Biotechnology Department, the University of Sheffield.

4. Ammonium sulfate precipitation

This step was done to fractionate the secreted proteins on both wheat straw and carboxymethyl cellulose media. Different percent saturations of ammonium sulfate (25 %, 50 %, 65 % and 90 %) were used to achieve these fractionations and protein concentrations were measured after each precipitation step. Firstly, *Pseudomonas putida* was cultivated on both WS and CMC media for 4 days at 30°C, and then the media were centrifuged (Refrigerated Centrifuge, Beckman Avanti J-251, UK) for 20 minutes at 4°C and 13000 xg to remove the bacterial cells. The final volumes were 500 ml and 400ml of cells free extracts of wheat straw and carboxymethyl cellulose media respectively. The amount of ammonium required to achieve each saturation was calculated according to the standard table provided by Harris and Angal, (1995). Ammonium sulfate was added gradually, while these media were stirred at 4°C. After dissolving all ammonium particles, these media were centrifuged using a refrigerated centrifuge at 17000 xg for 20 minutes, and pellets were collected and

supernatants used to prepare next percent saturation at 4°C with continuous stirring. Protein concentrations were calculated for all pellets using Bradford method, and the enzymes activities were also measured for all pellets using protocols described above.

3.2.2 Ozonolysis-microbe synergetic approach

3.2.2.1 Material and culture medium preparation

Two sets of experiments were conducted: the first was simply pretreatment with ozone-rich microbubble, referred to as microbubble mediated ozonolysis pretreatment (MMO). The second, however, was pretreatment with ozone-rich microbubbles followed immediately with the microbial application, referred to as microbubble mediated ozonolysis and microbial pretreatment (MMO-M). The untreated wheat straw is referred to as the control.

Wheat straw was mechanically (Pestle and Mortar) prepared to obtain average particle size ~ 1 mm. The biomass was then washed with distilled water and oven-dried at 80°C for 18 h. Wheat straw solution (1 % w/v) was prepared with distilled water and the solution used for the MMO experiment. After MMO pretreatment, the wheat straw was collected and rinsed with distilled water for the MMO-M pretreatment.

The culture medium for the MMO-M experiment was prepared according to Abdul-kadhim and Jarallah, (2013), with a composition of: 1% MMO pre-treated wheat straw (collected after the MMO experiment), 0.5% yeast extract, 0.02% magnesium sulfate and 0.02% ammonium phosphate dibasic. The medium was then sterilized by autoclaving at 121°C and 1 bar for 15 minutes before cultivating with *Pseudomonas putida* KT2440 at 30°C and pH 6 for four (4) days. The pH was set with NaOH or concentrated HCl (Sigma-Aldrich, UK).

3.2.2.2 Ozone generation and quantification

An ozone generator (Dryden AQUA, UK) was used to generate ozone, and the concentration of the generated ozone was determined using the method described by Rakness et al., (1996). 100 ml/min flow rate was calibrated to ascertain the ozone concentrations. Two ozone concentrations -- 6.67 mg/L and 8.87 mg/L -- were explored at varying exposure times (2, 6, 12, 24 h) to determine a reaction time long enough to allow substantial oxidation of the biomass.

The fluidic oscillator was connected to the ozone generator that fed a sintered glass diffuser (16-20 µm pore size) to produce ozone microbubbles (Figure.3.2).

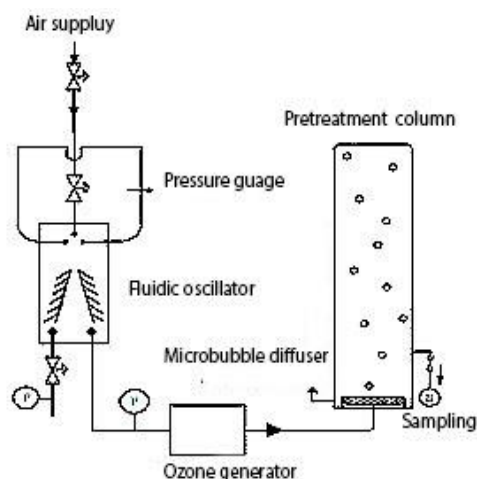


Figure 3.2: Experiment set up. Gas from the fluidic oscillator passes through the fluidic oscillator to the ozone generator. The gas emerges as microbubble-rich ozone. The overall volume is 0.15 L and the working volume of the pretreatment column is 0.1L.

3.2.3 Analytical methods

3.2.3.1 Determination of glucose concentration

Glucose concentration was determined enzymatically using Sigma-Aldrich(UK) reagent kit, which used hexokinase enzyme to phosphorylate glucose to glucose-6-phosphate and the latter product is dehydrogenised with glucose-6-phosphate dehydrogenase to 6- phosphogluconate and this reaction is combined with NAD^+ reduction to NADH, combining with increasing in the absorbance at 340 nm. The spectrophotometer was used to measure the optical density at 340 nm with a Spectrophotometer (DTSTM-1700, 1900 NIR). Samples preparation and procedures were achieved using methodologies, which were described by Sigma-Aldrich (UK) guidance sheet. Glucose concentration is also measured using the protocol described by Miller, (1959) to validate the glucose concentration.

Microbial biomass concentration was determined using the optical density at 600 nm using a spectrophotometer (DTSTM-1700, 1900 NIR)

3.2.3.2 Scanning Electron Microscope (SEM)

Scanning Electron Microscopy (SEM) was used to examine morphological changes in lignocellulosic biomass after each pretreatment and compare it with untreated biomass. The biomass was dried at 80°C for 24 hours in the oven and then coated with gold and examine with SEM (Model S-360, Phillips), which it operated at 15KV.

3.2.3.3 Fourier transform infrared spectroscopy- Attenuated Total Reflectance (FTIR-ATR)

FTIR-ATR (Perkin Elmer, UK) was used to examine changes in functional groups of biomasses after each pretreatment. These samples were examined with a spectrum range from 4000-650 cm^{-1} and resolution 4 cm^{-1} . Spectrum Software (V5.1) was used to show the results, which were background adjusted and normalized them at 1.5 A° . It is worth mentioning that it is not always easy to detect small changes in functional groups absorbances, hence Essential FTIR software (V3.20.009 from operant LCC infrared, trial version) has been used to show these changes as it has a magnification tool to check the absorbance at each wavelength.

3.3 Inactivation with CO₂-enriched microbubbles

3.3.1 Material and culture medium preparation

Pseudomonas putida was cultivated at 30°C for 24 hrs on the nutrient broth, and this culture used in the inactivation process. Normal saline solution was prepared and kept in the fridge for 24 hrs to cool down to reach 6°C. The diluted bacterial culture was prepared by mixing 900 ml of cold saline with 100 ml of bacterial culture, which was grown for 24 hrs, and the final temperature was set at 6°C.

The system was erected where the reactor was connected to CO₂ (100 %) gas cylinder through a diffuser (Ceramic diffuser, point four systems LTD, UK) at 100 ml/min (Figure 3.3). These experiment sets have stood for 90 min, and samples were drawn every 15 minutes except the first sample, which was drawn after 7 minutes. pH and temperature profiles were measured at the same time of drawing samples. Drawn samples were diluted with normal saline and aseptically cultivated on nutrient agar using inoculation loop at 30°C for 24 hrs, and then grown colonies were counted manually. Also, the colonies number was also confirmed by using two software packages: ColonyCount, 2015 © Promega Corporation and a colony counter (Bio Spectrum 410 imaging system, UVP, UK). Petri dishes with 30 – 300 colonies were only counted, and colony-forming unit per ml was calculated for each sample.

Survivor ratio is calculated and plotted by using Log (N/N₀) on Y-axis and time on X-axis. While N refers to the number of colony forming unit for treated samples, N₀ refers to the initial number of colony forming unit before CO₂ treatment, which was calculated for each experimental set prior of application of carbon dioxide-enriched microbubbles.

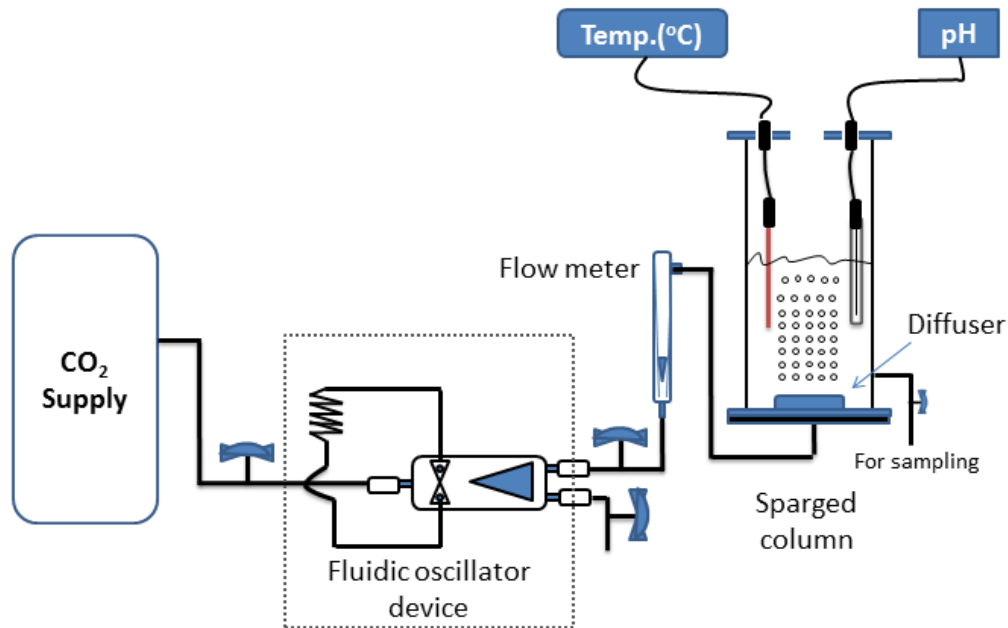
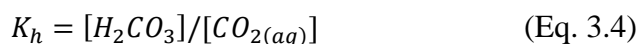


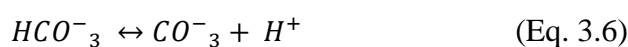
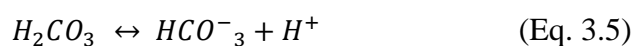
Figure 3.3: Experiment set up. Carbon dioxide gas from the gas cylinder passes through the fluidic oscillator to feed the microbubbles diffuser. The gas emerges as microbubble-rich carbon dioxide at 100 ml/min flow rate and the working volume of the inactivation column is 1L.

3.3.2 Determination of carbon dioxide concentration

Kinetically, conversion of carbon dioxide into carbonic acid is very slow, and there is only 0.2 % of carbon dioxide can be converted to carbonic acid and its ions, while 99.8 % of carbon dioxide tends to remain as a dissolved gas, which can be shown in the dissociated equilibrium constraint (Al-Mashhadani et al., 2011):



Carbonic acid is a diprotic acid, and it contains two hydrogen atoms ionizable in water and dissociates into bicarbonate and carbonate ions according to the following equations:



It is possible to infer the concentration of dissolved carbon dioxide from the pH assuming equilibrium and well-mixed system.

The equilibrium constraint for each dissociation reaction (Eq. 3.6) and (Eq. 3.6) are

$$K_{a1} = [HCO_3^-][H^+]/[H_2CO_3] \quad (\text{Eq. 3.7})$$

$$K_{a2} = [CO_3^{2-}][H^+]/[HCO_3^-] \quad (\text{Eq. 3.8})$$

The system should satisfy the electroneutrality constraint, therefore

$$[H] = [OH^-] + [HCO_3^-] + 2[CO_3^{2-}] \quad (\text{Eq. 3.9})$$

Dissociation of water to hydrogen and hydroxide ions with dissociation of carbon dioxide can give five equations, and the definitions of the pH relate with six unknowns, which are $[H^+]$, $[OH^-]$, $[HCO_3^-]$, $[H_2CO_3]$, $[CO_3^{2-}]$ and $[CO_2(aq)]$, which can be solved through set of nonlinear algebraic equations in standard packages such as MATLAB (Table 3.1). Accordingly, carbon dioxide concentration can be inferred from pH measurements as following:

$$[CO_2(aq)] = \frac{(10^{-pH}) ((10^{-pH})^2 - 10^{-14})}{K_{a1}K_h [10^{-pH}] + 2K_{a1}K_{a2}K_h} \quad (\text{Eq. 3.10})$$

Therefore, the concentration of dissolved carbon dioxide was measured using (Eq. 3.10) based on pH values, which were measured by pH (Mettler Toledo™ S220) meter. It is worth to note that addition of ethanol to the inactivation solution did not influence the pH of the solution and thus, the same (Eq.3.10) above was used to calculate the concentration of dissolved carbon dioxide in the experimental sets when ethanol used as an additive. On the other hand, addition of acetic acid 0.5% (Fluka, UK) was strongly affected the pH value (pH dropped to 3.34) and therefore, the above (Eq. 3.10) was integrated to include the dissociation of acetic acid in the new (Eq. 3.11) and the concentration of acetic acid in (Eq. 3.12).

$$[CO_2] = \frac{(10^{-pH})^2 \left(10^{-pH} - \frac{1.75e-05[A_A]}{10^{-pH}} - \frac{10^{-14}}{10^{-pH}} \right)}{[K_a K_b 10^{-pH} + 2K_a K_b K_h]} \quad (\text{Eq. 3.11})$$

$$[A_A] = \frac{(10^{-pH})^2 - 10^{-14}}{1.75e-05} \quad (\text{Eq. 3.12})$$

Table 3.1: Shows the chemical reactions with their correspondent reaction rate constants used to integrate the carbon dioxide concentration equations in the current study

Chemical reaction	Reaction rate constant	Unit	Reference(s)
$H_2O \xrightarrow{K^f} H^+ + OH^-$	$K^f = 5.5 * 10^{-6}$	1/s	Chartterjee et al., (1983) Zhang and Houk, (2005) Garrett et al., (2005)
$H^+ + OH^- \xrightarrow{K^r} H_2O$	$K^r = 3 * 10^3$ $K_{eq} = 1.8 * 10^{-16}$ $K_w = 1 * 10^{-14}$	1/mole/sec	
$CO_2 + H_2O \xrightarrow{K^f} H_2CO_3$	$K^f = 0.043$	1/mole/sec	Zhang et al., (2008)
$H_2CO_3 \xrightarrow{K^r} CO_2 + H_2O$	$K^r = 14.98$	1/s	
	$K_{eq} = 2.87 * 10^{-3}$		
$H_2CO_3 \xrightarrow{K^r} HCO_3 + H$	$K^f = 10^{6.9}$	1/mole/sec	
$HCO_3 + H^+ \xrightarrow{K^r} H_2CO_3$	$K^r = 4.67 * 10^{10}$ $K_{eq} = 1.7 * 10^{-4}$		
$HCO_3 \xrightarrow{K^f} CO_3 + H^+$	$K_{eq} = 5.62 * 10^{-11}$	1/mole/sec	
$HC_2H_3O_{2(aq)} + H_2O \xrightleftharpoons{K^f} H_3O_{(aq)} + C_2H_3O_{2-(aq)}$	$K_{eq} = 1.75 \times 10^{-5}$	mole /L	Skoog et al., (2000)

3.3.3 Morphological examination of the bacterial cells

3.3.3.1 Combined microscopy

For the first experimental set, two slides for bacterial smear before and after the inactivation process were prepared and stained with Gram stain according to the standard protocol, which was described by Harely, (2002). After that, the combined microscopy (Olympus microscope,

CX23) was very limited to differentiate morphological changes on the microbial cells and thus, the microbial samples were examined using Scanning electron microscopy.

3.3.3.2 Scanning electron microscopy

Microbial specimens were fixed chemically. Initially, the specimens were kept in normal saline to avoid any changes as a result of osmolality, and normal saline is the isotonic solution. After that, the specimens were placed in 2-3% Glutaraldehyde in 0.1 M sodium phosphate for 3 hours at 4°C and then washed in 0.1M phosphate buffer pH 7.4, twice with 10 minutes intervals at 4°C. The second fixation with 1-2% aqueous osmium tetroxide for 1 hours at room temperature is followed. The samples, then dehydrated through series of ethanol concentrations (75, 95 and 100) % respectively for 15 minutes before drying in absolute ethanol (100%) oven hydrous copper sulphate for 15 minutes. Specimen then dried overnight again after placing them in 50-50 mixture of 100% ethanol- 100% Hexamethyldisilazane for 30 minutes followed by a further 30 minutes with 100% Hexamethyldisilazane. After drying, the specimens were mounted on 12.5mm diameter stubs, attached with Carbon-Sticky Tabs, and then coated in an Edwards S150B sputter coated with approximately 25 nm of gold. The specimens were finally examined in a Philips/FEI- XL-20SEM at an accelerating voltage of 20Kv.

3.4 Fermentation integrated with *in situ* separation of bioproducts

3.4.1 Material preparation

Zymomonas mobilis ZM4 (ATCC® 31821) was first activated using RM medium which was suggested by the provider (ATCC in partnership with LGC Standards), in 1L Erlenmeyer flask with continuous shaking at 100 rpm. Thereafter, the bacterium was cultivated on pre-inoculum medium and second stage inoculum medium (See appendix A) before starting the fermentation process using the fermentation media (See Appendix A).

3.4.2 Experimental procedures

Zymomonas mobilis was cultivated on the fermentation medium after pre-cultivating it on both pre-inoculum and second stage inoculum media. This bacterium was incubated at 30°C and pH 5.5 for several days (30-50 h), and acetaldehyde and ethanol concentrations were measured using gas chromatography (See Appendix F). Firstly, the fermentation process was achieved under standard conditions without sparging microbubble (Preliminary studies). This step was done to study different aspects of bacterial growth and bioproducts production under standard conditions without sparging microbubble and with using the wild-type strain (*Zymomonas mobilis* ZM4). Secondly, the fermentation process was conducted using initial and periodical

sparging strategies with air microbubbles. Both durations of sparging and flow rate were chosen according to the experimental data (However, the flow rate was stabilized at 0.3 L/min). This process was achieved using an airlift loop bioreactor (See figure 3.4). Samples were taken every 1 hour for the trial experiments to evaluate the system and to better understanding of the whole process, and then the sampling time was determined to be two hours. These samples were analyzed using GC to quantify the products (Acetaldehyde and Ethanol) and also glucose concentration using the protocol described by Miller, (1959). However, the biomass concentration was measured on an hourly basis and no samples were drawn overnight due to the safety rules of the university.

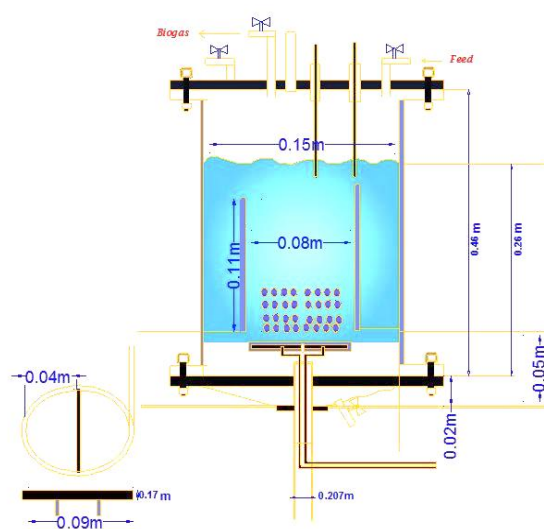


Figure 3.4: Experiment set up. Air from the fluidic oscillator passes through the fluidic oscillator to feed the microbubbles diffuser. there are two outputs from the fluidic oscillator with two bleeding on both sides to control the oscillatory flow.

Two identical bench-scale fermenters were used in the current study. Each fermenter has an overall volume of 15 liters with working volume of 9 liters (Figure 3.4). The time of each experimental set was determined according to the glucose consumption, biomass concentration and the results gained from the preliminary studies. These fermenters were operating under mesophilic conditions ($\sim 30^{\circ}\text{C}$).

A PID controller was used to control the temperature in the reactor at 30°C . The reactor was also provided with a pH controller, type ON/OFF controller (Model BL931700 pH mini controller) to control the pH in the fermenter. The solution used to adjust the pH during the fermentation process, is 1M sodium bicarbonate, and this solution has several advantages over other bases such as sodium hydroxide. For example, this solution is less corrosive and toxic than NaOH, it does not cause any precipitation in the fermenter, and more importantly, this

solution adjusts the pH gradually, and it does not cause change the pH value significantly with excessive doses. No acidic solutions were used to adjust the pH in the current study as the pH tends to decrease in the fermentation process due to carbon dioxide and acids production during the fermentation process and thus, only alkaline solutions were needed to adjust pH.

Produced biogas (carbon dioxide) was measured every day, and this measurement was achieved by displacement of the aqueous acid solution ($\text{pH} \leq 3$). All volumes of produced biogases mentioned in this study were corrected to 1 atm and at room temperature ($\sim 20^\circ\text{C}$). The carbon dioxide concentration was measured using carbon dioxide monitor (Data gas analyzer, Model 0518) at 1 atm pressure.

Vapour and gas collectors were designed to collect the stripped products and to measure the final concentration of each product (Carbon dioxide and acetaldehyde) after finishing the fermentation process, while ethanol accumulates in the fermentation broth. Figure 3.5 shows the experimental design of the fermentation process.

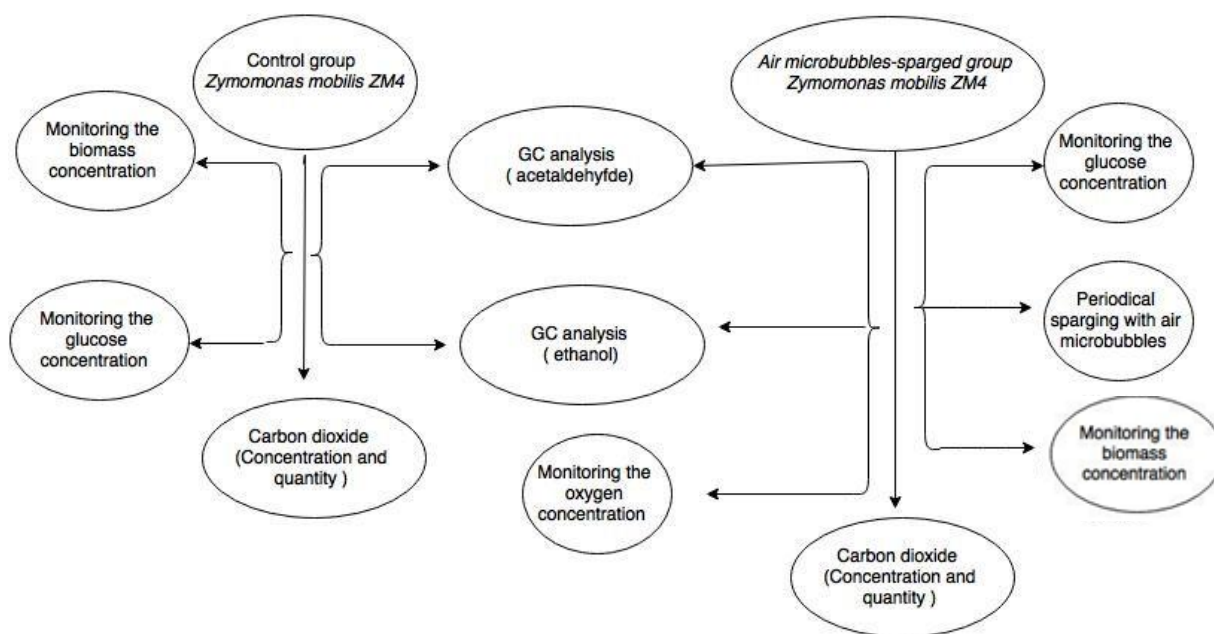


Figure 3.5: Experimental design of the fermentation process using wild strain of *Zymomonas mobilis* ZM4. The initially sparged group is referred to as control group.

3.4.3 Vapour collectors

Two collection systems were tested to collect the stripped volatile compounds from the fermentation broth. The first system is a trapping system and the second is a condensation system. Regarding the trapping system, two solutions can be used to trap the produced acetaldehyde, either sodium bisulphite (Sodium hydrogen sulphite) at 0.02% concentration

(Wecker, 1987) or cold water (Tanaka et al., 1990) (Figure 3.6). While, using cold water can trap 93.2% of the produced acetaldehyde, sodium bisulphide solution, in contrast, can trap 79% of the produced acetaldehyde at pH equals or less than 2 (Tanaka et al., 1990).

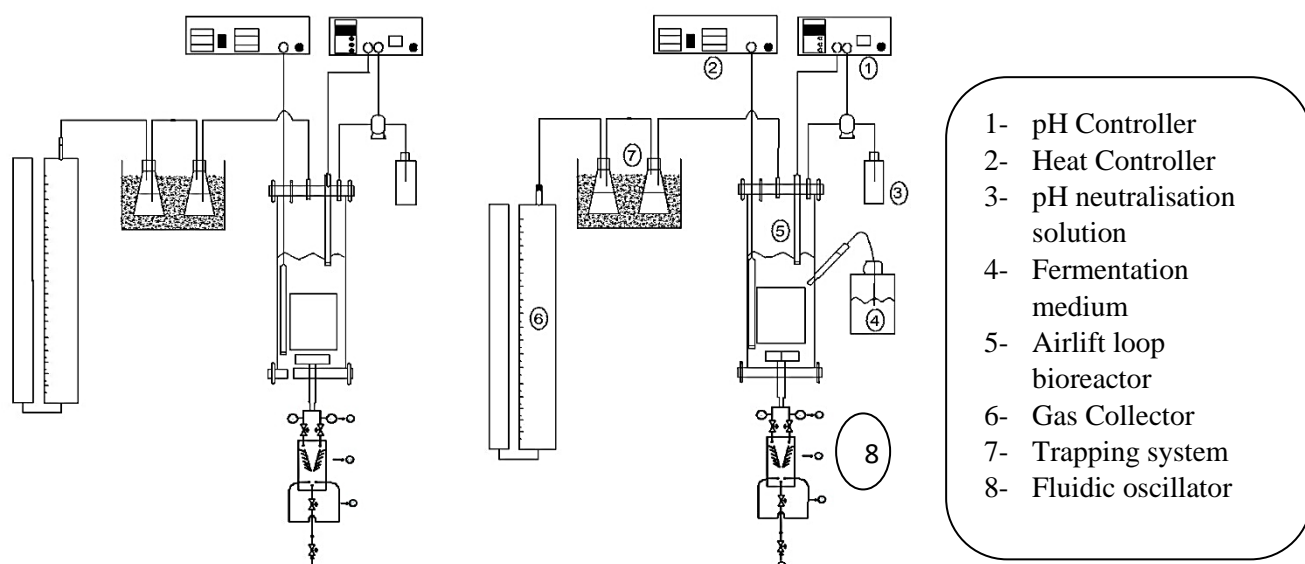


Figure 3.6: Schematic flow diagram of the fermenter connected with both trapping system and gas collector.

However, cold water followed by 3-methyl-2-benzothiazolinone hydrazone hydrochloride solution (MBTH) at 0.05% concentration was used in this study as it has the highest trapping efficiency (Tanaka et al., 1990) (Figure 3.6).

The cold-water trapping system was made of 1 of 500 ml gas washing bottle containing 400 ml cold water (at around $\sim 5^{\circ}\text{C}$) cooled by ice, and the trapped acetaldehyde was measured by gas chromatography. In addition, the gas leaving the system was bubbled through 250 ml gas washing bottles containing 150 ml of 0.05% (w/v) 3-methyl-2-benzothiazolinone hydrazone hydrochloride solution to monitor any acetaldehyde leakage from the trapping system. The cold water in the system was quickly replaced with new one as soon as the white precipitate seen in MBTH washing bottle. The trapped acetaldehyde in water does not need any treatment before analyzing it with GC in comparison with the one trapped by sodium bisulphite solution, which needs further treatment (Wecker, 1987). More importantly, acetaldehyde is highly volatile compound, and some of the produced acetaldehyde might be lost during the treatment of acetaldehyde-sodium bisulphite solution, resulting in inaccuracy of the results.

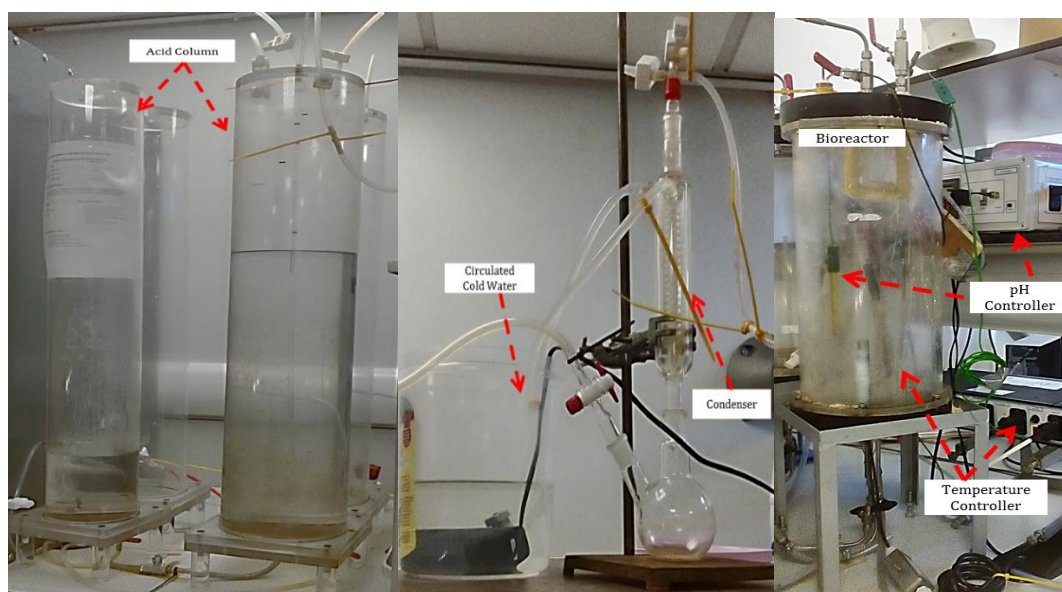
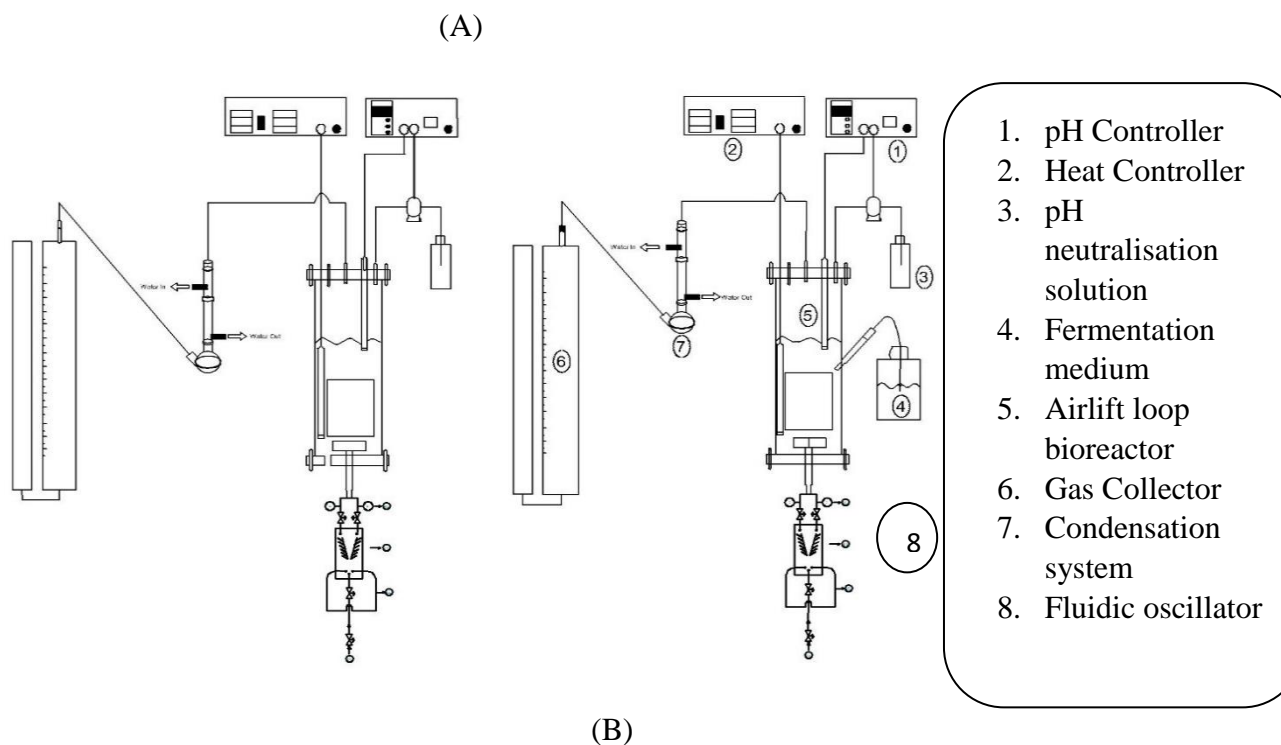


Figure 3.7: (A) Schematic flow diagram of the fermenter connected with both condensation system and gas collector. (B) A picture of the final set up used in this study.

Figure 3.7 shows the chosen system used in the current study to collect the volatile compounds. A condensation system was made from a condenser (C6/13/SC), approximal surface area ($2.5 \times 10^{-2} \text{ m}^2$, Pyrex quickfit, UK) connected to 250 ml two neck round bottom Flask (Pyrex quickfit, UK). Cold water ($\sim 5^\circ\text{C}$) was supplied to the inlet of the condenser by a pump (superfish aqua-flow 50, flow rate 20L/hr). The gas leaving the system was bubbled through 250ml gas washing bottles containing 150ml of 0.05% (w/v) 3-methyl-2-benzothiazolinone

hydrazone hydrochloride solution to make sure that all stripped acetaldehyde was condensed in the system, and the rest of the flow with carbon dioxide passes to the next collector, gas collector. This system avoids many difficulties associated with the cold-water trapping system such as the need to increase the flow rate to overcome the resistance in the gas washing bottles due to the pressure of the liquid height, which also affect the gas collection in the gas collector.

3.4.4 Gas collector

The main concept behind the design of gas collector is the communicating vessels phenomena. This phenomenon shows that the pressure of the liquid does not depend on the size or shape of containers, but instead, it depends on liquid height in these containers. Liquids with the same height have the same constant pressure regardless the shape or the size of containers. This fact can be changed if the ends of these vessels are closed, and vacuum pressure will be generated within these vessels. Therefore, this project uses the vacuum pressure to withdraw the gaseous products from the headspace of the fermentation vessel and eventually capture them in the storage column.

The used collector consists of two cylinders; while the first cylinder is called the reference cylinder and its dimensions are 15 cm diameter and 1m height, the second cylinder is called the collection cylinder and its dimensions are 20 cm diameter and 1 m height as shown in Figure 3.8. The upper end of the reference cylinder is exposed to the atmosphere, while the top end of the collection cylinder is provided with four exits, two of them will be used for samples withdrawal and gas analysis. The another exist was used to connect this collector with the vapour collector, while the fourth exist is for water supply.

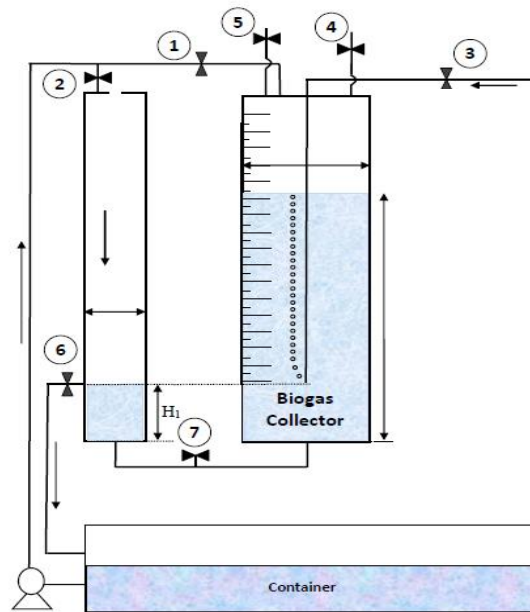


Figure 3.8: The used gas collector which is connected to the vapor collector

This vacuum is governed using the following mathematical equation:

$$P = p g \Delta H \quad (\text{Eq. 3.13})$$

Where P is a hydrostatic pressure, ΔH is the height difference between two cylinders, p is the liquid density (kg/m^3), and g is the gravitational acceleration (9.81 m/s^2).

The liquid levels must be kept the same in both collection cylinder and fermenter to prevent vacuum pressure formation among them. Avoiding vacuum formation between fermenter and collection tube can keep both headspaces of fermenter and collection cylinder at the same pressure, and stripping of gases can be achieved under atmospheric pressure (1 atm). It is worth mentioning that changing the liquid level can lead to either re-dissolution of produced gasses in the fermentation media (negative vacuum pressure), or it might extract some gasses from the fermentation medium (positive vacuum pressure). Therefore, it would be very helpful to establish a calibration between the fermenter and the collection tube.

All produced gasses leave the headspace of the fermenter under the vacuum pressure leading to reduce the partial pressures of these gasses in the fermenter. Also, the current fermentation process is a closed system, where all products are collected at different stages. All produced carbon dioxide is collected and thus; the bespoke system reduces carbon dioxide emissions from the fermentation processes but importantly, the collected carbon dioxide can be recycled and used in other useful applications such as cultivation of algae.

In addition, the volume of gas (carbon dioxide) was measured using the following equation:

$$V_g = \frac{\pi}{4} D_c^2 H_{hs} \quad (\text{Eq. 3.14})$$

Where V_g is the volume of gas (m^3), D_c is the diameter of the collection tube (m^2), and H_{hs} is the height of collected gas (m).

Carbon dioxide solubility is decreased with decreasing the pH in the solution. Therefore, acid water (\sim pH 3) was used to fill the gas collector and to minimize the dissolved carbon dioxide to its lowest.

3.4.5 Analytical methods

3.4.5.1 measurement of glucose concentration

Miller, (1959) protocol was used to measure the glucose concentration during the fermentation process. A calibration standard curve was made for glucose concentrations with this method and used to work out the glucose concentration in a given sample.

3 ml of a sample was mixed with 3 ml of solution 1 (1 % dinitrosalicylic acid, 0.2 % phenol, 0.05 % sodium sulfite, and 1 % sodium hydroxide) and then the mixture was heated in water bath at 100°C for 15 minutes. 1 ml of solution 2 (40 % Rochelle salts) was added into the mixture after heating. When the mixture is cooling down, the optical density of glucose was measured using spectrophotometer at 575 nm. Mixture of water with solution 1 and 2 was used as the blank.

3.4.5.2 Biomass calibration curve

Biomass was determined by the optical density at 600 nm using the uninoculated medium as a blank (Douka et al., 1999). Samples were centrifuged and the biomass at the bottom of the tube was dried in an oven at 80°C for 18 hrs. A turbidity- dry weight calibration standard curve was then made and prepared to be used for calculating the biomass concentration.

3.4.5.3 Detection of acetaldehyde production using acid fuchsin

Acid fuchsin was used as an indicator for acetaldehyde production. This pigment has specificity toward aldehydes and acetaldehyde specifically. This test consists of two parts. In the first part, *Zymomonas* wild strain was cultivated upon 4SSM agar plate for 48 hours. The second part includes overlaying previous plates with acid fuchsin contained agar medium (The overlay medium consisted of the following (in g/100 ml of distilled H_2O): acid fuchsin, 0.02; KH_2PO_4 , 3.18; $\text{Na}_2\text{HPO}_4 \cdot 7\text{H}_2\text{O}$, 0.88; and agar, 2.0. Molten acid fuchsin medium at 45°C was decolorized with 0.5 M NaOH (Holman et al., 1914) before it was used as an overlay. The latter part was

stood for 3-16 hours to appear pink to red colour range as a result of acetaldehyde production (Wecker, 1987).

3.4.5.4 Selection of overproducing strains using allyl alcohol

0.2 mM allyl alcohol was used to select bacterial strains with decreased or altered alcohol dehydrogenase activity. Allyl alcohol can be oxidized by alcohol dehydrogenase to produce acrylaldehyde (Acrolein). The latter chemical is a toxic compound for a bacterial strain with normal or overactive alcohol dehydrogenase activity. Therefore, only cells with decreased or altered alcohol dehydrogenase activity can grow in the presence of allyl alcohol (Rando, 1974). The mechanism of alcohol dehydrogenase in converting allyl alcohol into acrylaldehyde can be shown in Figure 3.9.

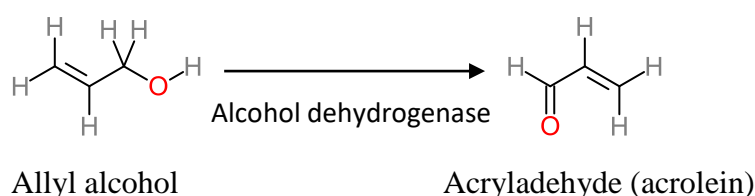


Figure 3.9: The conversion of allyl alcohol to toxic acrylaldehyde by alcohol dehydrogenase (Adapted from Rando, 1974)

Allyl alcohol was added to the molten culture medium (4SSM agar) to reach a final concentration 0.2 mM before pouring into Petri dishes. These dishes were inoculated with three-day-old *Zymomonas* strain, and after four days of incubation, the grown colonies were streaked onto fresh 4SSM Agar. The concentration of allyl alcohol was increased gradually (2 mM, 10 mM, 20 mM, 100 mM and 200 mM) by following the same procedure mentioned with 0.2 mM concentration and the final grown colonies were transferred to fermentation medium to determine acetaldehyde production (Wecker, 1987).

3.4.5.5 Measuring of the relative alcohol dehydrogenase activity

To measure the relative activity of alcohol dehydrogenase in both wild type and mutant type *Z.mobilis*, permeabilized cells need to be prepared. The permeabilized cells can be prepared by taking 1 ml of 24 hr grown cells suspended in 30 mM K_2HPO_4 buffer pH 6. These cells are collected by centrifugation for 5 mins at 1000 xg and the pellet is resuspended in 200 μ l 30 mM K_2HPO_4 (pH6) with 1 g/l lysozyme (Sigma-Aldrich, UK). 15 μ l chloroform was then added and vortex for 45 s, and immediately place on ice. The samples kept on ice for 10 min, then 800 μ l 30 mM K_2HPO_4 added. To measure the relative activity of alcohol dehydrogenase, 10 μ l permeabilized cells was mixed with 990 μ l of 30 mM TrisHCl buffer pH 8,5 contained 1M

ethanol and 33 mg NAD⁺, while the blank measurement is conducted with the buffer and ethanol plus NAD⁺ only. Changing in the optical density at 340 nm was recorded using a spectrophotometer (Ultraspec 2100 Pro, Biochem, UK) for 60 s. The absorbance for the wild strain is considered as a 100 % activity, the measurement for the mutant strain is then used to calculate the relative activity.

3.4.5.6 Sampling

Samples from the fermentation systems are collected hourly for biomass measurements, while samples are collected per two hours for glucose, acetaldehyde and ethanol measurements. Samples for bioproducts measurements are filtered with syringe filter unit (Whatman® Anotop® 25 Plus syringe filter, pore size 0.2 µm, Sigma- Aldrich, UK), and kept in airtight vials in an inverted position. These vials are fitted with crimp-top lids, accommodating septa in an airtight seal that can be pierced with a syringe needle. The septa is made of rubber and coated with teflon. Using these vials is to assure that all produced acetaldehyde is considered as this compound tends to be in a vapour phase at the room temperature as well as other volatile compounds such as ethanol. Figure 3.10 shows pictures for the used vials in the current study. These samples were analyzed instantly, and if the GC instrument is not available on the day, the samples were kept in the freezer at 4°C.



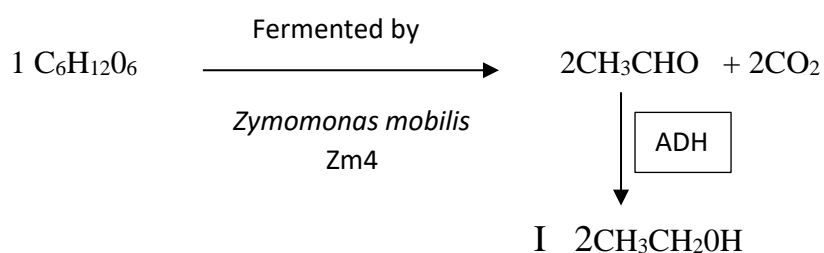
Figure 3.10: Pictures for the airtight vials used to storage the withdrawal samples.

3.4.5.7 Product yield calculations

The fermentation products were measured using millimolarity unit (mM), which prescribes mass of material to the volume of liquid. The yields of the fermentation bioproducts (acetaldehyde and ethanol) were calculated by considering 1 mole of glucose can be metabolised to produce 2 moles of acetaldehyde / ethanol with 2 moles of carbon dioxide. The percentage

yield is the ratio between the actual yield and the theoretical yield multiplied by 100%. It indicates the percent of theoretical yield that was obtained from the final product in an experiment. The actual yield is the amount of product (acetaldehyde and ethanol) actually produced in the fermentation process, which is mass of product formed per mass of substrate (glucose) consumed multiplied by 100.

The chemical equation for acetaldehyde and ethanol production from glucose can be seen below:



According to above equation, each mole of glucose, if *Zymomonas mobilis* was able to ferment 100% of 1 mole of glucose, should yield 2 moles of acetaldehyde/ ethanol and 2 moles of carbon dioxide. To calculate the theoretical yield, the molar mass of each chemical involved in the above equation needs to be determined using the periodic table. After that, the theoretical yield was calculated by multiplying the number of produced moles by both actual moles and the calculated molar mass of each chemical.

Regarding carbon dioxide, only the volume and concentration of carbon dioxide were reported in this study. No carbon dioxide yield was calculated because this gas can be produced as a byproduct by many reactions such as conversion of Phosphoenolpyruvate to Oxaloacetate, reduction of Acetyl-CoA to malate and conversion of pyruvate to acetaldehyde and carbon dioxide. Also, it tends to dissolve in the fermentation broth, and some of the dissolved carbon dioxide is dissociated into carbonic acid, bicarbonate, and carbonate, leading to decrease in the pH of the broth. Practically, the fermentation broth was kept at pH 5.5 and sodium bicarbonate was pumped to the fermentation broth to control any decrease in the pH.

The calculation of biomass yield was based on that 10.5 g dry weight of *Zymomonas mobilis* is the highest biomass yield, which can be generated for each mole of glucose being consumed (Kalnenieks, 2006) and thus, 10.5 is considered as 100% yield.

3.5 Bacterial Propagation

3.5.1 Experimental procedures

Duran Conical Flasks Wm 2000ml were used in both stationary and shaking flask cultures. 1.5L cylindrical Airlift Loop Bioreactor (ALB) made of PerSpex measuring 0.16m and 0.125m in height and base respectively (Figure 3.11). The reactor was fitted with a microporous sprayer for bubble generation. The ALB supported pH, temperature and DO probe (Mettler Toledo, UK). The culture temperature was controlled using a microbiological incubator operating at 30°C. Sterile 4% glucose standard medium (4GSM) is prepared according to (Feigl, 1955), was used for the experiment. Before culturing, the medium was autoclaved for 15 minutes at 121 °C. Next, 1L of growth medium was used to conduct stationary, shaking flask and ALB experimental sets. 18hrs old inoculum was used to inoculate all the experimental sets. With stationary culture, 2000 mL Erlenmeyer flask with 1000 ml pre-inoculated medium was left static 8 hrs at 30°C. With shaking culture, 2000 mL Erlenmeyer flask with 1000 ml pre-inoculated medium was kept in a rotary shaking incubator (INFORS HT, Germany) at 30°C on 100 rpm. The control of pH was achieved using a pH controller, type ON/OFF controller (Model BL931700 pH mini controller) using 1M sodium bicarbonate solution to adjust the pH.

3.5.2 Determination of K_La

Based on the metabolic oxygen uptake rate of the organism during propagation, the overall oxygen transfer coefficient was determined by the yield coefficient method. The oxygen transfer rate was calculated using the equation below:

$$\frac{d C_L}{dt} = K_L a (C^* - C_L) \quad (\text{Eq. 3.15})$$

Where

- K_L = is the liquid –phase mass transfer coefficient(m^2/hr).
- a = is the interfacial surface area (m^2).
- C^* = is the oxygen concentration at saturation conditions (mol/L).
- C_L = is the oxygen concentration in the culture medium (mol/L).

Alternatively, the dynamic method suggested by Bandyopadhyay and Humphrey, (1967) was also used. This method is based on monitoring the dissolved oxygen concentration during a short period of aeration. Under steady state conditions, the oxygen uptake rate can be calculated from the following equation:

$$\text{O}_2 \text{ uptake} = rX \quad (\text{Eq. 3.16})$$

$$\text{O}_2 \text{ transfer rate} = K_{La}(C^* - C) \quad (\text{Eq. 3.17})$$

Where:

- r = is the specific oxygen uptake rate per unit mass of fermenting microorganisms.
- X = is the mass concentration of fermenting microorganisms in the fermenter.
- K_{La} = is the volumetric oxygen transfer coefficient.
- C^* = is the concentration of oxygen in the liquid that might be equilibrium with the partial pressure of the oxygen in the air.
- C = is the concentration of the oxygen at a particular point in the fermenter.

This method has two stages, which are gassing and non-gassing stage. In the latter, change in the dissolved oxygen concentration can be calculated from the following equation:

$$\text{Change in the dissolved oxygen concentration} = \frac{dC}{dt} = -rX \quad (\text{Eq. 3.18})$$

It is worth to note that this equation cannot be applied immediately after turning off the air supply, and sometimes need to escape the air bubbles from the bioreactor. The dissolved oxygen concentration is monitoring until it reaches to around the critical value, after which the airflow is turned on again. The former stage is called gassing stage, in which change in dissolved oxygen concentration can be calculated from the following equations:

$$\text{Change in dissolved oxygen concentration} = \frac{dC}{dt} = K_{La}(C^* - C) - rX \quad (\text{Eq. 3.19})$$

rX value can be worked out from the non-gassing period.

It is important to note that specific oxygen uptake rate is constant as long as the dissolved oxygen concentration is above the critical biological oxygen concentration when the organisms have not been starved yet. The exact value of the critical oxygen concentration depends on the microorganism; however, this value usually falls between 5% and 10 % of the air saturation under the average operational conditions (Doran, 2013).

On the other hand, the oxygen transfers rate (OTR) between the gas and liquid phase in shaking flasks can be described as:

$$\text{OTR} = K_{La}(C^*_L - C_L) = K_{La}(p_{\text{O}_2} * L_{\text{O}_2} - C_L) \quad (\text{Eq. 3.20})$$

Where

K_L = is the liquid –phase mass transfer coefficient (m^2/hr).

a = is the interfacial surface area (m^2).

C^* = is the oxygen concentration at saturation conditions (mol/L).

C_L = is the oxygen concentration in the culture medium (mol/L).

p_{O_2} = the oxygen partial pressure (bar)

According to above equation, oxygen saturation concentration depends on the oxygen solubility in the culture medium and the oxygen partial pressure in the headspace of the cultivation flask p_{O_2} . Moreover, the solubility of oxygen depends on both the medium composition and electrolyte concentration (Klößner and Büchs, 2012). The maximum oxygen transfer rate can be calculated using the following equation when $C_L=0$:

$$OTR = K_L a * p_{O_2} * L_{O_2} \quad (\text{Eq. 3.21})$$

$K_L a$ in shaking flasks can be calculated from the below equation, which was developed by Henzler and Schedel, (1991):

$$K_L a = 0.5 * d^{\frac{73}{38}} * n * d_0^{\frac{1}{4}} * V_L^{\frac{-8}{9}} * D^{\frac{1}{2}} * \nu^{\frac{-13}{54}} * g^{\frac{-7}{54}} \quad (\text{Eq. 3.22})$$

Where

d = is the maximum inner flask diameter (m)

n = is the shaking frequency (1/s)

d_0 = is the shaking diameter (m)

V_L = is the filling volume (m^3),

D = is the diffusion coefficient (m^2/s)

ν = is the kinematic viscosity (m^2/s)

g = is the acceleration of gravity (m/s^2).

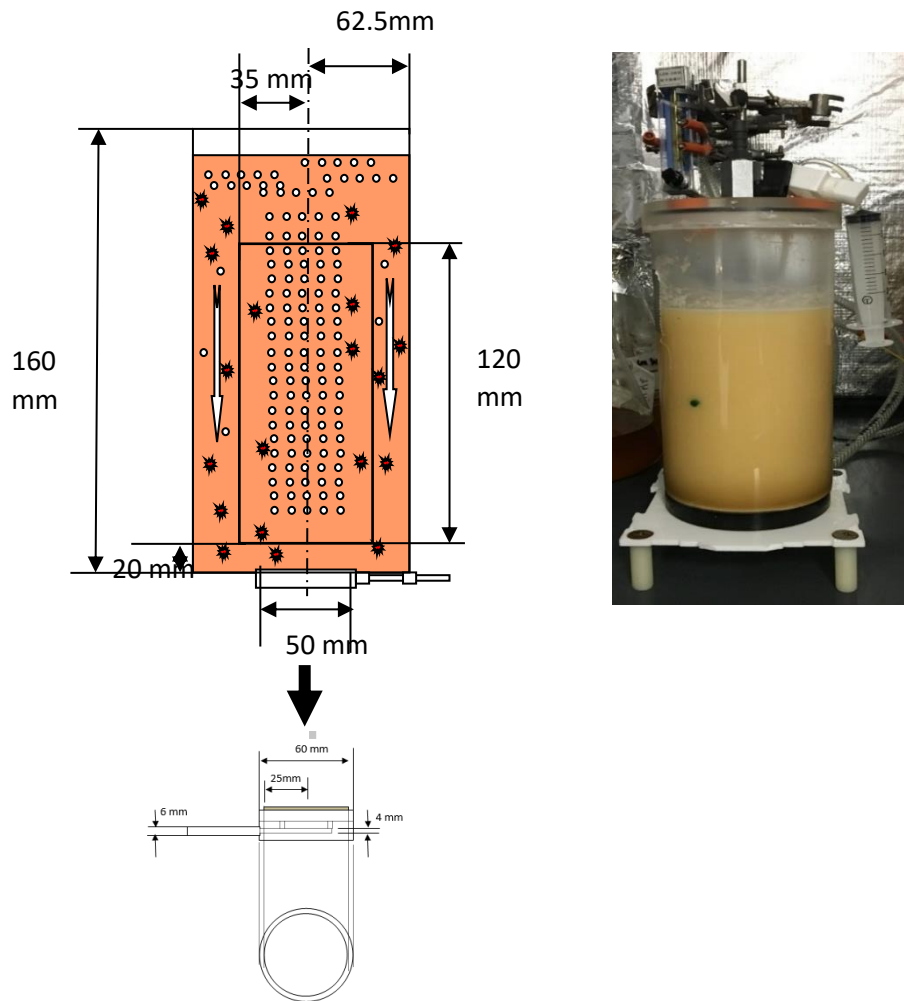


Figure 3.11: Schematic representation of the Airlift Loop Bioreactor. Microfiltered air was supplied through the sparger for bubble generation. The ALB is also fitted with pH, DO, thermocouple sensor. This reactor was incorporated in the microbiological incubator to regulate the temperature

Chapter 4

Exploiting microbubble-microbe synergy for biomass processing: Application in Lignocellulosic biomass pretreatment

Overview

The potential of lignocellulosic biomass as a sustainable biofuel source is substantial. The development of an efficient and cost-effective pretreatment approach remains challenging. In this chapter, an attempt was made to explore a new, relatively cheap pre-treatment option that works at ambient temperatures. By using microbubbles generated by fluidic oscillation, free radicals around the gas-liquid interface of the microbubble readily attack and degrade lignocellulosic biomass, rendering it more amenable to digestion. The combination of microbubbles and *Pseudomonas putida*—a robust delignification and cellulolytic microbe, further improved biomass degradation and consequently, increased glucose production from wheat straw in comparison to solo pretreatment of the biomass with microbubbles and *Pseudomonas putida* respectively. The microbubble-microbe approach to making biomass more amenable to sugar production is potentially a valuable alternative or complementary pretreatment technique. *Pseudomonas putida* KT2440 was tested for its ability to secrete cellulases and lignin hydrolysis enzymes, and these enzymes catalyse the degradation of cellulose and lignin polymer to its fundamental units, glucose, and aromatic compounds respectively. *Pseudomonas putida* is proven an effective pretreatment agent and can be used alternatively with the existing methodologies.

4.1 *Pseudomonas Putida* growth on culture medium

Figure 4.1 shows the growth pattern of *Pseudomonas putida* on different cellulosic and lignin media: carboxymethylcellulose (CMC), lignin medium (LM) and more complex biomass, wheat straw medium (WM). Selection of these three media was essential to ascertain the ability of the bacterium in utilizing and growing on different carbon sources. While *Pseudomonas* growth on CMC medium can be clearly seen as a monoauxic growth due to the single C-source, growth on LM was a diauxic growth as the two carbon sources (glucose and lignin) are available for metabolism by the microbe. WM culture, however, revealed a significant *Pseudomonas putida* growth due to several carbon sources found in wheat straw such as: hexoses, pentoses, and their complexes. The higher growth is attributable to the simultaneous utilization of the substrates, which is a typical microbial behavior when exposed to a mixture of carbon sources (Lendenmann et al., 1996). The limitation of carbon and energy sources explains the relatively

low growth rate and growth pattern recorded for both WS and LM media (Hadiati et al., 2014), in contrast to high nutritional performance and typical growth pattern recorded in CMC.

It is noteworthy to mention that due to the maximum cellulolytic activities observed after four days, further experimentations on biological pretreatment were conducted for four days.

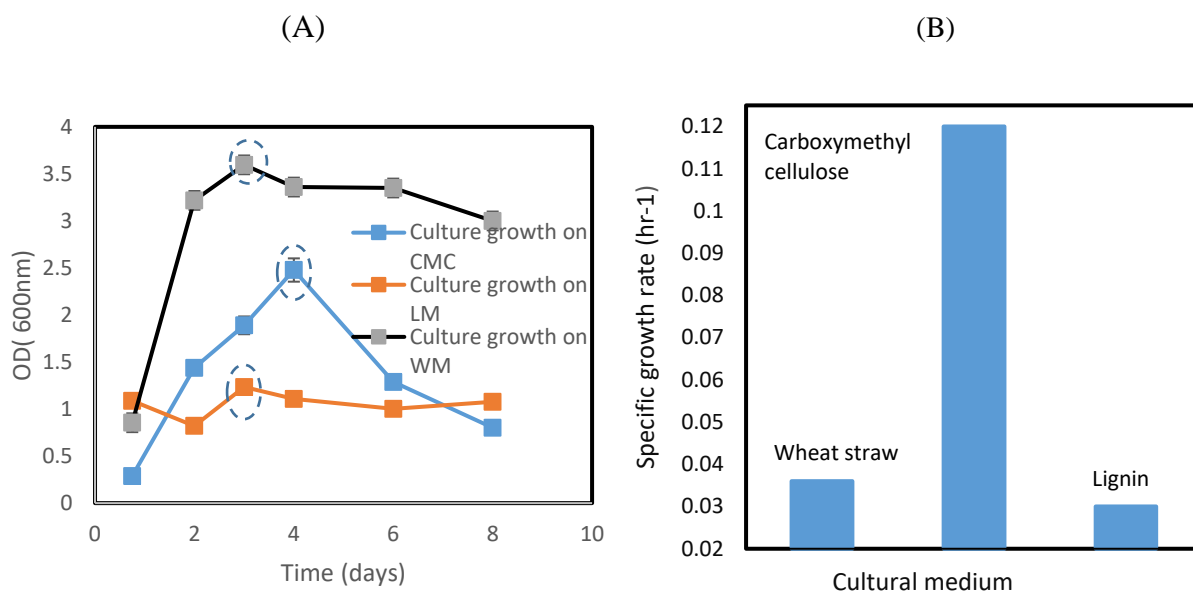


Figure 4.1: Plot of the growth pattern of *Pseudomonas putida* KT2440 on three different culture media. (A) growth pattern on Carboxymethyl cellulose medium (CMC), Lignin medium (LM) and Wheat straw medium (WM). (B) Specific growth rates on the three different media. Error bars are representative of the standard error of triplicate results

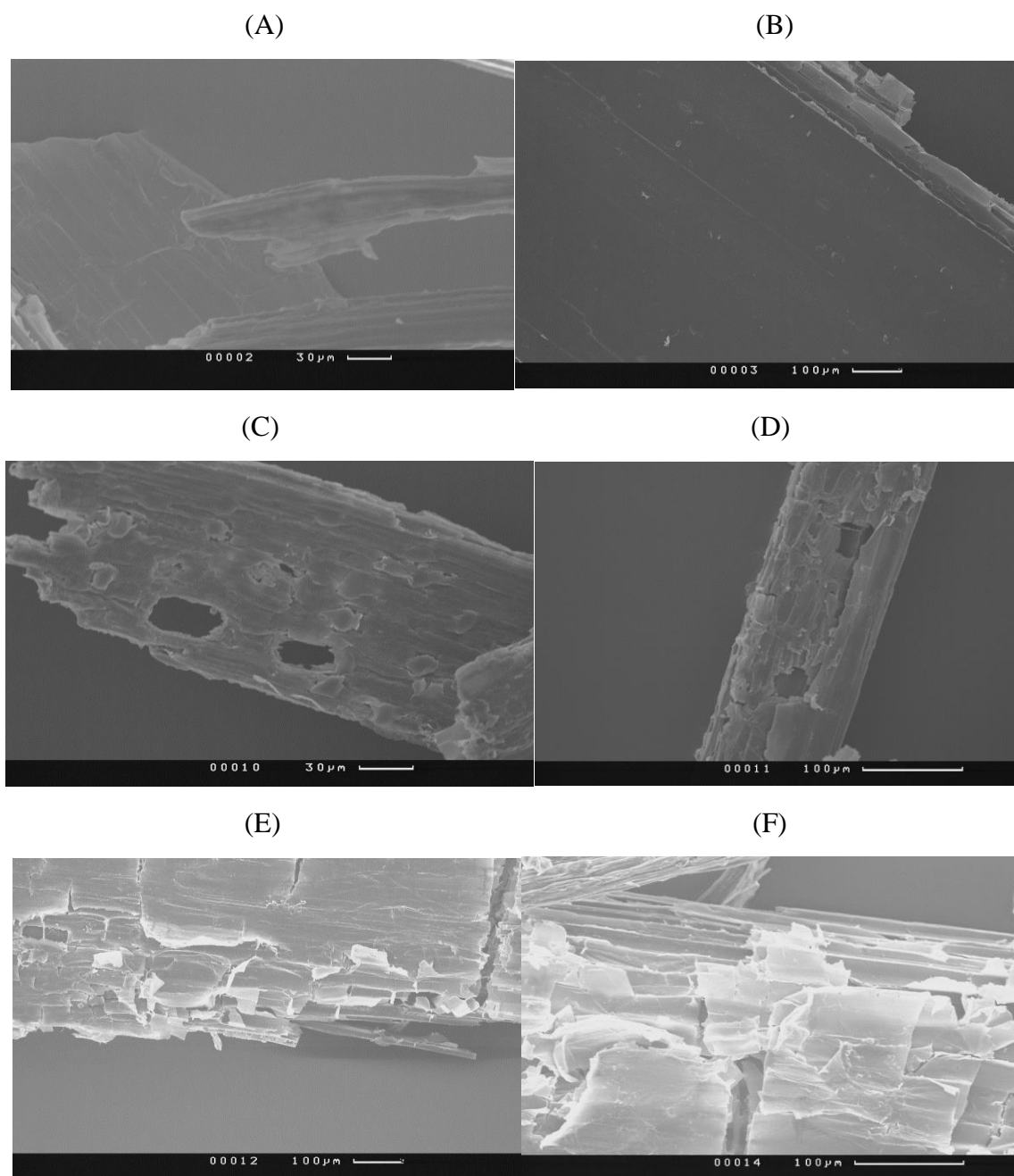
Figure 4.1B shows Specific growth rates of *Pseudomonas putida* on three different media, which are calculated using an equation described by Widdel, (2010):

$$\mu = \frac{2.303 (\log OD_2 - \log OD_1)}{(t_2 - t_1)} \quad (\text{Eq. 4.1})$$

Specific growth rate of *Pseudomonas* on CMC medium was the highest among specific growth rates on other media as the glucose was used as a carbon source for its growth and propagation, and it was around 0.12 hr⁻¹. While specific growth rate on wheat straw medium was 0.039 hr⁻¹, the growth on lignin medium was 0.030 hr⁻¹. Structurally, wheat straw has high carbohydrates content such as hexoses and pentoses, with less lignin content, however the microbe showed a comparable specific growth rate on both wheat straw and lignin media. In general, the bacterium would be expected to need more time to adapt and survive in these harsh conditions.

4.2 Morphological changes on wheat straw

Structural and physical changes are essential indicators of the effectiveness of a pretreatment process. To observe and characterize the morphological changes on the biomass, samples were examined by each pretreatment method under a SEM and result presented in Figure 4.2.



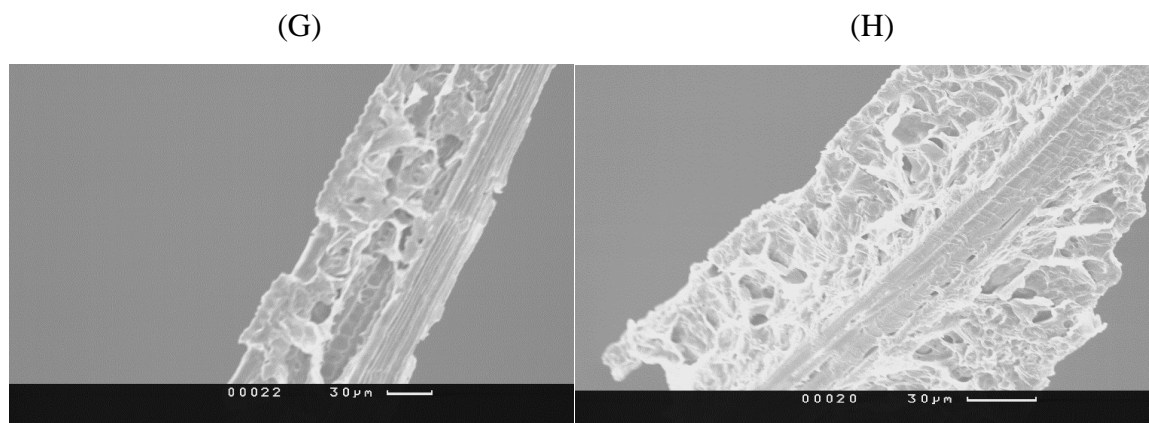


Figure 4.2: Morphological changes on wheat straw after different pretreatment conditions. Images (A) and (B) are the untreated wheat straw; (C) and (D) are wheat straw after pretreatment with microbubble; (E) and (F) are the wheat straw after biological pretreatment with *Pseudomonas putida*; (G) and (H) are the wheat straw after the combined pretreatment with both microbubbles and the biological organisms

Untreated straw (Figure 4.2 A and B) was observed to be physically intact with its morphology preserved, which is evidenced by the relatively smooth, densely packed surfaces. In contrast, the microbubble (see Figure 4.4 for size distribution) mediated treatment (Figure 4.2C and D) revealed wheat straw with clear porous structures on and through the straw surfaces. This effect results from the decreased rigidity and the re-ordering of fibers during pretreatment. This observation is corroborated by the findings of Cui et al., 2012 who reported a similar porous structure on wheat straw after pretreatment with a steam explosion at 200-220°C. Microbubble boundaries are highly charged interfaces, carrying and releasing potent free radicals in the containing medium. When in contact with a solid body (particles), the charges are readily deposited and effectively attack the surface, consequently degrading the particle physical structure. Ragnar et al., (1999) found that excited hydroxyl radicals resulted in the capture of one hydrogen from either the methyl groups or the carbon in the middle structure of lignin. The extent of surface damage can vary depending on the bubble surface charge magnitude, bubble, and particle size and carrier gas. Dosing charge-laden microbubbles can play a crucial role in the catalysis and cleavage of cellulose and hemicellulose and inadvertently, facilitating the release of sugar from the biomass.

Glucose concentration measurement reveals a slight increase (0.08mg/ml after 3:30hrs) with the incorporation of microbubbles during lignocellulosic biomass pretreatment (see Figure 4.3A). Typically, long glucose chains in cellulose link with each other via hydrogen bonds and are responsible for the formation of microfibril structures in cellulose. These bonds also connect microfibrils with hemicellulose moiety of the biomass (Roman, 2004). The energy of these

interfibrillar hydrogen bonds must be overcome to break up these microfibrils into separated fibers, and eventually release glucose moieties from the separated fibers (Janardhnan and Sain, 2011). The low result, likely due to the relatively short retention time with microbubbles, demonstrates, however, the potential of a microbubble in the pretreatment of lignocellulosic biomass.

In Figure 4.2 (E and F), there is a significant morphological change on wheat straw after pretreatment with *Pseudomonas putida*. The images reveal the presence of debris - crust-like fragments -- covered surface, known as fractions of the middle lamella. The presence of crust-like fragments indicates the absence or partial degradation of hemicellulose since the middle lamella is mainly made from hemicellulose (Kristensen et al., 2008). This improved result (0.159 mg/ml Figure 4.3B), compared to microbubble pretreatment, suggests that enzymes play a more influential role in biomass hydrolyses. Degradation of lignocellulosic biomass by *Pseudomonas putida* is attributable to the secretion of various groups of enzymes. Cellulases attack cellulose chains at random sites to produce glucose as a final product (Ibrahim and El-diwany, 2007). On the other hand, oxygenases cleave carbon double bonds in lignin by inserting oxygen atoms to form carbon monoxide as a final product (Bauer and Max, 1996). These results are consistent with the findings of Putnina et al., 2012 and Cui et al., 2012, when the authors pre-treated hemp fibers and wheat straw by steam explosion.

The result of combined pretreatment - microbubbles and *Pseudomonas putida* is presented in Figure 4.2 (G and H). Under this pretreatment condition, the wheat straw structure appears relatively loose, largely irregular and highly fibrous. But equally remarkable are the pores observed across the material surface. Similar structural changes were also reported by Gould, 1985 and Singh et al., 2013, who investigated the pretreatment of agricultural residues by alkali delignification combined with microwave. Considering the principal structure of lignocellulosic biomass, lignin is the most complicated component, and poses the greatest physical barrier for biomass hydrolysis. By disrupting the lignin structure of the biomass, microbubbles provide an easier and faster access for the enzymes realized from the microbe for cellulose digestion. The hydroxyl and superoxide radicals generated from collapsed microbubbles (Takahashi et al., 2007) readily attack hydrogen and β - glycosidic bonds in the biomass (Li et al., 2009a and b). In addition, hydroxyl radicals are easily transformed into superoxide radicals and vice versa (Ragnar et al., 1999), intensifying the metabolic process of *P.putida*.

This microbubble-microbe synergy should release more sugar than either of the individual methods. To test this, glucose concentration was measured for the combined pretreatment (see Figure, 4.3B). Here, wheat straw was first pre-treated with microbubbles for over three hours and the pretreatment continued with the addition of *Pseudomonas putida* for four (4) days. The final glucose concentration obtained from the combined pretreatment, was 0.27 mg/ml. The result of the combined technique is higher than either solo operations. However, the exact order in which the microbubble-microbe delignification of biomass occurs is largely unknown and therefore subject to further investigation.

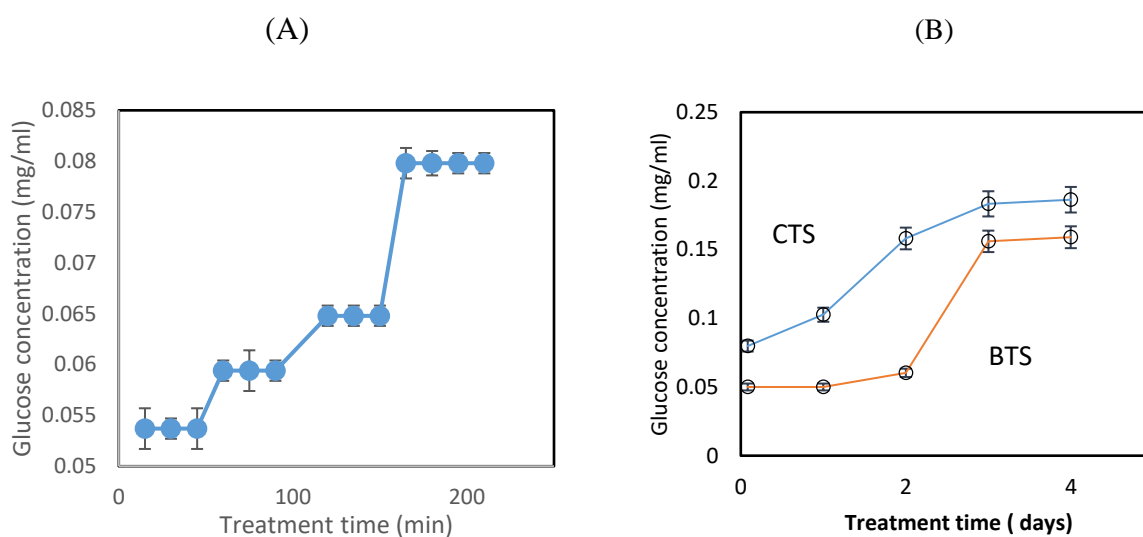


Figure 4.3: Plot of glucose concentration with time during pretreatment of lignocellulosic biomass. (A) Microbubble pretreatment. (Bi) Biological pretreatment of straw (BTS) (Bii) Combined pretreatment of straw (CTS) –microbubble and biological method. Increased glucose yield was reordered for combined pretreatment method. Error bars depict the standard deviations.

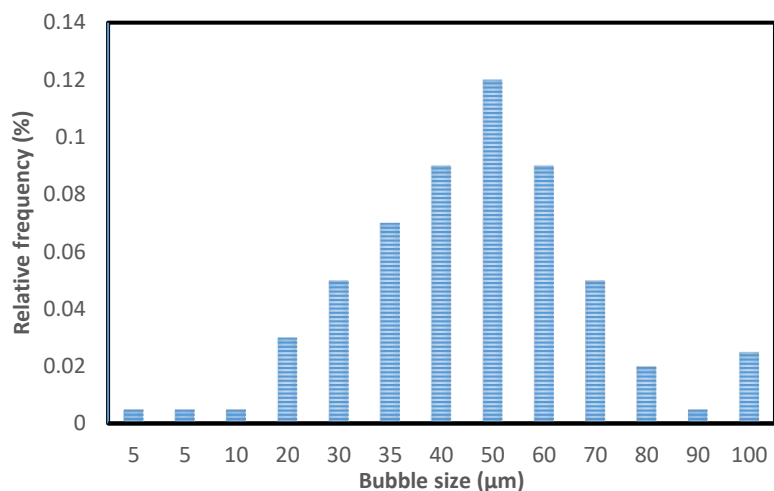


Figure 4.4: Microbubble size distribution plot. Sub-100 μm bubbles were largely produced. Second visible peak exists as a result of slight production damage on the microporous sparger

Figure 4.4 shows the microbubble size distribution used in this study. In average, these bubbles have diameters around 50 μm . Bubbles around this diameter tend to have a high interior pressure, leading to the shrinkage and collapse of the microbubble beneath the solution surface because of the dissolution of the interior gas by the surrounding solution but crucially, the surface of these bubbles becomes charged due to the adsorption of ions at the gas-liquid interface. The interior gas pressure increases as bubbles become smaller but importantly, free radicals can be generated by the collapse of microbubbles, resulting in a hot spot with extremely high pressure and temperature (Li et al., 2009).

4.3 Changes in the functional groups of the biomass

Apart from the physical changes, chemical changes to the biomass were assayed to characterize the variations in functional groups under the experimental conditions studied.

Figure 4.5 (A) presents FTIR-ATR readings of untreated wheat straw samples and wheat straw after treatment with microbubbles. At $750/710\text{ cm}^{-1}$ - a ratio of crystalline cellulose ($1\alpha/1\beta$) in the biomass (Yamamoto et al., 1996; Boisset et al., 1999 and Kumar et al., 2009). There was a slight but noticeable decrease in the absorbance, suggesting a crystalline cellulose decrease in the biomass. The decrease was in favor of the microbubble treated samples in comparison with the untreated samples. Boisset et al., (1999) observed a similar reduction on cellulosic substrate contents after treating with *Clostridium thermocellum* as did Yamamoto et al., (1996). Typically, the crystalline cellulose is more difficult to hydrolyse than amorphous cellulose. Therefore, reducing its amount in the biomass is crucial to the liberation of some inherent

glucose molecules and consequently, making the biomass more accessible for further digestion by cellulases (Boisset et al., 1999 and Yang et al., 2011).

Further, the $1098/900\text{ cm}^{-1}$ ratio defines the ratio of crystalline cellulose to amorphous cellulose. The result reveals a slight decrease in this ratio after microbubbles pretreatment compared with the untreated samples. This decrease was consistent with the result at 900 cm^{-1} , which is related to amorphous cellulose (Laureano-Perez et al., 2005). However, the amorphous cellulose absorbance at 900 cm^{-1} was unchanged after microbubbles pretreatment. The absorbance at 1745 nm , which relates to the carbonyl groups - the side chains of lignin molecules (Windeisen et al., 2007), was slightly decreased after microbubbles pretreatment.

The FTIR-ATR readings for both untreated wheat straw and bacterially treated wheat straw is presented in Figure 4.5(B). The absorbance of the crystalline ratio ($1\alpha/1\beta$) decreased significantly after biological pretreatment compared to the untreated straw. Interestingly, this outcome differs from results from previous studies. For example, Yang et al., (2011) reported a decrease in amorphous cellulose degradation by cellulases compared to crystalline cellulose. Fan et al., (1980) also reported the inability of cellulases to attack the crystalline portion of cellulose, which led to an increase in crystalline. In their study, the amorphous cellulose content decreased after pretreatment with the bacterium (Fan et al., 1980) in comparison with untreated samples as well as with different microorganisms (Yang et al., 2011). Crystalline cellulose is less hydrolysable than its amorphous counterpart, especially to microbes. However, *Pseudomonas putida* is unique for its metabolic versatility, effectively producing enzymes for degrading crystalline cellulose.

Additionally, the current results also revealed a decrease in the absorbance of carbon double bonds content of the biomass at 1595 cm^{-1} , which is related to the aromatic ring in lignin. Cleavage of the carbon double bond has been reported as one activity of this bacterium. Bauer et al., (1996) found that dioxygenase enzymes present in *Pseudomonas putida*, facilitate the cleaving of the carbon double bond in N-heterocyclic rings by inserting oxygen atoms, leading to the formation carbon monoxide as a final product. Also, Tu et al., (2013) demonstrated that *Pseudomonas spp* are effective in degrading ciprofloxacin as a result of carbon double bond cleavage via oxidation with manganese.

Further, the 1720 cm^{-1} absorbance identifies the carboxylic acids or ester groups in both hemicellulose and lignin (Sun et al., 2005). The result here shows a decrease in absorbance with

the microbe in comparison with the untreated biomass. At 1745 cm^{-1} , there was a significant reduction in the absorbance in comparison with untreated samples. This absorbance relates to the carbonyl bonds as well as the side chains of lignin (He et al., 2008 and Windeisen et al., 2007). Deconstruction of cellulose is problematic by the presence of lignin and hemicellulose as well as their derivatives. Delignification therefore, is an inevitable crucial step in deconstructing cellulose and eventually releasing exploitable monomers for microbial metabolism. *Pseudomonas putida* acts as a delignification agent, effectively decreasing the lignin content and complexes.

Application of microbubbles and *Pseudomonas putida* for the pretreatment of lignocellulosic biomass has improved the hydrolysis of the biomass, showing both physical and chemical changes and the consequent production of glucose. To improve the commercial viability of the pretreatment technique, therefore, further work is necessary for understanding the key physicochemical and biochemical mechanisms underpinning the technique and exploring options to improve glucose yield. One option is to increase the surface area of microbubbles by further decreasing bubble size as cellulose is a composite material with the surface structure of 3-5nm size. Dosing with hot microbubble to liberate cellulose is yet another. Crucially however, future studies to investigate methods to improve *p. putida* growth and consequently production of enzyme as the latter play a more influential role in glucose production is expedient. Provided substantial glucose yield can be obtained; the microbubble-microbe biomass processing technique offers many benefits including: decrease in capital and production cost in comparison to traditional techniques that utilize a substantial amount of chemicals and enzymes and high temperature and pressure.

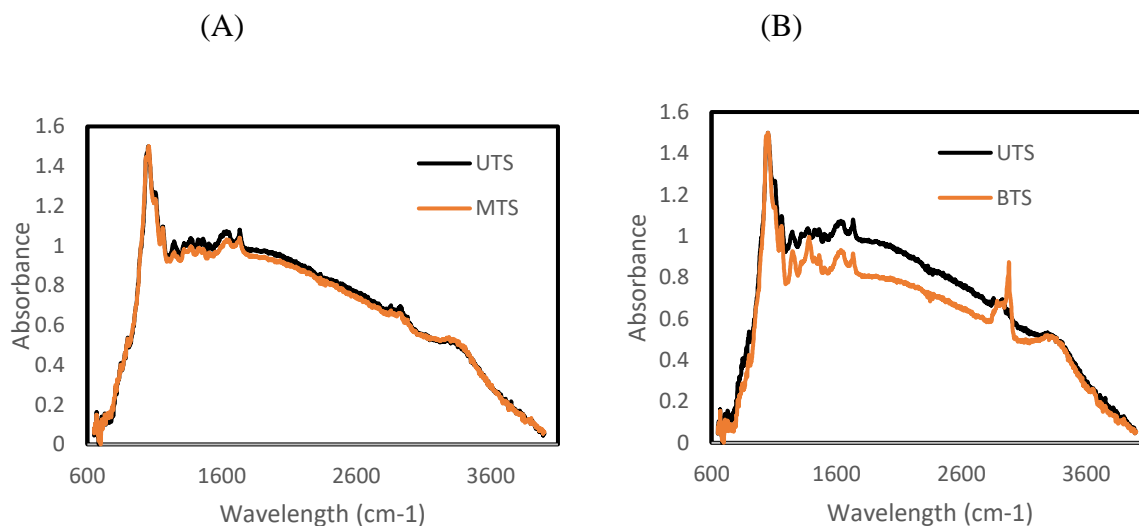
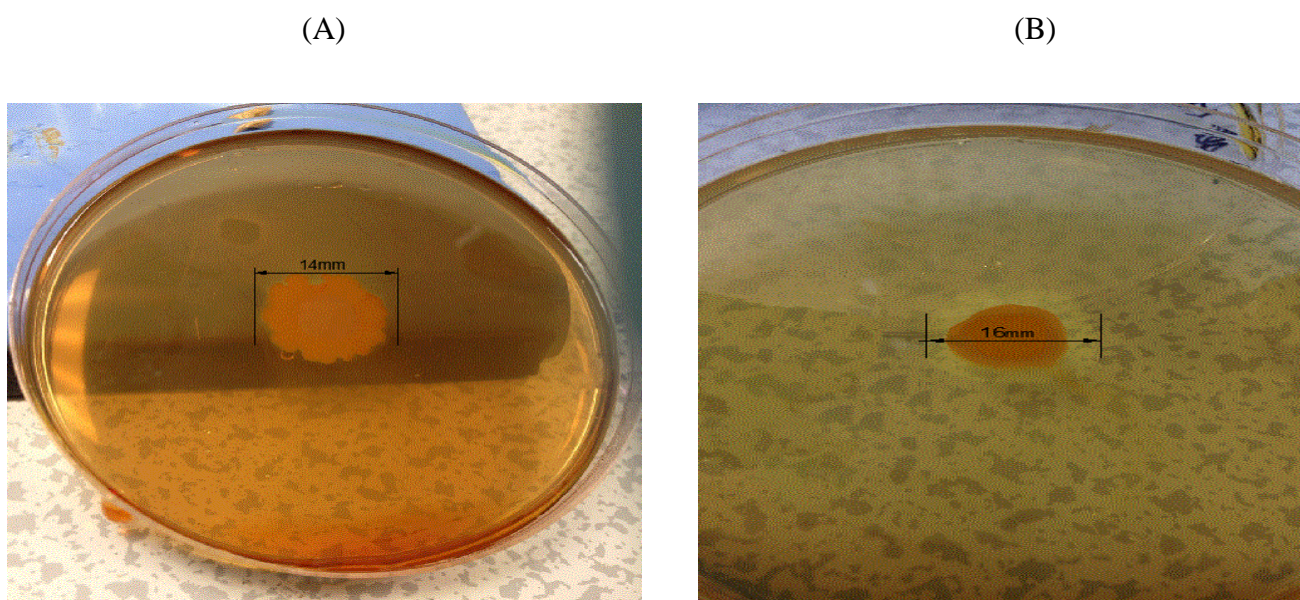


Figure 4.5: (A) FTIR-ATR spectrum of biomass after pretreatment with microbubbles (MTS) (B) FTIR-ATR spectrum of biomass after pretreatment with a bacterium (BTS). A more pronounced difference in the mid part of the absorbance spectrum, showing the effect of *Pseudomonas putida* on lignocellulosic biomass pretreatment. UTS is untreated samples.

4.4 *Pseudomonas* cellulolytic activities on Petri dishes

The cellulolytic activity of *Pseudomonas putida* KT2440 was tested qualitatively using Petri dishes and quantitatively by measuring enzymes activities, proteins concentrations, and specific enzymes activities. Figure 4.6 shows the average of the cellulolytic activities of *Pseudomonas Putida* KT2440 on both carboxymethyl cellulose and wheat straw agar media.



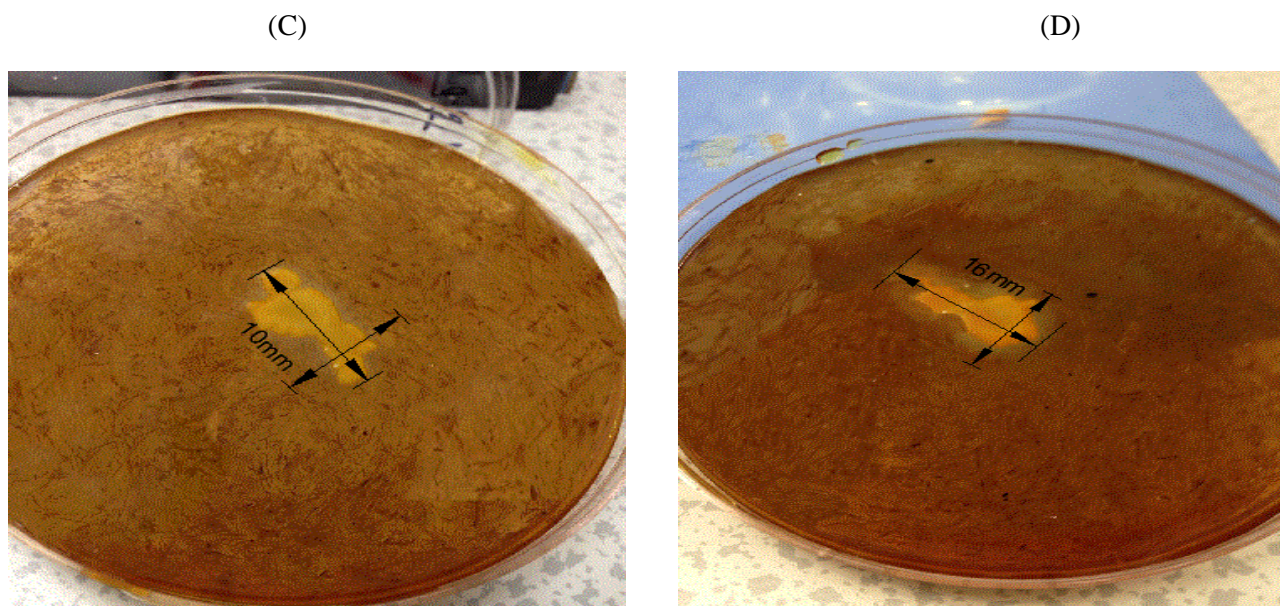


Figure 4.6: Cellulolytic activities of *Pseudomonas putida* on two media. A and B represent the cellulolytic activity on CMC after 3 and 4 days respectively. C and D represent cellulolytic activity on WSM after 3 and 4 days respectively.

Table 4.4.1: cellulolytic activities of *Pseudomonas putida* on Petri dishes

Culture media / Cellulolytic activity	After 3 days (Diameter mm)±SD	After 4 days (Diameter mm)±SD	After 5 days (Diameter mm) ±SD
Carboxymethylcellulose	14 ±1	16±1	16±1
Wheat straw	10±1	16±0.5	16±1

Cellulolytic activity of *Pseudomonas putida* was observed at its highest between 3- 5 days as it can be seen in Figure 4.1A; however, there was not significant change between the activities after 4 and 5 days of incubation as shown in the Figure 4.6 and Table 4.1. Therefore, 4 days of incubation at 30°C was chosen to collect cultural filtrates, to do the enzymatic activity tests and to finish the biological pretreatment with *Pseudomonas putida*. These results were consistent with the growth patterns on CMC and wheat straw media, which showed that the microbial activity on CMC medium is higher than on WS medium and therefore; it can be concluded that the cellulolytic activity on CMC is greater than on WS as cellulose is the main carbon source in both media.

4.5 Proteomics of cellulases enzymes

After the qualitative study, the next step was to measure this activity quantitatively by measuring the enzymes activities, protein concentrations, and specific enzymes activities. Knowing these parameters can build a milestone for future use and optimization of cellulases production and utilization from *Pseudomonas putida* KT 2440.

4.5.1 Crude enzymes activities

Sodium dodecyl sulfate - Polyacrylamide gel electrophoresis (SDS-PAGE) was used to run the samples after concentrated them with amicon tubes. Different protein bands were seen on SDS-PAGE, and their molecular weights were determined using the standard proteins M12 marker (See Figure 4.7). Crude enzymes activities were measured according to protocols described before at fourth day, when the cellulolytic activities reached its highest. Using amicon tubes increased the enzymes activities as a result of increasing the enzymes concentration. Using the amicon tubes increased the protein concentrations to about 280 % in wheat straw medium and about 61.5 % in CMC medium (Table 4.2). The membranes used in the amicon tubes have the ability to retain molecules above a specific molecular weight. However, the solutes with a molecular weight close to the nominal molecular weight limit may be only partially retained. Two factors can play important roles in the membrane retention, which are the molecular size and molecular shape. It is worth to note that the amicon Ultra 10K device — 10,000 NMWL was used in this study, and this is at least two times smaller than the molecular weight of protein solute mentioned in the literature reviews (Schell, 1987 and Lejeune et al., 1988). Concentrated proteins were applied on SDS-PAGE for 36 minutes and 200 voltages, and the resulting proteins bands with their approximate molecular weight can be seen in Figure 4.7.

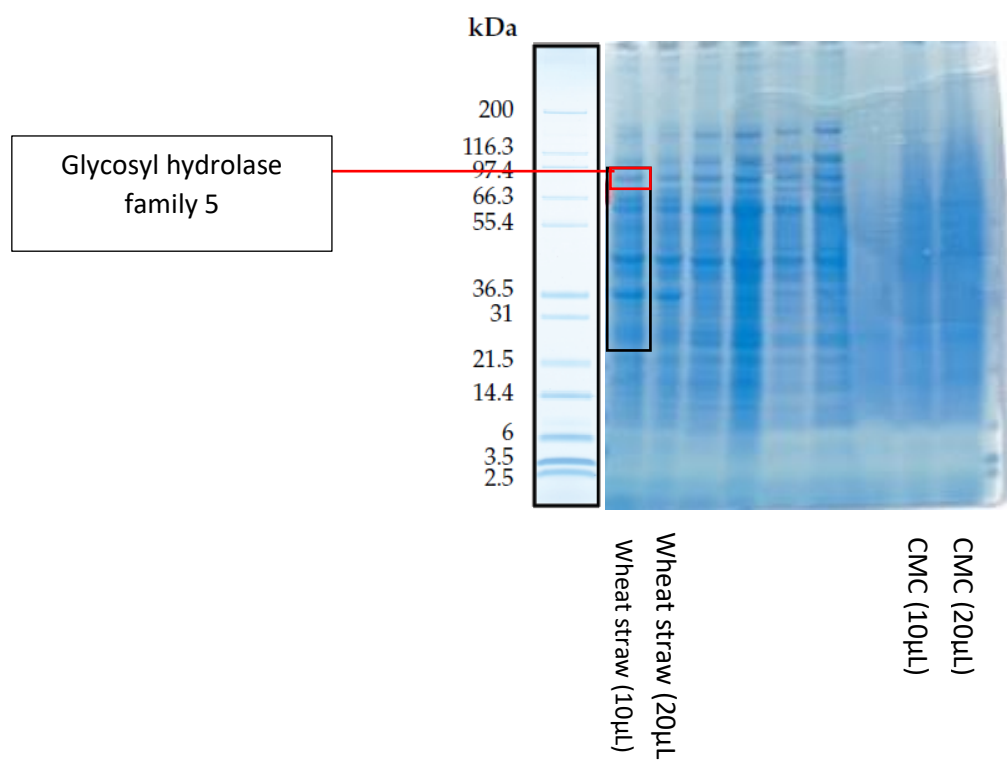


Figure 4.7: SDS-PAGE of *Pseudomonas putida* KT 2440 cultural filtrates showing the produced proteins. The black-coded bands represents the bands used in the In-gel digestion and analysed with LC-MS/MS, while the red-code band shows the identified protein, which has molecular weight around 96 kDa.

Table 4.2: Initial protein concentrations and concentrated protein concentrations with corresponding cellulases activities. Results are rerepresentative of triplicate readings.

Samples (Cultural filtrates)	Initial Protein concentration (mg/ml)	Concentrated Protein concentration (mg/ml)	CMCcase activity (U/ml)	FPase activity (U/ml)	β -glucosidase activity (U/ml)	Specific activity of CMCcase (U/mg)	Specific activity of FPase (U/mg)	Specific activity of β -glucosidase (U/mg)
Wheat straw	0.15	0.57	0.014	0.004	0.011	0.093	0.026	0.073
Carboxymethyl cellulose	0.13	0.21	0.012	0.002	0.011	0.092	0.015	0.084

4.5.2 Partial purification and precipitation of cellulases enzymes using ammonium sulfate salt

Ammonium sulfate was used to fractionate the produced proteins using different saturation concentrations. Following this step, enzymes activities were measured in every fraction. Different salt concentrations were used to precipitate different proteins in different fractions; however, 25 %, 50 %, 65 % and 90 % saturations with ammonium sulfate were utilized in this study. These saturations were chosen according to the protein concentrations in each step, precipitation of CMC material with proteins and depending on the information mentioned in

the literature reviews. Table 4.3 shows protein concentrations in each step of ammonium sulfate precipitation for both cultural media.

It can be seen from Table 4.3 that the highest protein precipitation was observed in 65% saturation in both culture media. However, at 25 % saturation, 11mg/ml of protein were precipitated from carboxymethyl cellulose medium in compared to 13.2 mg/ml in wheat straw medium. While, 0.8 mg/ml of protein was precipitated in CMC medium at 50 % saturation, 6 mg/ml of protein were precipitated from WS medium. Finally, 4.2 mg/ml of protein precipitated from WS medium at 90 % saturation compared to 2.2 mg/ml of protein in CMC medium. The amounts of precipitated proteins are dependent on the ionic strength in the medium. Generally, proteins have low solubility in pure water; however, this solubility can increase with increasing the ionic strength as there are extra organic ions bound to the protein's surface and this will prevent the aggregation of proteins. Adding ammonium sulfate to the protein's solution can withdraw the water molecules from these proteins and this leads to aggregate and precipitate of protein's molecules within the solution. While, the first case is called 'salting in', the second case is called 'salting out' (Koolman and Roeham, 2005). These samples were run on SDS-PAGE for 36 minutes and 200 voltages, to identify proteins, which were precipitated in each fraction of ammonium sulfate saturation concentrations. However, there was an undesirable interaction between CMC material and the ammonium salt, and this led to form a gel-like aggregation at the bottom of precipitation vessel. Accordingly, it was suggested that using ammonium sulfate in precipitation of cellulases produced on CMC medium is not recommended and alternative method needs to be used for precipitation and purification purposes. Figure 4.8 shows SDS-PAGE for each fraction of ammonium sulfate saturation concentration.

Table 4.4.3: Enzyme activity of various cellulolytic enzymes during different steps of ammonium sulfate fractionation. The results are representative of triplicate readings.

Medium	Ammonium sulphate precipitation (% saturation)	Precipitated volume (ml)	Protein concentration mg/ ml	Total protein concentration mg	CMCase activity (U/ ml)	FPase activity (U/ml)	β -glucosidase activity (U/ml)	Specific activity of CMCase (U/mg)	Specific activity of FPase (U/mg)	Specific activity of β -glucosidase (U/mg)
CMC	0	44	0.11	4.84	0.012	0.002	0.011	0.092	0.015	0.084
	25	11	1	11	0.09	1.26	0.03	0.008	0.114	0.003
	50	5	0.16	0.8	0.10	0.093	0.019	0.12	0.116	0.024
	65	25	0.08	4	0.022	0.031	0.058	0.006	0.008	0.015
	90	22	0.1	2.2	0.03	0.010	0.024	0.012	0.004	0.011
Wheat straw	0	40	0.08	3.2	0.014	0.004	0.011	0.092	0.015	0.084
	25	11	1.2	13.2	0.006	0.054	0.051	0.0004	0.004	0.004
	50	5	1.2	6	0.2	0.093	0.19	0.03	0.02	0.03
	65	5	0.85	4.25	0.023	0.073	0.287	0.006	0.017	0.067
	90	6	0.7	4.2	0.06	0.040	0.08	0.014	0.001	0.02

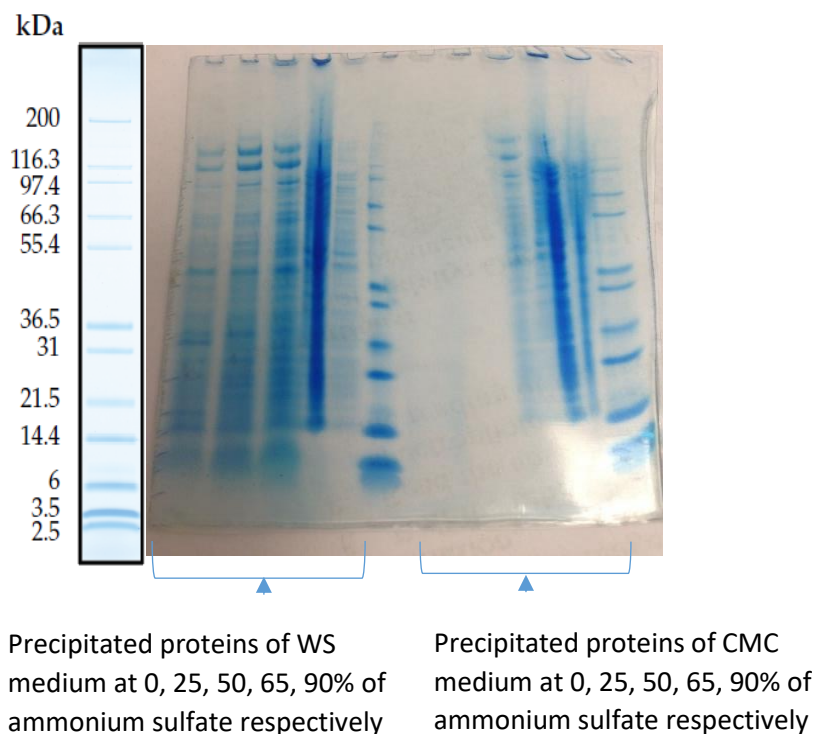


Figure 4.8: SDS-PAGE for proteins after fractionation with ammonium sulfate.

Figure 4.9 shows the enzymes activities in two cellulose-contained media, CMC, and wheat straw after different ammonium sulfate saturations. From Figure 4.9, it can be seen that CMCase enzymes were precipitated at 25 % and 50 % in CMC medium (Figure 4.9A), and at 50% in wheat straw (Figure 4.9B). On the other hand, FPase enzymes were precipitated at 50% in both CMC and wheat straw media. In contrast, β -glucosidase enzymes were precipitated at 65% in both CMC and wheat straw media. It is worth to note that the ammonium salt could not precipitated these enzymes at any particular saturation and thus, the enzymes activities were observed in almost all the saturations with different percentages and this might suggest that cellulases are not recommended to be precipitated and/or purified using ammonium sulfate salts and other purification techniques need to be explored. Figure 4.10 shows the specific enzymes activities in two cellulose-contained media, CMC, and wheat straw after different ammonium sulfate saturations by dividing the enzymes activities over the protein concentration at each saturation.

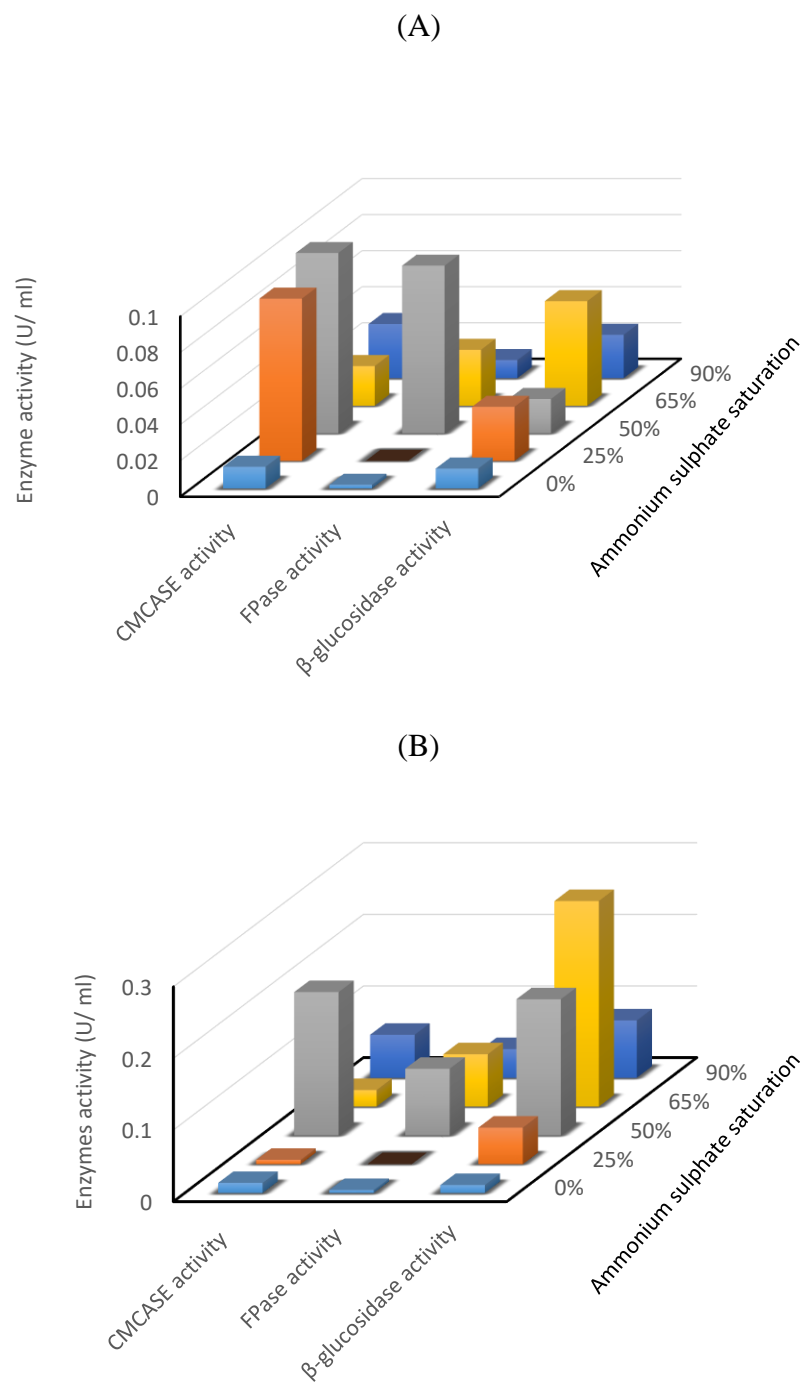


Figure 4.9: Enzymes activities of cellulases on different media. (A) CMC medium (B) Wheat straw medium

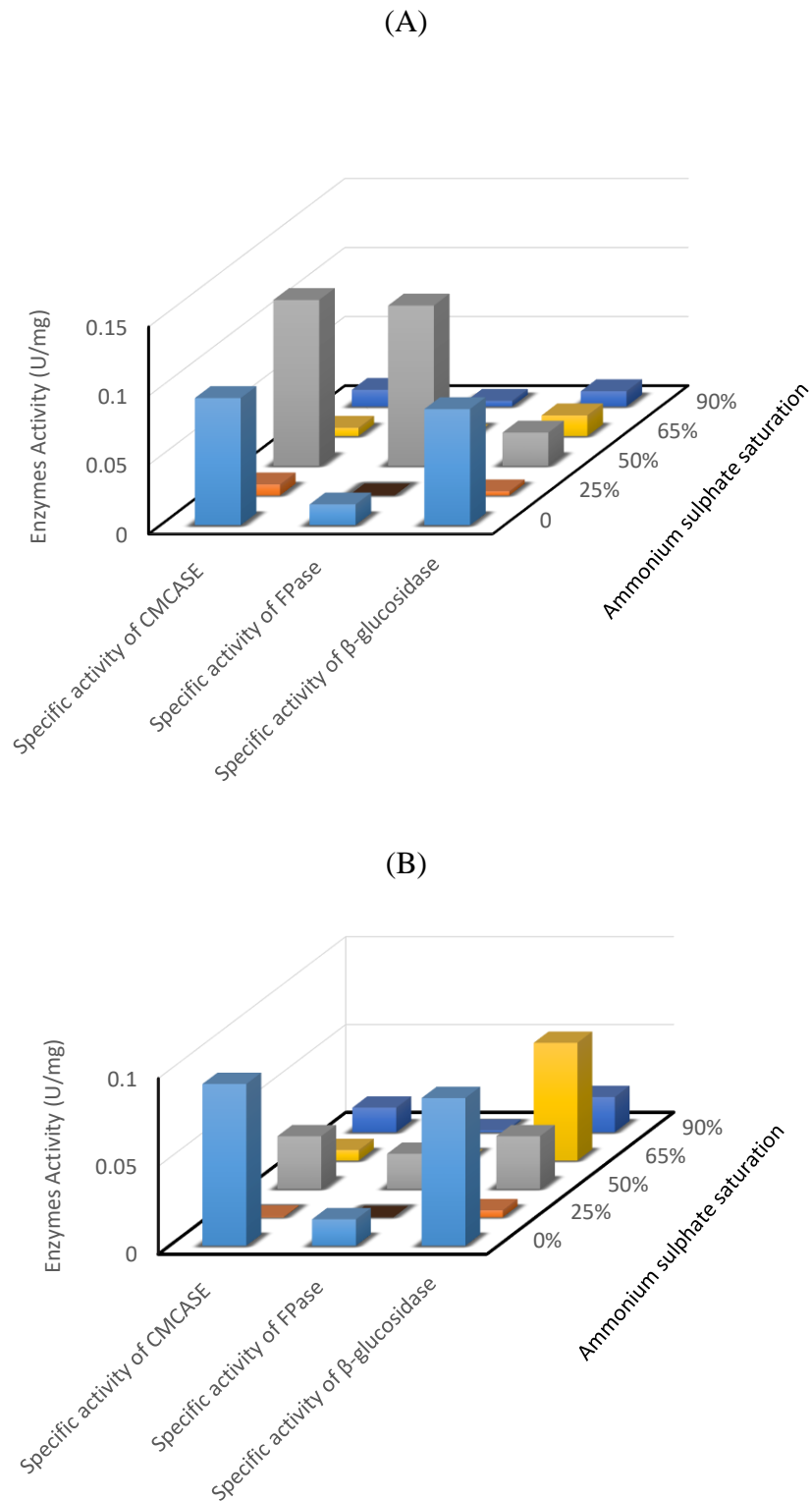


Figure 4.10: Specific enzymes activities on different cellulose contained media (A) CMC (B) wheat straw

Interestingly, this bacterium showed reasonable cellulolytic activity in comparison with other cellulolytic microbes reported previously. For example, Sethi et al., (2013) have studied the optimization of the cellulases production from bacterial species isolated from soil. The isolated species were *Pseudomonas fluorescens*, *Bacillus subtilis*, *E. coli*, and *Serratia marcescens* and comparing the cellulolytic activity of *Pseudomonas putida* KT 2440 with all the isolated species, it can be clearly observed that this bacterium has higher cellulolytic activity than all these isolates, except *Pseudomonas fluorescens*, which shows higher cellulolytic activity when the glucose concentration increased to 5% (Sethi et al., 2013). On the other hand, the fungal species were also isolated from soil by Ram et al., (2014), and all these fungal isolates showed a lower cellulolytic activity than *Pseudomonas putida* KT 2440, when the highest zone of clearance observed was 7 mm by PISS-3 fungal strain (Ram et al., 2014), while the highest zone clearance noticed in the current study was 16 mm on both carboxymethyl cellulose and wheat straw media. Also, this bacterium shows a comparable cellulolytic activity with *Cellulomonas*, *Bacillus*, and *Micrococcus spp*, which showed 0.0172, 0.0165 and 0.0121 U/ml respectively (Immanuel et al., 2006) in comparison with 0.014 U/ml obtained in the current study.

4.5.3 LC-MS/MS analysis of cellulolytic proteins

Trypsin is known as the most commonly used protease for in-gel protein digestion and it hydrolyses the peptide bonds in which the carbonyl group is followed by either Lysine (Lys) or Arginine (Arg) moiety, with one exception when Lysine and Arginine are N-linked to aspartic acid (Asp). In addition, this cleavage will not happen if the amino acid, Proline, is connected the carboxyl side of Lysine and Arginine. Because the long digestion times, the digestion process was kept overnight, and the post-digestion preparations steps were followed in the next day (Hustoft et al., 2010). Before Liquid chromatography–mass spectrometry (LC-MS) analysis (See appendix H), removing the buffers and salts added during the sample preparation were carried out using ZipTip, which helped to concentrate and purify the samples for delicate downstream analysis (Capelo et al., 2009). The results from the Proteome Discoverer 1.4 software package showed that the cellulases were secreted by *Pseudomonas putida* KT 2440 to hydrolyse the cellulose content of wheat straw. Typically, these enzymes are classified into families, and the produced enzymes can be identified as a family rather than as an individual enzyme. LC-MS/MS analysis of cellulolytic proteins showed that glycosyl hydrolase family 5 was produced with an average molecular weight about 96.6 (kDa), and the calculated isoelectric point was 6.40. The number of amino acids in the identified glycosyl hydrolase family protein was 868. This result is crucial for further production and purification of these enzymes and

represents supporting evidence about the ability of *Pseudomonas* to produce cellulases during its growth on wheat straw as a carbon source. The produced cellulases are different from what have been mentioned in the literature reviews of *Pseudomonas* as a genus (Schell, 1987 and Lejeune et al., 1988). Knowing the molecular weight, calculated pI and the number of amino acids are very important details for future separation and purification of cellulases enzymes from *Pseudomonas putida* KT2440. It is worth mentioning that the identified protein family was a part of large protein library, which was identified from around 500 proteins with various structural and catalytic activities.

4.6 Conclusions

An alternative lignocellulosic biomass pretreatment technique using microbubbles and *Pseudomonas putida* at room temperature has been investigated. Physical changes to the biomass structure as well as changes in the functional groups are aspects that were affected by the pretreatment technique. Microbubbles generated free radicals that attacked and disintegrated biomass lignin, making cellulose more accessible for hydrolysis. Further pretreatment with *Pseudomonas putida* caused considerable changes in both the morphology and functional groups content of the biomass, enhancing the glucose yield. The synergy between microbubbles and microbes in biomass processing offers some prospective benefits as a pretreatment technique for biofuel production. Finally, the cellulolytic activity of *Pseudomonas putida* KT 2440 was thoroughly investigated and cellulases activities were measured. Also, the molecular weight of glycosyl hydrolase family 5 (the family has all the cellulases enzymes from *Pseudomonas*) was determined as an outcome of this study as well as measuring the enzymatic activities. However, the main drawback to this pretreatment technique is the low glucose yield, which can be improved by increasing the biodigestibility of the biomass, and consequently release more glucose. To increase the biodigestibility of the biomass, a synergistic approach between ozonolysis and cellulolytic microorganism-*Pseudomonas putida* at room temperature will be investigated in the next chapter. Subsequently, the produced glucose can be used as a carbon source in the fermentation process, which will be carried out by *Zymomonas mobilis* cells.

Chapter 5

Exploiting ozonolysis-microbe synergy for biomass processing: Application in lignocellulosic biomass pretreatment

Overview

Pretreating lignocellulosic biomass is an energy and time-consuming process. To enhance the pretreatment method in chapter 4, a synergistic approach between ozonolysis and cellulolytic microorganism-*Pseudomonas putida* at room temperature is explored in this chapter. Ozone is a strong oxidative agent that reacts with lignin by attacking the carbon-carbon double bonds, while *P. putida* preferentially hydrolyses the exposed cellulolytic parts of the biomass to simple sugars. The results from SEM and FTIR-ATR show a significant reduction in lignin and cellulose contents, leading to relatively high sugar recovery. The glucose concentration increases coincidentally with the ozonation duration, and After 24 h however, the concentration reached 1.1 mg/ml, a 323 % increase compared with results after 2 h. Increasing the ozonation time to 24 h reduced the biological pretreatment time by 50% but crucially, increases microbial biomass. This approach has potentially high ramifications particularly for industries exploiting lignocellulosic biomass as a feedstock for bioethanol production.

5.1 Measuring the ozone concentrations

An ozone generator (Dryden AQUA, UK) was used to generate ozone, and the concentration of the generated ozone was determined using the method described by Rakness et al., (1996). 100 ml/min flow rate was calibrated to ascertain the ozone concentrations and used in all following experiments as it has the highest ozone concentration. Two ozone concentrations - 6.67 mg/L and 8.87 mg/L -- were explored at varying exposure times (2, 6, 12, 24 h) to determine a reaction time long enough to allow substantial oxidation of the biomass.

Table 5.1: Ozone concentrations with flow rate

Ozonation level	mg/L	
1	8.869	
2	6.678	
3	6.12	

5.2 Effect of pH and ozone on the functional groups

Figure 5.1 presents the FTIR-ATR spectrum for wheat straw biomass after microbubble-mediated ozonolysis (MMO) for 2 h at two pHs (3, 7) and ozone-rich microbubbles followed immediately with the microbial application (MMO-M). Two regions were identified as reaction sites for both ozone and microbial pre-treatment. The first is related to the cellulose content of the biomass, which ranges from $\sim 710\text{ cm}^{-1}$ to $\sim 1100\text{ cm}^{-1}$ wavelength for both amorphous and crystalline cellulose (Yamamoto et al., 1996; Boisset et al., 1999; Kumar et al., 2009 and Laureano-Perez et al., 2005). The second region is related to the lignin content of the biomass, $\sim 1595\text{ cm}^{-1}$ (Bauer et al., 1996). Under the acidic condition, the MMO-M pre-treatment (Figure 5.1B) resulted in a considerable decrease in both amorphous and crystalline cellulose as well as lignin content, particularly at an ozone concentration of around 8 mg/L. There was not much difference however between MMO and MMO-M pretreatment under acidic condition and 6 mg/L ozone concentration (Figure 5.1A). Pretreatment under neutral pH (Figure 5.1 C and D), only resulted in a slight decrease in cellulose and lignin contents of the biomass at ozone concentration around 6 mg/L and at higher ozone concentration, proved counter-productive. Also, there was no observable difference in performance between MMO and MMO-M

pretreatments. pH is a system parameter that significantly affects the release and yield of radicals as well as their reaction rate during the ozonation process (Ragnar et al., 1999). Radical species yield increases under an acidic condition in comparison with the higher pHs, leading to more effective hydrolysis of organic substrates (Ragnar et al., 1999). Furthermore, microbubble's acceleration of the formation of hydroxyl radicals during ozonation (Ragnar et al., 1999), contributes to the improved yield recorded.

The cellulose crystalline ratio (α/β), calculated by dividing absorbance at 750 cm^{-1} by absorbance at 710 cm^{-1} , was slightly decreased during all pretreatment combinations, suggesting that cellulose crystallinity was decreased by ozone. Sakai and Uprichard, (1991) have reported the effect of ozone on β -glucosidic bonds of cellulose, and showed its cleavage rate as 1.8 times faster than α -glucosidic bonds. This rate relies, however, on diffusion rate of ozone in water (Sakai and Uprichard, 1991). The decrease in cellulose crystallinity means decreasing the complexity of cellulose hydrolyses by cellulases. The complexity of crystalline cellulose hydrolyses was reported by Fan et al., (1980) as a major barrier to cellulose digestibility by cellulases. Similarly, Park et al., (2010) also showed that amorphous cellulose was the easier part of cellulose to hydrolyse.

The crystalline to amorphous cellulose ratio result was obtained by reading absorbance at 1098 cm^{-1} and 900 cm^{-1} . After MMO-M pretreatment, there was a small change recorded in the absorbance at 900 cm^{-1} (circled region in Figure 5.1B), which is absorbance of amorphous cellulose. The slight decrease in amorphous cellulose demonstrates the cellulolytic capability of *Pseudomonas putida*, but crucially, highlights its delignification tendencies. The implication of the latter is that *Pseudomonas putida* can also utilize lignin as a carbon source, and when present with cellulose, causes a diversion in the metabolic activity of the microbe. This outcome corroborates the earlier findings of Mulakhudair et al. (2016) who cultured *Pseudomonas putida* in lignin medium and observed an increase in microbial biomass.

Clearly, there was a visible change in absorbance at 1595 cm^{-1} (circled region in Figure 5.1B), which is the carbon double bonds absorbance. Carbon double bonds are typically the primary target site for cleavage by ozone. The result agrees with the findings of Kuvshinov et al., (2014) and García-cubero et al., (2009), who reported that ozone application was effective in attacking carbon double bonds, producing non-toxic esters. Kaneko et al., (1983) also reported the selective reaction of ozone with unsaturated carbon double bonds.

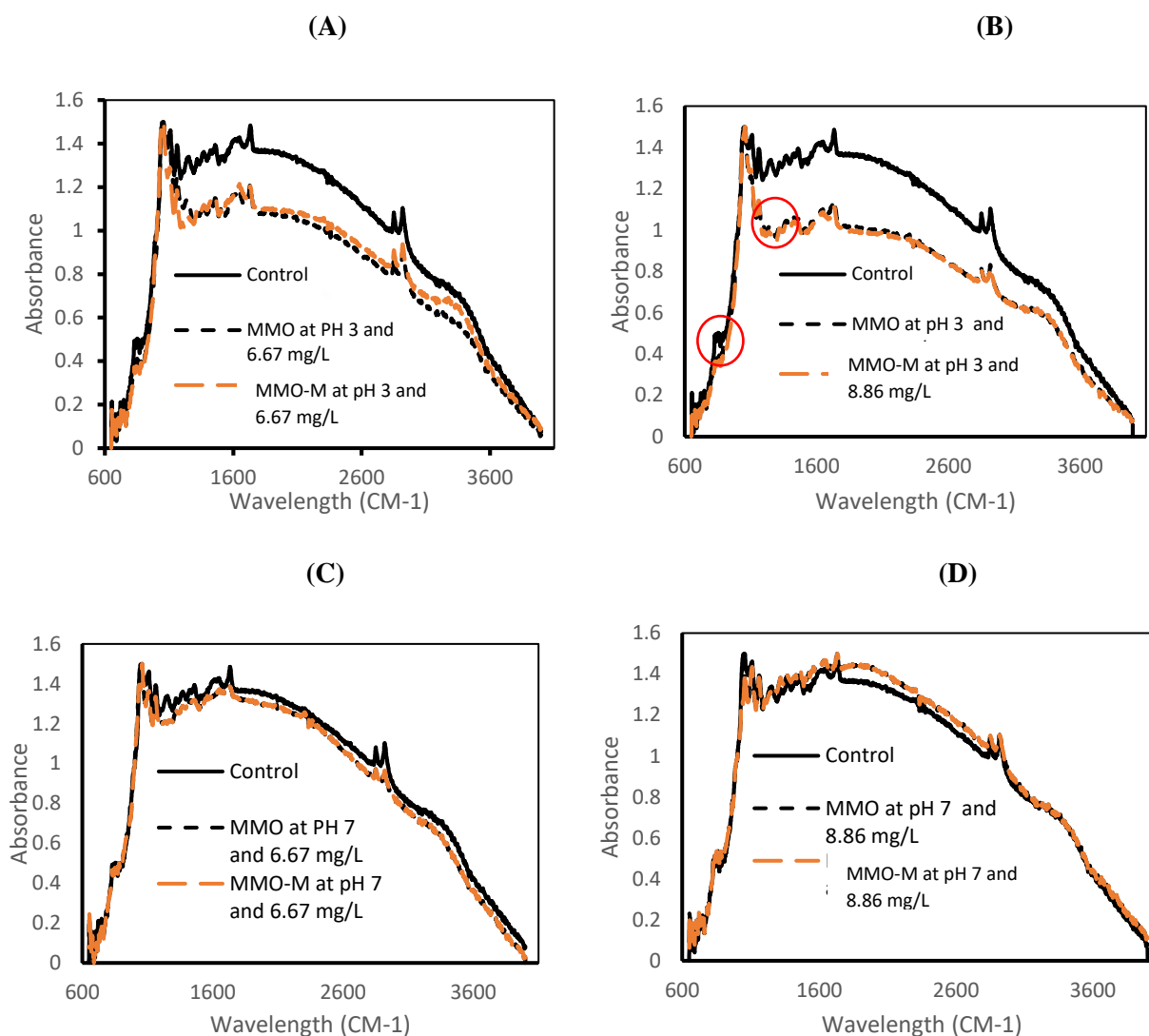


Figure 5.1: FTIR-ATP spectrum of lignocellulosic biomass after MMO and MMO-M pretreatments. (A) MMO at pH 3 and 6.67 mg/L ozone concentration and MMO-M at pH 3 and 6.67 mg/L ozone concentration (B) MMO at pH 3 and 8.86 mg/L ozone concentration and MMO-M at pH 3 and 8.86 mg/L ozone concentration (C) MMO at pH 7 and 6.67 mg/L ozone concentration and MMO-M at pH 7 and 6.67 mg/L ozone concentration. (D) MMO at pH 7 and 8.86 mg/L ozone concentration and MMO-M at pH 7 and 8.87 mg/L ozone concentration. The readings are representative of triplicate results.

5.3 Effect of pH and ozone on the morphological characteristics

Figure 5.2 shows a comparison between untreated and treated wheat straw under various pretreatment conditions. In Figure 5.2A, untreated biomass with its physical and morphological integrity are seen to be relatively intact. This is evident in the largely smooth surface with fewer cracks, and densely packed surface with ordered structure.

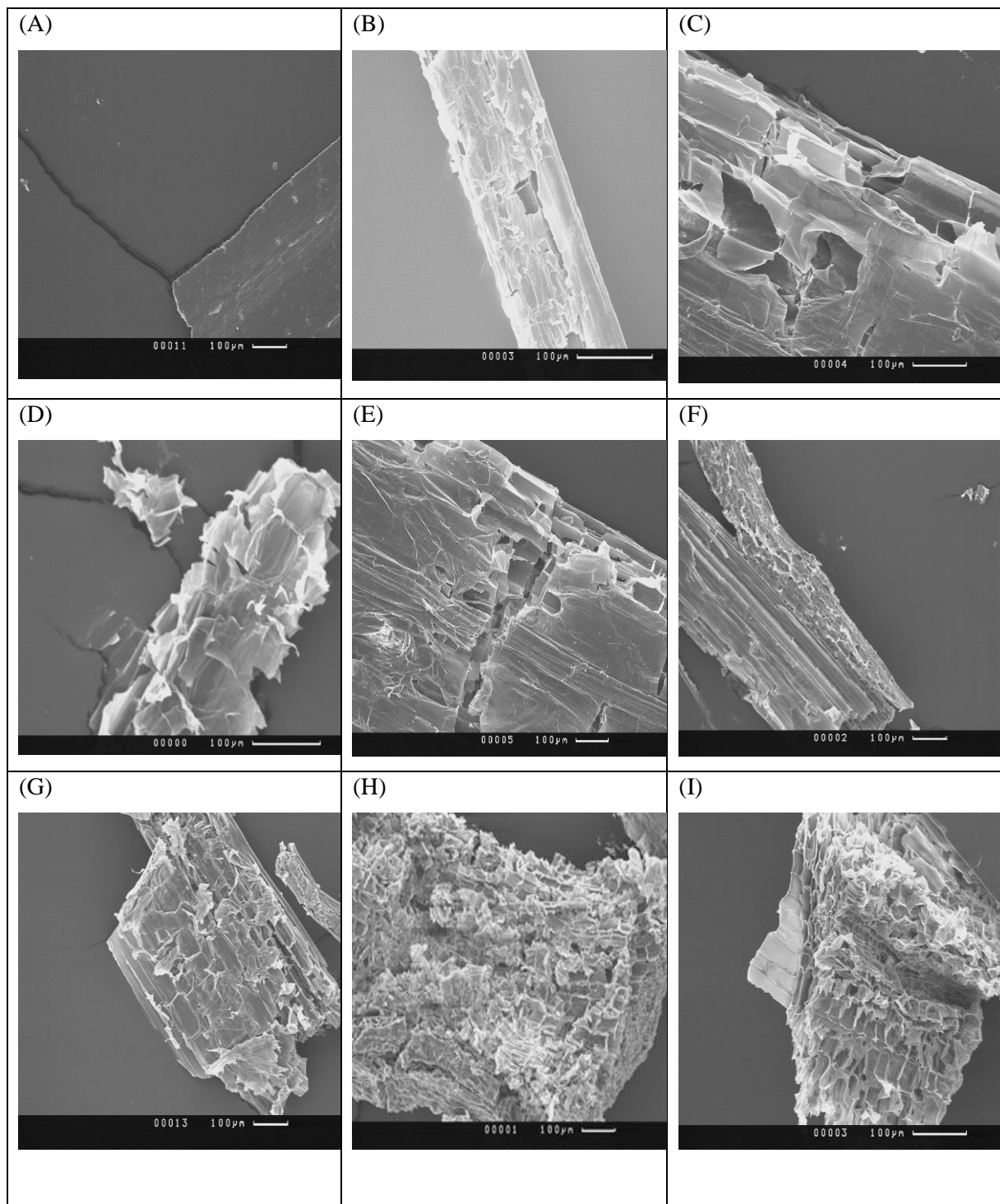


Figure 5.2: Morphological changes on wheat straw after MMO and MMO-M pretreatments for 2 h. (A) Untreated wheat straw. (B) MMO at pH 7 and 6.67 mg/L ozone concentration. (C) MMO-M at pH 7 and 6.67 mg/L ozone concentration. (D) MMO at pH 7 and 8.86 mg/L ozone concentration. (E) MMO-M at pH 7 and 8.86 mg/L ozone concentration. (F) MMO at pH 3 and 6.67 mg/L ozone concentration. (G) MMO-M at pH 3 and 6.67 mg/L ozone concentration. (H) MMO at pH 3 and 8.86 mg/L ozone concentration. (I) MMO-M at pH 3 and 8.86 mg/L ozone concentration.

In contrast, Figure 5.2 (B, C, D, E, F, G, H and I) shows morphological changes in wheat straw after MMO pretreatment for 2 h at both pHs (3, 7), and ozone concentrations (6.67 and 8.87 mg/L). From these images, it can be seen that there were substantial changes in the morphology of wheat straw and loss of its structure after pretreatment as well as rugosity on wheat straw surface (Figure 5.2B, C, D and G). However, MMO pretreatment at pH 3 and 8.86 mg/L (Figure 5.2H and I) caused a substantial removal of lignin and some of the internal microfibers clearly appeared in comparison with other pre-treatments. Some of these changes have already been previously reported by others authors. For examples, Souza- Correia et al., (2013) observed surface morphology in sugar cane after 4 h of ozone treatment and confirmed that these changes were due to oxidation by ozone. In addition, De Barros et al., (2013) exposed sugar cane bagasse and straw to ozone and observed the formation of multi-porous structures on the biomass surface after treatment for ~1 h. The reaction of ozone with organic substrates is achieved by ionic cyclo-addition, resulting in the cleavage of unsaturated bonds and activation of the aromatic bonds (Sakai and Uprichard, 1991).

Figure 5.2I shows morphological changes on wheat straw after MMO-M (at pH3 and ozone concentration 8.87 mg/L). Holistically, there is a dramatic change in the visual aspect with much debris on its surface. Kristensen et al., (2008), described this debris, as part of the middle lamella (composed mainly from hemicellulose) of the cell wall, which separates primary and secondary cell walls in plants. The porous structures observed on the wheat straw used in this study is consistent with the result reported by Mulakhudair et al. (2016), when the authors explored microbubble mediated pretreatment of lignocellulosic biomass.

Interestingly, glucose was liberated during the MMO process. This is largely attributable to microbubble as the free radicals generated around the gas-liquid interface can attack the lignin, facilitating hydrolysis (Doe., 2006 and Mulakhudair et al., 2016). The glucose concentration measured reached its highest after MMO at 8.87 mg/L and pH3 (Table 5.2) combined with MMO-M. These observations with other results from FTIR-ATR and SEM strongly suggest that acidic pH and 8.87 mg/L ozone concentration are effective conditions in the pretreatment of lignocellulosic biomass using MMO method.

Table 5.2: Glucose production at varying ozone and pH levels under both MMO and MMO-M pretreatments.

Treatment	Ozonation time (h)	Glucose Produced (mg/ml)±SD	
		MMO	MMO-M
6.67 mg/L at pH7	2	0.0145±0.002	0.071±0.005
8.87 mg/L at pH7	2	0.022±0.007	0.16±0.004
6.67 mg/L at pH3	2	0.015±0.002	0.057±0.008
8.87 mg/L at pH3	2	0.057±0.005	0.26±0.01

5.4 Effect of ozone exposure time on lignocellulosic biomass

Results from table 5.2 reveals that acidic pH and an ozone concentration of 8.87 mg/L gave the best result. Subsequent experiments were conducted under these conditions while varying the exposure time (6, 12, 24) h to ascertain the effect of ozone exposure time. It is worth mentioning that in the subsequent tests, the morphological changes in the biomass were not reported, as no difference was noticeable on the physical appearance of the lignocellulosic biomass with prolonged pretreatment beyond 2 h. Therefore, the two parameters monitored in the subsequent experiments, are FTIR-ATR spectrum and glucose yield.

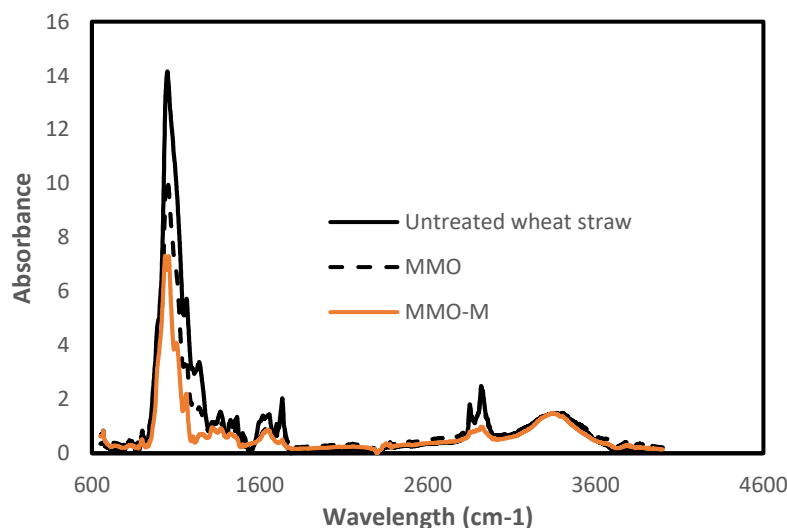


Figure 5.3: FTIR-ATR spectrum of biomass after MMO and MMO-M pretreatment for 6 h at pH 3 and ozone concentration of 8.87 mg/L. Spectra have been normalised at 710-1100 cm^{-1} and 1500-1600 cm^{-1} . The readings are representative of triplicate results.

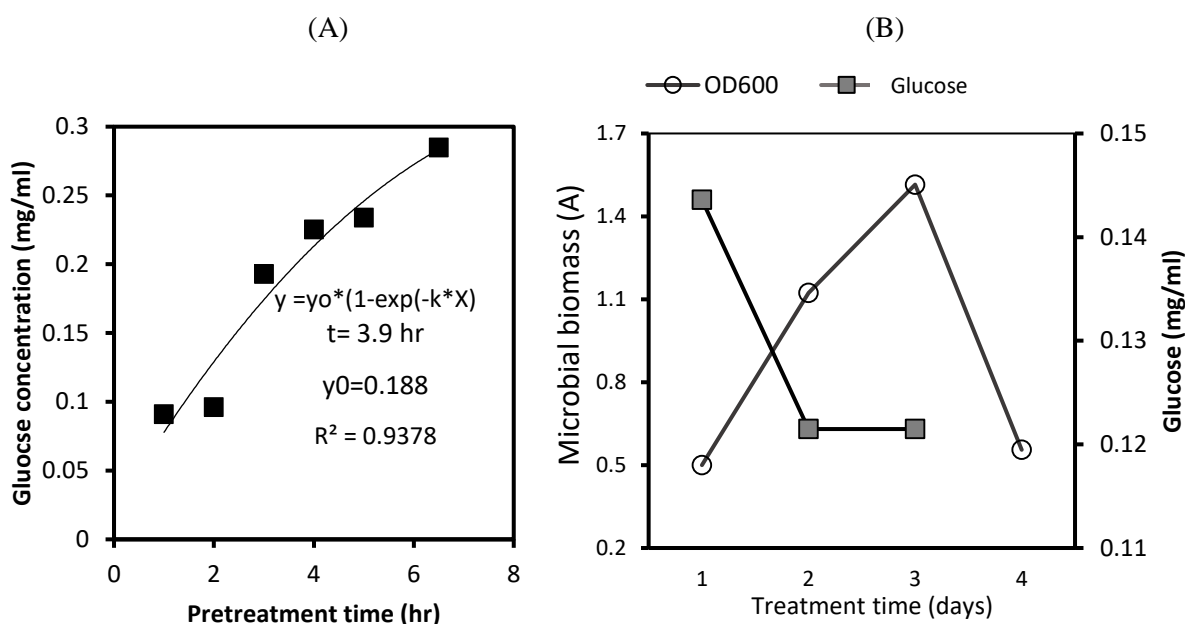


Figure 5.4: Graph of glucose production after 6 h pretreatment. (A) MMO pretreatment (B) MMO-M pretreatment. Glucose at day fourth in the biological pretreatment was not reported due to its low concentration. The readings are representative of triplicate results.

Increasing the MMO pretreatment duration to 6 h was expected to increase the biodigestibility of the biomass, and consequently, release more glucose. The results from the FTIR-ATR spectrum (Figure 5.3), shows a decrease in both the cellulose and lignin regions respectively. Additionally, the glucose concentration produced reached ~ 0.25 mg/ml at the end 6 h MMO pretreatment (Figure 5.4A), five times higher than the glucose produced after 2 h MMO pretreatment (Table 5.2). With the MMO-M pretreatment, two outcomes were observed during pretreatment: the first is that the microbial density increased, reaching maximum density in < 72 h. The second is the decreased glucose level (see Figure 5.4B).

Glucose production curve versus time was exponentially fitted to determine the average time constant of action during the MMO. The time constant (τ) of action of ozone on the lignocellulosic biomass to produce glucose was 3.9 h, and y_0 was 0.188 mg/ml according to the following equations:

$$y = y_0 * (1 - \exp(-k * t))$$

$$\tau = \frac{1}{k}$$

Where y represents glucose concentration (mg/ml), y_0 is the initial glucose concentration (mg/ml), t is the treatment time (h), and τ is the time constant.

The reactions kinetics of ozone with an organic compound (lignocellulosic biomass) commonly displays as a time constant (exponential constant) during the decay of the reactant (lignocellulosic biomass). This constant characterizes the time response of glucose released during the MMO. In other words, time constant gives a timescale for first order kinetics process.

Similarly, further exposure to 12 h MMO pretreatment caused a further decrease in the absorbance for both lignin and cellulose as seen in the absorbance at 710 cm^{-1} to around 1100 cm^{-1} for both amorphous and crystalline celluloses (Figure 5.5).

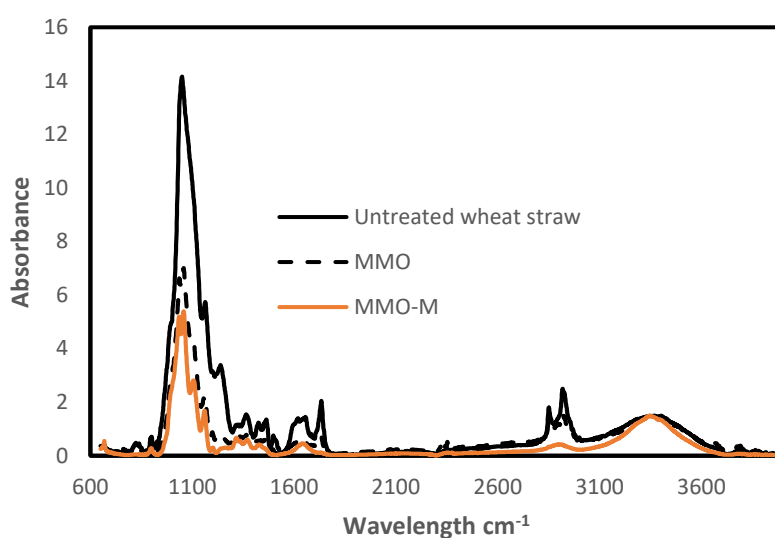


Figure 5.5: FTIR-ATR spectrum of lignocellulosic biomass after MMO and MMO-M pretreatment for 12 h at pH 3 and ozone concentration of 8.87 mg/L. Spectra have been normalised at $710\text{-}1100\text{ cm}^{-1}$ and $1500\text{-}1600\text{ cm}^{-1}$. The readings are representative of triplicate results.

The glucose concentration, however, after 12 h MMO pretreatment reached $\sim 0.3\text{ mg/ml}$ (Figure 5.6A), greater than five times more glucose produced after 2 h MMO pretreatment (Table 5.2).

Under MMO-M pretreatment, microbial biomass density increased and reached its maximum in $\sim 72\text{ h}$. There was an obvious decrease in the glucose concentration. The possible explanation for the result is that liberating glucose in the first pretreatment caused a decrease in the cellulose content of the lignocellulosic biomass, consequently reducing the extractable glucose from the biomass. Additionally, pretreatment of biomass for 12 h with MMO caused a substantial reduction in the main barrier of the biomass, lignin (Doe, 2006), and consequently accelerated *Pseudomonas putida* growth to reach its highest (Figure 5.6B).

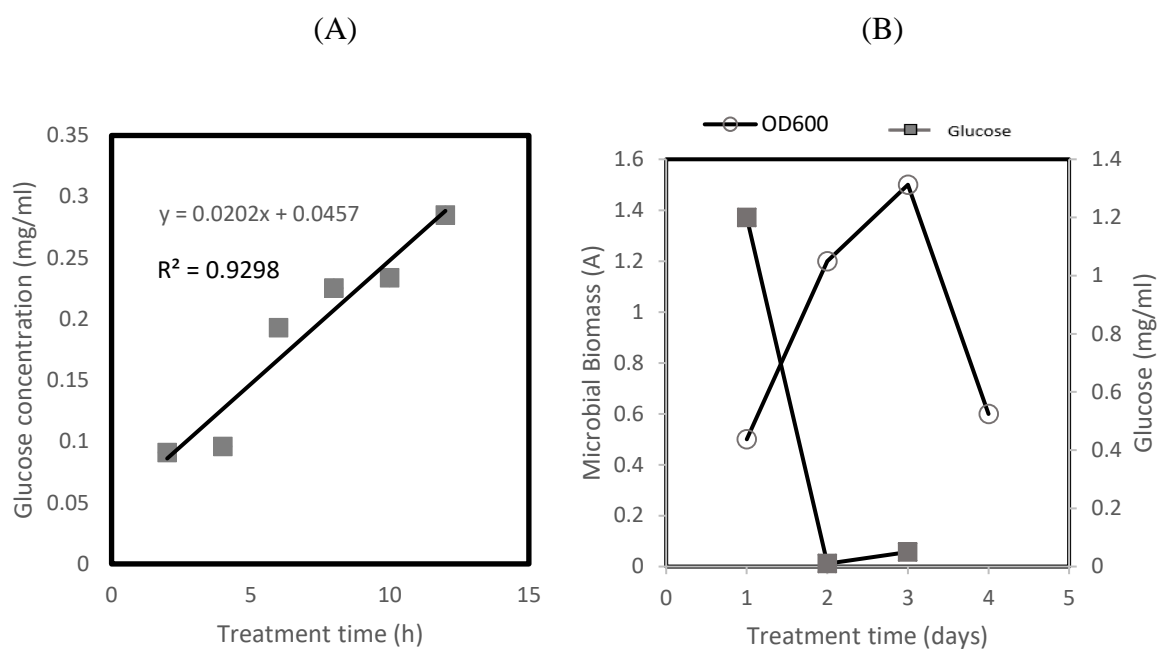


Figure 5.6: Graph of glucose production after 12 h pretreatment. (A) MMO pretreatment (B) MMO-M pretreatment. Glucose at day fourth of the biological pretreatment was not reported due to its low concentration. The readings are representative of triplicate results.

The change in functional groups after 24 h MMO pretreatment (Figure 5.7) shows a considerable decrease in both the cellulose and lignin regions respectively. On the other hand, during MMO-M pretreatment there was a substantial decrease in the cellulose region of the biomass. In addition, the delignification activity by the microbe was observed and can be seen as a reduction in absorbance at 1595 cm^{-1} . *Pseudomonas putida* can concurrently exhibit cellulolytic and delignification activities (Mulakhudair et al., 2016).

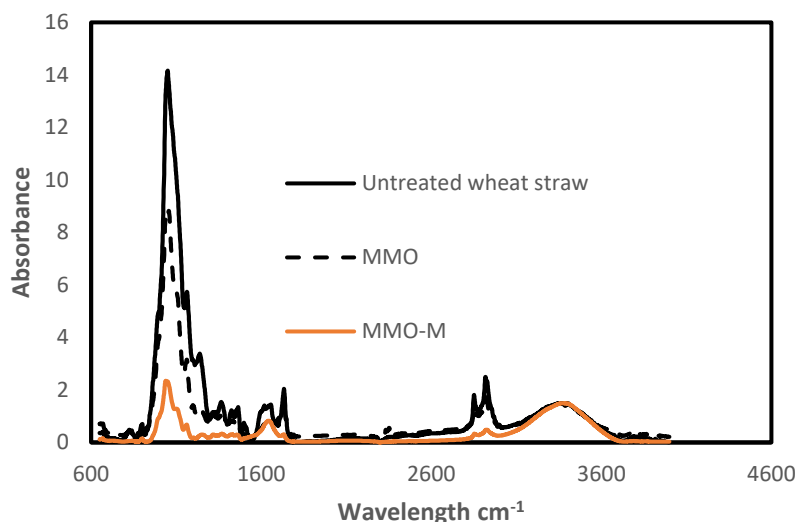


Figure 5.7: FTIR-ATR spectrum of lignocellulosic biomass after MMO and MMO-M pretreatment for 24 h at pH 3 and ozone concentration of 8.87 mg/L. Spectra have been normalised at 710-1100 cm⁻¹ and 1500-1600 cm⁻¹. The readings are representative of triplicate results.

After biological treatment, 85% of the cellulose in straw was degraded. Figure 5.8 presents the result of 24 h pretreatment. From Figure 5.8A, the glucose concentration reached 0.6 mg/ml, double the concentration at 24 h MMO-M pretreatment. Also, under 24 h MMO-M pretreatment, the *Pseudomonas* strain reached its peak growth density after 48 h (Figure 5.8B), a 50% reduction in the pretreatment time in comparison with the preliminary result at 2 h ozone pretreated sample. Further, this represents ~ 25 % reduction in the pretreatment time in comparison with MMO-M pretreatment at both 6 and 12 h respectively (Figures 5.4B and 5.6B). However, the difference between the slope calculated from glucose production during 12 h (Figure 5.6A) and the slope calculated from glucose concentration during 24 h (Figure 5.8A) is not significantly different from each other with P-value 0.64 (p-value > 0.05).

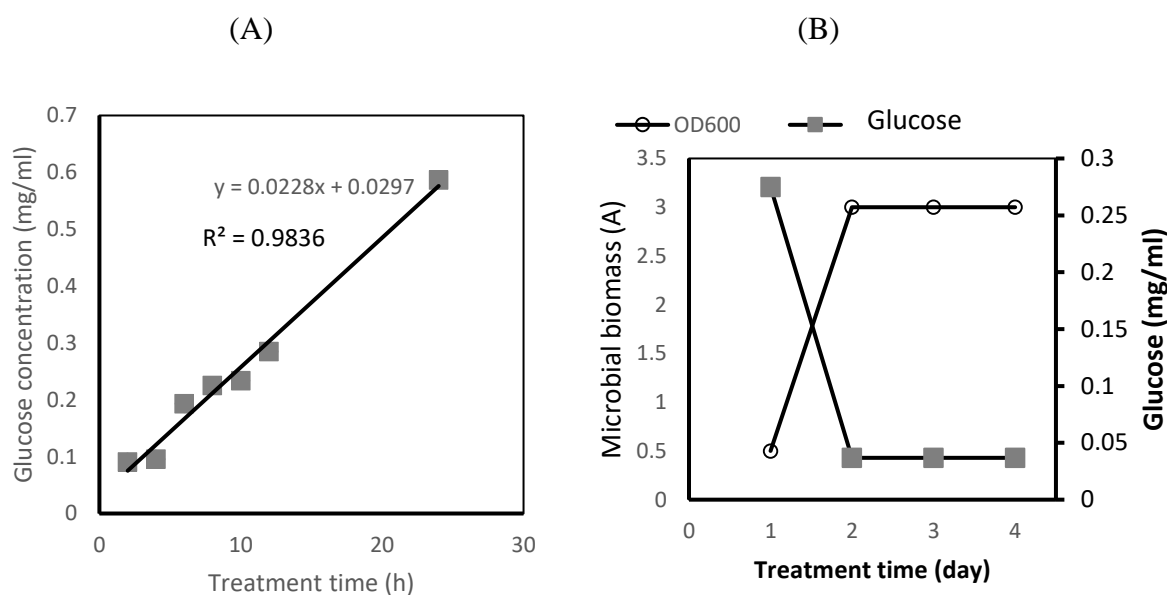


Figure 5.8: Graph of glucose production after 24 h pretreatment. (A) MMO pretreatment (B) MMO-M pretreatment. The readings are representative of triplicate results.

Table 5.3 summarizes and presents the comparison between total glucose concentrations after MMO and MMO-M at various treatment durations. There is a clear relationship between glucose yield and pretreatment duration. Increasing the exposure time is proportionate to the glucose production.

Table 5.3: Glucose production and accumulative produced glucose at the end of MMO and MMO-M of various prolonged exposure times.

Ozonation Time (h)	Glucose Produced (mg/ml)±SD	
	MMO	MMO-M
2	0.057±0.005	0.26±0.01
6	0.255±0.01	0.47±0.05
12	0.3±0.06	0.5±0.07
24	0.6±0.1	1.1±0.09

The MMO and MMO-M techniques explored in degrading have proved effective in solubilizing lignocellulosic biomass and consequently, releasing glucose crucial for bioethanol production. The results here are both promising and offer huge prospects on an industrial scale as one of the shortcomings in bioethanol production is not only the high cost of enzymes but also, the difficulty in effectively degrading lignin with ozone due to the mass transfer limitations.

Obviously, some improvements can be made to the study results. For instance, in exploring the limit of ozone concentration as well as the pretreatment exposure time. Nonetheless, the study outcome provides a significant background for future works.

5.5 Bubble analysis

The fluidic oscillator was connected to the ozone generator that fed a sintered glass diffuser (16-20 μm pore size) to produce ozone microbubbles. Several authors have extensively reported the fluidic oscillator, its mode of operation and application for microbubble generation. Readers are referred to earlier publications of Zimmerman et al., (2008), Tesař and Bandulasena, (2011), Hanotu et al., (2012) for more detailed information.

After collecting photographs of the bubbles in the bubble column using the high-speed camera and analysis with ImageJ software, the bubble size distribution was plotted (Figure 5.9). More than 300 bubbles were measured for reliable results and the highest percentage of microbubbles ranges between 250-750 μm .

The efficacy of the ozonation process depends on the diffusion coefficient of ozone, which is dependent on the gas-liquid contact time and interfacial area. The low-rise velocity of microbubbles and high surface to volume ratio can ensure efficient mass transfer. Direct ozone dosing is the most efficient way to deal with such highly reactive and short-lived chemical. Ozone can be dissolved into an aqueous solution from the gas- liquid interface, and this process is mass transfer limited. To enhance the mass transfer, ozone should be introduced to the bulk of liquid as microbubbles with high surface area to volume ratio. Microbubbles allow higher driving force in terms of mass transfer in the solution (Zimmerman et al., 2009 and Kuvshinov et al., 2014). However, the average of bubble sizes generated in the ozonation process is more than 4 times the average of ones generated in the previous experimental set (Chapter 4) and this might be attributed to several reasons such as surface wettability, channelling in a nozzle bank of diffusers (Ceramic and glass) and pore size, which had been extensively studied by Zimmerman et al., (2008) and Wesley, (2015).

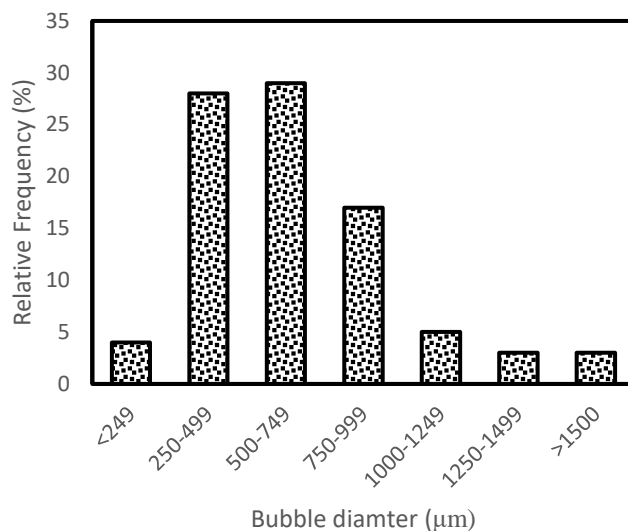


Figure 5.9: Microbubble size distribution plot

5.6 Comparison of traditional methods with the microbubble-mediated technologies developed in the current study for lignocellulosic biomass pretreatment

To illustrate how the various pretreatment technologies compare with the developed technologies, a comparison was made between the microbubble-mediated technologies developed in the current study with dilute-acid hydrolysis, which is the most widely used pretreatment technology for lignocellulosic biomass (Dussán et al., 2014). Diluted sulfuric acid at 0.75 % was used to do the pretreatment of 1 % wheat straw at 100 °C for 1 hr and the glucose concentration was measured at the end of the pretreatment duration using glucose assay kit (Dussán et al., 2014). This comparison is based on energy consumption, as this parameter is suitable for all pretreatment technologies. Calculating of the energy consumption was based on the consumed energy of air compressor, air compressor plus ozone generator and heating system in microbubble mediated technology, microbubble-mediated ozonolysis and dilute acid hydrolysis method respectively. Cost calculations of the chemicals consumption, however, shows that both the developed technologies and dilute acid hydrolysis method have almost similar costs for the chemicals added to prepare the growth medium of *Pseudomonas putida* and sulfuric acid used in the dilute acid pretreatment process.

Table 5.4: Energy calculation of pre-treatment processes

Processes	Duration	Glucose concentration (mg/ml)	Energy consumption kWh/0.1L
Microbubble-mediated technology	3.30 hr	0.2	0.05
Microbubble-mediated ozonolysis	24 hrs	1.1	0.068
Dilute acid hydrolysis	1hr	1.4	0.55

Therefore, the energy consumption can be considered the main parameter of the comparison between these technologies. From Table 5.4, microbubble-mediated technology and microbubble-mediated ozonolysis were consumed 0.05 kWh and 0.068 kWh for more than 3 hrs and 24 hrs respectively, while the dilute acid pretreatment consumed 0.55 kWh for just 1 hr. Interestingly, dilute acid pretreatment consumed around 89 % more energy than the energy consumed by the microbubble-mediated ozonolysis and 91 % more energy than microbubble-mediated technology. This high-energy consumption by dilute acid pretreatment produced just 21.5% higher glucose yield than microbubble mediated ozonolysis, but 86% higher glucose yield than microbubble-mediated technology. Also, the diluted sulphuric acid in the outcome slurry needs to be separated from the pretreatment slurry by the use of membranes before feeding this slurry to the fermentation process as this acid might show an inhibitory effect of the growing microbes in the downstream fermentation process. Thus, separating this acid will add additional costs to the pretreatment operational costs. Therefore, both technologies developed in the current study represent promising technologies to pre-treat lignocellulosic biomass

5.7 Conclusions

Lignocellulosic biomass from wheat straw was pre-treated with microbubble-rich ozone and a cellulolytic and delignification microbe. Both physical and chemical changes to the biomass were observed. Ozone attacks the carbon double bonds in lignin, substantially degrading it and making cellulose more accessible for hydrolysis. pH, ozone concentration and pretreatment time are all factors affecting hydrolysis and glucose yield with the latter varying directly proportionate with ozone concentration and pretreatment time. Further pretreatment with *Pseudomonas putida* caused considerable changes in both the morphology and functional groups content of wheat straw as well as enhanced the glucose yield. The produced glucose has been improved greatly using microbubbles enriched ozone and *Pseudomonas putida* synergetic approach in comparison with microbubble-microbe synergetic approach shown in

the previous chapter. However, using ozonolysis –microbe synergetic approach leaves the pretreatment slurry contaminated with *Pseudomonas* cells, which need to be inactivated before feeding this slurry to the fermentation vessel. Therefore, the next chapter will be investigated the inactivation process of *Pseudomonas putida*.

Chapter 6

Inactivation combined with cell lysis of *Pseudomonas putida* using a low-pressure carbon dioxide microbubble technology

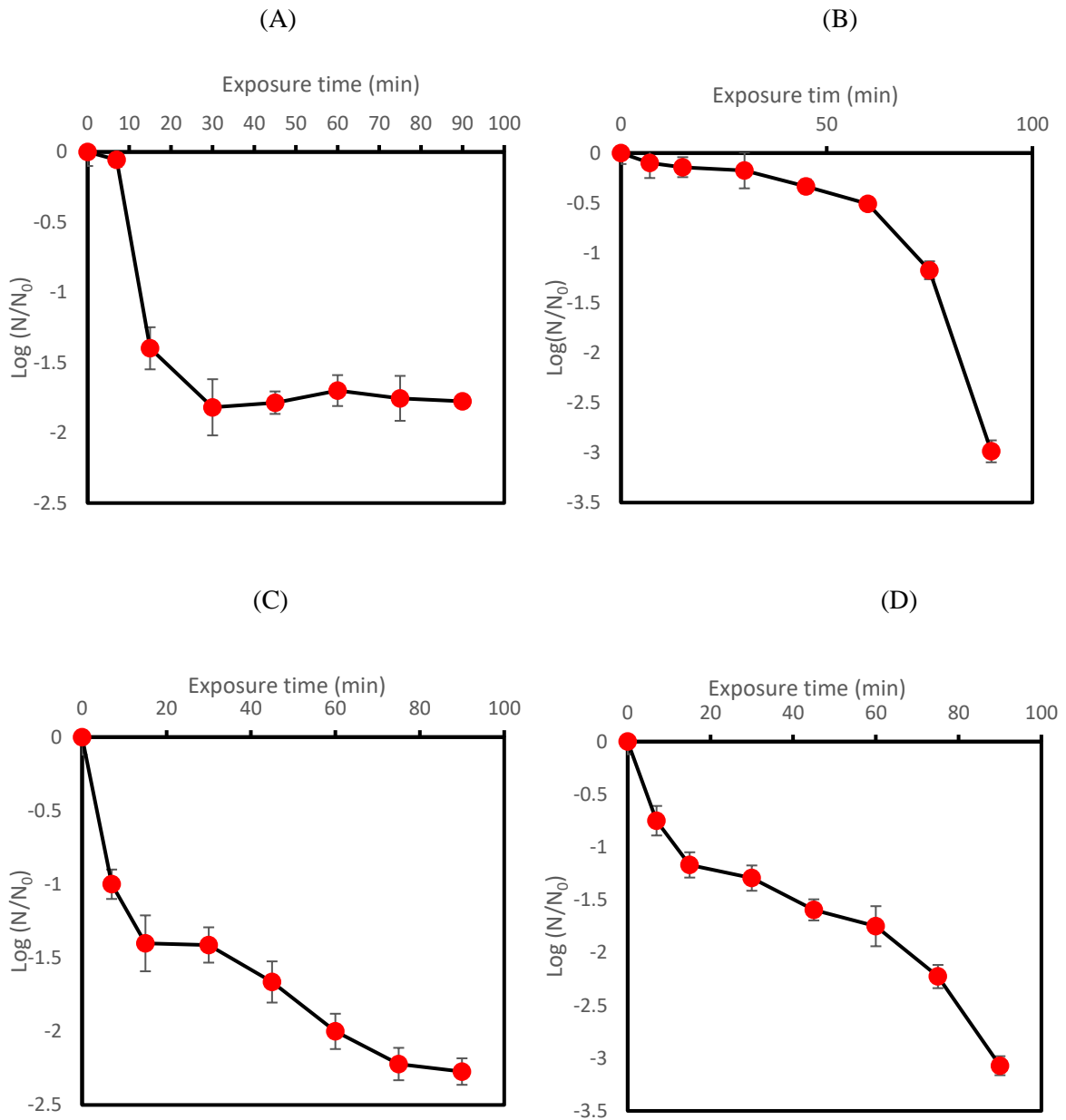
Overview

The sugar content in the pre-treatment slurry produced from the previous pre-treatment processes (Chapter 4 and 5) is contaminated with *Pseudomonas putida*, which was used in the biological pre-treatment. This chapter investigates the inactivation of this microbe before feeding the slurry into the fermentation process in the coming chapters. The ability of carbon dioxide enriched microbubbles to inactivate *Pseudomonas putida* suspended in physiological saline at low pressure (~ 1 bar) and temperature (6 -12 °C) was investigated. This process can be classified as a non-thermal sterilisation method, and it has many operational advantages over both traditional thermal and non-thermal sterilisation methods such as autoclaving, ethylene oxide treatment, and γ -radiation. The advantages come from efficient energy consumption (no heat source), avoidance of toxic and corrosive reagents, and *in situ* treatment. Introducing carbon dioxide enriched microbubbles can achieve ~2-Log reduction in the bacterial population after 90 min of treatment, addition of ethanol to the inactivation solution enhanced the inactivation process to achieve 3, 2.5 and 3.5-Log reduction for 2%, 5% and 10 % (v/v) ethanol respectively. Additionally, using acetic acid as an additive decreased the survivor ratio of *Pseudomonas* cells to more than 2.5-Log reduction. A range of morphological changes were observed on *Pseudomonas* cells after each treatment, and these changes were extended from changing cells shape from rod shape to coccus shape to severe lesions and cell death. *Pseudomonas putida* was used as a model of gram-negative bacteria, and many observations from this study might apply on the other gram-negative bacteria.

6.1 Inactivation of *Pseudomonas putida* using CO₂ microbubbles with and without the additives

P. putida cells were treated with CO₂ microbubbles for 90 min at 100 ml/min flow rate and ~1 bar. At equilibrium state, the inactivation efficiency was measured using two values, D-value and L-value. D-value is defined as the time required for 1 log cycle reduction in microbial population, and calculated from the negative reciprocal of the slope of regression line from the straight part of the survivor curve (Watanabe et al., 2003) in Figure 6.1A. On the other hand, L value is the time during which the number of microbial cells remains constant before starting the inactivation of microorganisms (Oulé et al., 2006). The D-value for treatment with CO₂

microbubbles was ~ 64.8 min, while there was ~ 2 -log reduction in *P. putida* population. In contrast, L value was ~ 9.6 min. Two mechanisms are suggested to play a central role in this process: oxidative stress and the CO_2 effects.



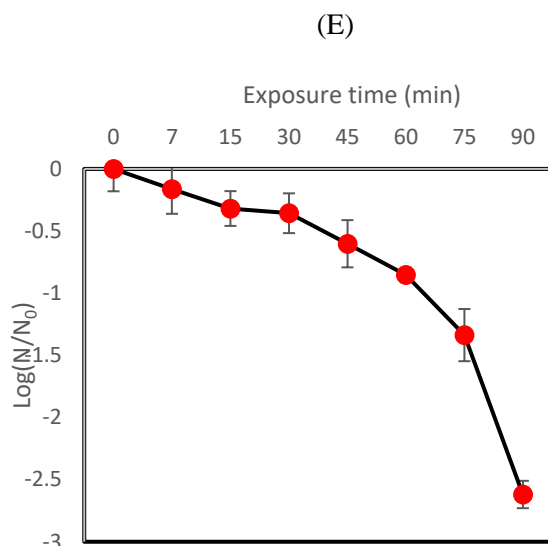


Figure 6.1: Survivor ratio of *Pseudomonas putida* after treatment with. (A) CO₂ microbubbles. (B) CO₂ microbubbles plus 2% (v/v) ethanol. (C) CO₂ microbubbles plus 5% (v/v) ethanol. (D) CO₂ microbubbles plus 10% (v/v) ethanol. (E) CO₂ microbubbles plus 0.5% (v/v) acetic acid. Error bars depict standard deviation.

Regarding the oxidative stress, during microbubbles shrinkage and subsequent collapse, some hydroxyl radicals are generated (Li et al., 2009). In addition, the generated hydroxyl radicals are readily converted to the superoxide radicals and vice versa (Ragnar et al., 1999). Previously, *P. putida* was reported to go through an oxidative stress, when exposed to the free radicals (Kim and Park, 2014). Free radicals are reactive oxygen species (ROS), and are injurious species, reacting with different components of cellular systems such as lipids, proteins and DNA (Imlay, 2003). Fundamentally, lipids seem to be the major targets for these species during an event of oxidative stress, and interestingly, the free radicals that are formed, can directly react with the polyunsaturated fatty acids in the cell membrane, provoking lipid peroxidation. The latter reaction can change membrane properties and disrupt the membrane-bound proteins (Cabiscol et al., 2000). The amplification to this reaction occurs when more radicals are generated and more polyunsaturated fatty acids are broken down into other highly reactive products such as aldehydes. These highly reactive products can cause severe damage to vital compounds such as proteins (Sheu and Blass, 1999).

The mechanisms of the action of CO₂ were described in depth (Garcia-Gonzalez et al., 2007). CO₂ is not a ‘natural product’ of the glucose metabolism pathway of *P. putida*, however, it can be produced during the catabolising of aromatic compounds by the β-Ketoadipate pathway (Ornston and Stanier, 1966). All these factors work together to achieve the elevated log reduction observed in *P. putida* using CO₂ microbubbles. In contrast, other microorganisms

such as *Zymomonas mobilis* (another example of gram-negative bacteria) are expected to show high degree of adaptation to CO₂ as it is produced naturally during metabolism in both aerobic and anaerobic conditions (Nipkow et al., 1985, Veeramulla and Agrawal, 1986 and Conway, 1992). Figure 6.2 shows the temperature profile during the inactivation processes.

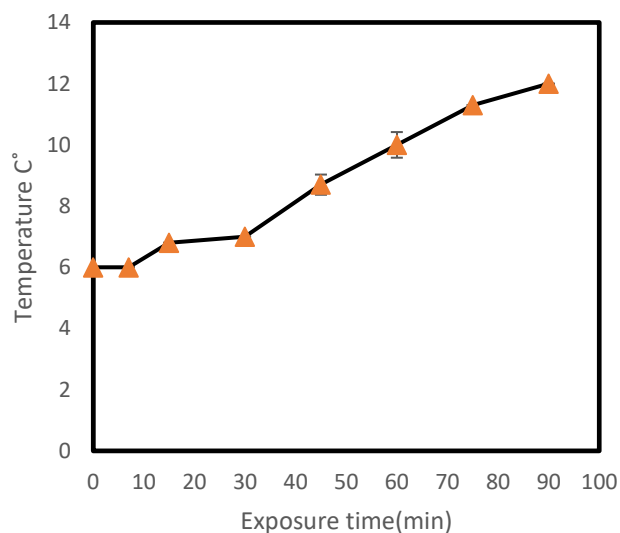


Figure 6.2: Temperature profile during CO₂ enriched microbubbles inactivation process, highlighting the range of temperatures used in the current study. Error bars depict standard deviation.

Low temperature was used to increase the CO₂ solubility in order to enhance the inactivation activity. At 0°C, the CO₂ solubility is around 1.3 mol/L, decreasing to ~1 mol/L at 10 °C. Moreover, increasing the temperature to 20 °C will decrease the CO₂ solubility to ~0.7 mol/L (Carroll et al., 1991). From Figure 6.2, there was a gradual increase in temperature of the solution from ~ 6 °C to ~ 12 °C.

To enhance the inactivation activity of CO₂ microbubbles, organic solvents, are employed. These solvents are toxic to some microbial cells due to their tendency to partition preferentially in the cytoplasmic membranes, increasing the fluidity of the cell membrane, and ultimately causing an increase in the unspecific permeabilization of the cytoplasmic membrane (Heipieper et al., 1991 and Heipieper et al., 1994). Moreover, the fatty acid composition in the cytoplasmic membrane of microbial cells can change significantly by these membrane-active solvents (Ingram, 1976 and Ingram, 1977). Isomerisation is a mechanism employed by *P. putida* to adapt its cytoplasmic membrane to ethanol toxicity. In this mechanism, the Cis-unsaturated fatty acids are isomerised to Trans unsaturated fatty acids, and the bacterial cells become much more robust to the ethanol stress (Heipieper et al., 1996). Figure 6.1B shows the survivor ratio of *P.*

putida cells after treatment with CO₂ microbubbles combined with 2 % (v/v) ethanol for 90 min at 100 ml/min flow rate and ~1 bar.

Adding 2% ethanol enhanced the inactivation process, and caused ~3-log reduction in the microbial population after 90 min. Interestingly, the time during which the number of microbial cells remains constant--L value-- was ~30 min, ~4 times longer than the previous experimental set while the D value was almost identical between both experiments. Enhancement of the inactivation activity can be attributed to mechanisms of action of both ethanol and CO₂ on the cytoplasmic membrane of *Pseudomonas* cells and the combined action of both elements. Both CO₂ and ethanol work mainly on the fatty acid composition of the membrane.

Changing the composition of the cytoplasmic membrane is not straightforward mechanism and certain threshold needs to be reached before observing any changes on the membrane. The exact duration to reach this threshold has not been studied yet for both CO₂ and ethanol. However, previous studies on the changes in the fatty acids profile are helpful to predict the duration. For example, Mejia et al., (1999) reported the changes in the fatty acids profile of *Escherichia coli* (gram-negative bacterium) after exposure to heat shock stress for 30 min. Another example is the study by Boylan et al., (1993), where *Bacillus subtilis* (gram-positive bacterium) was exposed to environmental stresses such as salt stress and 15-30 min were required to accumulate β -galactosidase.

During the first 30 min, the level of the *Pseudomonas* population was almost constant before the number of bacterial cells gradually decreased with time until the CO₂ concentrations reached the equilibrium state.

Additionally, it has been suggested that increasing the amount of ethanol used (the organic solvent) could intensify the inactivation process with CO₂ microbubbles. Therefore, the concentration of ethanol was increased to 5% (v/v) to test this hypothesis. Figure 6.1C shows the survivor ratio of *P. putida* after the treatment with CO₂ enriched microbubbles plus 5% ethanol. Interestingly, there was almost a 2.5 log reduction of *Pseudomonas* population after treatment. Further, it can be noticed that the time when the cell number remained constant was much less than the previous experiments, as well as the D-value, which reached around 46.8 min. This observation might not be expected but on the other hand, the L value was much lower than the previous experiment. While decreasing the log reduction in this treatment might have resulted from the increase in bacterial tolerance to ethanol, the microbial exposure to a sub-lethal level of ethanol might promote a cellular response to encounter this stress. For example, Vanbogelen et al., (1987) and Waston, (1990) reported induced expression of stress proteins as

a result of exposure to sub-lethal level of ethanol and the same proteins were expressed as a result of heat shock. Therefore, there might be a cross-protective response induced to face environmental stresses in the same manner. Indeed, this cross-protective response was seen previously in *Pseudomonas* spp, on exposure to different aromatic compounds and heat. In all three cases, stress shock proteins were produced (Park et al., 2001).

Furthermore, the concentration of the additive (ethanol) was increased to 10 % (v/v) to verify the combined effects of ethanol and CO₂ and to enhance the whole inactivation process. It can be observed from Figure 6.1D that there was around 3.5 log reduction in the bacterial population after this treatment. In addition, the D-value for this experimental set was 82.8 min, while the L-value was around 4.8 min. Both values were higher than the previous experimental set, and consistent with the original hypothesis. Indeed, the magnitude of ethanol toxicity is associated with its used concentration (Mrozik et al., 2004). Increasing the ethanol concentration to 10% can represent a chemical stress on the bacterial cells, and this stress might be analogous to other stresses (Ingram, 1986). As mentioned above, *P. putida* can evolve adaptative mechanisms as a response for stresses (Ingram, 1977; Vanbogelen et al., 1987 and Heipieper et al., 1996). Therefore, it was speculated that increasing the ethanol concentration above a certain threshold could exceed the ability of *Pseudomonas* cells to tolerate and respond to the elevated level of toxicity, causing serious injuries to the cytoplasmic membrane and eventually failure to keep the biological system balanced. Another important concept to be considered is Chaotropicity. Ethanol is known as a Chaotropic solute, resulting in water stresses in bacteria at concentrations similar to levels in the environment (Hallsworth et al., 2003). Hallsworth et al., (2003) showed that ethanol did not affect cell turgor, but instead, perturbed macromolecule–water interactions and thereby destabilized cellular macromolecules, inhibited growth. This bacterium responded to ethanol chaotropicity by specifically up-regulating the synthesis of proteins involved in stabilizing protein structure, in lipid metabolism, and in membrane composition (Hallsworth et al., 2003). However, destabilization of macromolecules in the biological system is an elastic process in comparison with the specific inactivation (such as inactivation with carbon dioxide). Macromolecules destabilization can be reversed up to a critical thermodynamic point by using kosmotropic solutes that increase entropy and affect hydration of macromolecules, such as trehalose (Hallsworth et al., 2003). These solutes tend to order water, and strengthen electrostatic interactions within organic macromolecules (Mansure et al., 1994; Shah et al., 1998 and Cray et al., 2015).

Acetic acid is another additive used in this study and it is a weak organic acid but it is stronger than carbonic acid (carbon dioxide dissociated species), and it shows toxic effects to a range of microorganisms at concentration as low as 0.5% and its dissociation inside the microbial cells represents the cause of this toxicity. These toxic effects include decreasing the intracellular pH, and the metabolic disturbance through releasing anion and other deleterious effects (Trček et al., 2015). Additionally, the acetic acid dissociation constant is directly associated with the quantity of protonated and ionic forms of acetic acid as a function of the pH value of the inactivation solution. At a pH of 3.75, 90% of acetic acid is in its undissociated form (CH_3COOH), and the undissociated acetic acid molecules are lipophilic molecules, which can permeate the cytoplasmic membrane by passive diffusion, thereby dissociating in the cytosol of bacterial cells directly. This dissociating causes a decrease of internal pH to values that might not be tolerable, leading to a strong reduction of metabolic activity and thereafter, to cell death. Cytosol acidification has another consequence, which is dissipation of the electrochemical gradient retained across the cytoplasmic membrane, which is a crucial demand for the secondary transport across this membrane (Trček et al., 2015). Interestingly, there was almost a 2.5-log reduction of *Pseudomonas* population after treatment with CO_2 -enriched microbubbles plus acetic acid (Figure 6.1E).

Addition of this acid decreased pH of the inactivation solution to 3.34 before starting the sparging course (Figure 6.3E), and thereafter; pH was slightly increased during carbon dioxide sparging. Under acidic solution, carbon dioxide tends to be existed in an aqueous phase, and the concentrations of other carbonate species ($[\text{H}_2\text{CO}_3]$, $[\text{HCO}_3^-]$ and $[\text{CO}_3^{2-}]$) tend to be very limited at acidic conditions (Lower, 1999). As pH decreases below 4.5, the zeta potential of microbubbles has a positive value, and this increase with decreasing pH might cause a higher probability of negative charged bacterial cells (Bononi et al., 2008); which can be approaching the bubble interface (Li et al., 2009), and this might bring the bacterial cells in contact with CO_2aq in the bubble interface. This approaching might facilitate the penetration of CO_2 into microbial cells. Garcia-Gonzalez et al., (2007) hypothesised that CO_2 has a direct effect on the microbial membrane, and CO_2 in microbubbles at this low pH is probably the most important factor to explain the high penetration rate of carbon dioxide into bacterial cells.

Additionally, this acid has a limited inhibitory effect in this concentration (0.5%) even it remains in the treated samples, which might be used as a substrate for the next process such as the fermentation process or foodstuffs. Previously, this acid was used as an additive and it was shown to courage the inactivation process with carbon dioxide (Kamihira et al., 1987). Many

industries have been used acetic acid as a preservative because its ability to inhibit a wide range of microorganisms, although acetic acid tolerated microbial strains have recently been emerged (Trček et al., 2015).

6.2 CO₂ concentrations during CO₂-enriched microbubbles sparging with and without the additives

The CO₂ concentration was estimated using Eq. 3.10. Figure 6.3 (A, B, C, D and E) presents the CO₂ concentrations at different pHs for all experimental sets. From Figure 6.3, it can be noticed that the inactivation processes were increased in conjunction with increase in CO₂ concentration. This observation can be interpreted by the fact that the elevated CO₂ concentration tends to be accumulated in the phospholipid bilayers of cytoplasmic membrane, causing an increase in the penetrated CO₂ (Isenschmid et al., 1995 and Spilimbergo et al., 2002). Also, increasing the dissolved concentration of CO₂ was accompanied with decreasing the survivor ratio (Kobayashi et al., 2014).

Regarding CO₂ concentration when the acetic acid was added to the inactivation solution, the Eq. 3.11 was used to work out the CO₂ concentration (Figure 6.3E). Adding the acetic acid to the inactivation solution decreases pH to around 3.34 and this low pH is a barrier for CO₂ dissociation.

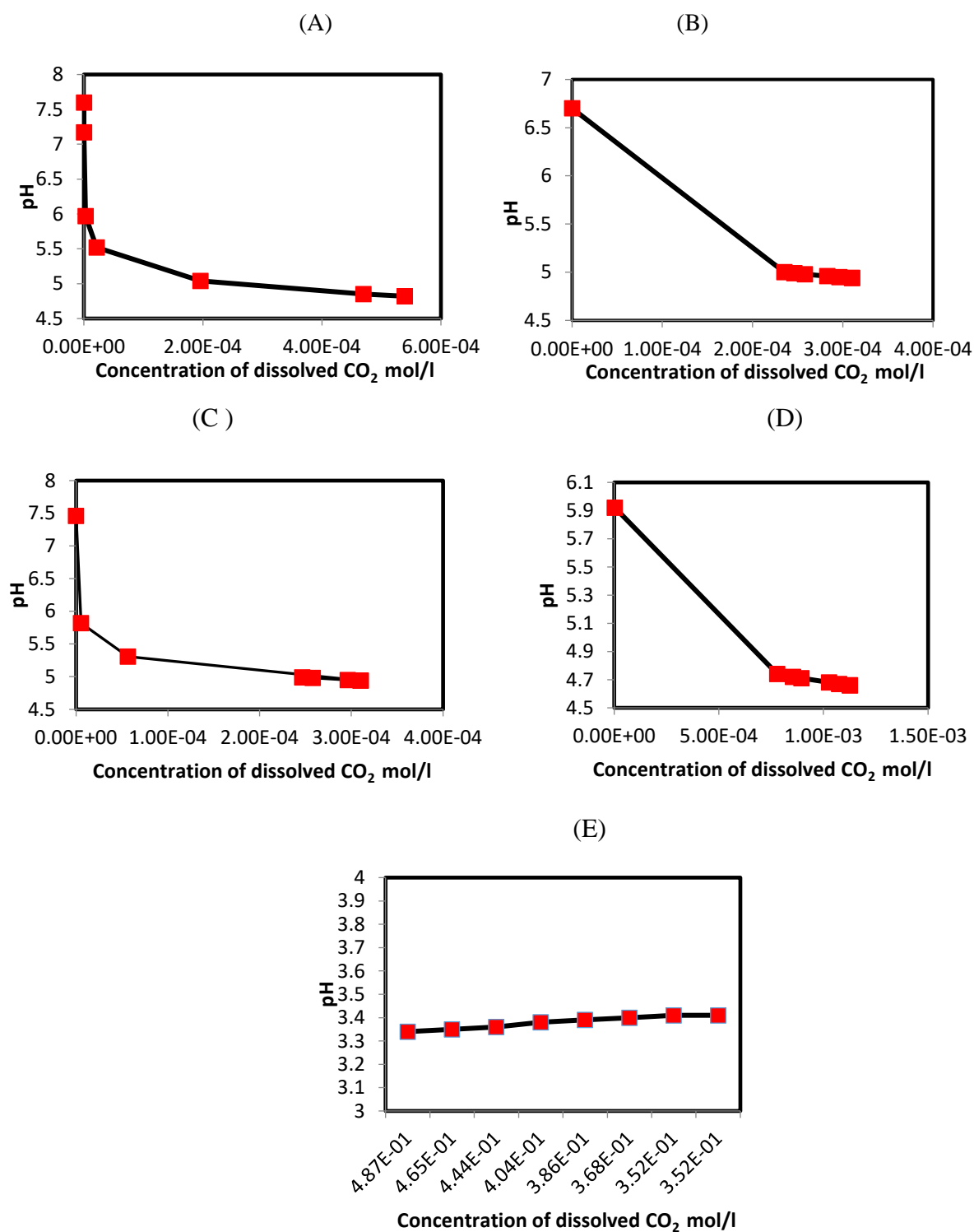


Figure 6.3: CO₂ concentrations with different pHs observed during sparging. (A) CO₂ microbubbles. (B) CO₂ microbubbles plus 2% ethanol. (C) CO₂ microbubbles plus 5% ethanol. (D) CO₂ microbubbles plus 10% ethanol. (E) CO₂ microbubbles plus 0.5% acetic acid. Readings are representative of triplicate results.

6.3 Morphological changes on *Pseudomonas putida* cells using CO₂ microbubbles with and without the additives

The inactivated cells with CO₂-enriched microbubbles treatment were examined using microscopy to observe the morphological/numerical changes on the bacterial cells after treatment (Figure 6.4). There was a clear reduction in the number in comparison with the untreated cells. Further observation revealed changes in the morphology such as shortening and shrinkage of the cells.

Much research was done on using supercritical CO₂ in the inactivation process of microorganisms. For example, it was hypothesized that application of supercritical conditions can facilitate CO₂ penetration into the cell membrane, consequently expanding the microbial cells and causing cell disruption (Darani and Mozafari, 2009). Indeed, the concept behind using supercritical CO₂ was originally described by Fraser, (1951), when bacterial cells were burst after injecting the CO₂ under high pressure. Thereafter, this concept was used to recover some cellular constituents such as intracellular enzymes and proteins (Lin and Chen, 1994). While, many of the previous studies on the inactivation with CO₂ were achieved under high pressure and elevated temperature (~73 bars and 31.1°C) to reach the supercritical state (Diaaz-Reinoso et al., 2006), the current study was achieved under a relatively low-pressure CO₂ (~1 bar) and low temperatures (6-12°C). Therefore, it suggests that high pressure and temperature are not the only factors affecting cell lysis by CO₂ application.

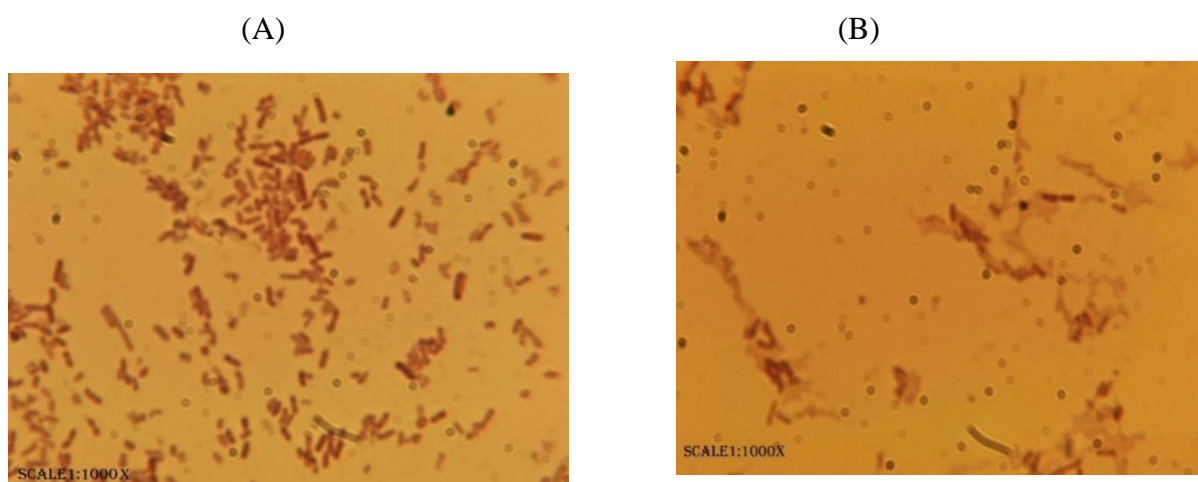


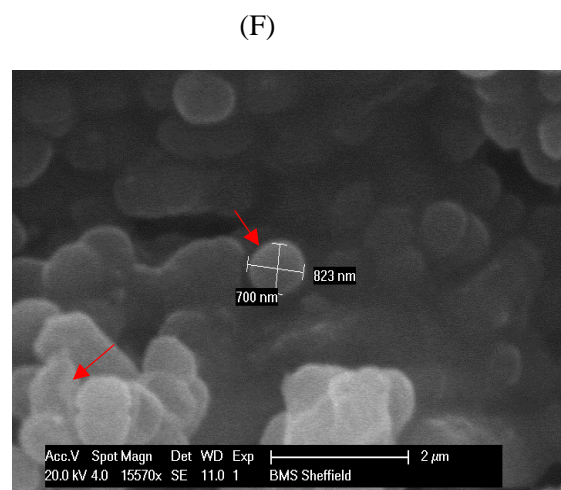
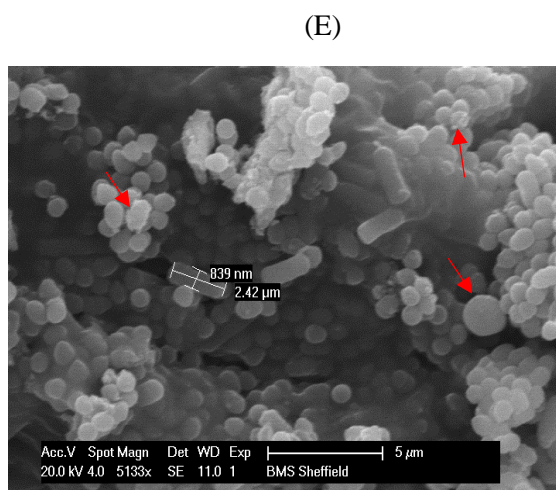
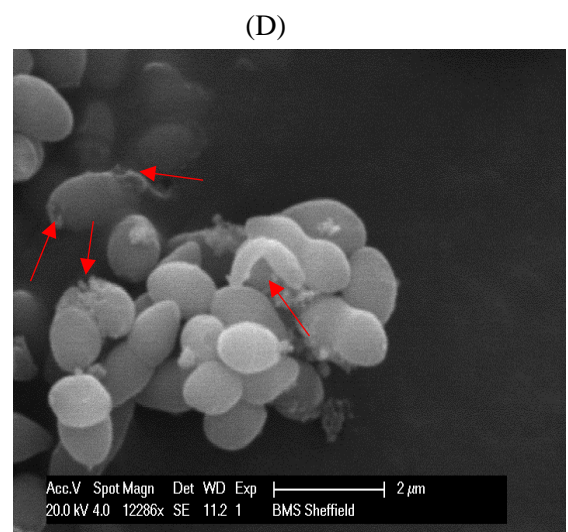
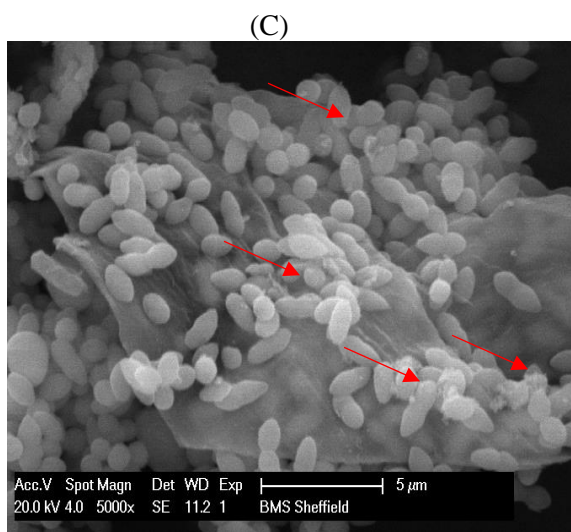
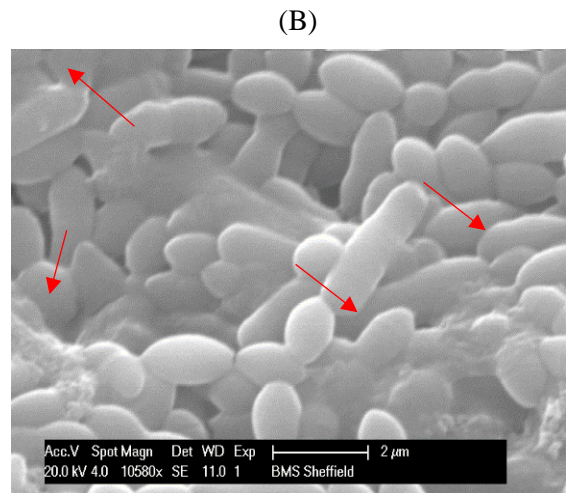
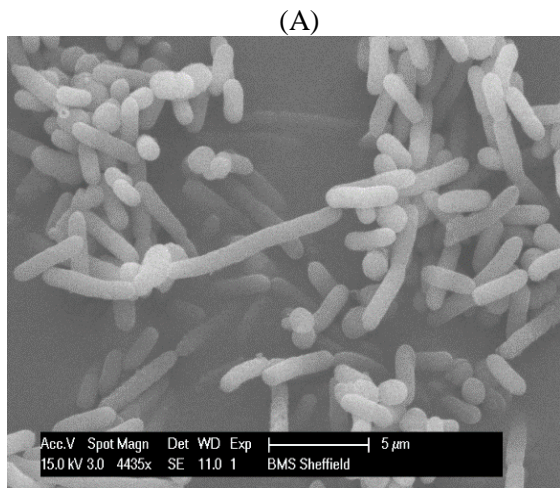
Figure 6.4: Numerical changes after treatment with CO₂ microbubbles on 1000X. (A) Bacterial smears before sparging CO₂. (B) Bacterial smear after treating with CO₂-enriched microbubbles for 90 min.

Figure 6.5 shows morphological changes on the *Pseudomonas* cells after treatment with CO₂ microbubbles plus ethanol as an additive. In Figure 6.5B, it is obvious that the *Pseudomonas* cells were aggregated after the treatment with CO₂-enriched microbubbles plus 2 % ethanol. Many conditions can provoke microbial flocculation such as substrate acquisition, slow growth or starvation, physical and chemical stress and aggregation to protect against predation (Bossie and Verstraete, 1996). Moreover, formation of microbial flocs can also increase the metabolic activity of the stressed cells (McFeters et al. 1990) and to enhance the microbial resistance to toxic compounds such as biocidal compounds (Costerton et al., 1987; Giwerzman et al., 1991 and Anwer et al., 1992). The changes in the cell shapes can also be noticed in Figure 6.5(B) in comparison with the normal bacterial cells in Figure 6.5(A) (the control); when *Pseudomonas* cells were observed to transition from rod cells to coccus cells. This transition might increase attachment of the bacterial cells, consequently leading to flocculation (Fakhruddin and Quilty, 2006). Occasionally, the size reduction is accompanied by an increase in population under various environmental stresses (Novitsky and Morita, 1976; Amy and Morita, 1983; Givskov et al., 1994, Mueller, 1996 and Makarov et al., 1998). Interestingly, the decrease in cell size was not accompanied with an increase in the bacterial population in the current study, as shown in Figure 6.1B. Changing the cells shape from rod to round shape increases the cell surface area to volume ratio; a useful metabolic response under starvation stress condition. Bacterial cells are known to adjust in order to effectively transport nutrients with minimum energy consumption (Sanin et al., 2003). However, alternating the *Pseudomonas* cells shape from rod

to round shape in the current study is likely a consequence of changes due to the environmental stresses mentioned above.

Figure 6.5 (C and D) shows the morphological changes that occurred in the *Pseudomonas* cells as a result of the treatment with CO₂ enriched microbubbles plus 5% ethanol. It is apparent that the cells have lesions with loss of membrane integrity. Cell injury and death were previously observed, due to high pressure CO₂ application (Hong et al., 1997). The current study however, was conducted under low pressure (~1 bar), and observing the same morphological changes on the bacterial cells is suggestive of an inactivation and subsequent cell lysis capability of CO₂ according to the mechanisms reviewed previously (Garcia-Gonzalez et al., 2007). Using CO₂ under high pressure can enhance the solubility of CO₂ and consequently, accelerate cell injury and death (Hong et al., 1997). These changes are irreversible (Hong and Pyun, 2001). Therefore, application of high pressure is a way to enhance the CO₂ inactivation activity but by no means the only factor responsible for inactivation.

The morphological changes during the treatment with the CO₂-enriched microbubbles plus 10 % ethanol are presented in Figure 6.5 (E and F). Increasing the ethanol concentration can increase the membrane permeability of the bacterial cells, which is associated with chemical activities, inducing narcosis in biological systems (Isenschmid et al., 1995). This effect is followed by leakage of protons and some vital ions such as potassium ions from the cytoplasmic membrane of the bacterial cells (Leao and Uden, 1984 and Cartwright et al., 1986). Interaction of these compounds with the phospholipid bilayers of the cytoplasmic membrane could cause substantial changes in the membrane structure. For example, lipophilic compounds tend to accumulate in the hydrophobic part of the cytoplasmic membrane, disturbing the interaction between acyl chains of the phospholipid bilayers as well as changing the fluidity of the membrane. Eventually swelling of the phospholipid bilayers of the bacterial cells can occur, resulting in a ball-like shape (Sikkema et al., 1995). Figure 6.5 (G and H) shows the morphological changes during the treatment with the CO₂-enriched microbubbles plus 0.5 % acetic acid. The size reduction might have resulted due to the inability of *Pseudomonas* to tackle the passive diffusion of acetic acid through the cytoplasmic membrane. Keeping the same cell size or reducing it (More relative area) can decrease the tolerance to acetic acid as this increases the relative area for passive diffusion and there is additional acid can be crossed the cytoplasmic membrane, which coincides with increasing the membrane permeability via CO₂ enriched microbubbles (Trček et al., 2015).



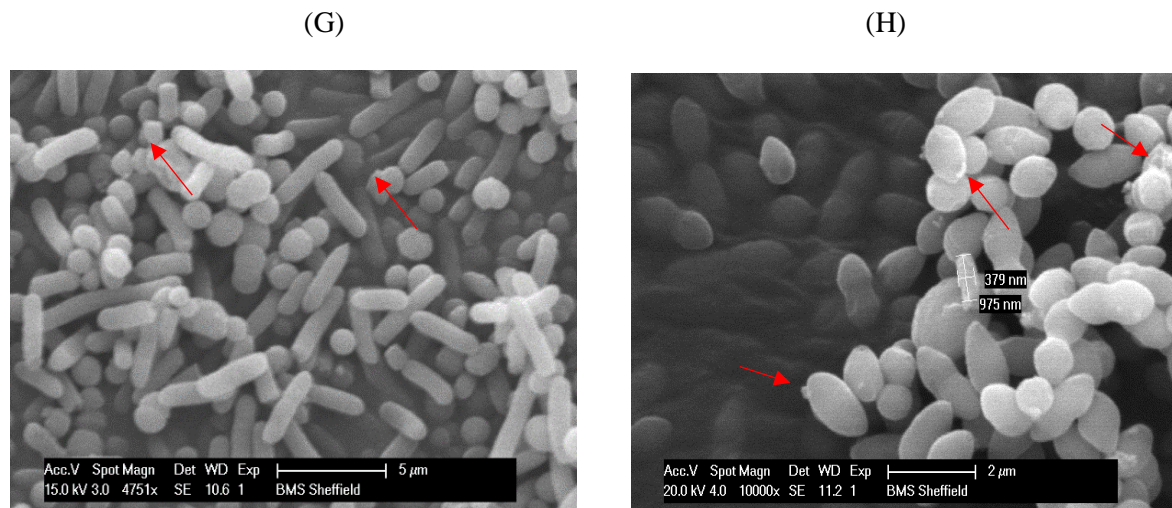


Figure 6.5: Morphological changes on. (A) Untreated *Pseudomonas* cells. (B) *Pseudomonas* cells after the inactivation process with CO₂ microbubble plus 2% ethanol. (C) (D) *Pseudomonas* cells after the inactivation process with CO₂ microbubble plus 5% ethanol. (E) (F) *Pseudomonas* cells after the inactivation process with CO₂ microbubble plus 10% ethanol. (G) (H) *Pseudomonas* cells after the inactivation process with CO₂ microbubble plus 0.5% acetic acid.

6.4 Conclusions

Pseudomonas putida was used to conduct the biological pretreatment in the previous chapters and it needs to be inactivated before feeding the pretreatment slurry to the fermentation process in the coming chapters. *P. putida* is also used a model for gram-negative bacteria in the current study. Survivor ratio after each experiment was calculated after streaking the bacterial samples on nutrient agar plates, and only the viable cells can grow to colonies on these plates. Using the additives to enhance the CO₂ enriched microbubbles inactivation activity was chosen with considering the final concentration of these additives and the potential downstream processes such as the fermentations process (In the coming chapters) and foodstuff manufacturing. The highest concentration of both additives (ethanol and acetic acid) was not exceeded the inhibitory effects of these chemicals on the next fermentative microorganisms such as *Zymomonas mobilis*, which is used to carry out the fermentation process. The initial log reduction with carbon dioxide enriched microbubbles alone was around 2 Log, while best Log reductions were achieved by 10 %, 2% 5% and 0.5% of ethanol and acetic acid respectively. Using microbubble technology for CO₂ sparging caused both an oxidative stress and disturbance to the biological system of *Pseudomonas putida* cells. Addition of ethanol and acetic acid were amplified the activities of CO₂ enriched microbubbles and decreased the survivor ratio of *Pseudomonas putida*. Several morphological changes were observed after each treatment, and these changes were ranged from changing the cells' shapes from rod shape to round shape, appearing lesions

on the bacterial cells, severe injurious signs and cells death. Finally, the CO₂ concentration was monitored during the inactivation process using pH values as a basis for its calculations.

Chapter 7

Aerobic fermentation integrated with *in situ* separation of bio-products using microbubble technology and wild type *Zymomonas mobilis* ZM4 strain

Overview

Zymomonas mobilis has long been known as the best microbial producer of ethanol, and it is widely used to produce a large quantity of ethanol in anaerobic conditions, offering many advantages over other ethanol producers such as *Saccharomyces cerevisiae*. This bacterium uses an Entner-Doudoroff (ED) pathway to metabolise glucose, which was seen to be produced from lignocellulosic biomass in Chapters 4 and 5, and being inactivated in chapter 6, to produce ethanol. Under aerobic conditions, however, this bacterium produces a reasonable amount of acetaldehyde and carbon dioxide with lower quantity of ethanol. This study investigates the performances of *Zymomonas mobilis* under aerobic conditions, whereby acetaldehyde is produced as a target product. Acetaldehyde and carbon dioxide accumulations in the fermentation broth severely inhibit the *Zymomonas* growth. Removing the accumulated acetaldehyde and carbon dioxide, however, reduces the chemical activity of the gaseous products with a negative value change in Gibbs free energy; hence the biological reactions become thermodynamically favourable and provides momentum for the formation of more products. Microbubbles generated by fluidic oscillation were used to remove both acetaldehyde and carbon dioxide from the fermentation broth. The fermentation conditions need to be aerobic and thus; so three scenarios of sparging with microbubbles were explored to choose the one most fit. In the first scenario, the fermentation process was achieved under standard conditions with the sparging of microbubbles at the beginning of the fermentation process. The second scenario was a continuous sparging strategy, whereby microbubble sparging continued throughout the duration of fermentation. Due to the inefficiency of this scenario in both acetaldehyde and carbon dioxide collection and because of high energy usage and gas wasting with a high operational cost, this scenario was avoided. In the third scenario, the fermentation process was conducted using a periodical sparging strategy, in which aeration took place at certain times during the fermentation process. Both the duration of sparging and flow rate were manipulated according to the experimental observations. The fermentation process was achieved using the bespoke airlift loop bioreactor.

7.1 Acetaldehyde accumulation and its inhibitory effect

During the aerobic fermentation of *Zymomonas mobilis*, acetaldehyde accumulates as a less reduced metabolite, and the accumulated acetaldehyde can cause an inhibition of *Zymomonas mobilis* growth, both growth rate (μ) and cell yield ($Y_{x/s}$) (Ishikawa et al., 1990, and Pentjuss et al., 2013). This accumulation starts immediately after the inoculation of *Zymomonas mobilis*, and acetaldehyde accumulation rate increases with time (Ishikawa et al., 1990). In an attempt to gain some insight into the inhibition mechanism of acetaldehyde, various concentrations of acetaldehyde were added extracellularly during the early stages of the exponential phase of *Z. mobilis* ZM4 growth (after 2 and 4 hours). Figure 7.1A shows that the microbial growth was strongly inhibited by the acetaldehyde addition after two hours, and the acetaldehyde inhibitory effect was proportional with its concentration.

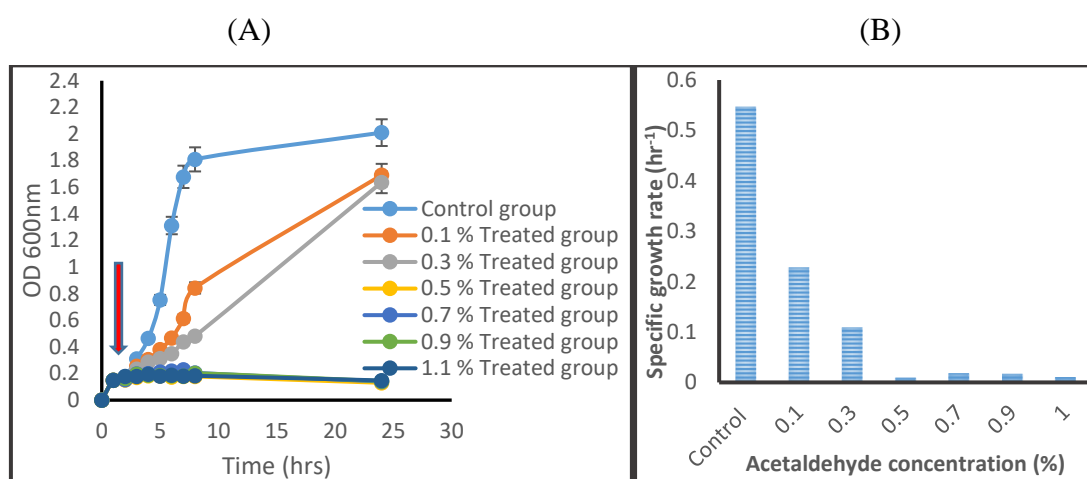


Figure 7.1: (A) Effect of added acetaldehyde on exponential cell growth of *Zymomonas mobilis* ZM4 after 2 hours. The red arrow shows the time of the acetaldehyde addition (B) Specific growth rate of *Zymomonas mobilis* ZM4 after adding various concentrations of acetaldehyde. Error bars depict standard deviation.

Figure 7-1B shows the specific growth rates of *Zymomonas* at various concentrations of acetaldehyde in comparison with the control group (without acetaldehyde addition). From Figure 7-1(A,B), increasing the acetaldehyde concentration is strongly inhibiting both the specific growth rate and cell biomass. Viikari and Korhola, (1986) were reported that the cell yield of *Zymomonas mobilis* decreased linearly with the acetaldehyde concentrations in the broth. The results of the current study were consistent with theirs. In an attempt to gain more information about the inhibitory mechanism of acetaldehyde on *Zymomonas mobilis* ZM4 cells, the inhibited cells were examined using a scanning electron microscopy to investigate the morphological changes, which might be resulted from acetaldehyde inhibitory effects. Figure

7.2 shows a comparison between *Zymomonas mobilis* cells before and after the acetaldehyde addition.

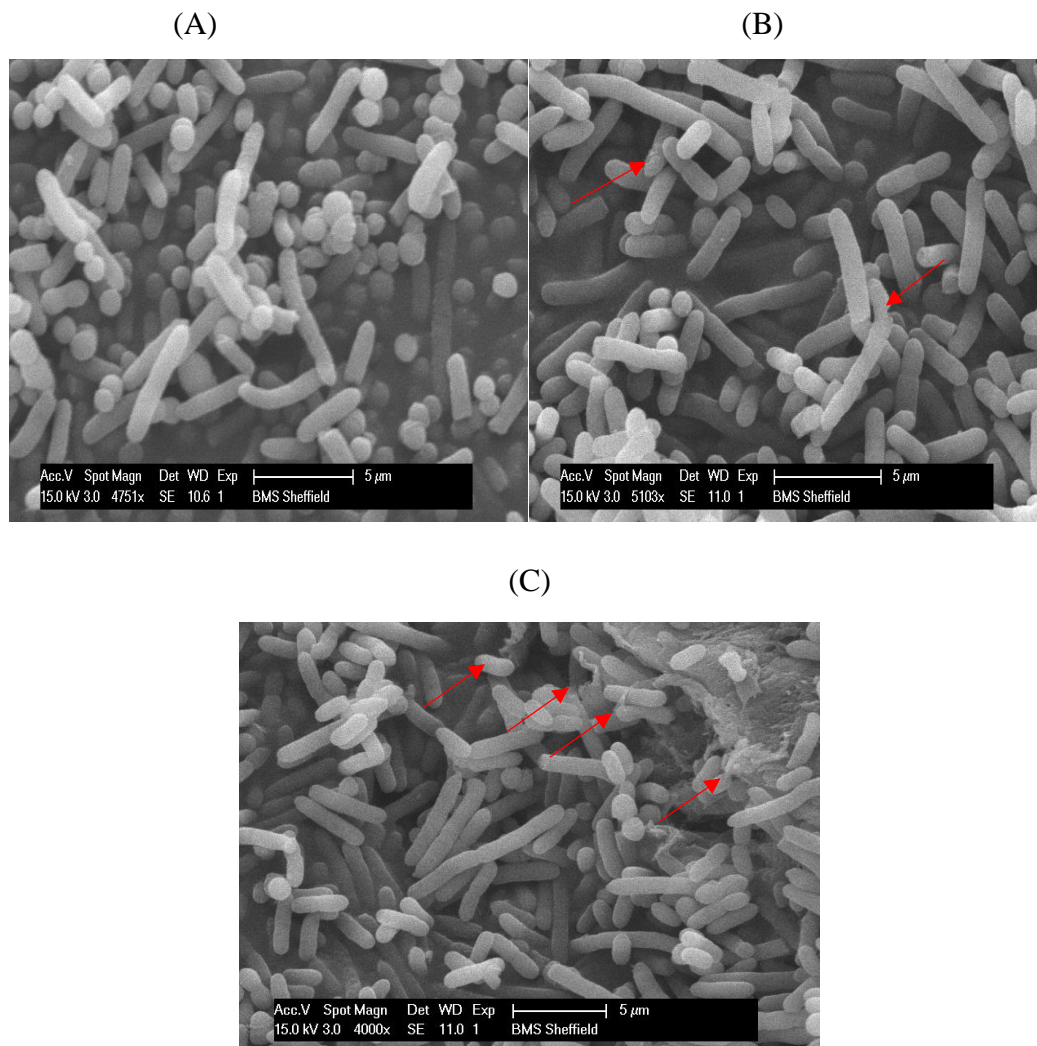


Figure 7.2: The morphological changes on *Zymomonas mobilis* ZM4 cells after acetaldehyde addition. (A) The control group without acetaldehyde addition. (B) the morphological changes on the cells after adding 0.5 % of acetaldehyde. (C) the morphological changes on the cells after adding 1.0 % of acetaldehyde.

From Figure 7.2B and C, bacterial cells have lesions on them, and that there was a loss of membrane integrity with cells' flocculation. Cells injury might be irreversible and lead to the cells death (Hong et al., 1997). Seeing these morphological changes on the bacterial cells under acetaldehyde stress might prove the inactivation combined cell lysis as a result of acetaldehyde toxicity.

To our knowledge, there is no clear mechanism of acetaldehyde inhibition mentioned previously. However, a mechanism was suggested by Bolstad, (2003), to show the combined

toxicity of acetaldehyde with oxygen radicals in mammalian liver cells. Figure 7.3 shows the suggested mechanism of acetaldehyde toxicity by Bolstad, (2003).

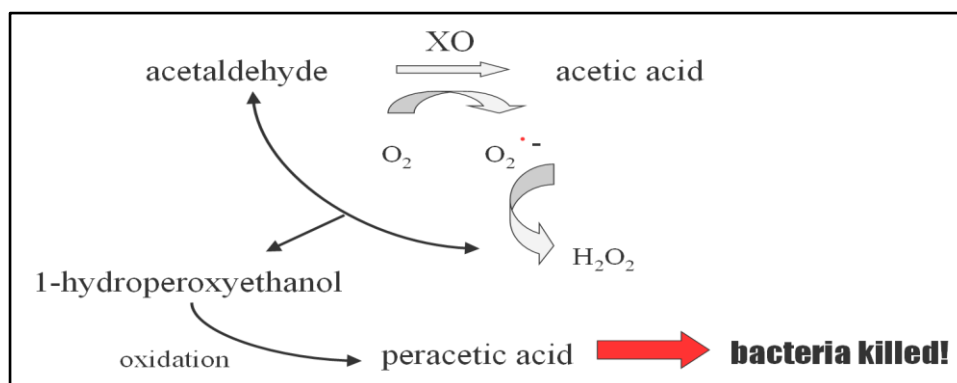
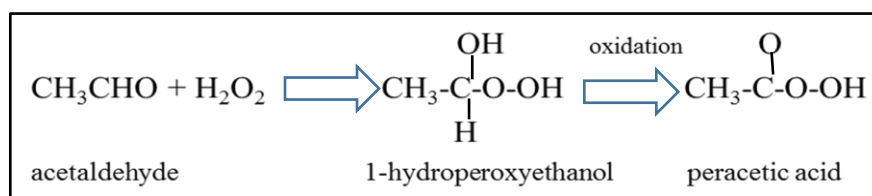


Figure 7.3: Mechanism of acetaldehyde toxicity (Adapted from Bolstad, 2003).

According to the above mechanism, it is unclear whether the toxicity is caused by producing oxygen radicals ($\text{O}_2^{\cdot-}$ / H_2O_2) or whether the toxicity comes from the acetaldehyde/ H_2O_2 adduct as shown below:



Therefore, it is hypothesised that acetaldehyde forms toxic adducts with superoxide radical, hydrogen peroxide, and hydroxyl radicals, and these toxic compounds would decrease the survival of bacterial cells such as *E.coli* (Bolstad, 2003).

Another scenario was tested by adding acetaldehyde after 4 hours of the inoculation. It was considered that four hours would be sufficient to accumulate acetaldehyde within the fermentation broth of *Zymomonas mobilis* under aerobic conditions compared with after two hours additions (Ishikawa et al., 1990). Figure 7.4A shows that the bacterial growth was strongly inhibited by the acetaldehyde addition after four hours, and the acetaldehyde effect was proportional to its concentration. Figure 7.4B shows that the specific growth rates of the *Zymomonas* culture at various concentrations of the added acetaldehyde in comparison with the control group (In which no acetaldehyde was added). Comparing the specific growth rates in Figures 7.1B and 7.4B, it is clear that acetaldehyde accumulation at the early stage (after 2 hours) of the exponential phase can substantially reduce the specific growth rates of

Zymomonas mobilis to about 83 % in comparison with acetaldehyde addition after 4 hours, which decreased the specific growth rates of the same bacterium to around 75 % for the same acetaldehyde concentration, 1 %.

Morphological and physiological features, as well as adaptation and genetic changes of various growth phases, are different. Susceptibility of bacterial cells for inhibition by chemicals such as acetaldehyde, is strongly related to the bacterial growth phase. Bacterial cells tend to be more susceptible to inhibitors at the early stages of exponential phase in the cell cycle than at the late stages of the exponential phase, but these cells become more resistance to the inhibitors in the stationary phase (Cherchi and Gu, 2011). Resistance during the exponential phase is associated with the induction of σ -independent resistance mechanisms, which are induced while going through this phase. On the other hand, resistance during the stationary phase is associated with the induction of other stress-resistant genes such as heat shock genes (Cherchi and Gu, 2011).

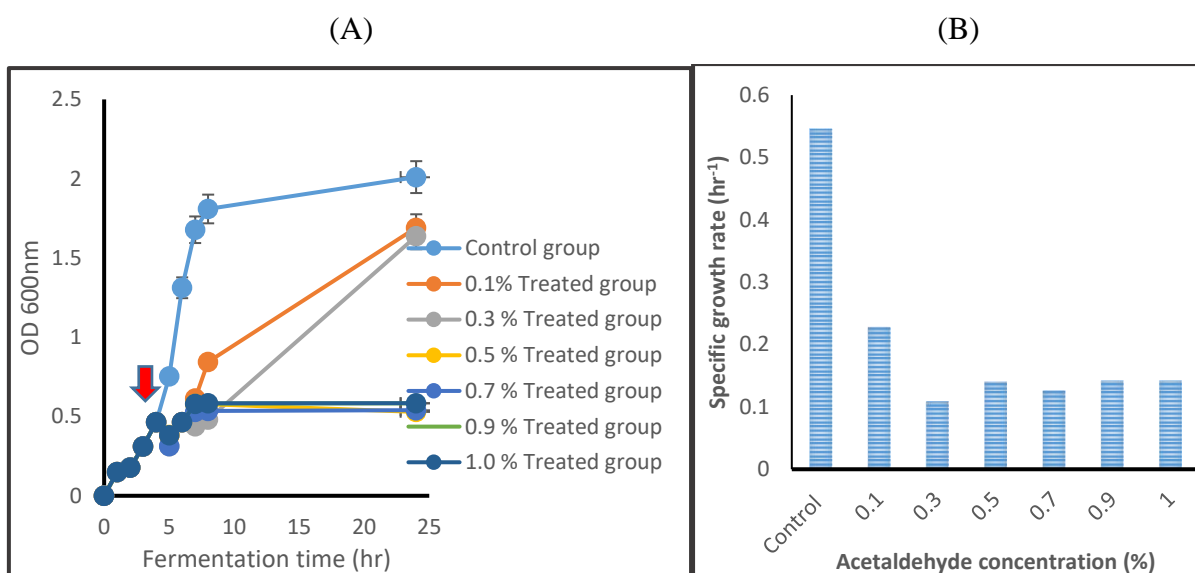


Figure 7.4: (A) Effect of added acetaldehyde on exponential cell growth of *Zymomonas mobilis* ZM4 after 4 hours. The red arrow shows the time of the acetaldehyde addition. (B) Specific growth rate of *Zymomonas mobilis* ZM4 after addition various concentrations of acetaldehyde at hour fourth. Error bars depict standard deviation.

7.2 Combined accumulation of both acetaldehyde and carbon dioxide with their inhibitory effects

In section 2.2, the potential scenarios of carbon dioxide accumulation were mentioned with a specific focus on the physiological effects of this accumulation, while in this section, attention is drawn to examine the potential morphological changes of carbon dioxide accumulation on *Zymomonas* cells. Additionally, the consequences of the combined accumulation of both carbon dioxide and acetaldehyde are also explored.

Two experimental sets were designed to study and to validate the morphological changes on the *Zymomonas* cells under the stresses of both carbon dioxide and acetaldehyde. In the first experimental set, samples were treated with carbon dioxide gas for around 20 mins until reaching an equilibrium concentration, where no further decrease in pH was noticed. Carbon dioxide is produced during the fermentation process in addition to acetaldehyde and ethanol, and some of the produced carbon dioxide remains dissolved in the liquid broth, and this broth reaches saturation during fermentation (i.e. contains the maximum possible amount of dissolved carbon dioxide) (Brown, 2001). In the second experimental set, *Zymomonas* cells were treated with both carbon dioxide for 20 mins and acetaldehyde then added to study the combined effect of both these products. Further, *Zymomonas* cells were collected from the real fermentation vessels in the initially-sparged group and periodically-sparged group to validate the observed morphological changes in the bacterial cells.

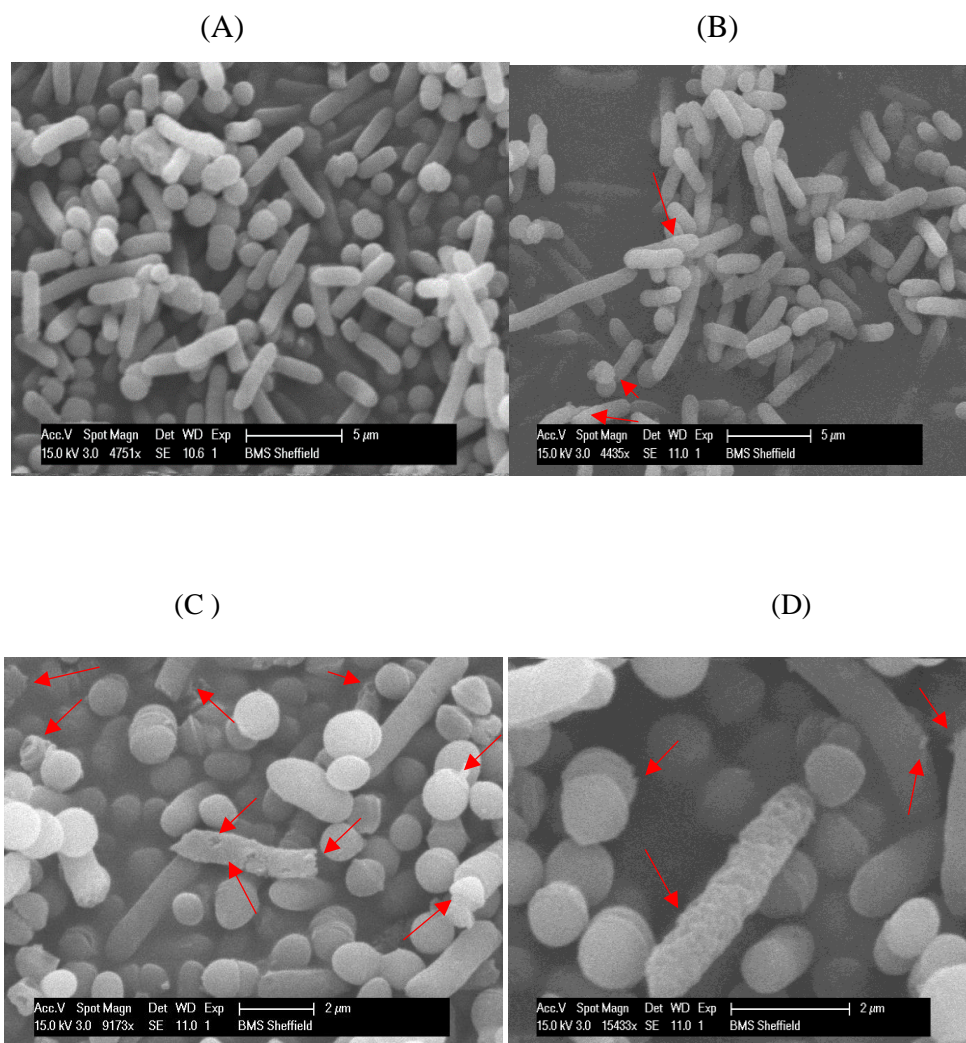


Figure 7.5: The morphological changes on *Zymomonas mobilis* ZM4 cells after carbon dioxide and acetaldehyde accumulation. (A) The control group before carbon dioxide and acetaldehyde

accumulation. (B) The morphological changes on the cells after carbon dioxide accumulation by sparging carbon dioxide for 20 mins at 0.3 l/min. (C) The morphological changes on the cells after addition of 0.5% of acetaldehyde after 2 hrs and carbon dioxide accumulation for 20 mins. (D) The morphological changes in the cells after addition of 1% of acetaldehyde after 2 hrs and carbon dioxide accumulation for 20 mins.

Figure 7.5B shows the bacterial cells that remained intact but with shortening in size of some of them. In addition, some lesions on the cells' membranes were observed, which might be resulted from the modification of the cell membrane composition and characteristics by increasing its fluidity and permeability due to the accumulated carbon dioxide (Garcia-Gonzalez et al., 2007). Figure 7.5C displays the *Zymomonas* cells after adding both acetaldehyde (0.5%) and carbon dioxide, and *Zymomonas* cells were transitioned from rod cells to coccus cells. This transition might increase the attachment activity of the bacterial cells and provoke cell flocculation (Fakhruddin and Quilty, 2006). Occasionally, the size reduction is accompanied by an increase in population under various environmental stresses (Novitsky and Morita, 1976; Amy and Morita, 1983; Givskov et al., 1994 ; Mueller, 1996 and Makarov et al., 1998), and the surface area to volume ratio. This response is useful under starvation stress, when the bacterial cells tend to increase their ability to transport nutrients with minimum energy consumption due to the increase of the diffusibility of these nutrients (Sanin et al., 2003). However, the morphological changes on the *Zymomonas* cells is thought to be a consequence of changing the shape-determining mechanism due to the environmental stresses (carbon dioxide and acetaldehyde). In Figure 7.5D, the concentration of the added acetaldehyde was increased to double, but the morphological changes of the *Zymomonas* cells were almost the same as in the previous experiment, 0.5 % acetaldehyde concentration. This observation agreed with what was observed in Figures (7.1A and 7.4A), where *Zymomonas* cells performed almost the same under these two acetaldehyde concentrations (0.5 % and 1 %). Therefore, it is suggested that the acetaldehyde inhibitory effect starts as low as 0.1 %, and this effect maximises and becomes severe after increasing the acetaldehyde concentration to 0.5% and upwards. The same observation was reported by Wecker and Zall, (1987), who found that *Zymomonas* growth was inhibited at concentrations as low as 0.05 % acetaldehyde.

7.3 Oxygen requirement of the fermentation system

Oxygen plays a very important role in the fermentation process of *Zymomonas mobilis* ZM4. Depending on whether the process is aerobic or anaerobic, the fermentation products can be changed. *Zymomonas mobilis* tends to accumulate less reduced metabolite, acetaldehyde under aerobic conditions, while ethanol preferentially accumulates under anaerobic conditions. Sparging air-microbubbles in the fermentation system can achieve two main purposes. The first

is to provide enough oxygen for *Zymomonas* growth and propagation. The second is to strip out some fermentation products such as acetaldehyde, carbon dioxide and, to a lesser extent, ethanol.

Three strategies can be used to provide oxygen to the bacterial culture, which are the initial sparging strategy, the continuous sparging strategy, and the periodical sparging strategy.

7.3.1 Initial sparging strategy

Oxygen uptake rate is constant during the fermentation process as long as the oxygen concentration is above the critical biological concentration, where the microbial cells have not yet been starved for oxygen (Bandyopadhyay and Humphrey, 1967). The exact value of the critical oxygen concentration depends on the microorganism, and this value usually falls between 5 % and 10 % of the air saturation under average operational conditions (Doran, 2013). Taking these values into account as well as considering studies from Ishikawa et al., (1990) and Bringer et al., (1984), 0.83 ppm was used as the critical oxygen concentration in these experimental sets, which equals more than 10 % of oxygen saturation in the fermentation medium. This oxygen concentration can be seen as a safe choice to keep the whole fermentation process aerobic.

In the initial sparging strategy, air microbubbles were sparged at the beginning of the fermentation process. This sparging can achieve two goals. The first is to provide oxygen to the bacterial culture until it reaches an equilibrium, at which point no further oxygen can be dissolved in the fermentation broth. The second is to distribute the bacterial inoculum within the fermentation broth evenly using fluid circulation generated by rising microbubbles in the airlift loop bioreactor. Oxygen concentration after turning off the air supply was monitored, and the initial $K_L a$ was calculated using nitrogen degassing method, when $\ln\left(\frac{C^* - C_0}{C^* - C_t}\right)$ is plotted against time, and the slope is $K_L a$.

Figure 7.6A shows the oxygen concentration profile during the fermentation process using the initial sparging strategy. The calculated $K_L a$ at 0.3 L/min and 30°C is 31.8 hr⁻¹. Figure 7.6B shows the typical plot for $K_L a$ estimation for 0.3L/min at 30°C, where the slope of the straight line indicates a mass transfer coefficient $K_L a$ (min⁻¹). The calculated $K_L a$ is valid as long as the following assumptions are met: the liquid phase is well mixed, the response time of the dissolved oxygen electrode is fast (the used oxygen electrode (Seven Dual pH and DO TM220, Mettler Toledo) has a response time is just over 10 seconds), while the gas-phase dynamics are ignored as there are no expected changes in the properties of the gas dispersion with time.

The oxygen concentration had fallen below the proposed critical oxygen concentration after just 270 minutes (4.5 hours) Figure 7.6A, leading to a shift from aerobic conditions to anaerobic ones, which accumulate ethanol preferentially. It is worth emphasising that aerobic conditions need to be kept in order to accumulate acetaldehyde (the target product) in the fermentation broth as well as ethanol but to a lesser extent. Therefore, another sparging strategy needs to be used in order to maintain aerobic conditions during fermentation.

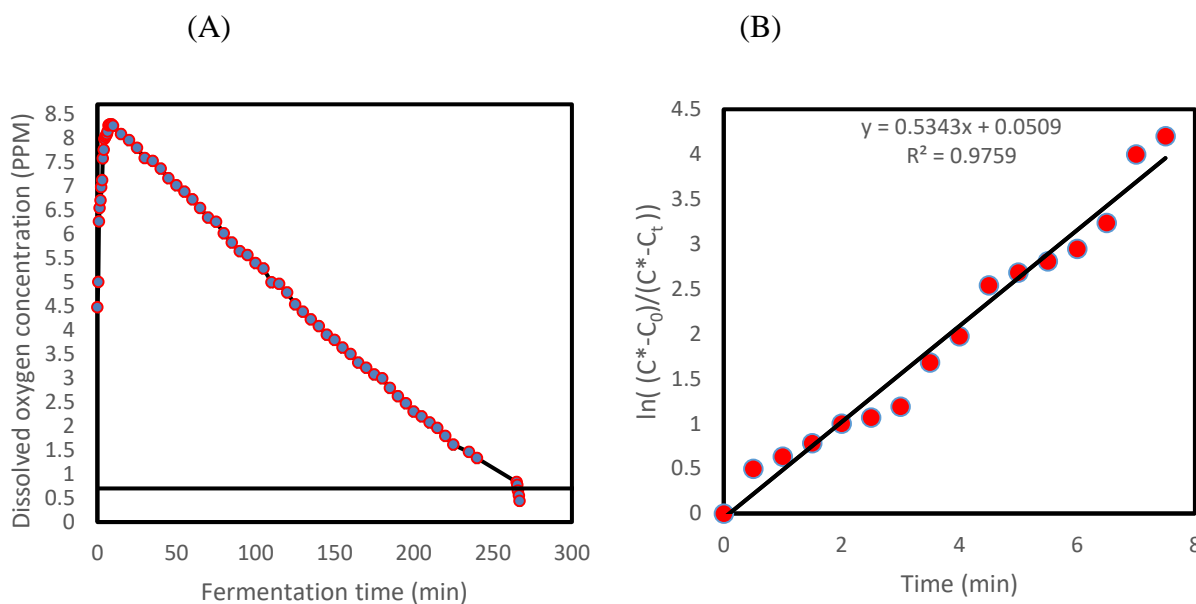


Figure 7.6: (A) The dissolved oxygen concentration against time during the fermentation process of *Zymomonas mobilis* ZM4 using the initial sparging strategy. (B) Typical plot of initial K_La estimation under initial sparging strategy, where the slope of straight line indicates mass transfer coefficient K_La (min^{-1}). The readings are representative of triplicate results.

7.3.2 Continuous sparging strategy

The dissolved oxygen concentration was monitored during the fermentation process under continuous sparging strategy (Figure 7.7). Using continuous sparging strategy kept the oxygen concentration high during the fermentation process with continuous mixing of the fermentation broth and stripping of the fermentation products such as acetaldehyde and carbon dioxide, and both of which are advantageous for the aerobic fermentation (Figure 7.7). On the other hand, using this strategy consumes high energy and gas with a high operational cost, because the used fluidic oscillator needs a high flow rate (60-80 L/min) to generate a pulse-jet stream. Dry air at only 0.3 L/min was fed to the diffuser, and the rest of the dry air (64.7 L/min) was purged as 65 L/min of dry air at 1.5 bars was fed to the fluidic oscillator.

Also, both biomass concentration and specific oxygen uptake rate are not considered in the K_La calculation when using the nitrogen degassing method, because they need to be

determined by considering other parameters such as oxygen solubility, which is susceptible to experimental inaccuracies. To avoid some of these complications and making K_La more representative to the real situation in the fermenter, a periodical sparging strategy was suggested to reduce cost, wasted gas and energy usage, and to make it more inclusive to the biomass concentration and ultimately to the oxygen uptake rate, r .

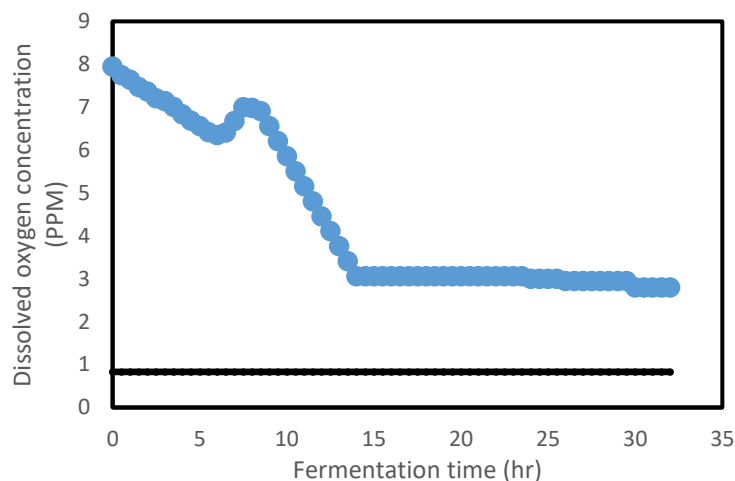


Figure 7.7: The dissolved oxygen concentration against time during the fermentation process of *Zymomonas mobilis* ZM4 using the continuous sparging strategy, whereby the concentration of the dissolved oxygen is kept far from the critical oxygen concentration. The readings are representative of triplicate results.

In addition, acetaldehyde and carbon dioxide cannot be collected efficiently under this strategy since both of those products are continuously stripped from the fermentation broth and; so their concentrations in the outlet stream are too low to be efficiently collected in both the vapour phase collection and the gas collection systems. Therefore, it is suggested that the continuous sparging strategy is more suitable in systems with high acetaldehyde and carbon dioxide productivities that need more oxygen supply. Such systems face inhibition problems due to the accumulation of by-products. Additionally, ethanol can be removed from the fermentation broth by the continuous stripping. This strategy can be a good option to provide enough oxygen to aerobically-grown microbial cultures, but using this strategy should be accompanied with high product concentrations.

7.3.3 Periodical sparging strategy

To save energy and to keep the operational cost low with efficient products stripping, air-microbubbles were sparged periodically. Air-microbubbles were introduced to the fermentation system until oxygen concentration equilibrium was achieved. Thereafter, the sparging was stopped, and the system was left to consume the provided oxygen. When the

oxygen concentration dropped to about the critical oxygen concentration, the air supply was turned on again. Two periods were identified during the aeration. The first period was at the beginning of the fermentation process, when the oxygen concentration reached its saturation concentration at 30°C to ~ 8.28 ppm. In the second period, the system had already started to produce the fermentation products such as carbon dioxide (gas) and acetaldehyde (which tended to be vapor at 30°C), and this changed the equilibrium of oxygen in the system. The new equilibrium concentration was reached ~4.7 ppm.

The rational interpretation for these two periods is that the oxygen mass transfer response follows the thin film theory, in which the mass transfer response is inherently transient in small microbubbles (Bredwell and Worden, 1998 and Worden and Bredwell, 1998). In the first period, the oxygen mass transfer is sufficiently fast. Therefore, the internal concentration of oxygen in the microbubbles is significantly reduced as there is a significant driving force for oxygen transfer from the microbubble to the fermentation medium and eventually to the microbial cells. This nonequilibrium driving force is decreased as microbubbles rise in the fermentation broth. Ultimately, if the bubble composition of gases reaches equilibrium with the bulk liquid concentration, this driving force for the mass transfer vanishes (Al-Mashhadani et al., 2011). Concurrently, the bacterial culture would be in the lag phase, and will have just started to consume the oxygen.

At the second period of the aeration, when the fermentation process has already begun, the bacterial culture started consuming oxygen, and many gaseous products have been produced. The equilibrium of the system changed and the bubble composition varied. During this period, the produced gases accumulated in the bulk liquid, and they tended to diffuse into microbubbles, and this might lead to reducing the equilibrium concentration, reducing the nonequilibrium driving force. Figure 7.8 shows the oxygen consumption pattern in the *Zymomonas* fermentation culture with a two-staged aeration pathway.

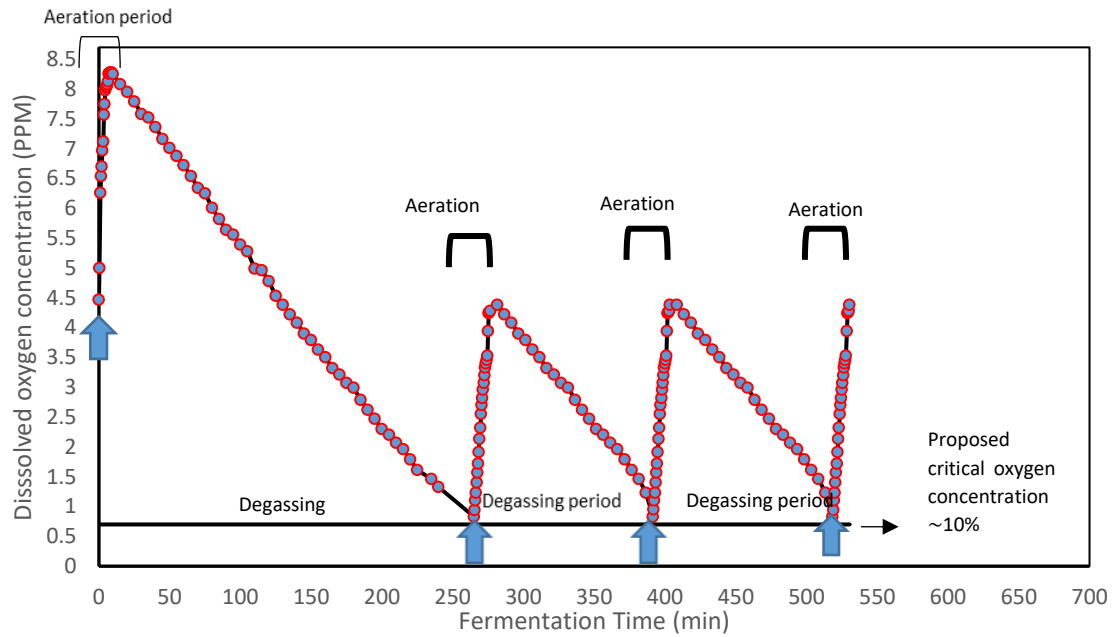


Figure 7.8: A model of periodical oxygen dosing and consuming in *Zymomonas* fermentation culture. Two periods were identified during the aeration. The first period was at the beginning of the fermentation process, while at the second period, fermentation process has already begun, and the cultured started consuming oxygen, and many gaseous products have been produced. The readings are representative of triplicate results.

Table 7.1: The oxygen mass transfer coefficient (for 0.3 L min⁻¹ dosing) with equilibrium concentrations and sparging time (mins) calculated during the experimental sets.

Period			r (specific oxygen uptake rate) mmol. g (dry weight) ⁻¹ .hr ⁻¹	
			Growth phase	r-value
The first period	182 hr ⁻¹	$K_L a$ (Mass transfer coefficient)	Lag phase	1.8
	8.11 PPM	C^* (saturation concentration)		
	8 mins	Sparging time	Log Phase	4.2
	265 mins	Time before the next sparging		
The Second period	237 hr ⁻¹	$K_L a$ (Mass transfer coefficient)	Stationary phase	2.88
	4.23 PPM	C^* (equilibrium concentration)		
	16.5 mins	Sparging time	Death phase	1.56
	110 mins	Time before the next sparging		

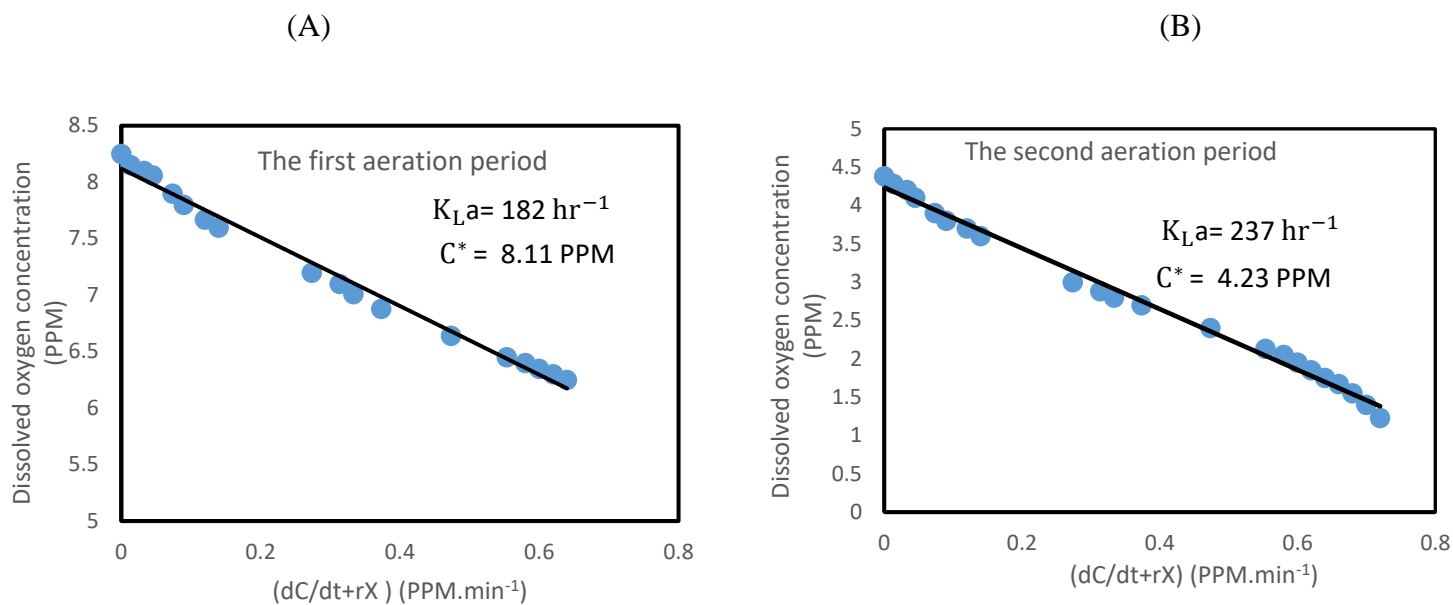


Figure 7.9: Graphic determination of Volumetric oxygen transfer coefficient for *Zymomonas mobilis* ZM4 culture (for 0.3 L min^{-1} dosing). (A) During the first period (8 mins). (B) During the second period (16.5 mins). The readings are representative of triplicate results.

Both Table 7.1 and Figure 7.9 show that the oxygen mass transfer coefficient in the first period is lower than that of the second period. Variations in the oxygen mass transfer coefficients happened at different bacterial growth stages (different growth rates) which can likely be attributed to the physicochemical features of the fermentation medium due to the bacterial propagation and product excretion from the cells. Both these two factors can play important roles in changing the characteristics of the fermentation broth (Bandyopadhyay and Humphrey, 1967). After inoculating the fermentation medium with the *Zymomonas* inoculum, sometimes needs to be spent in the lag phase (adaptation phase) before the bacterial culture launches the log phase (exponential phase). During the lag phase and the early stage of the log phase, the biomass concentration was as low as 0.5 g/L , and this concentration was almost constant across the first three hours of the fermentation process before the culture launched into the exponential phase, when the biomass concentration started to grow exponentially (Figure 7.10B).

The specific growth rate of the *Zymomonas* cells grown under the initial sparging strategy was around 0.39 hr^{-1} , while the cells grown under the periodical sparging strategy showed an increased specific growth rate, which reached 0.44 hr^{-1} , 13 % faster growth rate than the cells grown in the initially-sparged group.

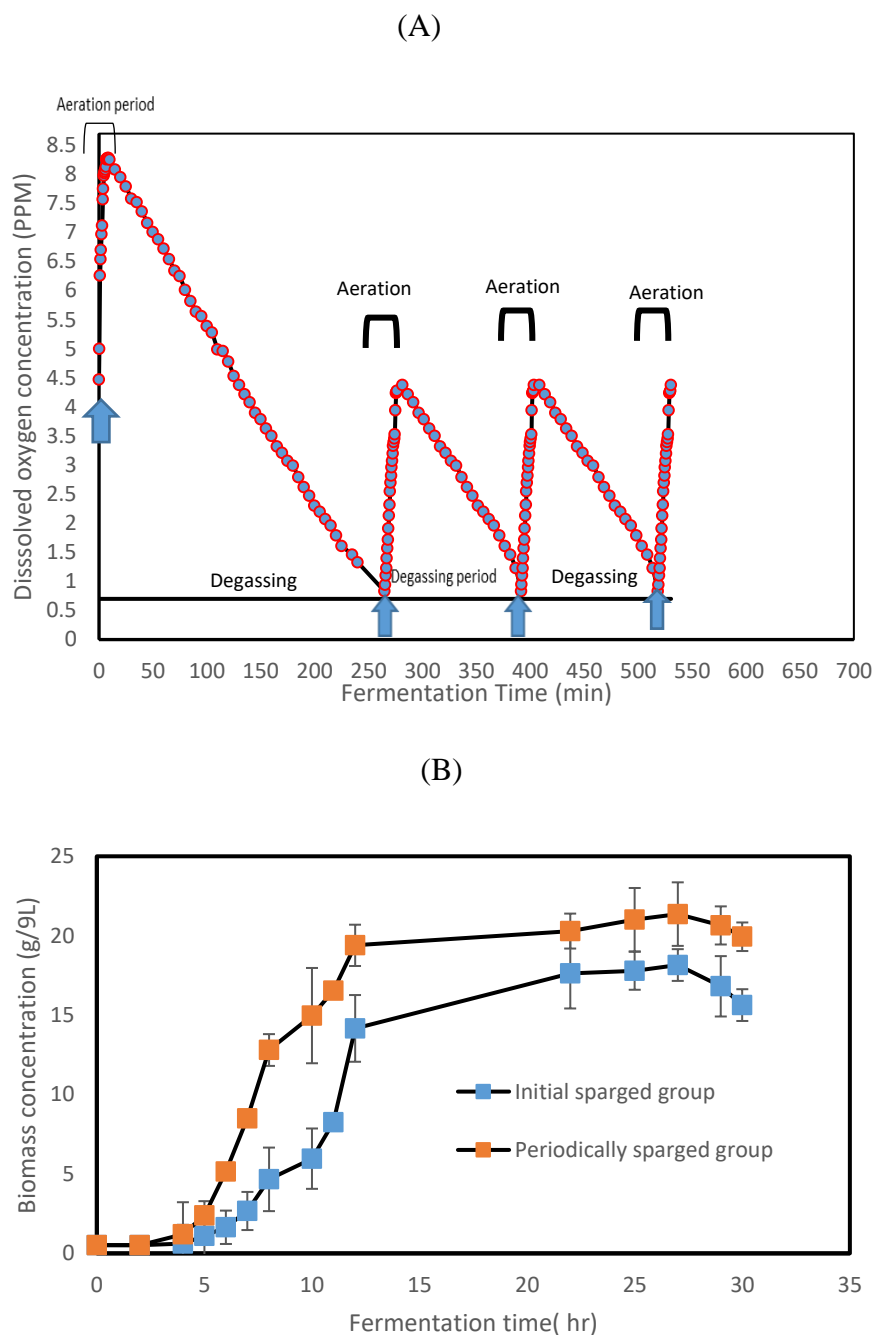


Figure 7.10: (A) A model of periodical oxygen dosing and consuming in *Zymomonas* fermentation culture. (B) Comparison between the growth pattern of *Zymomonas mobilis* under initial and periodical sparging strategies, highlighting the importance of keeping aerobic conditions. Error bars depict standard deviation.

7.3.4 Specific oxygen uptake rate patterns

Due to the low solubility of oxygen in fermentation broths, the dissolved oxygen concentration in these broths can become the limiting nutrient (Garcia-Ochoa et al., 2010). Decreasing the dissolved oxygen concentrations in the fermentation broth was described previously due to high demand during the fast growth in the exponential phase, however this demand became minor

in the stationary phase (Pinches and Pallent 1986). This behaviour fits most of the microbial cultures (García-Ochoa et al., 2000 and Çalik et al., 2006).

The specific oxygen uptake rate (r or qO_2) is characteristic for each microorganism, and it is commonly considered a constant during microbial growth but interestingly many experimental results show a disagreement with this presumption (García-Ochoa et al., 2000 and García-Ochoa et al., 2010).

The oxygen consumption and oxygen supply rate for *Zymomonas mobilis* cultures have been intensively studied (Mastroeni et al., 2003; Bringer et al., 1984; Kalnenieks et al., 2000 and Pentjuss et al., 2013). However, the specific oxygen uptake rate for various growth phases of *Zymomonas mobilis* has not been studied. Therefore, part of the current study was to monitor and to track the oxygen concentration profile during all phases of growth as well as working out the specific oxygen uptake rate for each phase of growth.

During the first 2 to 3 hours of the fermentation process, specific oxygen uptake rate (r , qO_2) was measured immediately after the inoculation, using the biomass dry weight concentration (from the biomass calibration curve) to calculate the initial biomass concentration in the fermenter. Figure 7.11 shows the growth curve of *Z. mobilis* in the periodically-sparged group labelled with specific oxygen uptake rates for each growth phase. In general, the specific oxygen consumption rate was proportional to the rate of the bacterial growth in the culture. Consequently, the highest value recorded in these experiments was related with the most rapid growth, during the exponential phase.

As it can be seen from Figure 7.11, the specific oxygen uptake rate in the lag phase was $1.8 \text{ mmol.g (dry weight)}^{-1}.\text{hr}^{-1}$ during the first two to three hours. After that, this rate was increased to more than double at the log phase to $4.2 \text{ mmol.g (dry weight)}^{-1}.\text{hr}^{-1}$, and it was almost uniformly constant from the 4 to 12 hours of the fermentation duration. The increase in the oxygen consumption coincides with an increase the metabolic rate in microbial cells, which occurs near the end of the lag phase and the log phase (Martin, 1932). The specific oxygen uptake rate in this study is defined as the population respiration rate normalised by the population biomass. This specific oxygen uptake rate is decreased as the microbial culture transited from the exponential phase to the stationary phase, when this rate reached $2.88 \text{ mmol.g (dry weight)}^{-1}.\text{hr}^{-1}$.

Carbon limitation is an important factor in the launching of a microbial culture to the stationary phase in complex media (Chubukov and Sauer, 2014). Many bacteria catabolise a variety of

carbon sources to generate energy and such carbon starvation in the stationary phase causes a lack of the required energy for stationary phase responses (Chubukov and Sauer, 2014). Interestingly, glucose had not been yet depleted when the bacterial culture launched the stationary phase. Therefore, other factors might accelerate the *Zymomonas* culture's entrance into the stationary phase. These factors such as accumulation of toxic metabolites, can provoke the launch to the stationary phase. The bacterial cells in this phase show a decrease in the resistance to antibiotics and other environmental stresses, and microbes need to resolve this dilemma, and solving it represents a trade-off between energy generation and resistance mechanisms (Benaroudj et al., 2001).

The specific oxygen uptake rate decreased further in the death phase, reaching $1.56 \text{ mmol.g (dry weight)}^{-1}.\text{hr}^{-1}$. This observation disagrees with what was mentioned by Riedel et al., (2013), who observed an increase in the specific oxygen uptake rate during the death phase. The interpretation of this observation might be due the cryptic growth. When nutrients are liberated from dead cells, these nutrients can be utilised by other cells for growth and propagation (Riedel et al., 2013). however, this rate was decreased in the death phase, and this probably happened because of the accumulation of the ethanol, increasing the death rate and depletion of the carbon source, glucose in this case.

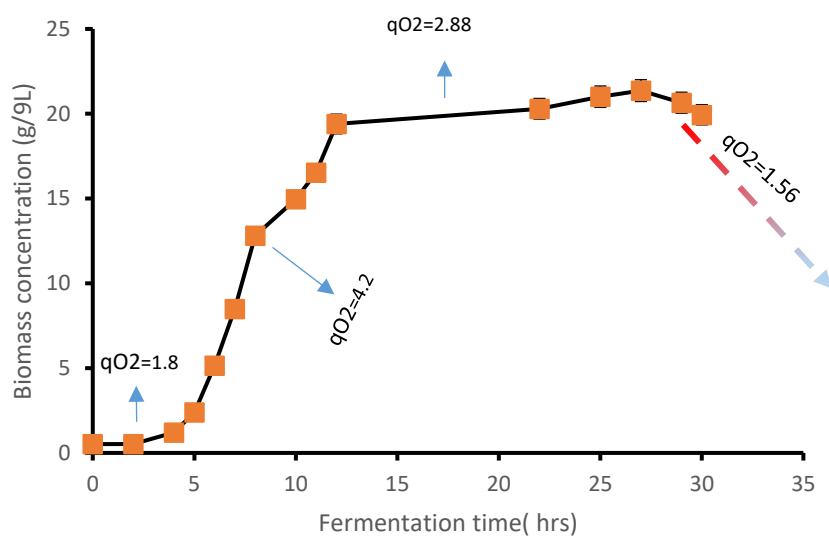


Figure 7.11: *Zymomonas* growth pattern during periodical sparging strategy (Flow rate 0.3 L/min) labelled with the specific oxygen uptake rate (qO_2) $\text{mmol.g(dry weight)}^{-1}.\text{hr}^{-1}$. The oxygen uptake rate hits its highest in the exponential phase, while it is gradually decreased in both stationary and death phases. The readings are representative of triplicate results.

7.4 Central metabolic routes

Zymomonas mobilis is a facultative anaerobic, obligatory fermentative bacterium (Rogers et al., 1982). It metabolises several sugars such as glucose, fructose and sucrose by an Entner-Doudoroff pathway in combination with the enzymes of pyruvate decarboxylase to convert the pyruvate into carbon dioxide and acetaldehyde, along with alcohol dehydrogenase to produce ethanol as a final product (Dawes et al., 1966).

Generally, *Zymomonas mobilis* catabolises around 95-98 % of the carbon source (glucose) into ethanol and carbon dioxide, while just 3-5 % of this carbon source can be used in biomass formation and to serve an anabolic role (Swings and De Ley, 1977 and Rogers et al., 1982). Figure 7.12 shows the glucose consumption pattern and glucose consumption rate in both initially sparging group and periodically sparging group.

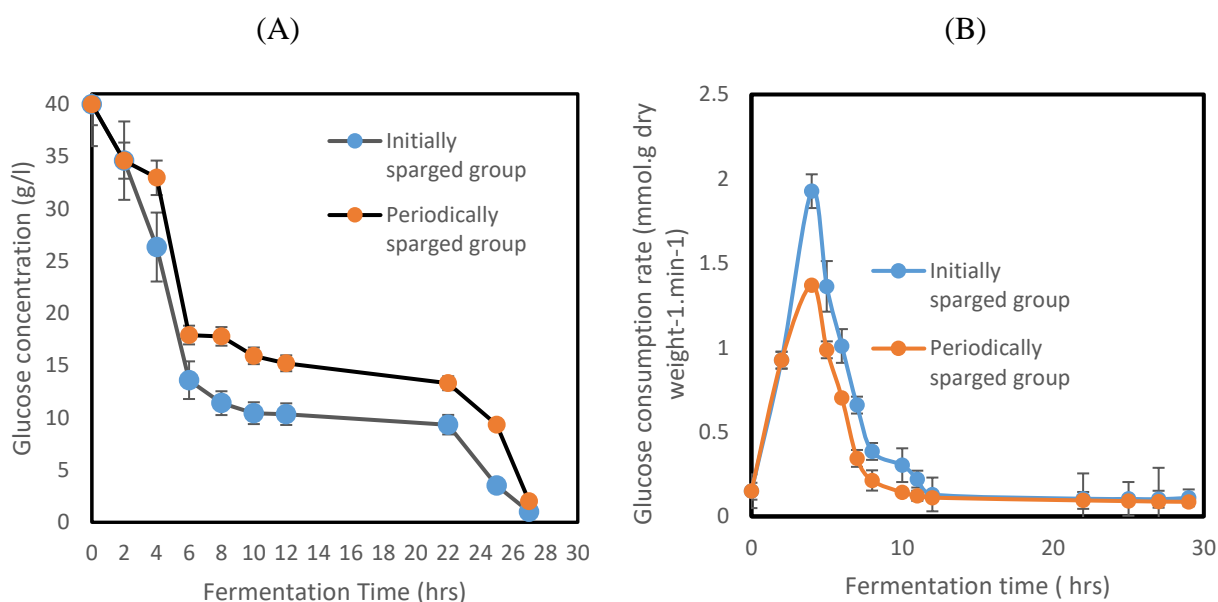
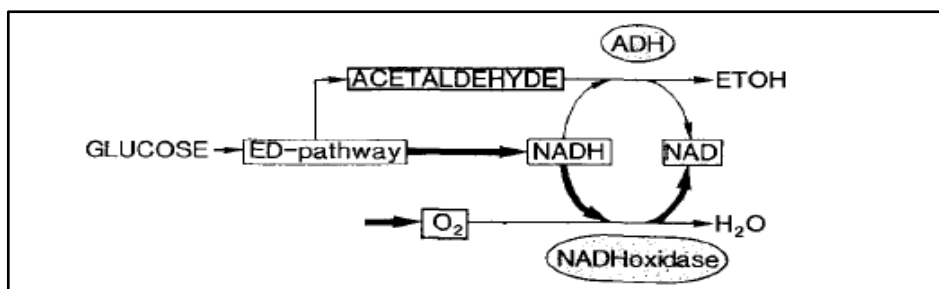


Figure 7.12: Glucose consumption pattern in *Zymomonas mobilis*. (A) Glucose concentration against time. (B) Glucose consumption rate in both initially and periodically sparged groups, whereby Initially sparged culture consumed more glucose than that the periodically sparged group under anaerobic conditions. Error bars depict standard deviation.

Carbohydrate metabolism in *Zymomonas mobilis* can be seen as a true catabolic highway (Sprenger, 1996). Anaerobically, *Z. mobilis* cells convert glucose into ethanol and carbon dioxide at 3 to 5 times faster than the glucose consumption rate in yeast (Rogers et al., 1982). Also, the glucose consumption rate in this bacterium is also 1.2 to 1.5 times faster than *Streptococcus bovis*, which is another promising obligatory fermentative microorganism (Cook and Russell, 1994).

Initially, both groups were started at the same level of oxygen, and both groups showed almost the same pattern of biomass production (Figure 7.10) and glucose consumption (Figure 7.12) at the first 3 hours of the fermentation process. Thereafter, the initial sparging group was kept without any oxygen supply, while the periodically-sparged group was regularly aerated. 4 hours were required to reach the critical level of oxygen in both groups (Table 7.1), and further oxygen starvation led to a shift in the metabolism pathway into the anaerobic fermentation. Ishikawa et al., (1990), reported the same observation. Two scenarios were expected depending on the dissolved oxygen level: the first happens under high concentration of the dissolved oxygen (higher than the critical oxygen level), and the second occurs at relatively low dissolved oxygen concentration (lower than the critical oxygen concentration). NADH oxidase is responsible for the oxidation of NADH with oxygen, and thus, the oxygen consumption happens because of this activity (Bringer et al., 1984). Under the first scenario, the activity of NADH oxidase is directly adapted with dissolved oxygen concentration, and its activity increases as the concentration of the dissolved oxygen increases (Bringer et al., 1984). When the concentration of the dissolved oxygen is above the critical oxygen level, the NADH becomes limited because of the NADH oxidation by NADH oxidase, and therefore, less NADH (which is formed by an Entner-Doudoroff pathway) is available to reduce the acetaldehyde into ethanol by the alcohol dehydrogenase. In the second scenario, the concentration of the dissolved oxygen is nearly zero (lower than the critical oxygen level) when most of the formed NADH becomes available for the reduction of acetaldehyde into ethanol by alcohol dehydrogenase (Ishikawa et al., 1990). Figure 7.13 shows these two scenarios.

(A)



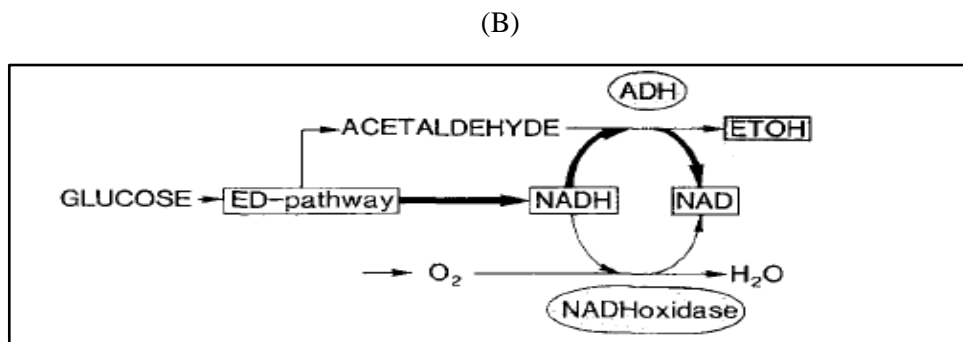


Figure 7.13: Proposed scenarios of the products shifting in *Z. mobilis*. (A) Under the aerobic conditions (Higher than the critical oxygen level). (B) Under anaerobic conditions (Lower than the critical oxygen level) (Adapted from Ishikawa et al., 1990).

Shifting from aerobic to anaerobic conditions can be observed in the changing of glucose consumption pattern in the initially- sparged group. Figure 7.12A shows that at the initial 3 hours of the fermentation, both experimental sets showed almost the same glucose consumption patterns as they started with the same dissolved oxygen concentration (around 8.28 ppm). After that, the groups diverged, and more glucose was consumed by the initially- sparged strategy group when almost 100 % of the glucose had been utilised at the end of the fermentation process (around 27 hours). In comparison, there was 99 % of glucose utilised after the same duration by the periodically sparged group.

Interestingly, the specific glucose consumption rate in initially- sparged group was almost double the specific rate in periodically-sparged group (Figure 7.12B). It can therefore be thought that more time is needed to consume the same amount of glucose by the aerobic culture.

Therefore, the presence of oxygen alternated both the glucose consumption and specific glucose consumption rate of *Zymomonas mobilis* in the fermentation system. There are many explanations for this behavior. For example: this observation could be attributed to the type of products: *Zymomonas mobilis* tends to produce less reduced metabolites under the aerobic condition with less ethanol (Swings and De Ley, 1977, Bringer et al., 1984 and Ishikawa et al., 1990). Also, *Zymomonas mobilis* ZM4 produces an increased amount of ethanol under anaerobic conditions, and growth in the presence of ethanol causes changes in the lipid composition as many lipids need to be synthesised (Tornabene et al., 1982 and Carey and Ingram 1983). The ability to synthesise a variety of lipids is essential to all organisms, and lipid biosynthesis pathways are endergonic: they use ATP as a source of the metabolic energy, and a reduced electron carrier as a reductant (Nelson et al., 2008). Therefore, it has been suggested that additional ATP needs to be generated to fulfill the energetic requirements of the lipids biosynthesis, which are used to change the composition of the bacterial membrane as an

adaptation strategy for the increasing ethanol concentration. This might also explain why anaerobically grown cells need to consume more glucose to meet this adaptation strategy. However, the difference in the glucose consumption at the end of the fermentation process was only 1 % between these two groups.

7.5 Fermentation products (Acetaldehyde, ethanol, and carbon dioxide)

Figure 7.14 (A, B) shows both acetaldehyde and ethanol production profiles during the fermentation process.

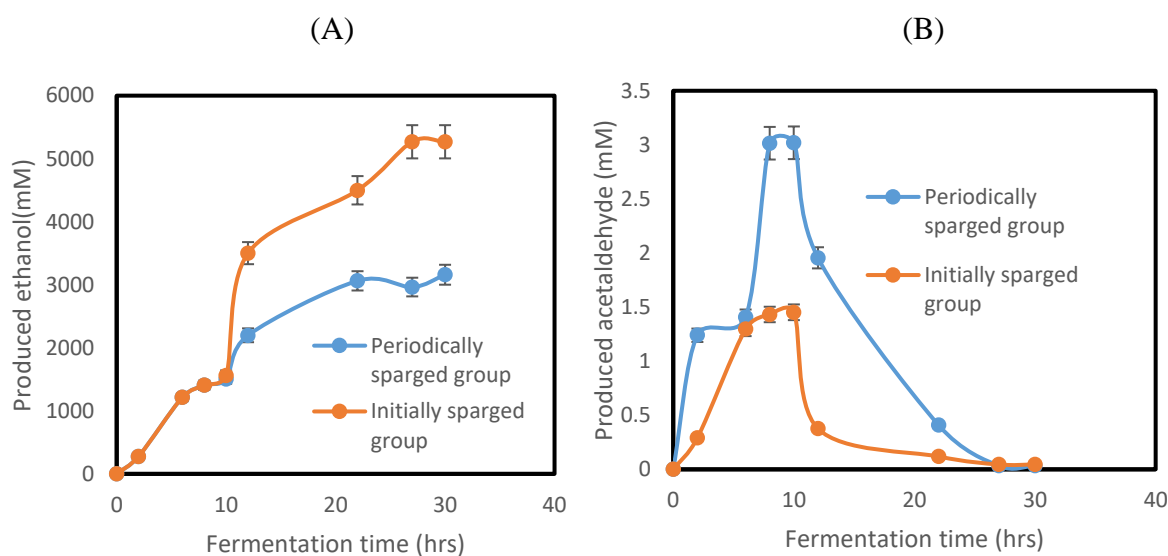


Figure 7.14: Acetaldehyde and Ethanol production during the fermentation course. (A) Ethanol production (B) Acetaldehyde production. Error bars depict standard deviation.

The ethanol production was almost the same between the two groups during the first 10 hours, and thereafter, the diversion between the two groups started and continued until the end of the fermentation process (Figure 7.14A). Interestingly, this deviation was expected to happen after almost 4 hours at the point at which the dissolved oxygen concentration was depleted and the metabolism was thought to shift to an anaerobic pathway gradually after this duration. In general, there was around 39 % more ethanol produced in the initially-sparged group in comparison with the periodically-sparged group. This result is consistent with the proposed scenarios in Figure 7.13, which suggested that there is less NADH available to the alcohol dehydrogenase to convert acetaldehyde to ethanol under aerobic conditions.

On the other hand, in Figure 7.14(B), acetaldehyde started to accumulate in the fermentation broth after just 2 hours from the beginning of the fermentation, and continued to accumulate within the broth and reached its highest point after 10 hours. Thereafter, the production decreased until the end of the fermentation process. The periodically-sparged group produced around 108

% more acetaldehyde than the initially-sparged group (Figure 7.14B). The accumulation of acetaldehyde in the periodically-sparged group during the first 10 hours might explain the increased concentration of ethanol, which was seen in this period as well. The concentration of substrate (acetaldehyde) is a key factor affecting the rate of reaction catalysed by an enzyme. Thus, increasing the acetaldehyde concentration in the periodically-sparged group increased the ethanol production by alcohol dehydrogenase, a linear increase with a concentration of acetaldehyde when it is at relatively low concentrations. With the further accumulation of acetaldehyde, the reaction velocity of alcohol dehydrogenase could increase by smaller and smaller amounts in response to an increase in the substrate (acetaldehyde) concentration. Eventually, the enzymatic reaction reaches a point, where the reaction velocity becomes very small as acetaldehyde concentration increases (Nelson and Cox, 2008). Figure 7.15 shows the total produced acetaldehyde and ethanol in both experimental groups.

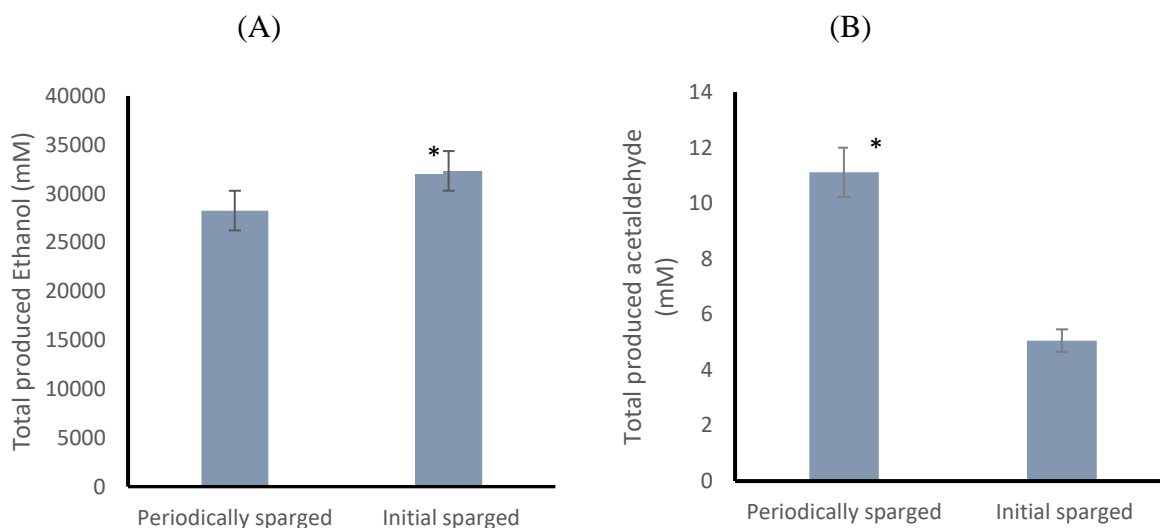


Figure 7.15: Accumulated fermentation products, considering both the produced and stripped products from the fermentation broth. (A) Total produced ethanol. (B) Total produced acetaldehyde. Error bars depict standard deviation. * The mean difference is significant at the 0.05 level.

7.6 *In situ* removal of some fermentation products

The production of acetaldehyde and its accumulation within the fermentation broth can severely inhibit the bacterial growth, and this might lead to deteriorate the culture progress before finishing the carbon supply. To solve this problem, a gas-stripping technique using microbubble technology is used to avoid the final product inhibition and to increase the substrate utilisation rate. In addition, *in situ* removal of the fermentation products (acetaldehyde and carbon dioxide) is accompanied with a decrease in the Gibbs free energy of the pyruvate decarboxylase reaction, and this will affect the driving force of the reaction in the direction of increased product

formation according to Equation 2.10. Removing both acetaldehyde and carbon dioxide has an entropic effect and replacing the removed acetaldehyde and carbon dioxide increases the entropy of the product-depleted state (Gary, 2004 and Al-Mashhadani et al., 2011).

The stripping of acetaldehyde can be modelled as a first order process according to the equation reported by Truong and Blackburn, (1984):

$$R_S = -\frac{dC_S}{dt} = K_S a C_S \quad (\text{Eq. 7.1})$$

Where R_S is the stripping rate, $-\frac{dC_S}{dt}$ is the change in the organic compound concentration with time and $K_S a$ is the stripping rate constant.

The gas-stripping rate increases proportionally for both changes in the concentration of organic solvent and the stripping rate constant, $K_S a$ (Eq. 7.1). Acetaldehyde is both the desired product and the inhibitory compound to *Zymomonas mobilis* and the relationship between stripping rate and the acetaldehyde concentration are both favourable. The stripping rate constant can be determined as the slope of a plot of $\ln \frac{C_{S_0}}{C_{S_t}}$ versus time t , as a linear best-fitted curve. As *Zymomonas mobilis* ZM4 produces acetaldehyde, the rate at which it is removed from the fermentation broth is likewise increased according to the Equation 7.1. Moreover, acetaldehyde is being both produced and stripped in the current system, and if it is continuously removed, the change in the acetaldehyde concentration is given by the following equation (Ezeji et al. 2005):

$$\frac{-dC_S}{dt} = R_S - R_P = K_S a C_S - R_P \quad (\text{Eq. 7.2})$$

At steady state ($\frac{dC_S}{dt} = 0$), the following equation can be obtained:

$$R_S = R_P = K_S a C_S \quad (\text{Eq. 7.3})$$

It can be concluded From Equation 7.3 that if $K_S a$ can be increased, then *Zymomonas mobilis* ZM4 will expose to a lower concentration of acetaldehyde for any given rate of solvent production. The gas-stripping rate constant can be modelled from the two-film mass transfer model for volatilisation processes as follows:

$$K_S a = \frac{a}{V} \left[\frac{1}{k_1} + \frac{RT}{H_C k_g} \right]^{-1} \quad (\text{Eq. 7.4})$$

The rate of mass transfer was increased by increasing the total interfacial surface area using microbubble technology, which gives a corresponding increase in $K_S a$ as illustrated by Equation 7.4. From Equations 7.1 and 7.4, important relationships can be obtained (Ezeji et al., 2005):

$$R_S \propto K_S a \quad (\text{Eq. 7.5})$$

$$K_S a \propto a \quad (\text{Eq. 7.6})$$

In addition, a correlation was developed between the gas flow rate and $K_S a$ for organic compounds in water (Truong and Blackburn, 1984):

$$K_S a \frac{V}{Q} = b(H_C)^{-1} \quad (\text{Eq. 7.7})$$

The important relationship that can be obtained from Equation 7.7 as follows:

$$K_S a \propto Q \quad (\text{Eq. 7.8})$$

Therefore, increasing the gas flow rate can increase $K_S a$ as well. However, only one flow rate was used in the current study, which is 0.3 L/min. Several reasons were considered before choosing this flow rate. For example, fluid foam was seen to appear at higher gas flowrates (more than 0.5 L/min), and this foam became even worse due to the generated microbubbles (~500 microns), when the traditional foam regions (the foam and the froth) were merged into one frothy mass (Vardar-Sukan, 1998). Another reason came from the simulation study conducted by Al-Mashhadani et al., (2015), which showed that using 0.3 L/min flow rate with a bubbles size of around 500 microns with the same fermenter geometry achieved maximum circulating eddy with limited dead zones.

On the other hand, the addition of antifoam compounds to the fermenter is well known to affect some parameters within the fermentation process such as hydrodynamics, bubble behaviour and interactions with other fermentation broth components, and it might also reduce the specific interfacial area available for mass transfer (Al-Masry, 1999). Importantly, 0.3 L/min is also suited both the vapour collection and gas collection systems because no acetaldehyde was detected in the output stream of the vapour collection system after passing it through 0.05% of 3-Methyl-2-benzothiazolinone hydrazone hydrochloride hydrate (MBTH) solution at random times during the sparging process.

Microbubbles provide high surface area to volume ratio (Zimmerman et al., 2009). Additionally, some fermentation products (such as acetaldehyde) flashes to its equilibrium

concentration of vapour on the surface layer of the microbubble, and the internal mixing of a microbubble is adequately rapid, and thus it reaches a uniformly-mixed status in a very short residence time (Zimmerman et al., 2013).

Therefore, using microbubbles provides a high interfacial area, a , which is directly related to both stripping rate constant ($K_S a$) and stripping rate (R_S) according to Equations 7.5 and 7.6.

Figure 7.16 shows the variation in acetaldehyde concentration during the fermentation process combined with air microbubbles sparging.

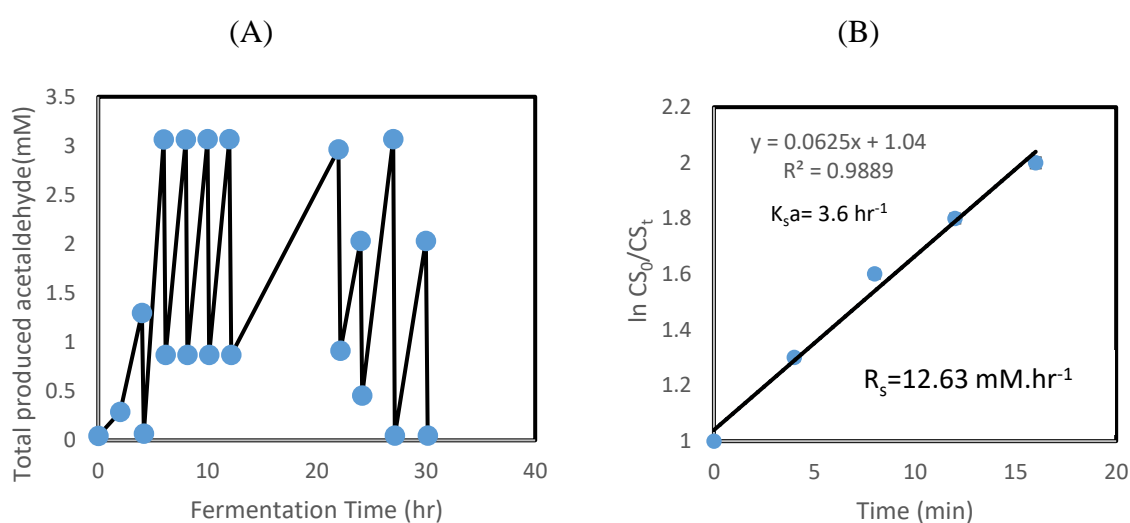


Figure 7.16: Stripping process of acetaldehyde from the fermentation broth using air microbubbles. (A) Fluctuation of acetaldehyde concentrations within the fermentation broth after stripping it with microbubble. (B) Variation of acetaldehyde concentrations with each sparging cycle and calculation of stripping rate constant $K_S a$. Error bars depict standard deviation.

The highest acetaldehyde concentration was 0.34 mM (0.015 g/L) (Figure 7.16A). This concentration is much lower than the inhibitory concentration of acetaldehyde. The stripping rate constant ($K_S a$) was calculated for the highest produced acetaldehyde at hour 10 when the acetaldehyde concentration reached around 0.34 mM. The application of microbubble technology decreased the acetaldehyde concentration to less than 0.022 mM after 16.5 minutes of sparging. Samples were withdrawn every 4 minutes and used to calculate the stripping rate constant ($K_S a$). The calculated stripping rate constant ($K_S a$) value was found to be 3.6 hr^{-1} . This value can be multiplied by the accumulated acetaldehyde concentration plus the produced acetaldehyde during the sparging time to work out the acetaldehyde removal rate or acetaldehyde-stripping rate, as acetaldehyde is both being produced and stripped during the sparging course. The acetaldehyde production rate (In hour 10 when the acetaldehyde

concentration reached its highest) was around $0.15 \text{ mmol. g(dry weight)}^{-1}.\text{hr}^{-1}$. Therefore; the stripping rate was around 12.63 mM.hr^{-1} .

Figure 7.17 shows the total carbon dioxide produced at the end of the fermentation process (27 hours) collected by the gas collection system.

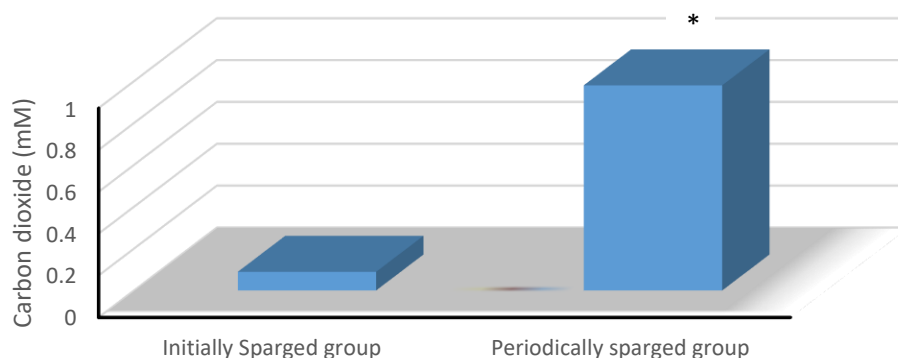


Figure 7.17: Cumulated collected carbon dioxide at the end of the fermentation process (27 hrs), which was collected using the gas collection system. The readings are representative of triplicate results. * The mean difference is significant at the 0.05 level.

Stripping carbon dioxide from the fermentation medium has many advantages for the fermentation process. For example, carbon dioxide is known to dissociate into carbonic acid, which can decrease the pH of the fermentation medium. To avoid pH variation, alkaline solutions need to be added to adjust the pH of the fermentation medium. The addition of the basic solutions means that it is expensive to maintain the suitable pH level for the fermentation process as well as increasing the maintenance and cleaning costs as some of these solutions are toxic and/or corrosive. Carbon dioxide accumulation can inhibit and inactivate the bacterial cells, and this might be combined with cell lysis, and then deteriorated the bacterial culture.

It is worth noting that removing some fermentation products (acetaldehyde and carbon dioxide) decreases the chemical activity of these products, and that drives the reaction in the direction of greater product formation according to Le Chatelier's principle.

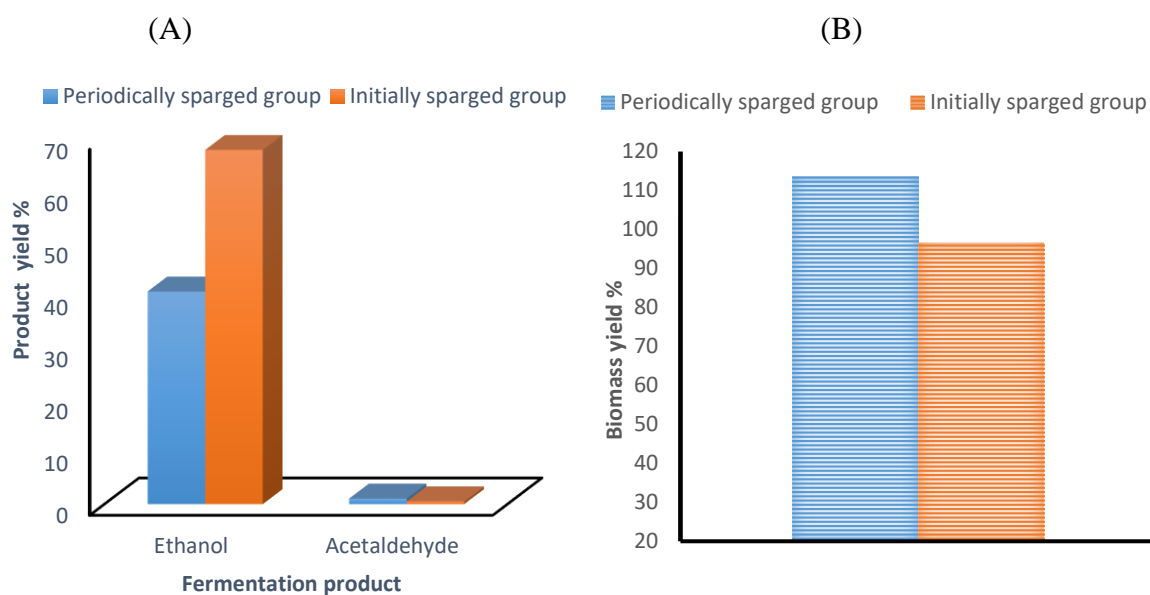


Figure 7.18: Bioproducts percent yields. (A) Ethanol and acetaldehyde yields. (B) Biomass yield.

Figure 7.18 shows the yields of the fermentation bioproducts (acetaldehyde, ethanol, and biomass), which were calculated by considering that 1 mol of glucose can be metabolised to produce 2 mol of acetaldehyde/ ethanol with 2 mol of carbon dioxide. The percentage yield is the ratio between the actual yield and the theoretical yield multiplied by 100. It indicates the percent of theoretical yield obtained from the final product in an experiment.

Ethanol yield reached 70 % in the initially-sparged group in comparison with 45 % in the periodically-sparged group, while acetaldehyde yield hit about 1 % and 0.5 % in the periodically-sparged group and the initially-sparged group respectively. Biomass yield was maximised in the periodically-sparged group and reached 110 %, while its yield in the initially-sparged group was around 90 %. The biomass yield calculation was based on the assumption that 10.5 g dry weight of *Zymomonas mobilis* cells can be generated for each mole of glucose being totally consumed (Kalnenieks, 2006).

7.7 Bubble analysis

Bubble size distribution was also considered in the current study, controlled using a ceramic diffuser with water as a liquid and air as a gas with a flow rate of 0.3 L/min. It is worth mentioning that the bubble analysis study was achieved using a high-speed camera photron 3 (EPSRC, UK). The reactor used in the experiments is cylindrical in shape to increase the efficiency of mixing, however, it proved difficult to measure bubble size in the cylinder because it gives an image bigger than reality. Therefore, the cylindrical reactor was replaced with a

rectangular reactor. Measurement of bubble size was carried out by image analysis software (ImageJ software 1.48V), which gives the area of the bubbles in two dimensions. Images containing more than 150 bubbles were analysed, and the average diameter of these bubbles was $\sim 500 \mu\text{m}$. The microbubbles with diameter of 400 to $600 \mu\text{m}$ have a relative frequency of 0.37 higher than other diameters, while the lowest relative frequency was in the range of 0 to $400 \mu\text{m}$. It can certainly be said that the number of microbubbles in the range of 400 to $600 \mu\text{m}$ was more dominant than other sizes, which represents around 60 % of the total generated bubbles (Figure 7.19).

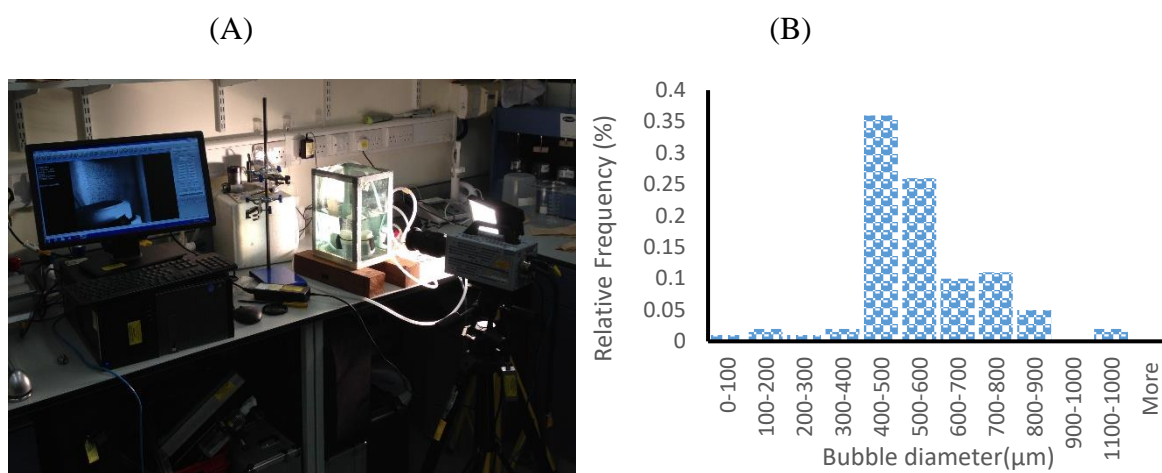


Figure 7.19: Bubble analysis. (A) bubble size measurement set up. (B) Bubble size distribution used in the current study, where the microbubbles with 400- $600 \mu\text{m}$ were dominant than other sizes. The readings are representative of triplicate results.

Using the fluidic oscillator helped to generate microbubbles with the reported size distribution. On the other hand, using a continuous air flow (after removing the fluidic oscillator) can generate much bigger bubbles ($1,000\text{-}2,000 \mu\text{m}$), which are no longer microbubbles (fine bubbles) at the same flow rate (0.3 L/min). Figure 7.20 shows a comparison between the oscillation flow fed by the fluidic oscillator and the continuous flow for the same flow rate, where micron-sized bubbles were generated from the diffuser with the oscillation flow without coalescence, and with almost uniform spacing/size (Zimmerman et al., 2013).

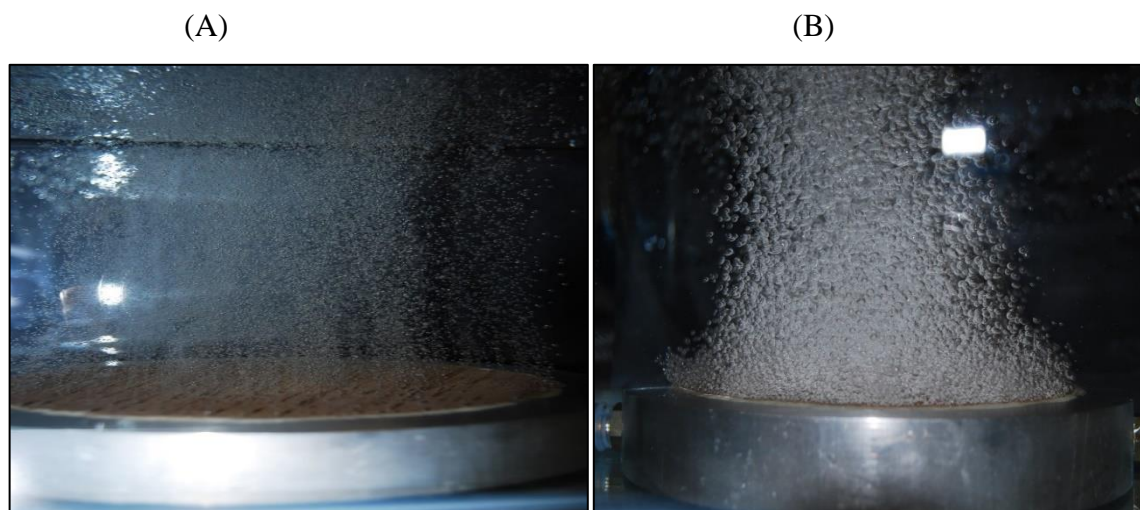


Figure 7.20: A comparison between an oscillated flow and a continuous flow in water at the same flow rate 0.3 L/min. (A) Oscillated flow fed by the fluidic oscillator generated microbubbles with uniform spacing between them. (B) Continuous flow generated fine bubbles, which tend to coalesce, producing even bigger bubbles (Adapted from Al-Mashhadani, 2013).

At 0.3 L/min and 400-600 μm bubble diameters, the gas bubbles were not present in the downcomer region of the airlift loop bioreactor and thus, there is zero volume gas fraction in this region, which represents more than 60 % of the overall working volume of the reactor. Therefore, both mass and heat transfer are restricted to the riser region because the downcomer region is free of gas bubbles as the liquid circulation cannot overcome the higher buoyancy of these bubbles and therefore, can not circulate them. Figure 7.21 shows the distribution of gas volume fraction and liquid velocity streamlines at 400 μm and 600 μm bubble diameters (Al-Mashhadani et al., 2015). In addition, the ratio of draft tube diameter to the bioreactor diameter (d/D) is an important parameter for internal loop bioreactors. $(d/D) = 0.6$ was used in the current study, which showed a good liquid circulation pattern that achieved good mixing within the fermentation reactor (Al-Mashhadani et al., 2015).

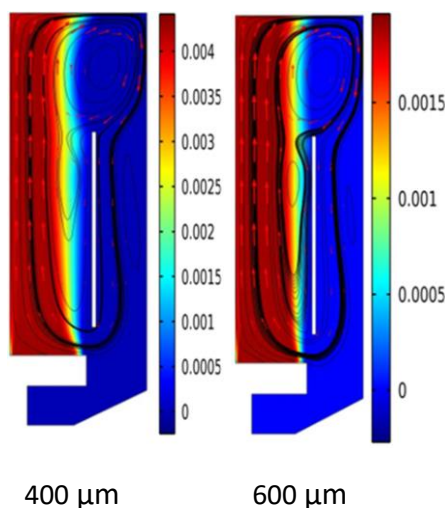


Figure 7.21: Snapshots of gas concentration (Kg/m^3) at two bubble diameters ($400 \mu\text{m}$ and $600 \mu\text{m}$) after steady state (Adapted from AL-Mashhadani et al., 2015)

7.8 Reducing the cleaning requirements in the airlift loop bioreactor using microbubble technology

An airlift loop bioreactor system was used in the current study. This bioreactor needs to be cleaned after finishing the batch culture and transferring the contents. Typically, the cleaning is done automatically using clean-in-place (CIP) techniques. Manual cleaning was used in the current study, and it achieved a contamination-free culture (which was examined by regular observation of the culture using both cultivations on the petri dishes and examination under a combined microscopy) and ensured consistency of the cleaning operation. Irrespective of the bioreactor type, i.e. stirred tank, bubble column, fluidised bed, external-loop airlift, or internal-loop airlift reactors, the general cleaning requirements are similar (Chisti and Moo-Young 1987). Controllable sensors, which can be replaced during the operation, have additional implications for the cleaning process. Applying microbubble technology, however, supplies oxygen to the culture and removes the fermentation products but importantly, prevention of microbial adhesion and detachment of adhering microorganisms on the bioreactor interface can also be achieved using this technology.

The production of toxic substances from *Zymomonas mobilis* during the fermentation process such as acetaldehyde, ethanol, or even carbon dioxide can substantially impede the bacterial growth and cause a dramatic reduction in the production of these chemicals (Todhanakasem et al., 2014). The tolerance to these toxic compounds can be enhanced by the formation of biofilms (Li et al., 2006). A microbial biofilm can be defined as a single species or communities of microorganisms that attach to surfaces (biotic or abiotic) and are embedded in an extracellular polymeric substance (EPS) (Todhanakasem et al., 2014). Microbial cells in biofilms might differ totally regarding phenotypic characteristics or adaptive responses to stresses from their

planktonic counterparts, and this can provide survival advantages and protection from a range of environmental conditions (Hall-Stoodley et al., 2004). *Zymomonas mobilis* ZM4 tends to form stable biofilms on hydrophobic plastic surfaces (Todhanakasem et al., 2014).

Poly (methyl methacrylate) (PMMA) was tested as the resin of choice for the fabrication of many biological-based polymers (Park et al., 2009), and can be modified to increase its hydrophobicity. The walls of the used bioreactor in the current study were made from this polymer. The hydrophobic–hydrophobic interactions cause the attachment of *Zymomonas mobilis* cells to the bioreactor ‘s walls and then the formation of biofilms on the internal walls of the bioreactor. The same adhesion observed on PMMA denture resins by *C. albicans* (Park et al., 2009).

Changing the carbohydrate concentration in the fermentation broth might change the cell surface’s hydrophobicity. Indeed, reducing of carbohydrates concentrations can enhance the development of the hydrophobicity of cell surface, lipopolysaccharide (LPS) fraction, of *Zymomonas mobilis* ZM4 cells (Shakirova et al., 2008), which tend to form dense, homogeneous biofilms in comparison with other *Zymomonas mobilis* strains (Todhanakasem et al., 2014).

Using microbubbles can detach these bacterial biofilms from the internal surfaces of a bioreactor (Sharma et al., 2005), and this observation was proved by taking snapshots of the internal walls of the bioreactor under both the initial sparging and the periodical sparging strategies.

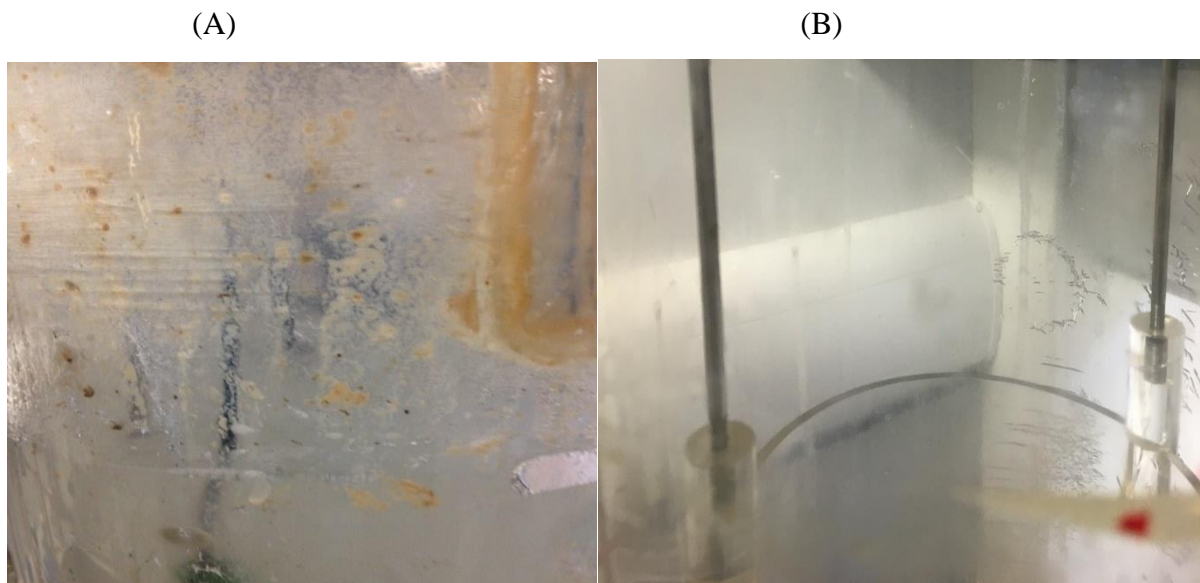


Figure 7.22: Snapshots of the internal walls of the bioreactor. (A) Under initial sparging strategy, where the internal walls have bacterial biofilms, giving them the dirty appearance. (B) Under periodical sparging strategy, where the internal walls were clean without any bacterial biofilms.

Passaging of air-liquid interfaces over substratum surfaces can involve in the detachment forces, which are perpendicular to the substratum surfaces and thus directly opposing the adhesion forces (Sharma et al., 2005). The surface tension forces involved in this detachment activity were previously reported for colloidal particles (Noordmans et al., 1997, and Suárez et al., 1999) and bacteria (Gómez-Suárez et al., 2001) in a parallel plate flow chamber. These sources are several orders of magnitudes larger than other forces that might act on microorganisms such as hydrodynamic, gravitational and buoyancy forces (Noordmans et al., 1997). Passing microbubbles is more effective when it is at low velocities and high interface tensions (Sharma et al., 2005), and these features are typical of microbubbles (Zimmerman et al., 2009). Also, the detachment activity increases when multiple microbubbles are periodically passing alongside these walls (Sharma et al., 2005).

7.9 Maintenance of asepsis conditions

One of the great advantages of the biochemical processes is that they can be conducted at low temperatures, near-neutral pH and in an aqueous environment. On the other hand, there is a significant cost associated with maintenance of asepsis, as some of these fermentation processes suffer from contamination with undesirable microbes. Therefore, raw materials and media must be sterilised by heating them up to 120°C and maintaining this temperature for 15-20 minutes at 1.1.5 bar before being cooled to operating temperature (autoclaving). Modern advances in sterilisation technologies have reduced costs, but these expenses are still considerable and has

a great impact on the bulk chemical market. However, the greatest cost is through the loss of production time (downtime) through contamination.

In the current project, there are some measures considered to reduce or avoid the contamination during the fermentation process. The fermenter used in this study is an airlift loop bioreactor, which is made of PMMA. EVONIK Industries have manufactured PMMA as a sheet with different dimensions. However, this polymer is not recommended for treatment at high temperatures, and if used as such it must have its temperature increases gradually. Therefore, this reactor cannot be sterilised using an autoclave, and another sterilisation method should be used to achieve this purpose. Accordingly, the fermenter was sterilised chemically using a liquid disinfectant (Pursept®-A Xpress Disinfection solution, BRAND, Germany). The ingredients of Pursept®-A Xpress Disinfection solution are 55 g ethanol, 0.03 g n-alkyl-aminopropyl-glycine, and auxiliary agents for each 100 ml of this solution. Surface disinfection with this solution can be as fast as 15 seconds and its activity can cover both bacteria and fungi (BRAND, Germany).

In addition, the cultural medium was sterilised using an autoclave for 20 minutes at 120 °C, a sterilisation technique that can destroy all microorganisms, including vegetative bacteria, mycobacteria, most viruses and most fungi (Doran, 2013). The sterilisation of air was also considered, and depth filters (Cole-Parmer, UK) were used in this process. Typically, the number of microbial cells in the air is in the order of 10^3 to $10^4/\text{m}^3$, and air filtration is the most common method used to sterilise air in bioprocesses, especially large-scale processes, while the heat sterilisation of the gasses is economically impractical. Depth filters can remove contaminants as small as 0.1 μm , and this pore size is up to 2 times smaller than the dimensions of the bacteria and spores to be removed (Doran, 2013). Samples were withdrawn at the beginning and the end of the fermentation process and used to prepare slides for microscopic examination. Figure 7.23 shows some pictures that were taken throughout this study to confirm that there was no or minimal contamination.

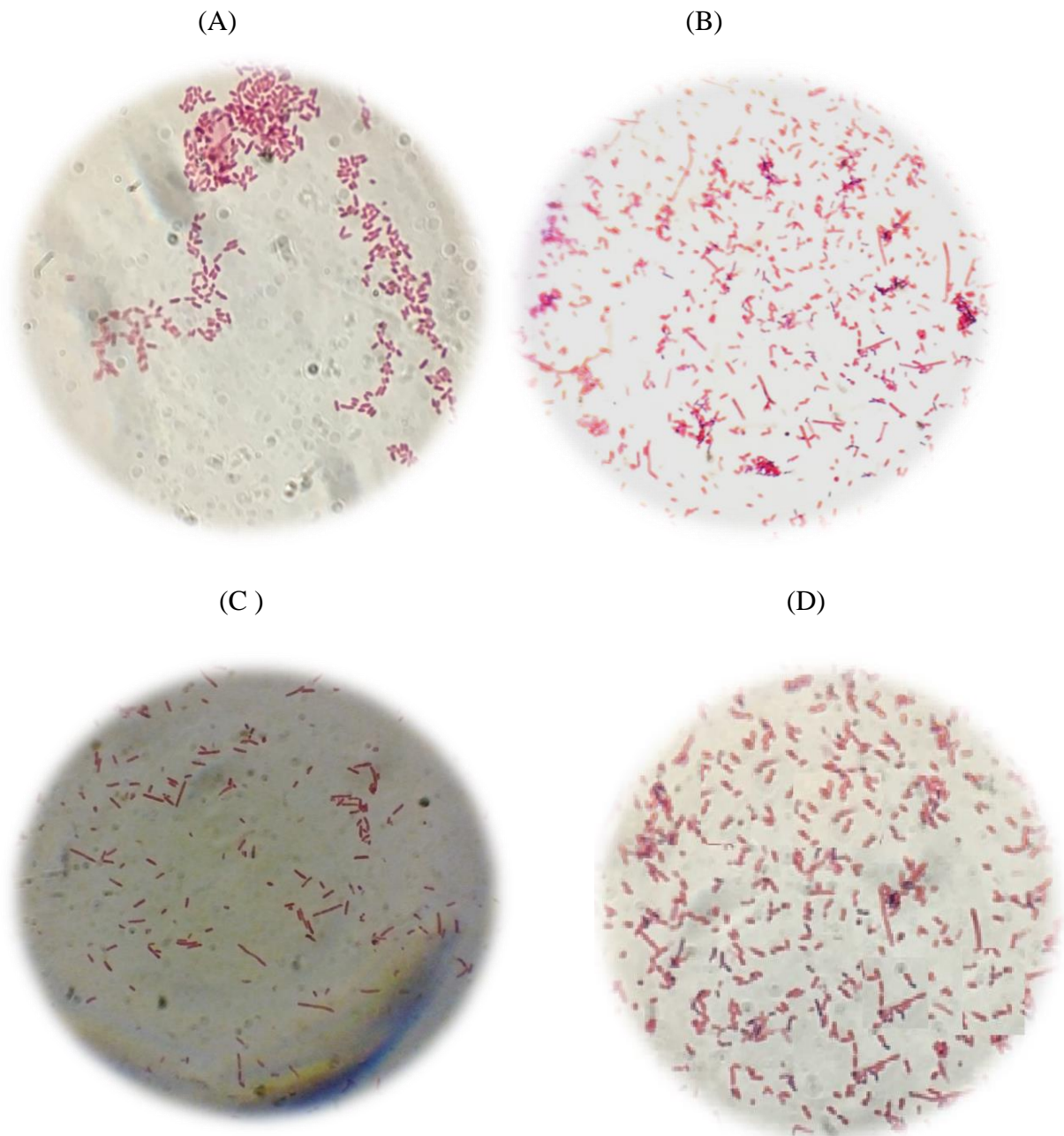


Figure 7.23: Microscopic pictures for the bacterial culture at the beginning of and after finishing the fermentation process for both Wild and 200 mM allyl alcohol selected strain (In the next chapter). (A) Wild strain culture at the beginning of the fermentation process. (B) Wild strain culture after finishing the fermentation process. (C) 200 mM allyl alcohol selected strain at the beginning of the fermentation process (Next chapter). (D) 200 mM allyl alcohol selected strain after finishing the fermentation process (Next chapter).

7.10 Conclusions

The aerobic fermentation process uses glucose as a carbon source, which was seen to be produced from the lignocellulose biomass pretreatment, as shown in Chapters 4 and 5 of the current study. Thereafter, the produced sugary content in the pretreatment slurry contaminated with *Pseudomonas putida* from the biological pretreatment was inactivated using carbon dioxide-enriched microbubbles, as shown in Chapter 6. This chapter focuses mainly on the fermentation process under aerobic conditions using *Zymomonas mobilis* ZM4 as a fermentative microorganism. Microbubble technology was used to supply oxygen to the bacterial culture in three different strategies: the initial sparging strategy, the periodical sparging strategy, and the continuous sparging strategy. While the initially-sparged group suffers from the oxygen starvation after around 3.5 hours, the continuously-sparged group keeps stable aerobic conditions, but this strategy causes a high-energy usage and gas wasting with a high operational cost. Beneficially, the periodical sparging strategy offers both enough oxygen supply and reduced energy usage, and provides efficient *in situ* separation of acetaldehyde, carbon dioxide, and to a much lesser extent ethanol. The results show that the *Zymomonas* growth is inhibited by acetaldehyde accumulation at a concentration as low as 0.1 % with several morphological changes seen on the bacterial cells by SEM. This inhibition can be avoided by stripping the inhibitors with microbubbles, which removes acetaldehyde from the fermentation broth with 99 % efficiency, leading to relatively high microbial growth. Using the periodical sparging strategy, however, gives 45 % yield of ethanol and 1 % yield of acetaldehyde with 110 % yield of microbial biomass in comparison with 70 %, 0.5 % and 90 % yield for ethanol, acetaldehyde and biomass, respectively, in the initially-sparged group. The periodically-sparged group produces 1,000% more carbon dioxide than the initially-sparged group. The oxygenation concurrent with the stripping process by the periodical sparging strategy efficiently maintained the oxygen concentration in the fermentation broth above the critical oxygen concentration, leading to stable aerobic conditions. The developed periodical approach has potentially significant ramifications, particularly for fermentation-based industries, and it promises to offset many traditional aerobic fermentation deficiencies.

The periodically-sparged group showed an elevated biomass and acetaldehyde production with less ethanol in comparison to the initially-sparged group.

Additionally, using microbubble technology helped to detach bacterial biofilms from the internal surfaces of the bioreactor and therefore, reduced the cleaning requirements in the airlift loop bioreactor.

To enhance the acetaldehyde production, alcohol dehydrogenase reaction needs to be attenuated or modified, and therefore, allyl alcohol will be used to select *Zymomonas mobilis* cells with decreased alcohol dehydrogenase activity, as will be shown in Chapter 8.

Chapter 8

Aerobic fermentation integrated with *in situ* separation of bio-products using microbubble technology and a mutant type *Zymomonas mobilis* ZM4 strain

Overview

Alcohol dehydrogenases catalyse the interconversion among ethanol and acetaldehyde (Lutstorf and Megnet, 1968; Beier et al., 1985). Alternatively, acetaldehyde can be oxidised to acetate by aldehyde dehydrogenases (Jacobson and Bernofsky, 1974; Dickinson, 1996 and Meaden et al., 1997). However, *Zymomonas mobilis* ZM4 does not show much activity of this enzyme and it was suggested that this bacterium might lack acetaldehyde dehydrogenase (Bringer-Meyer and Sahn, 1993). Also, acetate is not detected in the current study.

One way to enhance the acetaldehyde production in the fermentation process as a target product (as shown in Chapter 7) is to attenuate or modify the alcohol dehydrogenase activity. This can be achieved by using either physiological selection techniques such as the use of allyl alcohol or molecular biology-genetic engineering techniques such as a directed deletion mutation. However, using molecular biology-genetic engineering techniques is out of the scope of the current project, and so allyl alcohol was chosen to select the cells with attenuated alcohol dehydrogenase activity.

The acetaldehyde accumulation, however, can inhibit both the bacterial growth (as shown in Chapter 7) and pyruvate decarboxylase reaction by a product inhibition mechanism (Patel, 2007); leading to the inhibition of decarboxylation of pyruvate and as a result more pyruvate starts to accumulate (Juni, 1961). The increase of the substrate concentration (pyruvate) is induced the pyruvate dehydrogenase complex activity, which has an exclusively anabolic role in *Zymomonas mobilis* to produce acetyl coenzyme A, CO₂ and NADH (Sahn et al., 1992).

The results show that the acetaldehyde production in the periodically-sparged group was increased to around 932 % more than the initially-sparged group. The mutant strain produced around 1,566.7 % more acetaldehyde than the wild strain (Seen in the Chapter 7). Regarding the ethanol production, there was around 42 % more ethanol produced in the initially-sparged group than in the periodically-sparged group. The mutant strain produced around 97 % less ethanol than the wild strain. Using the microbubble technology, however, removes acetaldehyde from the fermentation broth with 88.5 % efficiency in comparison with 42 % efficiency achieved with the fine bubbles. Additionally, *Zymomonas* biomass is preferably generated under the periodical sparging strategy with 50 % yield, and this is halved under the initially sparging strategy. Interestingly, the biomass yield produced by the mutant strain is less

than half the yield produced by the wild strain. In addition, the oxygenation concurrent with the stripping process by microbubbles efficiently maintained the oxygen concentration in the fermentation broth above the critical oxygen concentration, leading to stable aerobic conditions.

8.1 Selection of acetaldehyde over-producing mutant strain using allyl alcohol

Allyl alcohol was used to select *Zymomonas mobilis* cells with attenuated or modified alcohol dehydrogenase activity. Allyl alcohol can be oxidised by alcohol dehydrogenase to produce acryldehyde (Acrolein). The latter chemical is a toxic compound to bacterial cells with normal or overactive alcohol dehydrogenase activity and subsequently, only cells with modified or attenuated alcohol dehydrogenase activity can grow in the presence of increasing allyl alcohol concentrations (Rando, 1974).

A mutant strain was selected using increasing allyl alcohol concentrations, which was ultimately expected to have higher acetaldehyde accumulation. Figure 8.1 shows the steps of the selection process using elevating allyl alcohol concentrations.

The initial concentration of allyl alcohol used was 0.2 mM, as given previously in a study by Wills et al. (1981) and thereafter, the allyl alcohol concentration was gradually increased to reach 200 mM, as can be seen in Figure 8.1.

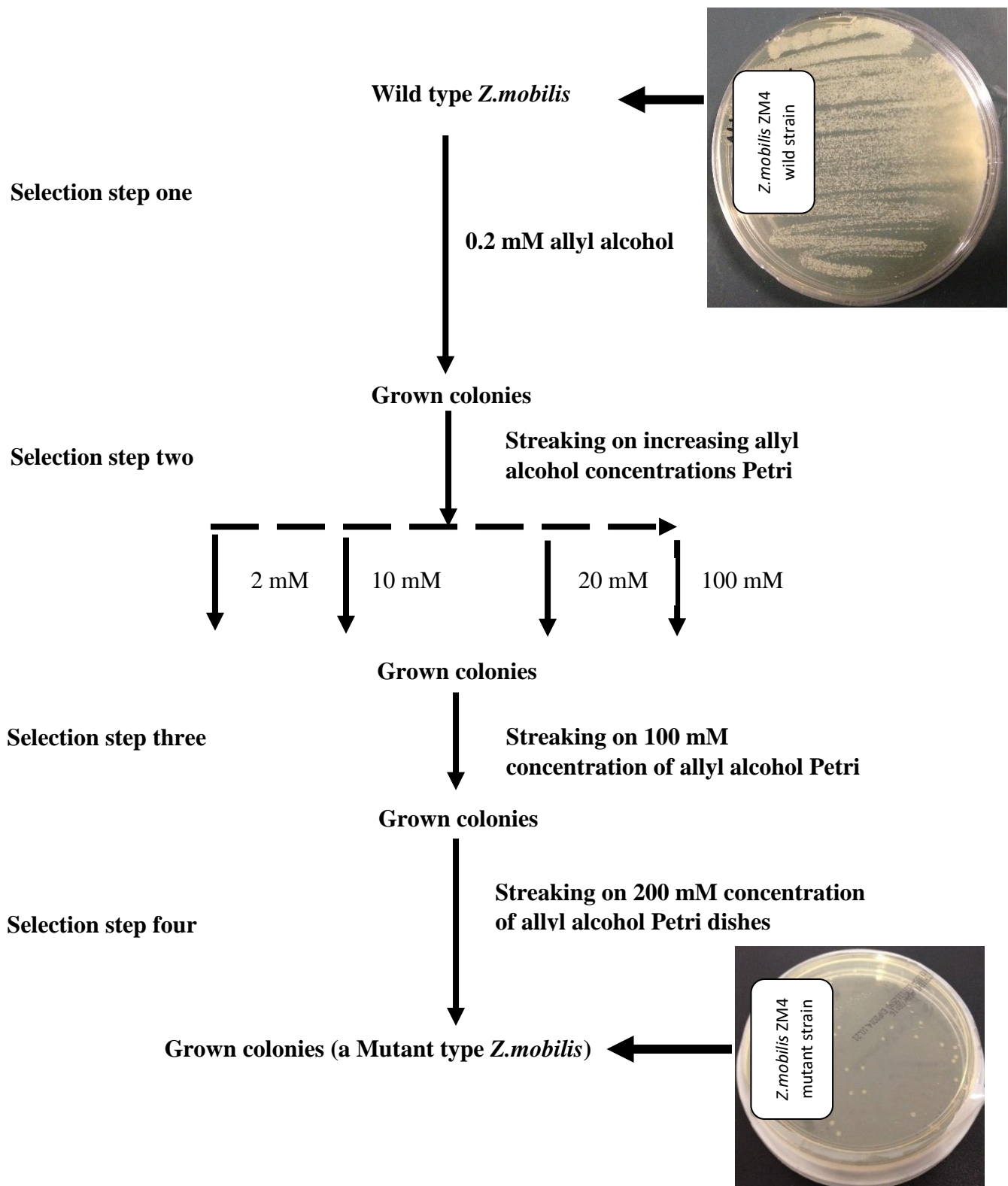


Figure 8.1: A sequential scheme using increasing allyl alcohol levels for the selection of *Z. mobilis* ZM4 mutant type with decreased or modified alcohol dehydrogenase activity.

Allyl alcohol is not known to change the metabolic pathway of *Zymomonas mobilis* but instead is just a methodology to select the bacterial cells with attenuated or modified alcohol dehydrogenase activity. Figure 8.2A shows that the increase in the acetaldehyde concentration corresponds with the increase in the allyl alcohol concentration to 100 mM, and also shows that the decrease in the ethanol concentration corresponds with the increase in the allyl alcohol concentration. In contrast, Figure 8.2B shows the shift in the *Zymomonas mobilis* ZM4 wild type population to a population with attenuated or modified alcohol dehydrogenase activity. It should be noted that allyl alcohol concentration was increased up to 200 mM during this study, and this concentration is double the concentration that was used in previous studies (Wecker, 1987 and Wecker and Zall, 1987) and therefore, the activity of alcohol dehydrogenase is modified or reduced greater than to what was achieved before.

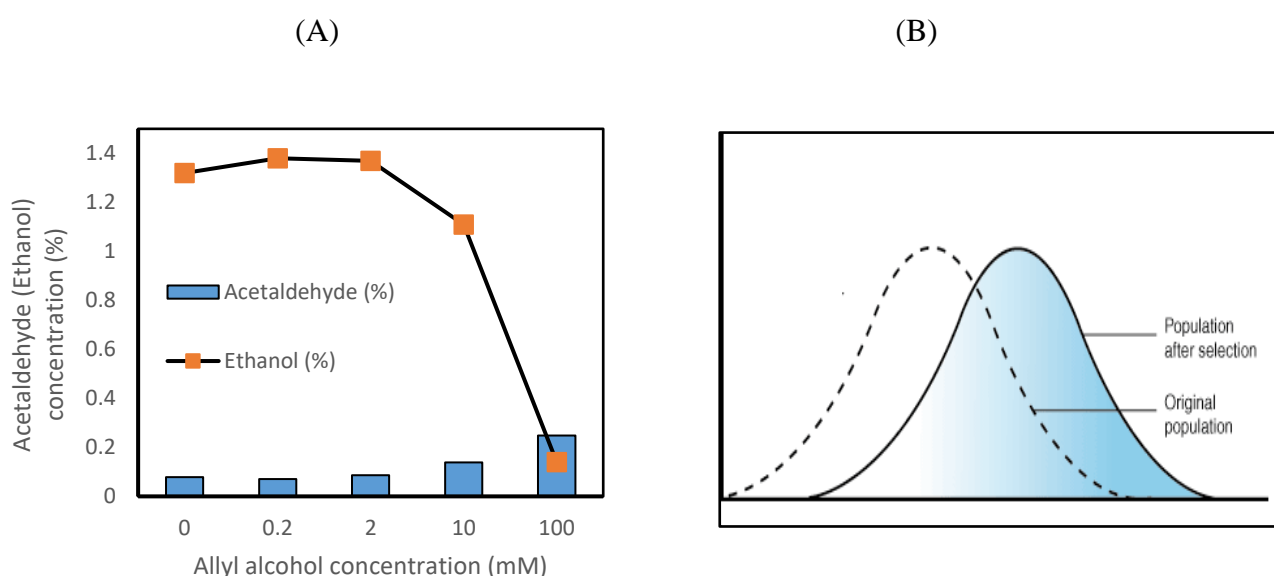


Figure 8.2: (A) Acetaldehyde and ethanol production against used allyl alcohol concentration (Adapted from Wecker and Zall, 1987). (B) Shifting of wild type *Zymomonas* population to a population with attenuated or modified alcohol dehydrogenase activity in the mutant strain.

Similar initial sparging and periodical sparging strategies described in the previous chapter were applied to the work described in this chapter with the mutant strain, considering the biomass concentration, X and the changing in the sparging duration.

It might be argued that the biomass concentration of the mutant strain is much lower than that of the wild strain and therefore, needs a shorter sparging duration. This is correct if the microbubble sparging is used to provide oxygen only. However, the microbubble technology is used to achieve two main goals: (i) to keep the oxygen concentration above the critical oxygen

demand (i.e. maintain aerobic conditions); and (ii) to strip out both acetaldehyde and carbon dioxide (primarily) along with ethanol and ethyl acetate (to a much lesser extent).

Table 8.1 shows the details of the periodical sparging strategy applied with the mutant strain to satisfy the oxygen demand and to strip out of the accumulated products, while the initial sparging strategy was applied at the beginning of the fermentation process.

The specific oxygen uptake rate was elevated in the mutant strain by an additional 6.67 %, 8.57 %, 4.17 % and 15.38 % in the lag, log, stationary and death phases, respectively, measured per gram (dry weight) of the biomass per hour, in comparison to the wild strain. This elevation could be due to increasing the activity of the respiratory chain. Indeed, ethanol synthesis and the respiratory chain are the two main sinks of NADH in *Zymomonas mobilis* metabolism, and they are competing for the reducing equivalents (i.e. NADH) (Rutkis et al., 2016). Modifying or attenuating the alcohol dehydrogenase activity leads to redirect some of the metabolically-available NADH towards respiratory NADH dehydrogenase (*ndh*), where oxygen, a final electron acceptor in the respiratory chain, is sufficiently plentiful in the fermentation broth.

Table 8.8.1: The oxygen mass transfer coefficient (for 0.3 L min⁻¹ dosing flow rate) with equilibrium concentrations and sparging time (mins) calculated during the experimental sets with *Zymomonas mobilis* mutant strain.

Period			r (specific oxygen uptake rate) mmol. g (dry weight) ⁻¹ .hr ⁻¹	
			Growth phase	r-value
The first period	182 hr ⁻¹	$K_L a$ (Mass transfer coefficient)	Lag phase	1.92
	8.11 PPM	C* (saturation concentration)		
	8 mins	Sparging time	Log Phase	4.56
	300 mins	Time before the next sparging		
The Second period	220 hr ⁻¹	$K_L a$ (Mass transfer coefficient)	Stationary phase	3
	4.23 PPM	C* (equilibrium concentration)		
	24 mins	Sparging time	Death phase	1.8
	125 mins	Time before the next sparging		

8.2 Differentiation of the overproduced strain with the use of acid fuchsin

Grown colonies of the mutant strain were overlaid with decolourised acid fuchsin agar. In the presence of the produced acetaldehyde, the acid fuchsin agar reacts with acetaldehyde and turns from nearly colourless to a range of colours from pink to red. The colour grade depends on the acetaldehyde concentration; a red colour can be seen as the highest acetaldehyde concentration. Figure 8.3 shows the acetaldehyde/acid fuchsin colony reaction in both wild and mutant strains.

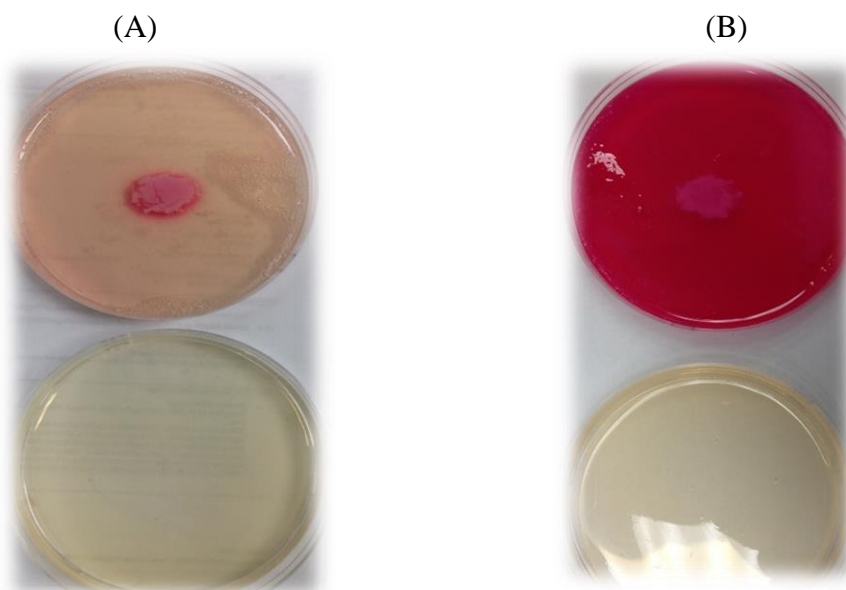


Figure 8.3: The acetaldehyde/ acid fuchsin colony reaction. (A) *Zymomonas mobilis* wild strain, where limited amounts of acetaldehyde are produced to give the pink colour. (B) *Zymomonas mobilis* mutant strain, where increased amounts of acetaldehyde are produced to give the red colour.

The degree to which acid fuchsin reacts with *Zymomonas* colonies is correlated to the concentration of acetaldehyde produced by these colonies. It is worth noting that using acid fuchsin to differentiate acetaldehyde-overproducing strains is a qualitative test, and it can only give an idea about the increases of the acetaldehyde concentrations based on a subjective observation of changing reaction colour. Indeed, the resolution of this test is limited and some of the produced acetaldehyde might diffuse within the agar, and it will not react with the acid fuchsin. The pictures in figure 8.3 show that the wild strain tends to produce a limited amount of acetaldehyde, as shown in the previous chapter, while using allyl alcohol helps to select the acetaldehyde-overproducing mutant cells, which have one or more mutations in the gene(s) of alcohol dehydrogenases with modifying or attenuating alcohol dehydrogenase activity. In addition, allyl alcohol is not known to be mutagenic. The selected mutant strain might be due to spontaneous mutations (Wecker and Zall, 1987). Consequently, it therefore may not be as

stable as those produced by other molecular and genetic engineering techniques, such as deletion mutations. The allyl alcohol-selected mutant strain results from amino acid substitutions (Wills and Jörnvall, 1979 and Wecker and Zall, 1987) and Therefore, it is be more likely to revert than mutants produced by deletion techniques.

Mutants that might have incidental mutations in their alcohol dehydrogenase without increasing the acetaldehyde production are not likely to be found, and this was verified in the experiments when more acetaldehyde was produced by the mutant strain.

The attenuation in the alcohol dehydrogenase activity was confirmed by measuring the alcohol dehydrogenase relative activity in both wild type and mutant type. The results show that the activity of alcohol dehydrogenase in the mutant strain was reduced by 77 % in comparison to the wild strain. Figure 8.4 shows the enzymatic relative activities in both mutant and wild type strains.

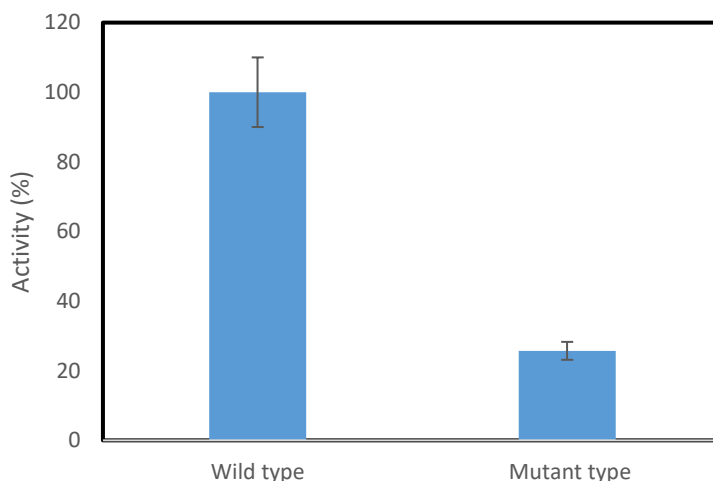


Figure 8.4: Alcohol dehydrogenase relative activity in mutant type in comparison with the wild type, showing around 77 % reduction in the activity in mutant type compared to the wild type.

8.3 Central metabolic routes

Figure 8.5 shows the glucose consumption patterns in the *Zymomonas mobilis* mutant strain, in which it can be seen that the mutant strain used around 50 % of the available glucose in the initially-sparged group compared to around 25 % in the periodically-sparged group after more than 50 hr from the start of the fermentation process (Figure 8.5A). Figure 8.5B shows the glucose consumption rate in both groups.

Both groups started at the same level of oxygen. However, the initially-sparged group was shifted to anaerobic conditions after more than 3 hours. It is not proposed that *Zymomonas* metabolism can be shifted into anaerobic growth directly, but instead a transition stage between aerobic and anaerobic growth is taking place, where the metabolism is gradually shifted from aerobic to anaerobic.

Additionally, these groups show different patterns of biomass production (Figure 8.6): at the first ten hours of the fermentation process, the initially-sparged group showed a hyperbolic growth pattern, while the periodically-sparged group showed a normal sigmoid growth pattern. The hyperbolic growth pattern might be attributed to the concentration of acetaldehyde (the inducer), which started to accumulate in the fermentation medium. Indeed, the existence of low concentrations of acetaldehyde can markedly reduce the lag phase of the growth curve (Stanley et al., 1993; Stanley et al., 1996; Hansson and Pamment, 2000; Aranda and del Olmo, 2004) and both sulphur amino acids metabolism and polyamine transporter genes can be induced by acetaldehyde (Aranda and Del Olmo, 2004). Two specific growth rates were observed during the growth in the initially-sparged group, the first specific growth rate was 0.168 hr^{-1} , which was seen during the first 10 hours of the fermentation. Thereafter, the specific growth rate dropped to 0.064 hr^{-1} during the rest of the exponential phase. In contrast, the periodically-sparged group showed almost consistent growth rate at the exponential phase, which was around 0.094 hr^{-1} .

Regarding the oxygenation process, the initially-sparged group was started at the same oxygen level as the periodically-sparged group but kept without any oxygen supply thereafter, while air-microbubbles were sparged into the periodically-sparged group at the fourth hour of the fermentation time. Five hours were required to reach the minimum threshold of the proposed oxygen critical level in both groups, and further oxygen consumption might lead to shift the metabolism to an anaerobic fermentation. Ishikawa et al. reported the same observation in their 1990 study. In Figure 8.5B, this observation is supported and the glucose consumption rate in the initially-sparged group increases further after shifting to anaerobic conditions (after more than five hours). The same proposed scenarios of the products shifting in *Zymomonas mobilis* in figure 7.13 are also applied here, with the same previous observations of the effects of oxygenation process.

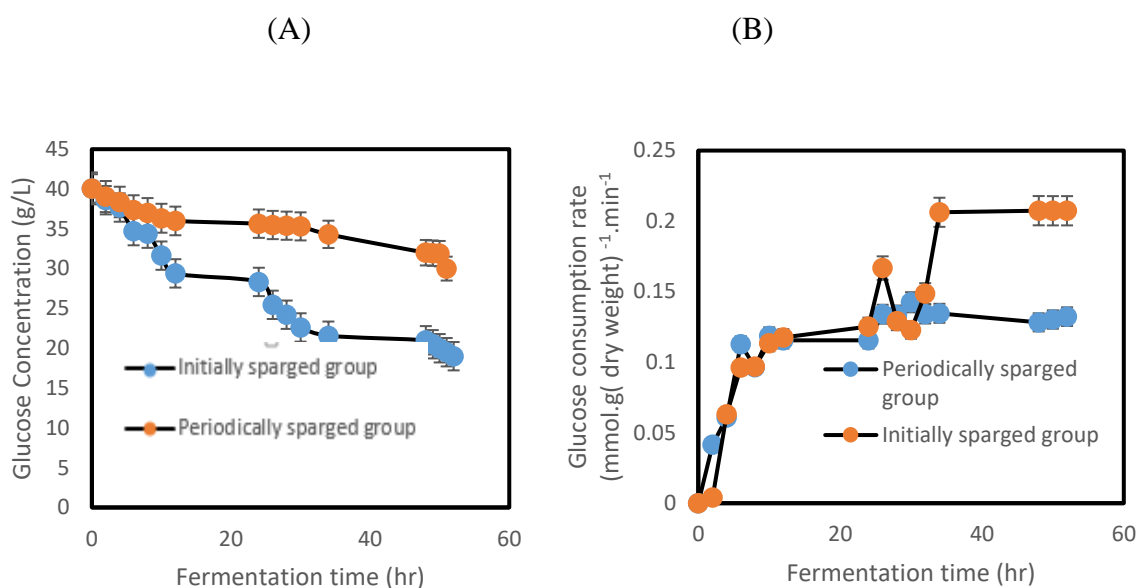


Figure 8.5: Glucose consumption pattern in *Zymomonas mobilis* ZM4 mutant strain. (A) Glucose concentration with time, whereby more glucose consumption was recorded under the anaerobic growth. (B) Glucose consumption rate in both initially and periodically sparged groups. Error bars depict standard deviations.

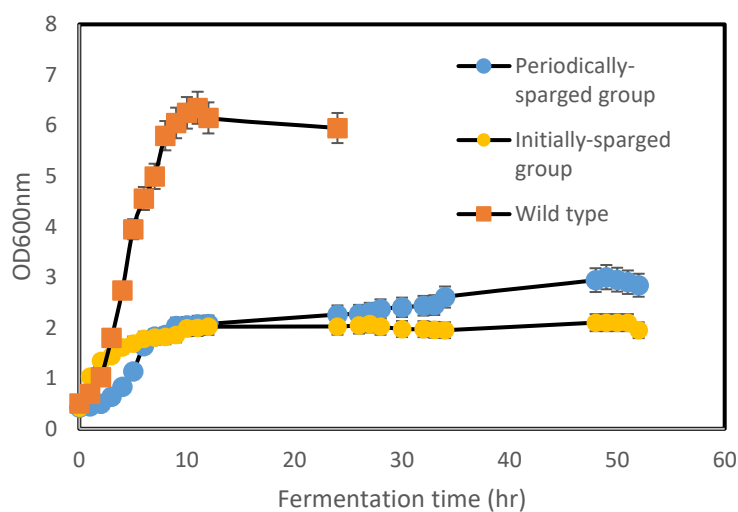


Figure 8.6: Comparison between the growth patterns of *Zymomonas mobilis* mutant strain in the initially sparged group and periodically sparged group with the wild strain of *Z.mobilis* ZM4. Error bars depict standard deviation.

8.4 Fermentation products (Acetaldehyde, ethanol, and carbon dioxide)

Figure 8.7 (A,B) shows both acetaldehyde and ethanol production pathways during the fermentation process.

Acetaldehyde started to accumulate in the fermentation broth after around 2 hours of starting the fermentation process in both groups, and it continued to be produced within the broth, and reached its highest concentration after around 5 hours in the initially-sparged group and after 20 hours in the periodically-sparged group. Thereafter, the production decreased until the end of the fermentation process (Figure 8.7A).

The acetaldehyde production can begin immediately just after inoculation (within 2 hours) (Ishikawa et al., 1990), but it starts to be detectable in the fermentation broth after some time has passed, as this chemical tends to diffuse poorly across the plasma membrane compared to ethanol, leading to its intracellular accumulation. The accumulated intracellular acetaldehyde concentration can build up to several folds higher than the prevailing extracellular concentration (Aranda and del Olmo, 2004).

The periodically sparged group produced around 433 % more acetaldehyde than the initially sparged group (Figure 8.7B). In addition, the accumulation of acetaldehyde in the periodically sparged group might also explain the increased concentration of ethanol, which also started to accumulate intensively during this period (Figure 8.7B) and this may be due to that the concentration of substrate (acetaldehyde) is a key factor affecting the rate of a reaction catalysed by an enzyme (alcohol dehydrogenase) (Nelson and Cox, 2008). Clearly, increasing the acetaldehyde concentration in the periodically sparged group has raised the ethanol production by alcohol dehydrogenase. This increase was linearly related to the concentration of acetaldehyde for the period between hour tenth to hour twenty. The reaction velocity of alcohol dehydrogenase would be increased by smaller and smaller amounts in response to any further increase in the substrate (acetaldehyde) concentrations (Nelson and Cox, 2008). Subsequently, the enzymatic reaction has reached to its Michaelis-Menton threshold, where the reaction velocity becomes very small as the acetaldehyde concentration increases (Nelson and Cox, 2008).

Another potential explanation for the increase in the ethanol production under the periodically-sparged group is the Le Chatelier's principle, whereby gaseous products are simultaneously produced and stripped out the fermentation broth (Al-Mashhadani et al., 2011). This removal can be accompanied by a decrease in the Gibbs free energy of the reaction, which would drive the reaction in the direction of greater volume of product (acetaldehyde, carbon dioxide and ethanol) formation, leading to their replacing the removed products (Gary, 2004). Figure 8.8

shows the concentrations of the accumulated fermentation products in both the initially and the periodically-sparged groups.

The ethanol production in the mutant strain did not deviated from the wild type behavior (Figure 8.7B). As expected, more ethanol was produced under anaerobic conditions in the initially sparged group and 42 % more ethanol was produced in the initially sparged group in comparison with the periodically sparged group.

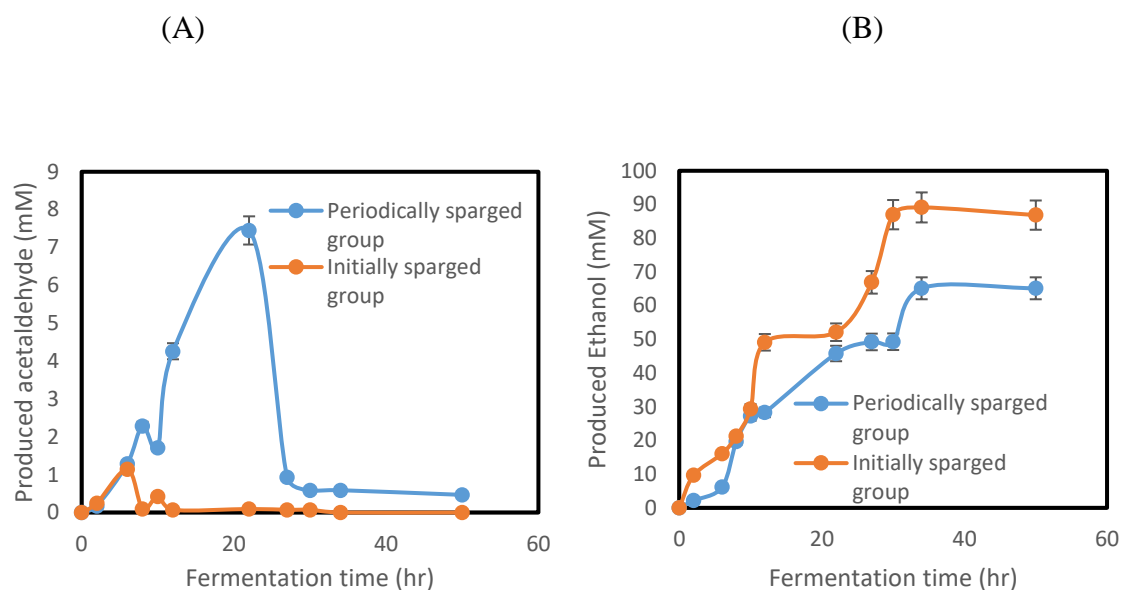


Figure 8.7: Acetaldehyde and Ethanol production during the fermentation process. (A) Acetaldehyde production with time, whereby acetaldehyde produced preferentially in the periodical sparged group. (B) Ethanol production with time, whereby ethanol produced preferentially in the initially sparged group. Error bars depict standard deviation.

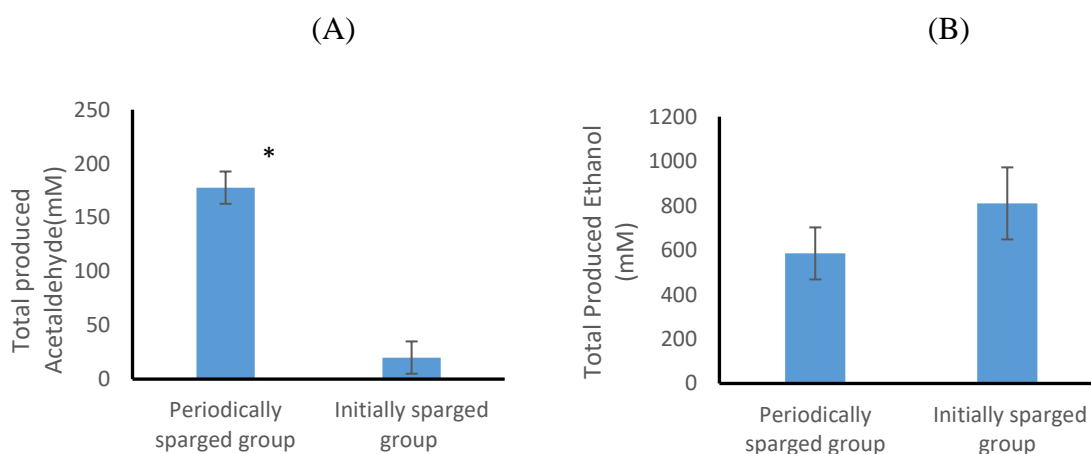


Figure 8.8: Accumulated fermentation products. (A) Produced acetaldehyde. (B) Produced Ethanol. Error bars depict standard deviation. * The mean difference is significant at the 0.05 level.

Figure 8.9 shows the amount of produced carbon dioxide at the end of the fermentation process in both initially and periodically-sparged groups. Carbon dioxide production in the periodically-sparged group was much higher than that produced by the initially-sparged group for the same duration (Figure 8.9). The reason for this carbon dioxide productivity might be due to the periodical stripping of the fermentation process according to Le Chatelier's principle. Also, the majority of the carbon dioxide produced in the initially-sparged group remains dissolved in the liquid fermentation broth, while it is regularly being stripped out of the fermentation broth in the periodically-sparged group.

When the fermentation broth in the initially-sparged reaches full saturation of carbon dioxide group (i.e. contains a maximum possible amount of dissolved carbon dioxide), the excess carbon dioxide might cause foaming (Brown, 2002), but also might inhibit the bacterial culture. On the other hand, stripping out carbon dioxide represents a removal of adverse effects of a potential inhibitor. Another advantage of the stripping out process is the reduction of the need to add more pH neutralisation solution (1M sodium bicarbonate) to neutralise the pH of the fermentation broth, and to keep it at pH 5.5 (the optimal pH level), as carbon dioxide can be dissociated into carbonic acid, bicarbonate and carbonate and the acidic species can decrease the pH of the fermentation medium (Mills and Urey, 1940 and Merlin et al., 2003).

Other authors also reported an enhancement of the bioprocess when carbon dioxide was stripped out, for example, the production of biohydrogen was increased when the partial pressure of carbon dioxide decreased (Tanisho et al., 1998; Park et al., 2005 and Alshiyab et al., 2008). According to those authors, the biohydrogen production increased by 43 % (Park et al., 2005) as part of a general increase in the biogas concentration after carbon dioxide removal (Alshiyab et al., 2008).

The carbon dioxide yield is challenging to calculate, for several reasons: (i) carbon dioxide is produced mainly from the decarboxylation of pyruvate, but importantly, it can also be produced from other metabolic activities such as carboxylation of phosphoenolpyruvate to oxaloacetate and acetyl-CoA to malate; (ii) carbon dioxide tends to dissolve in the fermentation broth; and (iii) the dissolved carbon dioxide can be dissociated into carbonic acid, bicarbonate and carbonate and the acidic species can decrease the pH of the fermentation medium. It can be argued that the carbon dioxide concentration can be worked out from the equations developed in Chapter 6, but the fermentation process needs to be kept at pH 5.5 by adding sodium

bicarbonate, and this makes challenging to monitor the decrease in pH during the fermentation process.

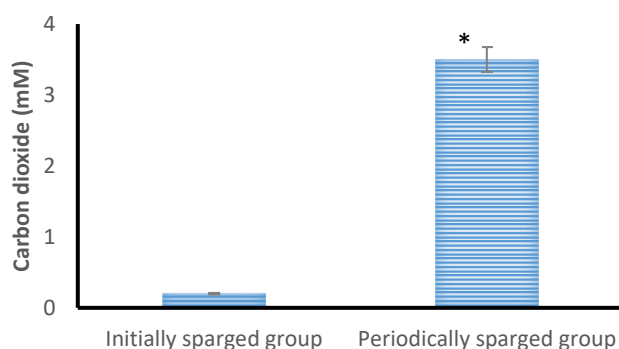


Figure 8.9: Accumulated produced carbon dioxide, whereby the amount of the produced carbon dioxide in the periodically sparged group was significantly higher than its counterpart in the initially sparged group. Error bars depict standard deviation. *The mean difference is significant at the 0.05 level.

8.5 *In situ* removal of some fermentation products

Stripping of both acetaldehyde and carbon dioxide was achieved using microbubble technology as well as a trace amount of ethanol (around 0.0017 mM was detected in the vapor collection system). Figure 8.9A shows the fluctuation in acetaldehyde concentrations in the fermentation broth after each sparging course. Microbubble technology was efficient to decrease the acetaldehyde concentration in the fermentation medium and kept its concentration less than 1.135 Mm (Figure 8.10A).

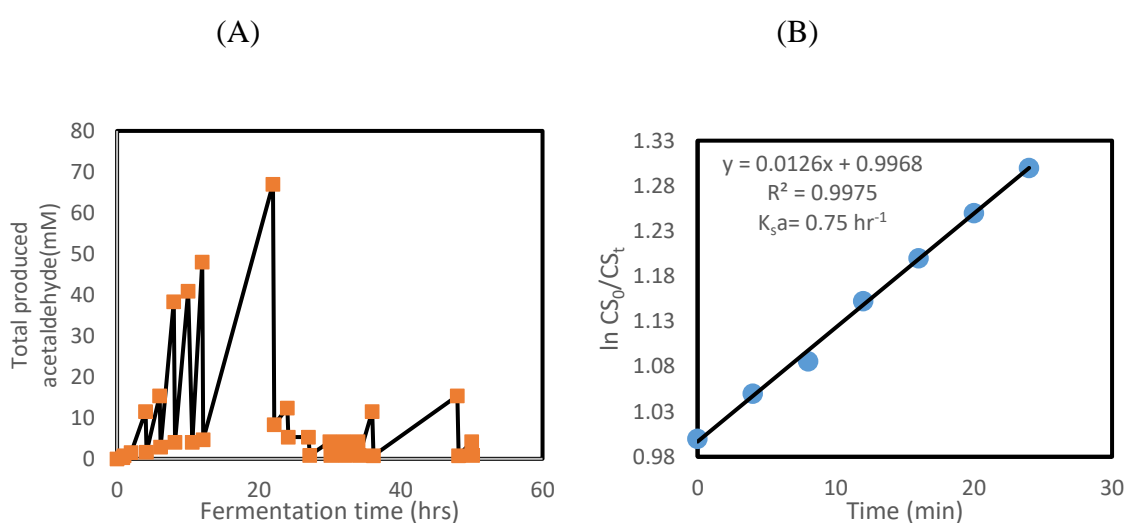


Figure 8.10: Stripping process of acetaldehyde from the fermentation broth using air microbubbles. (A) Fluctuation of acetaldehyde concentrations within the fermentation broth after each sparging course. (B) Variation of acetaldehyde concentrations with each sparging

cycle and calculation of stripping rate constant (K_{sa}). Error bars are representative of triplicate results.

Figure 8.10B shows changes in the acetaldehyde concentrations during each sparging course. The stripping rate constant (K_{sa}) was calculated for the highest concentration of produced acetaldehyde at hour 20 when acetaldehyde concentration reached 4.54 mM. Even with this relatively high concentration, microbubble technology was efficient in decreasing the acetaldehyde concentration to less than 1.135 mM after 24 minutes of sparging. Samples were withdrawn every 4 minutes and used to calculate the stripping rate constant (K_{sa}). The calculated stripping rate constant (K_{sa}) value was found to be 0.75 hr^{-1} . This value can be multiplied by the accumulated acetaldehyde concentration plus the produced acetaldehyde during the sparging time to work out the acetaldehyde removal rate or acetaldehyde stripping rate, as acetaldehyde is both being produced and stripped. The acetaldehyde production rate (during hour 20 when the acetaldehyde concentration reached its highest) was around $2.82 \text{ mmol. g(dry weight)}^{-1}.\text{hr}^{-1}$. Therefore the stripping rate was around $79.05 \text{ mM}.\text{hr}^{-1}$.

Figure 8.11 shows the yields of the fermentation bioproducts (acetaldehyde, ethanol and biomass), which were calculated by considering that 1 mol of glucose can be metabolised to produce 2 mol of acetaldehyde/ethanol with 2mol of carbon dioxide.

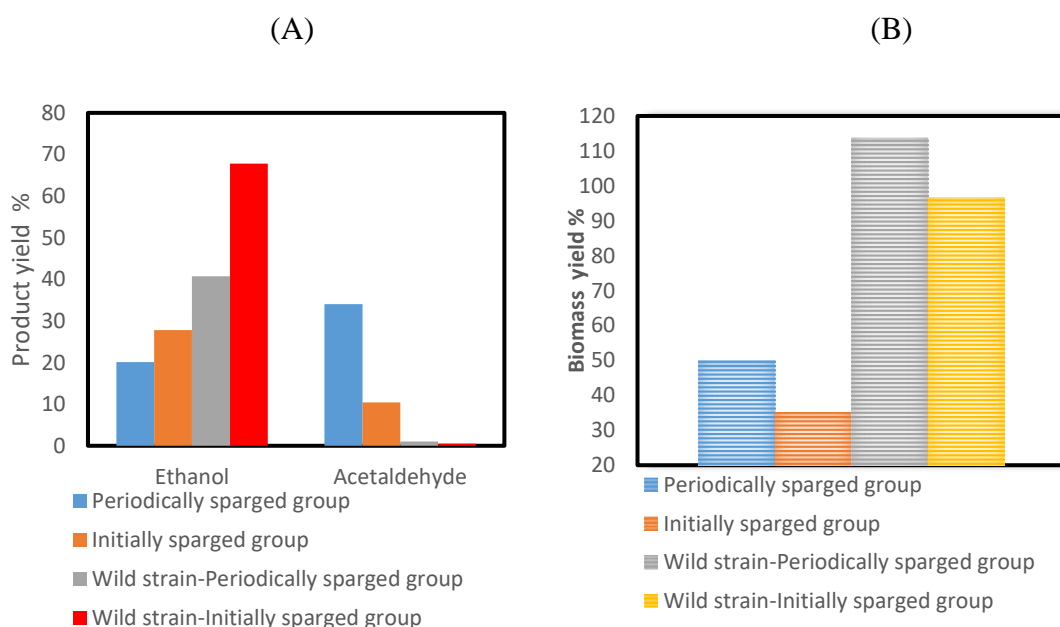


Figure 8.11: Bioproducts percent yields of mutant strain in comparison with the wild strain. (A) Ethanol and acetaldehyde yields. (B) Biomass yield.

The mutant strain shows a promising performance in the aerobic environment of the periodically-sparged group (Figure 8.11). While the ethanol percent yield reached about 20 %, the acetaldehyde yield was built up to 35 % under the aerobic conditions in the periodically-sparged group. On the other hand, the ethanol percent yield reached up to 30 %, while the acetaldehyde percent yield hit almost 10 % in the initially-sparged group. Regarding the biomass yield, the mutant strain flourished in the periodically-sparged group, and its yield reached almost 50 % in comparison with around 35 % under the anaerobic conditions of the initially-sparged group. Increasing biomass yield in the periodically-sparged group can be attributed to the *in-situ* removal of inhibitors by microbubble technology, especially acetaldehyde, as it tends to accumulate at the early stages of the exponential phase in the fermentation process under aerobic conditions. Also, microbubble technology removes carbon dioxide, which is another potential inhibitor of the fermentation process. Moreover, air microbubbles deliver oxygen efficiently to the fermentation medium and consequently to microbial cells, and this enhances the bacterial growth.

8.6 Changing the glucose concentration to optimize the fermentation process

The mutant strain consumed around 50 % of the provided sugar (40 g/L) in the batch culture of the initially-sparged group, while 25 % of glucose was consumed in the periodically-sparged group (Figure 8.5A). Consequently, the glucose concentration was halved to reduce the residual sugar, which would increase the performance and the productivity of the fermentation process. Bioproducts concentrations would tend to stay high as they depend on the consumed sugar rather than on the total provided sugar.

Figure 8.12 shows glucose consumption pathways during the fermentation process, supplied with 20 g/L glucose as a carbon source. The glucose was fully consumed by the mutant strain after 52 hr in the initially-sparged group, while some glucose was left over in the fermentation medium in the periodically-sparged group. Both groups showed similar glucose consumption patterns at the beginning of the process, and thereafter, a slight deviation was seen between these groups, and the initially-sparged group consumed more glucose than the periodically-sparged group. The glucose consumption rate was similar across both groups during the first 12 hours of the fermentation process and after that, the initially-sparged group showed an increased consumption rate, which was around 66.7 % higher than the rate in the periodically-sparged group.

Both groups, however, showed different patterns of the biomass production (Figure 8.13): at the first 10 hours of the fermentation process the initially-sparged group showed a hyperbolic growth pattern, while the periodically-sparged group showed a normal sigmoid growth pattern. Hyperbolic growth pattern was observed previously in the culture supplied with 40g/L glucose. The biomass concentration in the initially-sparged group was increasing even after shifting to the anaerobic conditions (after more than 5 hours) and the initially-sparged group showed two different specific growth rates: the first specific growth rate was 0.168 hr^{-1} , which was seen during the first 10 hours of the fermentation. Thereafter, the specific growth rate dropped to 0.064 hr^{-1} during the rest of the exponential phase (Figure 8.13). In contrast, the periodically-sparged group showed almost consistent growth rate at the exponential phase, which was around 0.094 hr^{-1} . Stripping out the fermentation products and providing high oxygen supply might be the reasons behind the enhanced growth in the periodically-sparged group in comparison with the initially-sparged group.

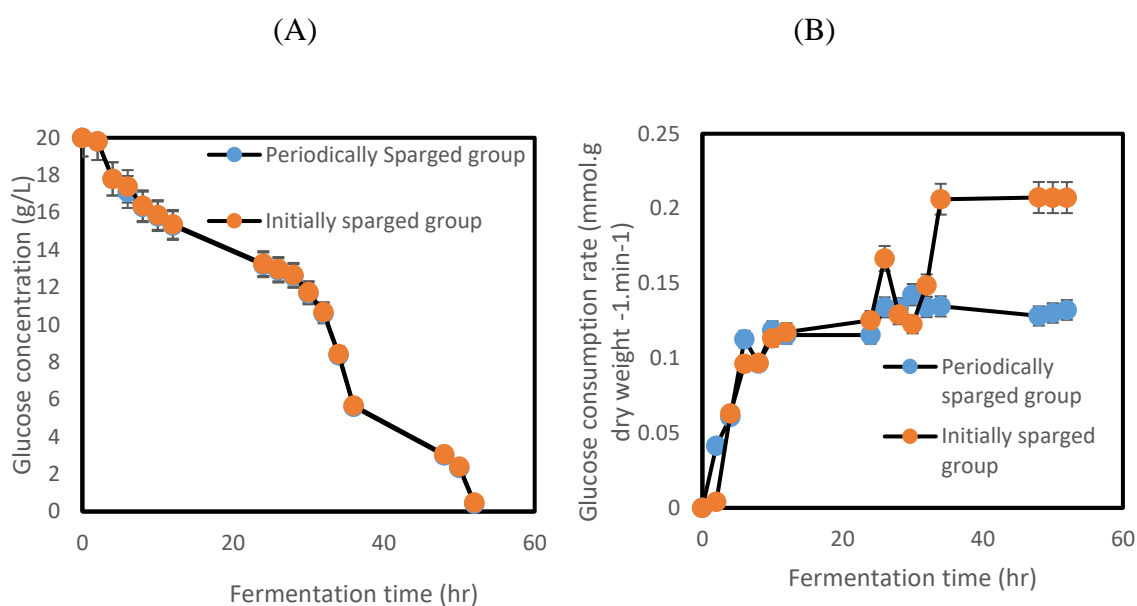


Figure 8.12: Glucose consumption pattern in *Zymomonas mobilis* ZM4 mutant strain grown on 20 g/l glucose supplied medium. (A) Glucose concentration with time. (B) Glucose consumption rate in both initially and periodically sparged groups. Error bars depict standard deviation.

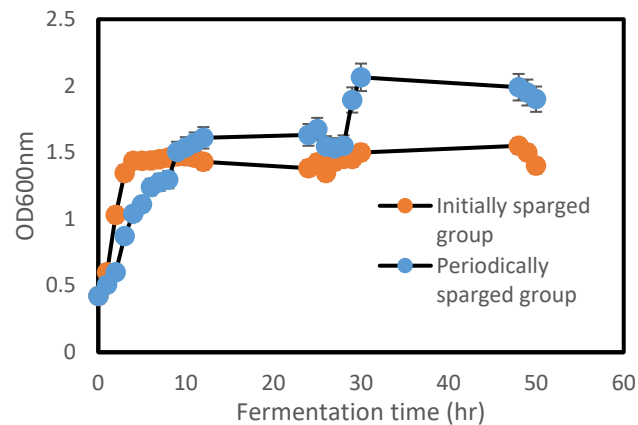


Figure 8.13: Comparison between the growth patterns of *Zymomonas mobilis* mutant strain in both initially and periodically sparged groups grown on fermentation medium supplied with 20 g/L glucose. Error bars depict standard deviation.

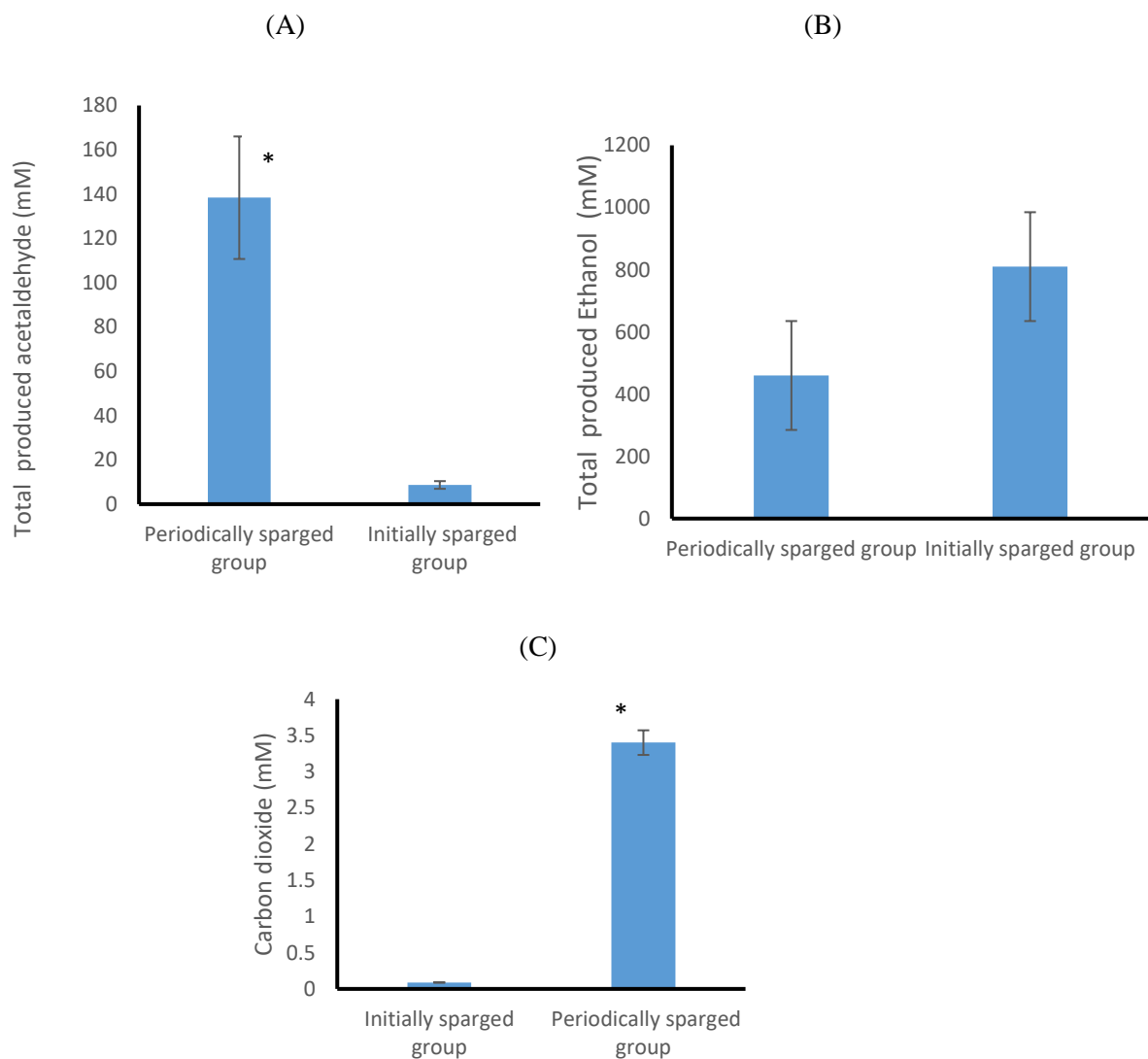


Figure 8.14: Accumulated fermentation products. (A) Produced acetaldehyde. (B) Produced Ethanol. (C) Produced carbon dioxide. Error bars depict standard deviation. * The mean difference is significant at the 0.05 level.

Figure 8.14 shows the accumulated fermentation products concentrations in both the initially- and periodically-sparged groups. The accumulative acetaldehyde concentration in the periodically-sparged group was 1,486 % higher than its concentration in the initially-sparged group. There was 95 % more ethanol produced in the initially-sparged group than in the periodically-sparged group. In addition, the amount of carbon dioxide produced in the periodically-sparged group was 1650 % higher than in the initially-sparged group, after it was collected and measured at the end of the fermentation process. These results might be due to the simultaneous production and separation of these products according to Le Chatelier's principle as well as the other reasons such as the removal of inhibitors, thereby removing the environmental stresses.

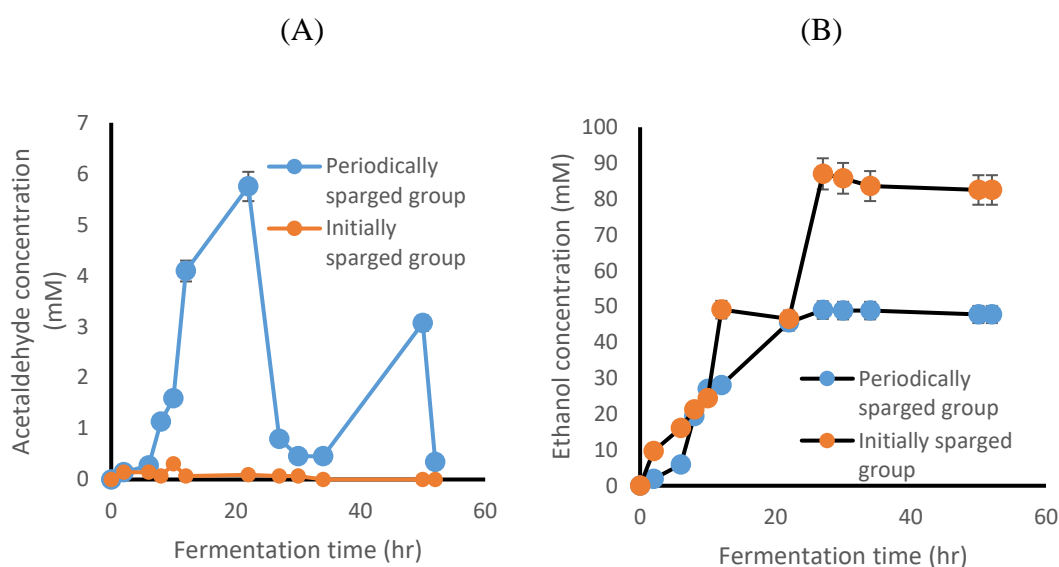


Figure 8.15: Acetaldehyde and Ethanol production during the fermentation process. (A) Acetaldehyde production with time. (B) Ethanol production with time. Error bars depict standard deviation.

Acetaldehyde started to accumulate in the fermentation broth after around 2 hours of the start of the fermentation process in both groups, and it reached its highest concentration after around 6 hours in the initially-sparged group (Figure 8.15). The periodically-sparged group, however, continues to produce acetaldehyde within the broth and reached its highest concentration after around 20 hr. After that, the production gradually decreased until the end of the fermentation process. At around 48 hours, the concentration of acetaldehyde built up to 3 mM as the culture was left without any sparging overnight. In Figure 8.15B, 80 % more ethanol was produced in the initially-sparged group than in the periodically-sparged group.

Figure 8.16A shows the fluctuation in the acetaldehyde concentration within the periodically-sparged culture. The acetaldehyde concentration reached its highest concentration of 5.67 mM after 20 hr. Acetaldehyde was stripped out of the fermentation broth and its concentration remained below 1.135mM (less than the minimum inhibitory concentration).

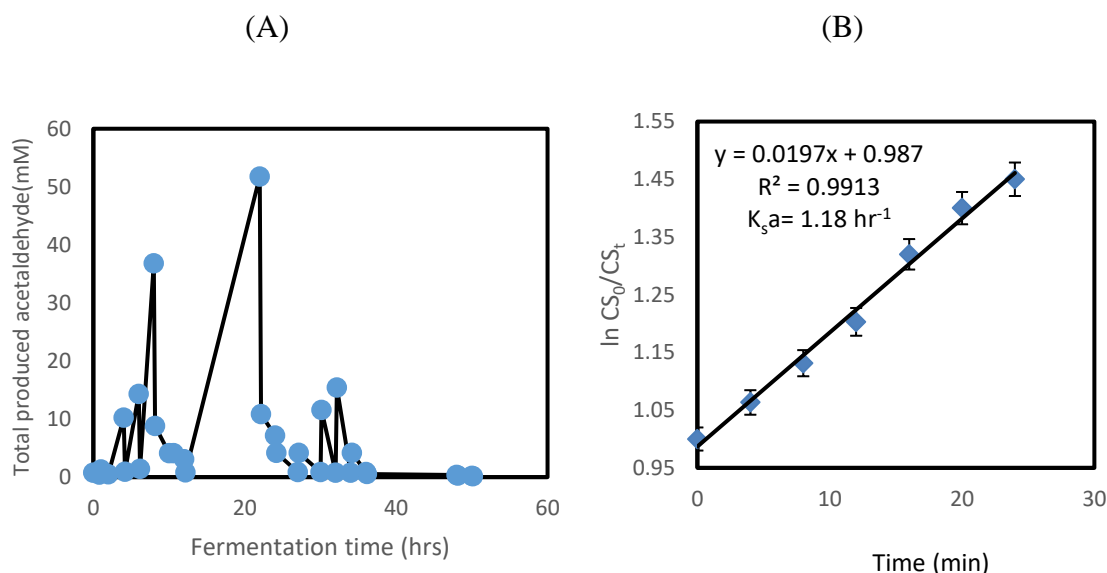


Figure 8.16: Stripping process of acetaldehyde from the fermentation broth using air microbubbles. (A) Fluctuation of acetaldehyde concentrations within the fermentation broth after each sparging cycle. (B) Variation of acetaldehyde concentrations with each sparging cycle and calculation of stripping rate constant (K_{sa}). Error bars depict standard deviation.

Microbubble technology was efficient in decreasing the acetaldehyde concentration in the fermentation medium and keeping its concentration less than 1.135 Mm (Figure 8.16A). The later concentration is less than the minimum inhibitory concentration. Figure 8.16B shows changes in the acetaldehyde concentrations during each sparging course. The stripping rate constant (K_{sa}) was calculated for the highest amount of produced acetaldehyde at the twenty hour when the acetaldehyde concentration reached around 5.67 mM. Even with this relatively high concentration, microbubble technology was efficient in decreasing the acetaldehyde concentration to less than 1.135 mM after 24 minutes of sparging. Samples were drawn every 4 minutes and used to calculate the stripping rate constant (K_{sa}).

The stripping rate constant (K_{sa}) value was found to be 1.18 hr^{-1} . This value can be multiplied by the accumulated acetaldehyde concentration plus the produced acetaldehyde during the sparging time to work out the acetaldehyde removal rate or acetaldehyde stripping rate, as acetaldehyde is both being produced and stripped. The acetaldehyde production rate (in hour

20 when the acetaldehyde concentration reached its highest) was around 3.92 mmol. g (dry weight)⁻¹. hr⁻¹. Therefore, the stripping rate was around 82.94 mM.hr⁻¹. Figure 8.17 shows the yields of the fermentation bioproducts (acetaldehyde, ethanol and biomass), which were calculated by considering that 1mol of glucose can be metabolised to produce 2mol of acetaldehyde/ethanol with 2 mol of carbon dioxide.

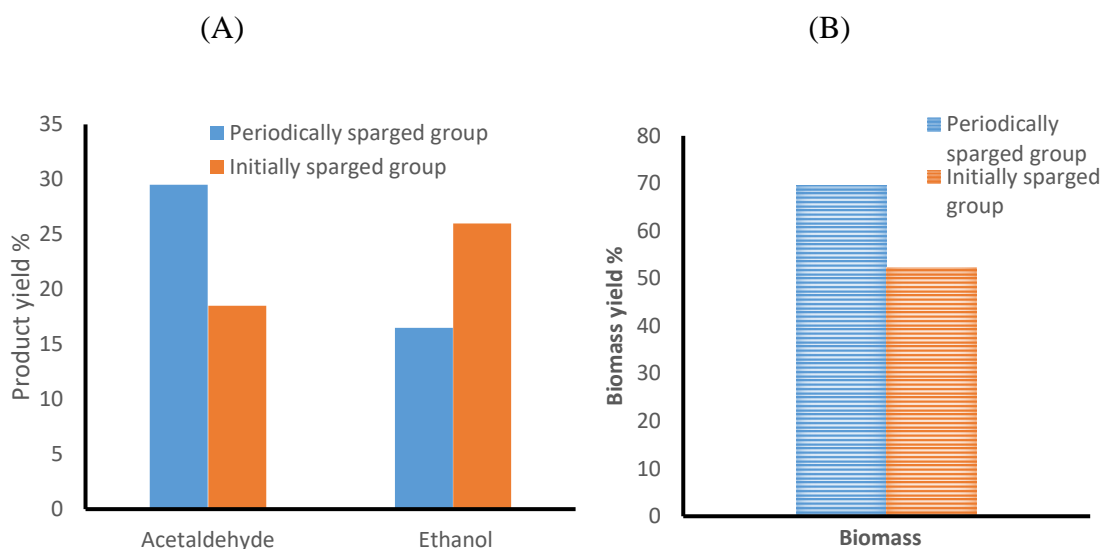


Figure 8.17: Bioproducts yields. (A) Ethanol and acetaldehyde yields. (B) Biomass yield.

The mutant strain shows an exceptional performance in the aerobic environment of the periodically-sparged group. While the ethanol percent yield reached more than 15 %, the acetaldehyde yield was built up to 30 % under aerobic conditions (periodically-sparged group). The ethanol percent yield reached almost 30 %, while the acetaldehyde percent yield hit almost 20 % in the initially-sparged group (Figure 8.17). Interestingly, the ethanol-to-acetaldehyde yields ratio was 1: 1.75 using 40 g/L glucose as an initial carbon source, while this ratio was increased to 1:87 (ethanol-to-acetaldehyde yields) when 20 g/L glucose was used in this experimental set. Therefore, using 20 g/L as an initial glucose concentration increases the performance of this mutant strain under periodically-sparged conditions, as almost all of the supplied glucose was consumed, and this enhances the overall yields of the process. These conditions can therefore be seen as the fitness conditions to produce acetaldehyde from the mutant strain.

Regarding the biomass yield, the mutant strain thrived in the periodically-sparged group and its yield reached almost 70 %, compared to around 50 % under anaerobic conditions (in the initially-sparged group) considering 10.5 g (dry weight) of biomass for each mole of glucose

being metabolised as a maximum biomass concentration produced by *Zymomonas mobilis* (Kalnenieks, 2006). In contrast, these yields were higher than the yields obtained with the group supplied with 40 g/L glucose. Its yield was 50 % in the periodically-sparged group and 35 % in the initially-sparged group. Again, this can be attributed to the initial glucose supply, which was consumed efficiently without any residual glucose in the culture.

To illustrate how the results obtained from the current study compare with previous studies, a comparison was made between the acetaldehyde results obtained from the bespoke microbubble-mediated systems with selected previous, promising studies. This comparison is based on the accumulative acetaldehyde concentration as this parameter is suitable for all studies and it represents the sum of the average concentrations of produced and stripped acetaldehyde from the fermentation process (Figure 8.18).

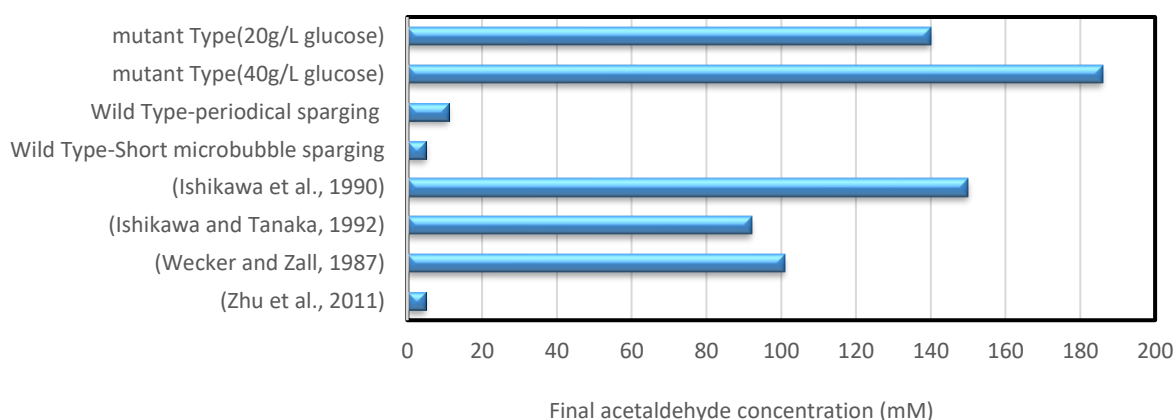


Figure 8.18: A comparison between the acetaldehyde results obtained in the current study with previous promising studies, whereby acetaldehyde is both produced and stripped out from the fermentation broth.

The obtained acetaldehyde in the current study was higher than that produced in previous studies, especially with the IFO 13757 *Zymomonas mobilis* strain grown in a 2 L jar fermenter (Ishikawa et al., 1990), where 24 % more acetaldehyde was produced by 200 mM of the allyl alcohol selected strain grown in the airlift loop bioreactor driven by microbubbles (Figure 8.18).

8.7 Separation of acetaldehyde-water mixture using air-microbubbles generated by fluidic oscillation

An acetaldehyde-water mixture was prepared with almost the same concentrations produced in the fermentation broth by the *Zymomonas mobilis* mutant strain to validate the obtained results

of the acetaldehyde stripping process. The temperature of the mixture was kept at 30 °C during the sparging time.

The stripping rate constant (K_{sa}) and the stripping rate were calculated during the sparging course for 24 minutes at 30 °C and 0.3 L/min flow rate, which is fed by the fluidic oscillator. It is worth noting that this experimental set represents the gas stripping efficiency in each sparging course at the point when the acetaldehyde concentration reached its highest. Figure 8.19B shows the decrease in the acetaldehyde concentration during the sparging course to less than 1.13 mM (less than the minimum inhibitory concentration). The removal efficiency was calculated by applying the following equation:

$$\% \text{ removal efficiency} = \frac{(X_0 - X_r)}{X_0} * 100 \quad (\text{Eq. 8.1})$$

where X_0 is the initial acetaldehyde concentration (mM) and X_r is the residual acetaldehyde concentration (mM).

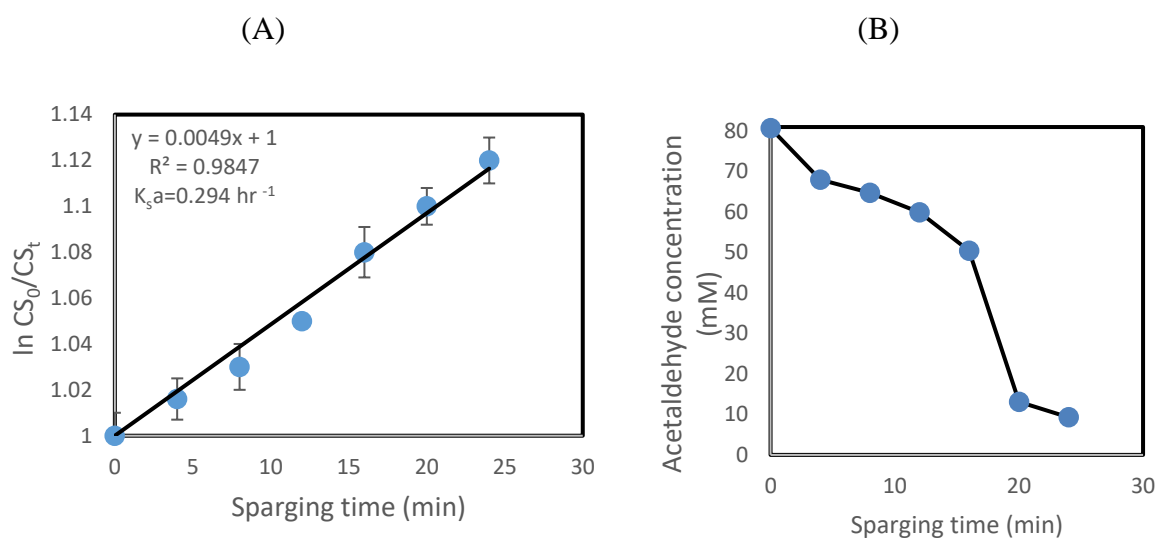


Figure 8.19: Stripping process of acetaldehyde from the acetaldehyde-water mixture using air microbubbles. (A) Calculation of stripping rate constant (K_{sa}) during sparging course. (B) Decreasing of acetaldehyde concentrations within the mixture after sparging course. Error bars depict standard deviation.

Figure 8.19A shows a decrease in the acetaldehyde concentration during the sparging course to calculate the stripping rate constant (K_{sa}). The stripping rate constant (K_{sa}) was calculated for the 81.72 mM acetaldehyde-water mixture, whereby microbubble technology was able to decrease the acetaldehyde concentration to less than 9.2 mM after 24 minutes of sparging.

Samples were drawn every 4 minutes and used to calculate the stripping rate constant (K_{sa}). The calculated stripping rate constant (K_{sa}) value was 0.294 hr^{-1} . This value can be multiplied by the initial acetaldehyde concentration to work out the acetaldehyde removal rate or the acetaldehyde stripping rate, which was $24 \text{ mM}\cdot\text{hr}^{-1}$.

In addition, the removal efficiency of acetaldehyde using microbubble technology reached 88.6%. This high efficiency can be explained as follows: Dry air microbubbles are injected into the liquid phase (acetaldehyde-water mixture) at $30 \text{ }^\circ\text{C}$, when a non-equilibrium driving force exists for mass transfer between the contact phases (bubble phase and liquid phase). The injected air microbubbles are dragged in a laminar regime which, in turn, acts to prevent the liquid and gaseous phases from reaching equilibrium rapidly, thereby ensuring a continuous mass transfer process. Subsequently, the acetaldehyde molecules (in a vapour phase at $30 \text{ }^\circ\text{C}$) are continuously transferred from the liquid side to the bubble side via both diffusion and internal convection due to bubble motion. Consequently, the equilibrium is disrupted according to Le Chatelier's principle, and shifts towards more vaporisation to compensate of the removed acetaldehyde molecules from the liquid phase. According to this scenario, the acetaldehyde concentration in the bubble phase would be higher than its concentration in the liquid phase.

In contrast, using continuous air flow (after removing the fluidic oscillator) generates much bigger bubbles ($1,000\text{-}2,200 \text{ }\mu\text{m}$), which are no longer considered microbubbles (fine bubbles) for the same flow rate (0.3 L/min). Increasing the bubble sizes decreases the stripping efficiency of acetaldehyde from the binary mixture as increasing the bubble sizes reduces the surface area-to-volume ratio and this minimises all interfacial transport phenomena such as heat, mass, and momentum transfers, which are heavily affected by surface area-to-volume ratio (Zimmerman et al., 2009). To validate this, a continuous air flow was fed to a ceramic diffuser at the same flow rate used before (0.3 L/min), and much bigger bubbles ($1,000\text{-}2,200 \text{ }\mu\text{m}$) were generated under these operational conditions (Figure 8.20).

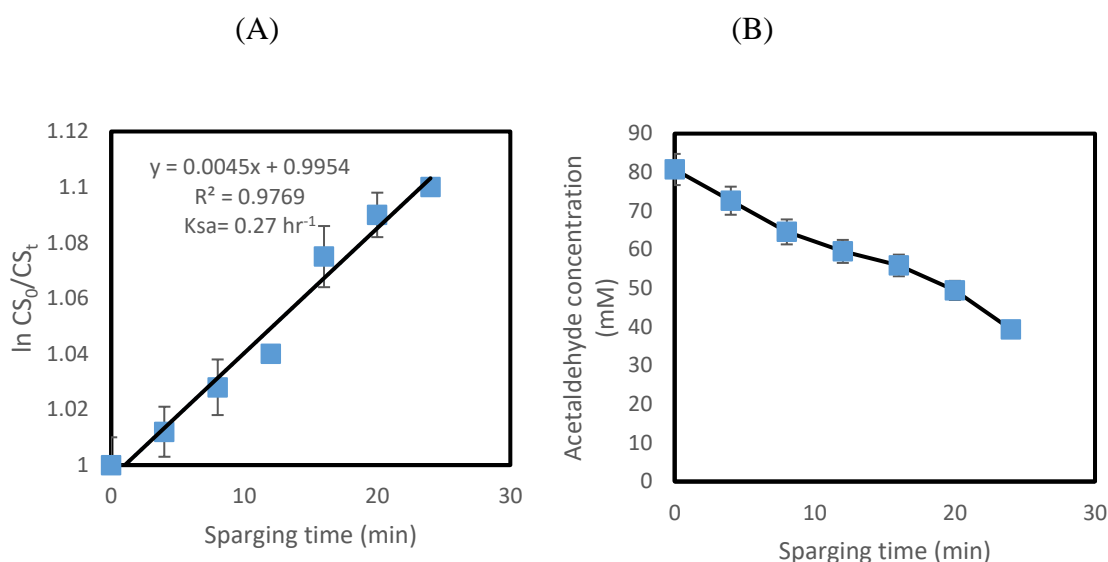


Figure 8.20: Stripping process of acetaldehyde from the acetaldehyde-water mixture using the continuous flow. (A) Calculation of stripping rate constant (K_{sa}) during sparging course. (B) Decreasing of acetaldehyde concentrations within the mixture after each sparging course. Error bars are representative of triplicate results.

The stripping rate constant (K_{sa}) was calculated for 81.72 mM acetaldehyde-water mixture, whereby fine air bubbles (without the use of a fluidic oscillator) were able to decrease the acetaldehyde concentration to 39 mM after 24 minutes of sparging. Samples were drawn every 4 minutes and used to calculate the stripping rate constant (K_{sa}). The calculated stripping rate constant (K_{sa}) value was found to be 0.27 hr^{-1} . This value can be multiplied by the acetaldehyde concentration to work out the acetaldehyde removal rate or the acetaldehyde stripping rate, which was $22 \text{ mM}\cdot\text{hr}^{-1}$ and this is 8 % decrease in the stripping rate in comparison with the microbubbles driven stripping process.

The removal efficiency of acetaldehyde using fine bubbles reached 52 %. Totally, the removal efficiency of acetaldehyde decreased 36.6 % when fine bubbles used instead of microbubbles. This decrease in the removal efficiency can be attributed to the limited surface area to volume ratio in the fine bubbles in comparison with microbubbles and thus; less mass transfer is taking place between the liquid and gaseous phases and also the relative internal circulation is less intensive (Zimmerman et al., 2013). Correspondingly, only limited acetaldehyde molecules are transferred from the liquid side to the bubble side and subsequently, these coarse bubbles in comparison with microbubbles can strip less acetaldehyde out.

8.8 Testing the performance of the mutant strain in a synthetic medium

All of the aforementioned works were done in a complex medium and only the glucose concentration was manipulated to optimise the performance in the complex medium. However, testing of the performance in a synthetic medium has many advantages, such as being very useful in understanding the bacterial metabolism as the chemical composition of this medium is exactly known. Another advantage is that this type of media can minimise variation in the results, since the results obtained using this medium are almost uniform and comparable, meaning that the bacterial metabolism stands out clearly amongst the results. This synthetic medium was reported to be used by Kremer et al., (2015). Two glucose concentrations were used to explore the performance of the *Zymomonas mobilis* mutant strain in this medium. Two glucose concentrations (20 g/L and 40 g/L) were used to show this performance and to compare it with the performance in the complex medium.

A. 20 g/L glucose concentration

20 g/L glucose concentration in the synthetic medium was used as an initial concentration to test both biomass and fermentation products formation using the bespoke periodical sparging strategy. Figure 8.21 shows biomass formation in the synthetic medium supplied with 20 g/L glucose.

Interestingly, the *Zymomonas mobilis* mutant strain showed a slowly growing trend with 0.16 hr⁻¹ specific growth rate and the final biomass yield reached 59 %. Using the mineral salts medium requires the addition of supplements of both pantothenate and biotin in the absence of amino acids (Montenecourt, 1985). The reason behind this addition is that the enzymatic reactions that produce the precursors of biosynthesis, are exceptionally weak in *Zymomonas mobilis* in comparison with the primary catabolic reactions of the pyruvate decarboxylase and pyruvate kinase (Bringer-Mayer and Sahm, 1988). In complex media, yeast extract is used as a nitrogen source as well as a pantothenate source as it is rich with pantothenate with double the amount that can be supplemented artificially (0.005 g/L was used in the current study to prepare the synthetic medium) (Belaïch et al., 1965).

Zymomonas mobilis catabolises around 95-98 % of the carbon source (glucose) into ethanol and carbon dioxide, while just 3-5 % of this carbon source can be served an anabolic role and biomass formation (Swings and De Ley, 1977 and Rogers et al., 1982).

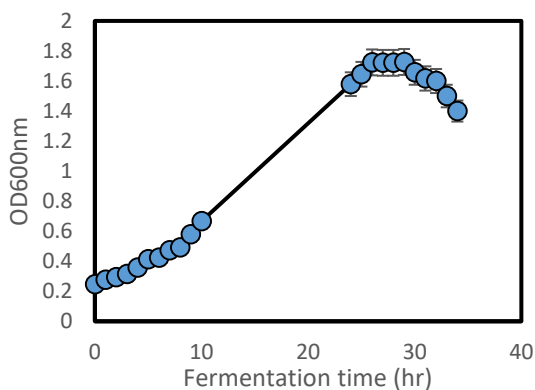


Figure 8.21: Growth pattern of *Zymomonas mobilis* mutant strain in the synthetic medium under periodically sparging strategy supplied with 20 g/L glucose. Error bars are representative of the triplicate results.

Figure 8.22 shows the glucose consumption pattern during the growth in the synthetic medium supplied with 20 g/L glucose.

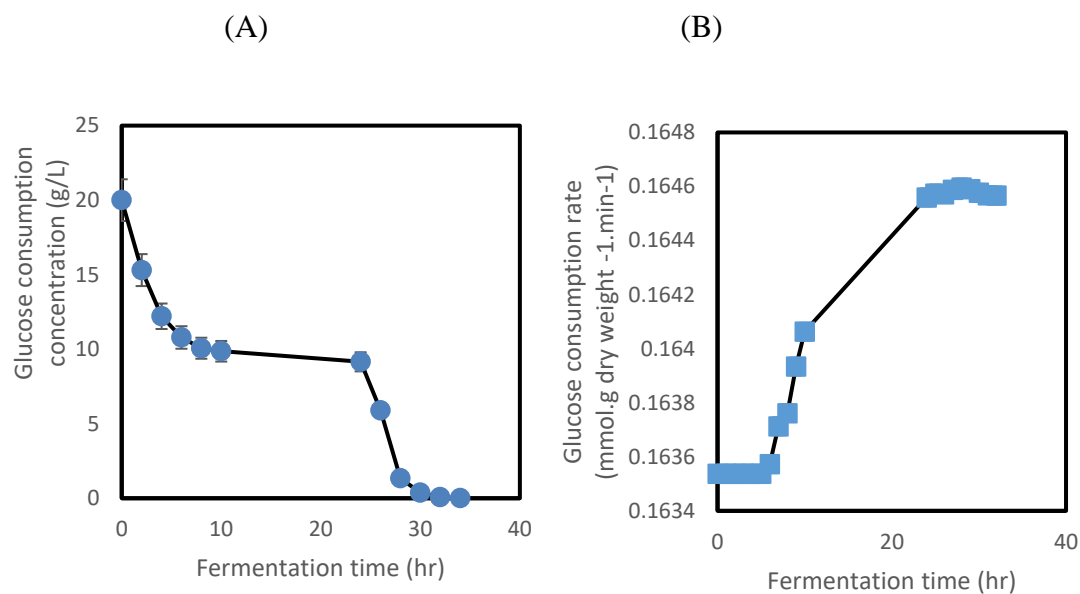


Figure 8.22: Glucose consumption pattern in *Zymomonas mobilis* ZM4 mutant strain grown in the synthetic medium supplied with 20 g/l glucose. (A) Glucose concentration with time. (B) Glucose consumption rate with time. Error bars depict standard deviation.

The provided glucose was totally consumed within 34 hours, while the glucose consumption rate gradually increased during the fermentation process and reached its highest at the end of the fermentation process.

Regarding the fermentation products, ethanol and carbon dioxide were only consistently produced in this experimental set, while acetaldehyde production was inconsistently produced

in the fermentation broth and its concentration was ranging from 0 to 2.58 mM. Figure 8.23 shows the ethanol production during the fermentation time in the defined mineral salts medium supplied with 20 g/L glucose. The low ethanol productivity is combined with low biomass formation and the final ethanol yield reached 21.5 %. The decrease in the ethanol concentration at the end of the fermentation process is attributed to the ethyl acetate formation as well as ethanol stripping.

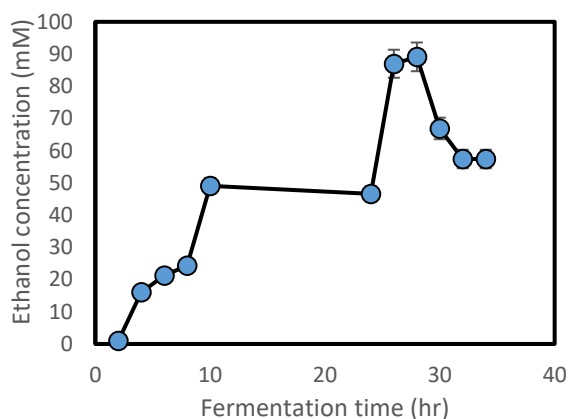


Figure 8.23: Ethanol production during the fermentation in the defined mineral salts medium supplied with 20 g/L, where the highest ethanol concentration was at hour thirty and thereafter, the concentration decreased due to the stripping process as well as ethyl acetate formation. Error bars depict standard deviation.

Under the aerobic fermentation of *Zymomonas mobilis*, numerous side products can be produced in addition to the main products, acetaldehyde, ethanol and carbon dioxide. These by-products have great importance as they contribute greatly to the aroma of the fermentation process. These products, such as acetate, lactate, acetoin (Yang et al., 2009), and ethyl acetate (Viikari and Berry, 1988) have frequently been detected in aerobically-grown *Zymomonas* cultures. The formation mechanisms of some of these by-products in brewer's yeast cultures were investigated previously (Genevois, 1951a, 1951b; Nordström, 1961, 1963; Yoshioka and Hashimoto, 1981 and Fukuda et al., 1998), and in *Candida utilis* culture (Armstrong et al., 1983). However, the formation mechanisms of these by-products have not been fully explored in *Zymomonas mobilis*, although they have frequently been detected in fermentation broths of *Zymomonas mobilis* under aerobic conditions (Viikari and Berry, 1988; Seo et al., 2005 and Yang et al., 2009).

Zymomonas mobilis catabolises glucose via the Entner-Doudoroff pathway to pyruvate, and up to 98 % of the produced pyruvate is converted to acetaldehyde and carbon dioxide (Neveling et al., 1998). However, only a small part (around 2 %) of the generated pyruvate is decarboxylated to acetyl coenzyme A, carbon dioxide, and NADH by the reaction of pyruvate dehydrogenase (PDH) complex (Sahm et al., 1992). Due to the lack of 2-oxoglutarate dehydrogenase complex and other enzymes of the tricarboxylic acid cycle in *Zymomonas mobilis*, the PDH complex plays an exclusively anabolic role in *Zymomonas mobilis*. This complex carries out 5 consecutive reactions in the decarboxylation and dehydrogenation of pyruvate to produce acetyl-CoA (Nelson and Cox, 2004).

Ethyl acetate is produced by alcohol acetyltransferase and hydrolysed by esterase. The combined action of these two enzymes determines the levels of ethyl acetate in fermentation broths. Various mechanisms are proposed to explain ethyl acetate formation, which are: (i) esterification of acetic acid in the fermentation broth using ethanol; (ii) enzyme-catalysed esterification in the fermentation broth; (iii) ester formation within the cell, and after that the ester diffuses into the fermentation broth; and (iv) transferring of the acetyl group from acetyl coenzyme A to ethanol, which is catalysed by alcohol acetyltransferase as ethanol accumulates in the fermentation broth. The formed ester (ethyl acetate) can be produced as a primary metabolite during the exponential phase's combined processes, requiring energy, and through the later stages of the fermentation process.

Seemingly, *Zymomonas mobilis* lacks the aldehyde dehydrogenase enzyme to oxidise acetaldehyde to acetic acid (Wecker and Zall, 1987; Bringer-Meyer and Sahm, 1993) and therefore ethyl acetate production using esterification of acetic acid is unlikely to take place. As a result, ethyl acetate is likely produced by transferring the acetyl moiety from acetyl coenzyme A produced by pyruvate dehydrogenase complex to ethanol (Figure 8.24). This mechanism was validated by monitoring the concentrations of both ethanol and ethyl acetate during the fermentation process, when the ethyl acetate yield reached 0.00044 (g/g) (Figure 8.25).

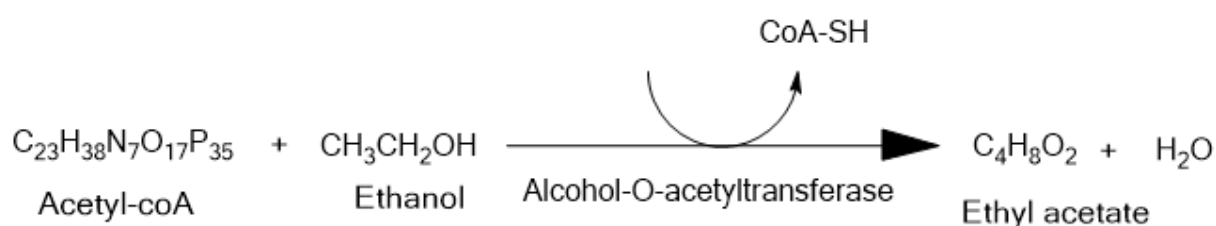


Figure 8.24: Proposed mechanism for ethyl acetate formation from both acetyl-coA and ethanol.

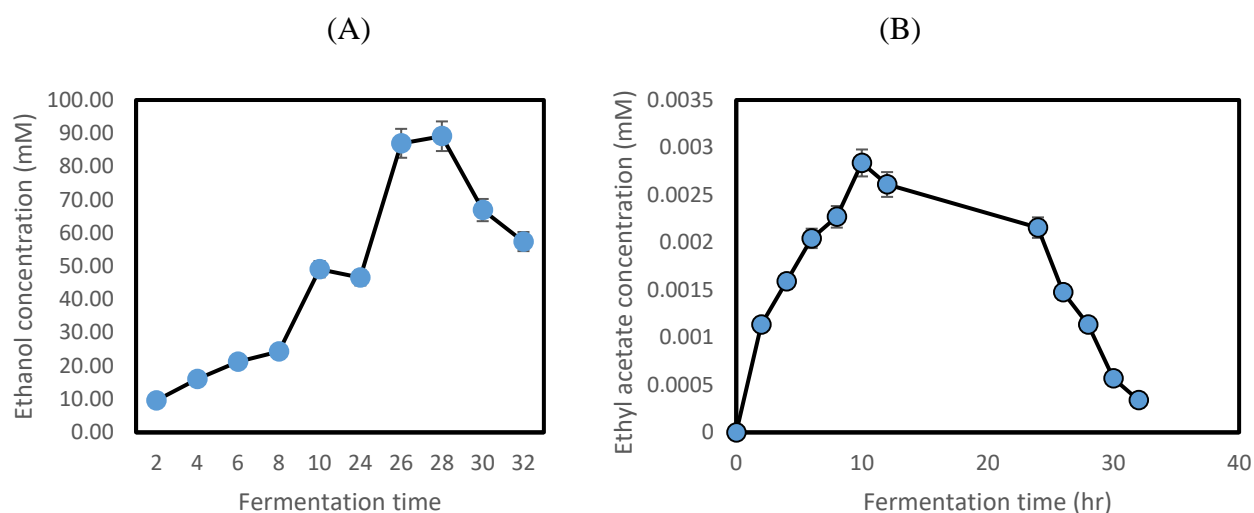


Figure 8.25: Ethyl acetate production corresponding with ethanol production. (A) Ethanol production during the fermentation process. (B) Ethyl acetate production during the fermentation process. Error bars depict standard deviation.

The ethanol accumulation in the fermentation broth can decrease both the rate of substrate conversion and the rate of product's formation (Osman and Ingram, 1985). The main action of the accumulated ethanol, which results in a decreased rate of fermentation, is to increase the membrane leakage, reducing the intracellular concentrations of cofactors and coenzymes that are essential for activities of enzymes involved in both glycolysis and alcohol production (Osman and Ingram, 1985).

The mechanism of the acetyl-CoA formation, which is another precursor for ethyl acetate formation, was described previously (Bringer-Meyer and Sahn, 1993).

An experimental set was designed to test the inhibitory effects of ethyl acetate on *Zymomonas mobilis* mutant strain growth after adding different concentrations of ethyl acetate. Figure 8.26 shows that the ethyl acetate accumulation has a minor effect on *Zymomonas* growth at various concentrations (ranging from 0.05 % (v/v) to 1 % (v/v)). Thus, this compound has a less inhibitory effect than both acetaldehyde and ethanol, which were studied previously. Indeed, the specific growth rate in the control group (the untreated group with ethyl acetate) was 0.60 hr^{-1} , while this rate decreased 35 % when 1 % (v/v) of ethyl acetate was added to the bacterial culture 2 hours after the beginning of the fermentation process. Interestingly, the addition of 0.05 % (v/v) of ethyl acetate to the bacterial culture decreased the specific growth rate by only 3 %, and the produced ethyl acetate in the current study was much lower than 0.05 % and therefore, no inhibitory effect is likely to happen due to the accumulation of ethyl acetate.

Physiologically, ethyl acetate has an unknown function, but its production is advantageous for *Zymomonas mobilis* as it is produced from ethanol and acetyl-CoA and therefore, its formation can be considered as a detoxification mechanism for ethanol under aerobic conditions, and also it can drive pyruvate dehydrogenase complex reaction forwards as acetyl-CoA is the final product of the pyruvate dehydrogenase complex activity.

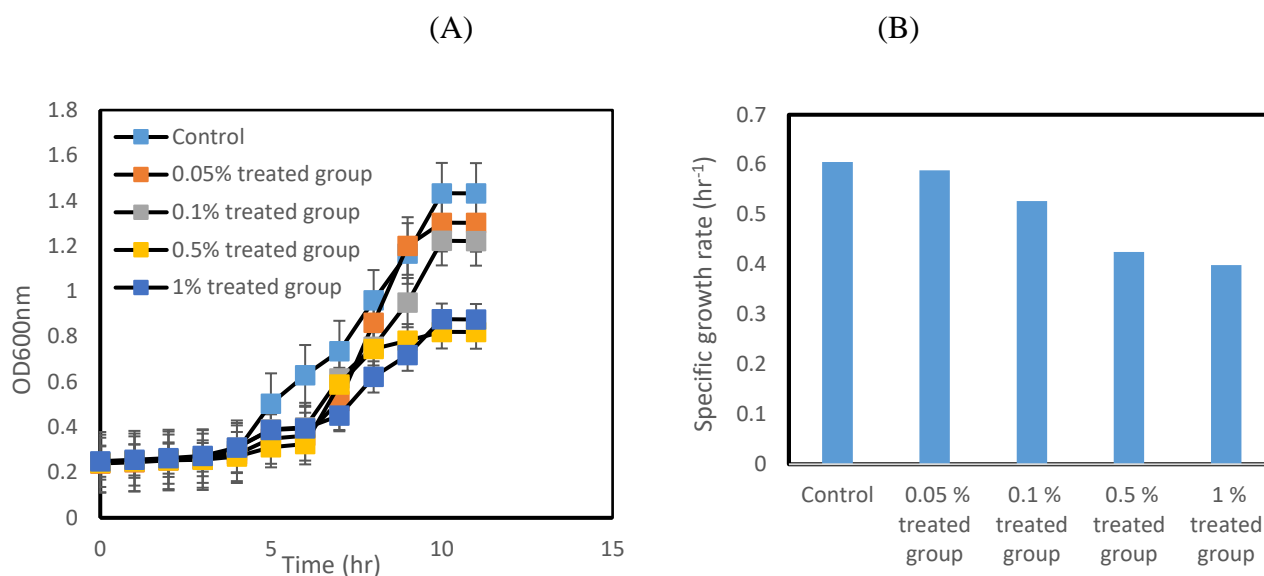


Figure 8.26: (A) Effect of added ethyl acetate on exponential cell growth of *Zymomonas mobilis* mutant strain after 2 hours, where the inhibitory effect of ethyl acetate is proportional to its concentration. (B) Specific growth rate of *Zymomonas mobilis* mutant strain after adding various concentrations of ethyl acetate. Readings are representative of triplicate results.

Carbon dioxide was produced during the fermentation process, and it is continuously collected during the fermentation process and its final concentration reached 4.3 mM.

B. 40 g/L glucose concentration

The concentration of supplied glucose was doubled in order to explore whether increasing the glucose concentration to 40 g/L could enhance the performance of the *Zymomonas mobilis* mutant strain in the defined mineral salts medium, compared to its performance with the 20 g/L glucose supplied medium.

Figure 8.27 shows the biomass formation in the synthetic medium supplied with 40 g/L. The *Zymomonas mobilis* mutant strain showed a slowly growing trend with 0.165 hr⁻¹ specific growth rate, while the biomass yield reached 54.9 %.

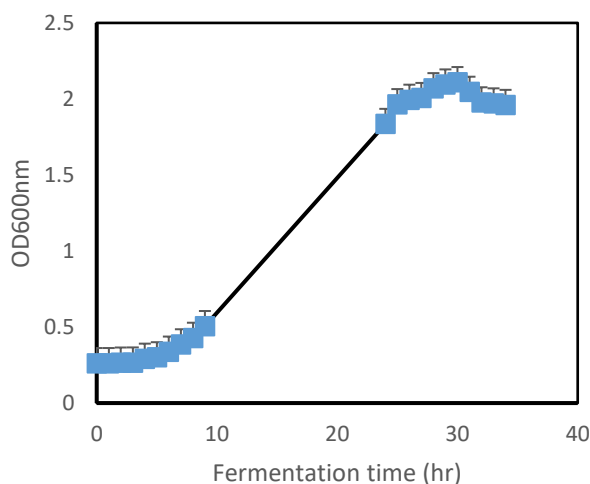


Figure 8.27: Growth pattern of *Zymomonas mobilis* mutant strain in the synthetic medium under periodically sparging group supplied with 40 g/L glucose. Error bars depict standard deviation.

Zymomonas mobilis generates 1 mol of adenosine triphosphate (ATP) per mole of glucose being metabolised, and its specific generation rate is considerably higher than the generation rate in some other microorganisms such as yeast. This high specific generation rate of ATP should be balanced by an equivalently rapid consumption rate. Undoubtedly, the cell-biomass formation is not the main consumer of ATP in *Zymomonas mobilis*, which grows in a low energetic efficiency (Kalnenieks, 2006). This relatively low biomass yield with high catabolic rate is caused by the presence of some ATP spilling reactions in this bacterium in the form of futile cycles or bypass reactions. The ATP spilling reaction allows glycolysis to proceed without coincidental biomass formation (Kalnenieks, 2006), under conditions when indispensable growth cofactors are absent or limited such as a pantothenate limitation condition (Belaich and Senez, 1965). The decoupling behaviour of biomass synthesis from bioproducts generation in batch cultures starts at relatively high glucose concentrations (e.g. between 4-6%) (Veeramallu and Agrawal, 1986).

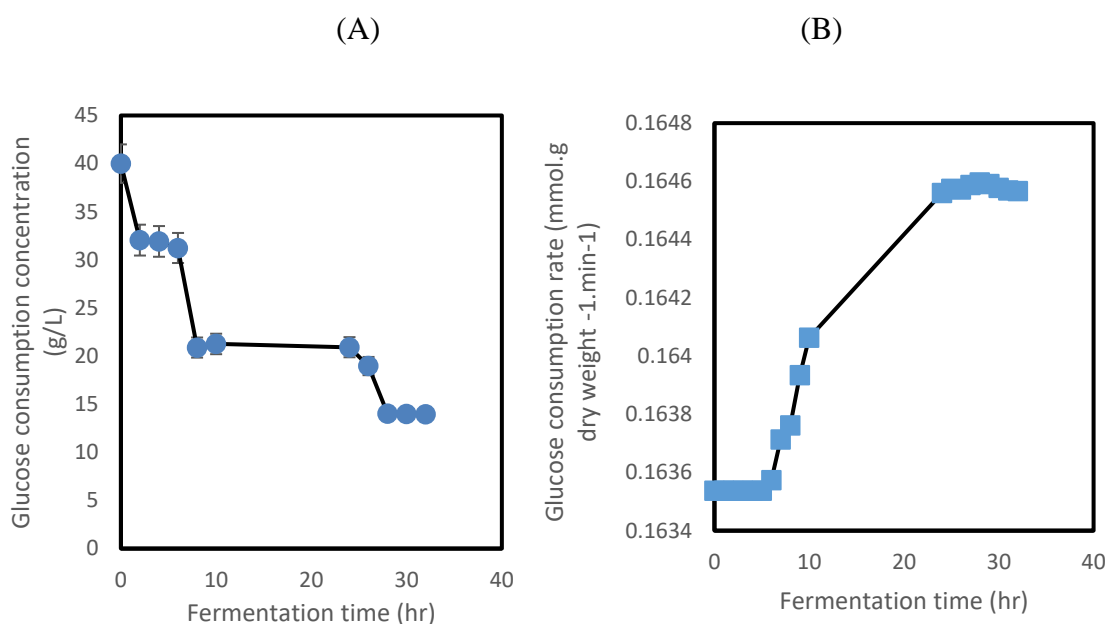


Figure 8.28: Glucose consumption pattern in *Zymomonas mobilis* ZM4 mutant strain grown on 40 g/l glucose supplied the synthetic medium. (A) Glucose concentration with time. (B) Glucose consumption rate with time. Error bars depict standard deviation.

65 % of the provided glucose was consumed by the *Zymomonas mobilis* mutant strain after 34 hours, and around 14 g/L of glucose was left over in the fermentation broth when the bacterial culture approached the death phase (Figure 8.28). Moreover, the bacterial strain showed comparable glucose consumption rate with the growth in supplied with 20 g/L glucose. The biomass concentration in the 40 g/L glucose supplied culture was 11 % higher than the concentration in the 20 g/L glucose supplied culture; but, the 40 g/L glucose supplied culture showed less biomass yield (54.9 %) than the 20g/L glucose supplied culture (59.5 %). This result agrees with the result reported by Lawford and Stevnsborg (1986), who observed a decrease in the biomass yield from 9.0 to 7.2 g(dry)wt. (mol glucose)⁻¹ when the concentration of glucose increased from 3 % to 6 % in the defined minimal medium. Decreasing the biomass yield can be attributed to two factors. The first is that the decoupling behavior of biomass synthesis from bioproducts generation in batch cultures begins at 40 g/L glucose concentration (Veeramallu and Agrawal, 1986). This behaviour is activated under high glucose excess conditions. The second is that the biomass yield is markedly decreased under nutrients limitations conditions such as nitrogen, phosphate or potassium limitations (Lawford and Stevnsborg, 1986 and Jones and Doelle, 1991). Therefore, it is recommended that optimisation research needs to be undertaken to determine the most suitable composition to avoid any nutrient limitation during the fermentation process.

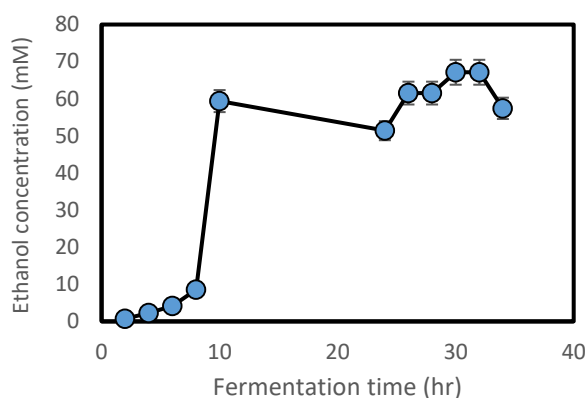


Figure 8.29: Ethanol production during the fermentation in the defined mineral salts medium supplied with 40 g/L. Error bars depict standard deviation.

Figures 8.29 and 8.30 show the concentrations of both ethanol and ethyl acetate respectively in the fermentation broth supplied with 40 g/L glucose. It can be clearly seen that the concentration of ethyl acetate is gradually built up in the fermentation broth and its yield reached 0.00047 (g/g), while there is a fluctuation in ethanol concentration especially at 26, 32 and 34 hours of the fermentation time and its yield reached 23 %. Acetaldehyde was also detected in the fermentation broth and its concentration varies from 0 to 5.5 mM. The fluctuated acetaldehyde concentration was also noted in the previous experiment, and this fluctuation is unclear to be interpreted. Carbon dioxide was produced during the fermentation, and it was continuously collected during the fermentation process and its concentration reached 4.3 mM.

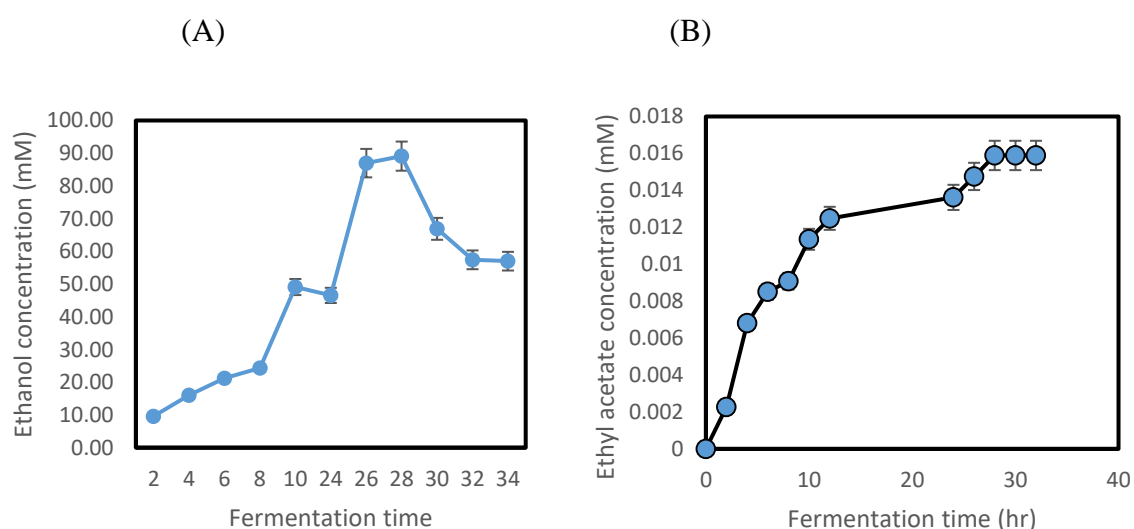


Figure 8.30: Ethyl acetate production corresponding with ethanol production. (A) Ethanol production during the fermentation process. (B) Ethyl acetate production during the fermentation process. Error bars depict standard deviation.

Importantly, the production of ethyl acetate was observed in the synthetic medium but it could not be detected in the complex medium under the same growth conditions. A reasonable interpretation for this observation is that the synthetic medium is a chemically known medium and is prepared by mixing compounds such as $\text{ZnSO}_4 \cdot 7\text{H}_2\text{O}$, $\text{FeSO}_4 \cdot 7\text{H}_2\text{O}$, $\text{MnSO}_4 \cdot 7\text{H}_2\text{O}$, $\text{CuSO}_4 \cdot 5\text{H}_2\text{O}$ and $\text{Co}(\text{NO}_3)_2 \cdot 6\text{H}_2\text{O}$. Many of these compounds are cofactors and required by many important metabolic pathways. Also, it is possible for the concentration of a single cofactor to affect the fluxes of many different pathways. For example, alcohol dehydrogenases (ADH) are metal-dependent oxidoreductases, particularly for zinc and iron (Moon et al., 2011), and both these metals are used to prepare the synthetic medium but not the complex medium. In addition, copper is another metal used to prepare the synthetic medium and it can be used as a transition metal for several families of enzymes as well as for the formation of periplasm protein in the cell membrane (Finney and O'Halloran, 2003). Consequently, the composition of the used synthetic medium might play a fundamental role in producing the elevated concentration of ethyl acetate.

8.9 Testing the performance of the mutant strain under anaerobic conditions

This study examines the shifting of metabolism of the mutant *Zymomonas* strain from the aerobic metabolism, which is favourable to accumulate acetaldehyde, to anaerobic metabolism, which is favourable to accumulate ethanol. The growing of the mutant strain under anaerobic conditions enriches and compliments the work under aerobic conditions.

The anaerobic conditions were achieved by sparging nitrogen-enriched microbubbles for less than 30 minutes at the beginning of the fermentation process and 15 minutes at the end of each day to remove any produced carbon dioxide and to maintain the anaerobic conditions. The lowest dissolved oxygen level achieved was 0.02 ppm at the end of the sparging course and the removal rate of dissolved oxygen was $0.6 \text{ mmol} \cdot \text{hr}^{-1}$ at 0.3 L/min flowrate of nitrogen, and this low dissolved oxygen concentration was maintained throughout the fermentation process (Figure 8.31).

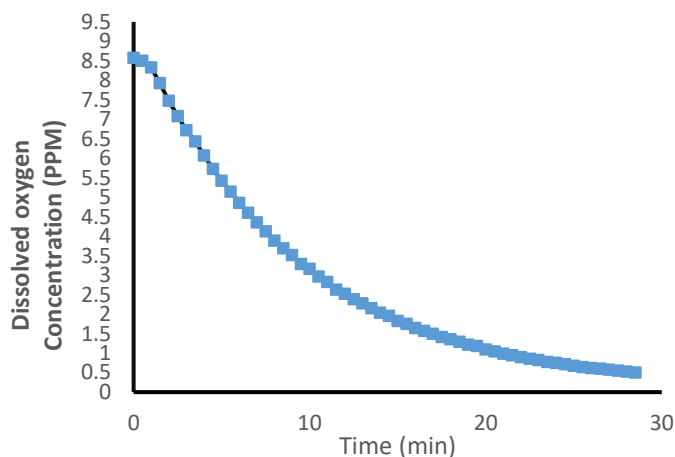


Figure 8.31: The dissolved oxygen profile in the fermentation broth during the sparging with nitrogen-enriched microbubble, showing the anaerobic conditions were maintained throughout the fermentation process. Points are representative of triplicate results.

Various parameters were monitored during the anaerobic fermentation, such as cell biomass, glucose concentration, and ethanol production. However, acetaldehyde was not detected in the fermentation broth under anaerobic conditions, as it is unlikely to accumulate in the fermentation broth at a detectable concentration under anaerobic conditions. The anaerobic fermentation process studied two glucose concentrations, 20 g/L and 40 g/L. It is worth mentioning that the anaerobic fermentation happened very intensively and bubbles (gaseous products) were generated from the fermentation activities, which rose within the reactor, creating a self-mixing inside the reactor, and ended up at the surface of the fermentation liquid. Although using a complex medium can provide greater biomass yields than a synthetic medium under anaerobic conditions, using a synthetic medium in physiological studies helps to focus on the metabolism and the regulation of the metabolic pathways, and the obtained data is easier to explain. As a result, a synthetic medium that supports both reasonable cell growth and products can be very useful in studies of gene regulation, protein expression, and metabolic fluxes. By systematically manipulating the components of the synthetic medium formulation, the specific nutritional and regulatory requirements for growth and targeted metabolic pathways can be determined. The unpredictability resulting from the complicated interactions among complex components and between the complex components and the products can also be minimised, or are at least easier to understand, and the cultivating environment is reproducible (Zhang et al., 2009).

8.9.1 Synthetic medium

Initially, a synthetic medium was used to conduct the fermentation process under anaerobic conditions in order to compare the mutant strain performance in both aerobic and anaerobic

conditions and to verify the original hypothesis, which stated that under anaerobic conditions acetaldehyde is unlikely to accumulate in the fermentation broth since all produced acetaldehyde is likely to be reduced to ethanol by alcohol dehydrogenase.

Table 8.2: Cell biomass concentration (OD), glucose concentration and ethanol concentration of the fermentation process with 20 g/L and 40 g/L glucose under anaerobic conditions. The readings are representative of triplicate results

Glucose concentration	Time (Hour)	Optical Density of Biomass at 600 nm (Absorbance)	Glucose Concentration (g/L)	Glucose consumption rate (mmol.g dry weight ⁻¹ .min ⁻¹)	Ethanol Concentration (mM) (error $\pm 1\%$)
20 g/l	0	0.476	20	0	0
	1	0.497	-	-	-
	2	0.746	8.45	0.034	16.93
	3	1.085	-	-	-
	4	1.444	6.6	0.069	96.39
	5	1.757	-	-	-
	6	2.042	4.96	0.034	227.42
	7	2.210	-	-	-
	8	2.329	0.807	0.004	286.15
	24	2.453	0.351	0.001	293.5
	25	2.408	-	-	-
	26	2.362	0.184	0.0009	288.76
27	2.297	0.137	0.0007	273.12	
40 g/l	0	0.640	40	0	0
	1	0.738	-	-	-
	2	0.910	15.260	0.119	19.64
	3	1.252	-	-	-
	4	1.596	13.140	0.123	92.16
	5	1.868	-	-	-
	6	2.081	12.660	0.169	202.01
	7	2.358	-	-	-
	8	4.120	10.250	0.093	357.57
	24	4.607	1.580	0.114	438.88
	25	4.57	-	0.116	-
	26	4.581	1.249	0.116	425.097
	27	4.54	-	-	-
	28	4.536	0.501	0.116	422.81
	29	4.426	-	-	-
30	4.321	0.35	0.116	405.66	

Both cell biomass and ethanol concentrations are proportionally related as the time of the anaerobic fermentation proceeded. On the other hand, the glucose concentration is inversely proportional to both cell biomass and ethanol concentrations (Table 8.2).

The highest optical density (OD) of biomass achieved was at 24 hours, while the highest ethanol concentration produced was 293.53 mM, and this was 67 % as a final yield. The final glucose concentration was 0.137 g/L at the end of the fermentation process (27 hours). The fermentation process reached its highest activity at 24 hrs, when both the biomass and ethanol concentrations hit their highest. Increasing the ethanol toxicity resulting from increasing its concentration and depleting the energy source (glucose concentration), can reduce the microbial activity within the fermentation process, leading the microbial culture to launch the death phase. Decreasing the ethanol concentration in the fermentation broth was a result of microbubble sparging as 15 minutes of nitrogen sparging was conducted at the beginning of the next day (after 24 hours), and some of the produced ethanol was stripped out the fermentation broth. In addition, the carbon dioxide was produced and collected during the fermentation process and its final carbon dioxide concentration was 2.05 mM.

Further, the glucose concentration was increased to 40 g/L and the results of cell biomass concentration, glucose concentration, and ethanol production are shown in Table 8.2. The overall fermentation time for the anaerobic conditions with 40 g/L glucose was 30 hours, compared to 27 hours in the previous experimental set.

The trend of cell biomass is similar to that with 20 g/L glucose and is inversely proportional to the glucose concentration, but it is proportional to the ethanol production. Increasing the carbon source (glucose) concentration from 20 g/L to 40g/L increases both the production of cell biomass and the ethanol concentration in the fermentation process.

The highest biomass concentration was reached at 24 hours, and at the same time the ethanol concentration hit its highest (438.88 mM), which was 50 % as a final yield, while the glucose concentration dropped to around 0.50 g/L at the end of the fermentation process. Carbon dioxide was produced and collected in this experimental set, and its concentration reached 3.47 mM, 41% more than the carbon dioxide produced in the 20 g/L glucose experimental set.

8.9.2 Complex medium

To test the performance of the mutant strain in the complex medium, a complex medium was used to conduct the fermentation process under anaerobic conditions. Ethanol is formed directly as the product of the energy generation and growth is normally the principal energy-requiring

process of the microbial cells. Therefore, this product (ethanol) is formed whenever there is growth within the fermentation process.

Firstly, 20 g/L glucose was supplied to the complex medium and used to conduct the fermentation process under anaerobic conditions. Table 8.3 summaries cell biomass, glucose and ethanol concentrations during the fermentation course.

Table 8.3: Cell biomass concentration (OD), glucose concentration and ethanol concentration of the fermentation process with 20 g/L and 40 g/L glucose supplied in complex medium under anaerobic conditions. The readings are representative of triplicate results.

Glucose concentration	Time (Hour)	Optical Density of Biomass at 600 nm (Absorbance)	Glucose Concentration (g/L)	Glucose consumption rate (mmol.g dry weight ⁻¹ .min ⁻¹)	Ethanol Concentration (mM) (error $\pm 1\%$)
20 g/L	0	0.22	20	0	0
	1	0.396	-		-
	2	0.817	6.16	0.35	33.86
	3	1.239	-		-
	4	1.43	4.54	0.22	132.87
	5	1.58	-		-
	6	2.48	4.2	0.17	285.93
	7	2.501	-		-
	8	2.54	1.82	0.12	297.87
	24	2.8	0.61	0.11	302.78
	25	2.93	-		-
	26	3.24	0.5	0.110	293.96
	27	3.36	-		-
	28	3.07	0.37	0.35	282.67
	29	3.08	-		-
30	3	0.35	0.22	293.96	
40 g/L	0	0.5	40	0	0
	1	0.56	-		-
	2	0.68	17.50	0.35	15.50
	3	0.91	-		-
	4	1.31	16.03	0.22	72.71
	5	1.784	-		-
	6	2.18	12.99	0.17	159.39
	7	2.808	-		-
	8	4.62	2.76	0.18	282.12
	24	4.668	-		-
	25	4.83	2.51	0.11	346.27
	26	4.82	-		-
	27	4.81	2.01	0.11	340.07

	28	4.78	-		-
	29	4.73	1.90	0.35	315.89

The overall duration of the fermentation process of complex medium supplied with 20 g/L glucose was 30 hours. The trend of biomass growth is inversely proportional to the glucose concentration, but it is proportional to the ethanol production; the general trends are similar with previous experimental sets.

The highest biomass concentration was reached at 27 hours but the ethanol concentration hit its highest (301.78 mM) at 24 hours, which was 69 % as a final yield, while the glucose concentration dropped to around 0.35 g/L. The ethanol yield using 20 g/L glucose in the complex medium was higher than its counterpart synthetic medium as well as the biomass concentration. However, the fermentation time in the complex medium was longer than the time in the synthetic medium for the same glucose concentration. Therefore, it can be concluded that the complex medium was more suitable to ethanol production from the mutant strain under anaerobic conditions with 20 g/L glucose concentration than the synthetic medium for the same glucose concentration and operational conditions. In addition, the collected carbon dioxide concentration was 4 mM, almost double of that produced in the synthetic medium for the same concentration of the used glucose.

The glucose concentration in the complex medium was then doubled, aiming to increase the produced ethanol. The overall fermentation time in this experimental set was 29 hours, compared to the 30 hours shown in the previous experimental set. As shown in all previous experimental sets under anaerobic conditions, the trend of cell biomass is inversely proportional to the glucose concentration, but it is proportional to the ethanol production. Both cell biomass and the concentration of ethanol at 40 g/L glucose were higher than the 20 g/L glucose supplied fermentation process. Therefore, increasing the carbon source (glucose) concentration from 20 g/L to 40 g/L also increases both the production of cell biomass and ethanol concentration in the fermentation process.

The highest biomass concentration achieved at 25 hours and at the same time; the ethanol concentration hit its highest (346.26 mM), which equals to 40 % as a final yield, while the glucose concentration was dropped to around 1.90 g/L at the end of the fermentation process. Interestingly, the ethanol yield produced in the complex medium supplied with 40 g/L glucose was less by 10 % than the ethanol produced in the synthetic medium supplied with the same glucose concentration. In contrast, the ethanol yield in the complex medium supplied with 20

g/L glucose was higher than its counterpart the synthetic medium for the same glucose concentration by 2 %. Finally, the collected carbon dioxide at the end of the fermentation process was 4.7 mM, and this was 35 % more carbon dioxide produced than the synthetic medium for the same glucose concentration and 17.5 % higher than the complex medium supplied with 20 g/L.

8.10 Conclusions

The performance of the wild type of *Zymomonas mobilis* under aerobic conditions and the production of acetaldehyde as a target product were investigated in chapter 7. To enhance the acetaldehyde production, a mutant *Zymomonas* strain was selected using increasing allyl alcohol concentrations up to 200 mM, which showed an elevated acetaldehyde accumulation in the fermentation broth. Two sparging strategies were used to supply oxygen, an initial sparging strategy, and a periodical sparging strategy. While the initially-sparged group suffered from oxygen starvation without any stripping activities, the bespoke periodical sparging strategy offered both enough oxygen supply and efficient stripping activities. Also, the periodically-sparged group showed an elevated biomass and acetaldehyde production with less ethanol in comparison with the initially-sparged group. Optimising the glucose concentration, however, switched the ethanol to acetaldehyde yields ratio from 1:75 to 1:78 when the glucose concentration was halved.

The mutant strain was also grown in the synthetic medium, and its performance was evaluated. In general, the performance of the mutant strain in the synthetic medium was not as good as in the complex medium, and the composition of the synthetic medium seems to have a major impact on this performance.

Interestingly, ethyl acetate was produced as a by-product in the synthetic fermentation broth by the mutant strain, and there is a good agreement that this product is likely produced by transferring the acetyl moiety from acetyl coenzyme A produced by pyruvate dehydrogenase complex to ethanol, providing a mechanism of self-detoxification of the ethanol accumulation. Curiously, the mutant strain is also grown under anaerobic conditions in both complex and synthetic media, and the metabolic pathways of this bacterium were directed to produce ethanol and carbon dioxide without any acetaldehyde detected in the fermentation broths. The growing of the mutant strain under anaerobic conditions enriches and compliments the work under aerobic conditions.

On the other hand, the mutant strain showed a weak biomass production and, to enhance the overall productivity of the fermentation process, an elevated biomass concentration needs to be

achieved. Chapter 9 explores various cultivating techniques to intensify the mutant strain growth.

Chapter 9

Intensification of the *Zymomonas* growth using various cultivating techniques: Bacterial Propagation

Overview

Zymomonas mobilis wild strain shows an increased biomass growth under aerobic conditions (Chapter 7). In contrast, 200 mM allyl alcohol selected mutant *Zymomonas mobilis* strain produces less biomass under aerobic conditions (Chapter 8). To enhance the biomass yield of the mutant strain, different techniques can be used to grow this bacterium aerobically, but maintaining sufficient oxygen concentration is a challenge in the bacterial propagation stage. Microbubbles are more efficient in mass transfer than larger bubbles due to their high surface area to volume ratio. The performance of the bespoke propagation unit equipped with a fluidic oscillator to generate microbubbles as well as traditional growing techniques such as stationary and shaking flask techniques are investigated. While the bacterial cells within traditional growing techniques suffer from oxygen limitation (and after that, shifting to a partial anaerobic state and anaerobic state), bacterial cells grown in microbubbles-dosed culture are kept distant from reaching to the oxygen-limited state. Oxygen is the limiting factor in the aerobically grown bacterial cultures, but similarly, the impact of mixing can be critical. The highest biomass yield was achieved using shaking flasks cultures for the mutant strain, while biomass yield reached its highest in microbubble-dosed culture for the wild strain. Also, a design and simulation study on the proposed propagation unit was also conducted for understanding both mass and flow aspects of this unit. The results of this study are crucial for bacterial-based industries such as biofuel, food, pharmaceutical industries for which the microbial biomass growth is premium.

9.1 Dissolved oxygen (DO) level

A- Stationary cultures

Figure 9.1 presents the profile of dissolved oxygen (DO) concentration in the stationary culture during the propagation stage. The oxygen concentration in the microbial culture decreased below the critical oxygen concentration (which was used as a 5-10 % of saturation concentration) about 40 minutes after inoculation (Figure 9.1). After 40 minutes, the DO concentration reached around 0.75 ppm, and the metabolism is started to switch to a partially anaerobic metabolism, and thereafter to anaerobic metabolism. Therefore, decreasing the dissolved oxygen concentration and changing the metabolism to the anaerobic growth would decrease the biomass yield (Zikmanis et al., 1999) and this what observed during measuring the biomass concentration. Under anaerobic conditions, the bacterial culture needs an extra time to

reach the same biomass concentration seen in the aerobically grown culture. In addition, using stationary culture causes microbial cells aggregation near the bottom of the flask with poor mixing, thereby a region above these crowded cells is rich in nutrients and oxygen, but not available to the cells and this would lead to the microbial starvation state (Bandyopadhyay and Humphrey, 1967). Under the starvation state, microbial cells become unable to sustain the normal state, the dynamic state (Roszak and Colwell 1987). Being in a dynamic state, microbial cells can be readily adapted to a range of environmental stresses using a wide variety of genotypic and phenotypic responses. For instance, enzymes synthesis rate can be regulated by an appropriate modification to take up growth-limiting nutrients, and uptake rates of nutrients available in excess can be modulated as well to face environmental stresses (Roszak and Colwell, 1987). These adaptive capabilities might account the ease with which microorganisms can respond to culture conditions in the laboratory as well as to their natural habits.

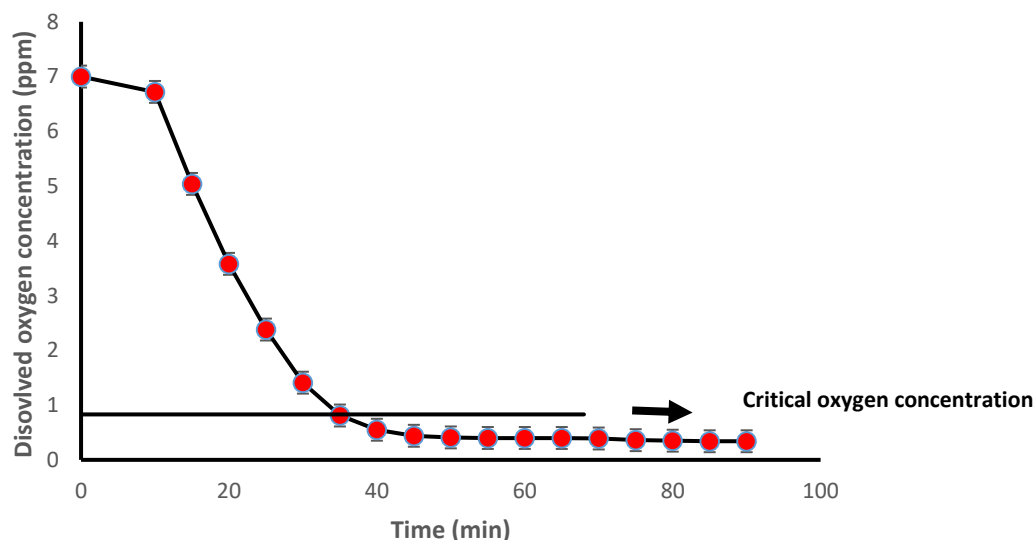


Figure 9.1: The profile of dissolved oxygen levels against time during stationary culture, whereby the concentration of dissolved oxygen dropped below the critical oxygen concentration after 40 mins. Error bars depict standard deviation.

B- Shaking flasks cultures

Figure 9.2 shows the dissolved oxygen concentration during the shaking flask culture in the propagation stage. The dissolved oxygen concentration was decreased gradually during the growth in the shaking culture, and it reached below the critical oxygen concentration (reached around 0.66 ppm) after just 200 minutes from the inoculation start (Figure 9.2). This decrease coincides with increasing the biomass concentration. Using the shaking strategy to grow microbial cells can achieve both aeration and mixing, which can result in better access to nutrients and increased mixing and more homogeneous cell distribution, encouraging the

microbial growth (Juergensmeyer et al., 2007). K_La in the shaking flask was calculated according to equation (3.23) and it found to be 0.45 hr^{-1} , while the oxygen transfer rate (OTR) was $0.002 \text{ mmol. g (dry weight)}^{-1} \cdot \text{hr}^{-1}$ according to equation (3.21) under 100 rpm shaking speed and at 30°C .

Clearly, using shaking flasks can achieve better aeration as well as mixing in comparison with the stationary culture. However, *Zymomonas* culture is still suffering from the oxygen limitation with shaking flasks strategy, and this problem becomes even worse with increasing the biomass concentration. The oxygen limitation can develop to partially anaerobic conditions, and after that to the anaerobic conditions. Therefore, even with the using of the shaking technique, another technique for oxygenation needs to be used to keep the microbial culture growing aerobically. Another option is to increase the shaking speed to achieve this purpose, but this option is not always applicable, depending on the container capacity and speed limitations of the shaking incubator. However, only one speed (100 rpm) was used in this study, which was mentioned in many studies related to the *Zymomonas* growing (Sootsuwan et al., 2013; Zhang et al., 2013 and Chou et al., 2015).

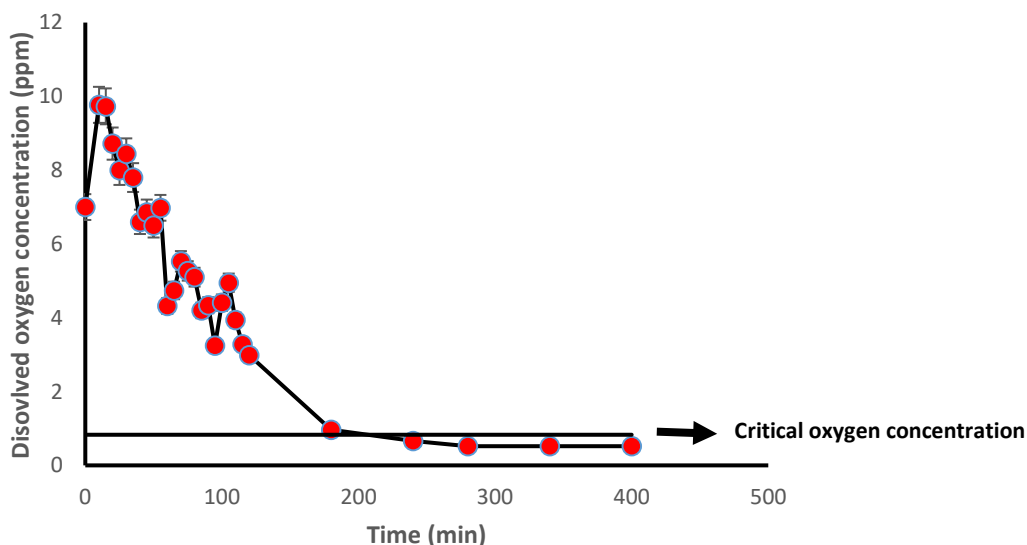


Figure 9.2: The profile of dissolved oxygen level against time during shaking flask culture, where the concentration of dissolved oxygen dropped below the critical oxygen level after 200 mins. Error bars depict standard deviation.

C- Microbubble-sparged cultures

Figure 9.3 shows the dissolved oxygen concentration in the microbubble-sparged culture during the propagation stage. the dissolved oxygen concentration was rapidly decreased in the airlift loop bioreactor (the proposed propagation unit), and reached to almost the critical oxygen

concentration after about half-hour (Figure 9.3). An oxygen-limited state can then be developed, where the biomass synthesis decreases in compared to the aerobic- grown biomass. To grow high cell density, *Zymomonas* culture needs to be kept growing aerobically (Zikmanis et al., 1999). Therefore, oxygen needs to be introduced periodically to the bulk of liquid using microbubbles, which rise slowly through the fermentation broth with its high surface area to volume ratio, allows efficient mass transfer to be achieved during the oxygenation process (Zimmerman et al., 2009). In addition, efficient mixing can maintain a balanced distribution of gaseous and cells within the reactor, minimizing the constraints of oxygen transfer to the culture medium and then to microbial cells (AL-Mashhadani et al., 2015).

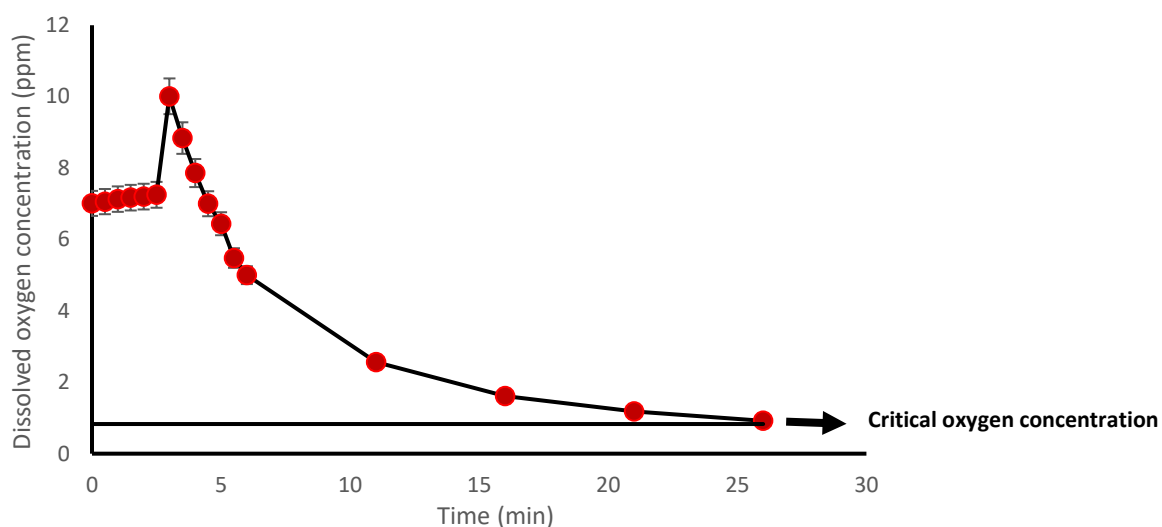


Figure 9.3: The profile of dissolved oxygen level against time during microbubbles-sparged culture, where the concentration of dissolved oxygen dropped below the critical oxygen level after 30 mins. Error bars depict standard deviation.

To avoid the oxygen limited state, oxygen was periodically introduced to the microbial culture to keep the dissolved oxygen concentration above the proposed critical oxygen concentration (Figure 9.4). An oxygen probe (SevenMulti™ dual meter pH/oxygen) was used to continuously monitor the oxygen concentration within the culture, and air-microbubbles were sparged to increase the oxygen concentration in the microbial culture until reaching to the equilibrium concentration when the air supply was turned off. A model for the periodical sparging strategy was developed to keep the oxygen concentration above the proposed critical oxygen concentration without the continuous sparging. The proposed model described the time needed to turn the air supply on until reaching to the equilibrium concentration and after that, turning off the gas supply. The periodical sparging strategy has many advantages over continuous sparging such as the periodical gas supply can reduce costs, wasted gas and energy used (Ying,

2013), and it also reduces the shear stress on the microbial cells and the foam formation (Smith, 2005).

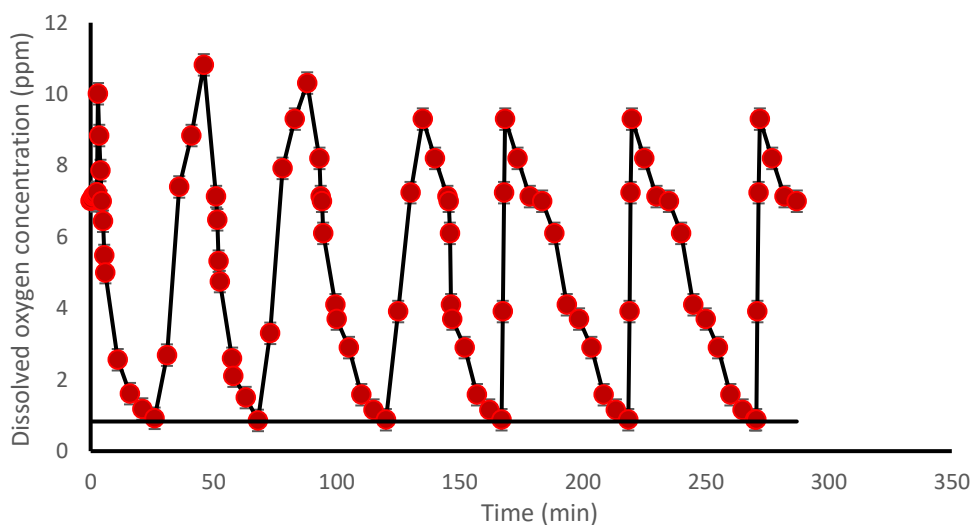


Figure 9.4: A model of periodical sparging strategy for the oxygenation process of the mutant strain of *Zymomonas* culture using microbubble technology, which describes the time needed to turn the air supply on and the time required to leave the culture before the next sparging course. Error bars depict standard deviation

In fact, the concentration of dissolved oxygen during the bacterial propagation depends on three main processes, which are the rate of oxygen transfer to the culture medium, the rate of oxygen transfer from the bulk medium to the bacterial cells and the rate of oxygen consumption by bacterial cells. However, the most important process from all three processes seems to be the dissolution of oxygen, considering the low dissolution of oxygen, which has been observed under traditional aeration systems. The calculated mass transfer coefficient $K_L a$ is presented in Figure 9.5 using the dynamic method.

Using microbubbles generated by the fluidic oscillator provided high surface area and long residence time, leading to increase the dissolved oxygen concentration. In addition, the aerobic conditions were maintained through the propagation period using the periodical sparging strategy.

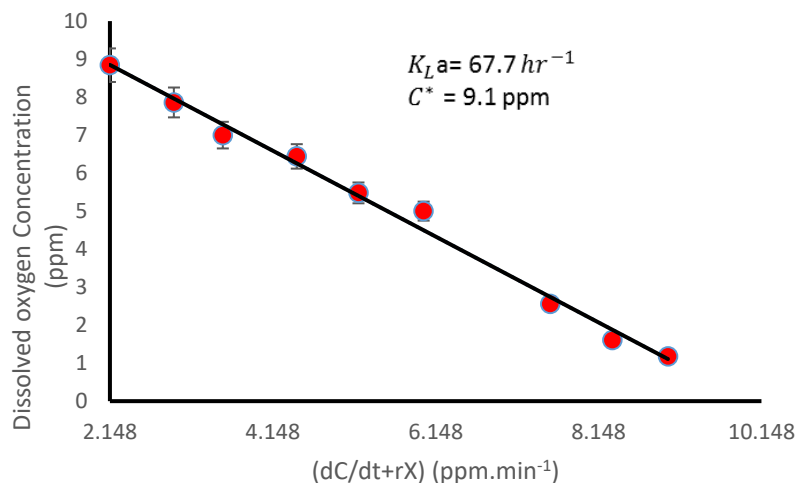


Figure 9.5: Calculation of the mass transfer coefficient and the equilibrium concentration. Error bars depict standard deviation.

The specific oxygen uptake rate was calculated to be $0.84 \text{ mmol. g (dry weight)}^{-1} \cdot \text{hr}^{-1}$. This rate is constant as long as the dissolved oxygen concentration is above the critical biological oxygen concentration when the microorganism has not been starved yet (Bandyopadhyay and Humphrey, 1967 and Doran 2013). The mass transfer coefficient was found to be 67.7 hr^{-1} using the dynamic method, while the oxygen equilibrium concentration was almost 9 ppm in the propagation culture. One of the most important features of this method is considering the oxygen transferred from microbubbles as well as the oxygen consumed by the growing bacterial cells as a dynamic parameter. Moreover, growing of *Zymomonas* cells aerobically can lead to accumulate less reduced metabolites such as acetaldehyde and acetate (Seo et al., 2005), and these metabolites can eventually inhibit the bacterial culture (Kalnenieks et al. 2000). Beneficially, microbubble sparging can effectively offset these toxic by-products and enhancing the biomass production during the propagation process.

Additionally, the oxygen mass transfer coefficient was also measured using the nitrogen de-gassing method (Figure 9.6). The rate of increase in the dissolved oxygen concentration is influenced by the aeration flowrate but equally, by the mixing effect in the airlift-loop bioreactor. The pressure-driven circulatory motion owing to the design is the main reason to use the airlift loop bioreactor in the biological processes in contrast to stirred tank reactors, which use impellers for mixing purposes, leading to consume a great deal of energy and limiting the total yield of the process.

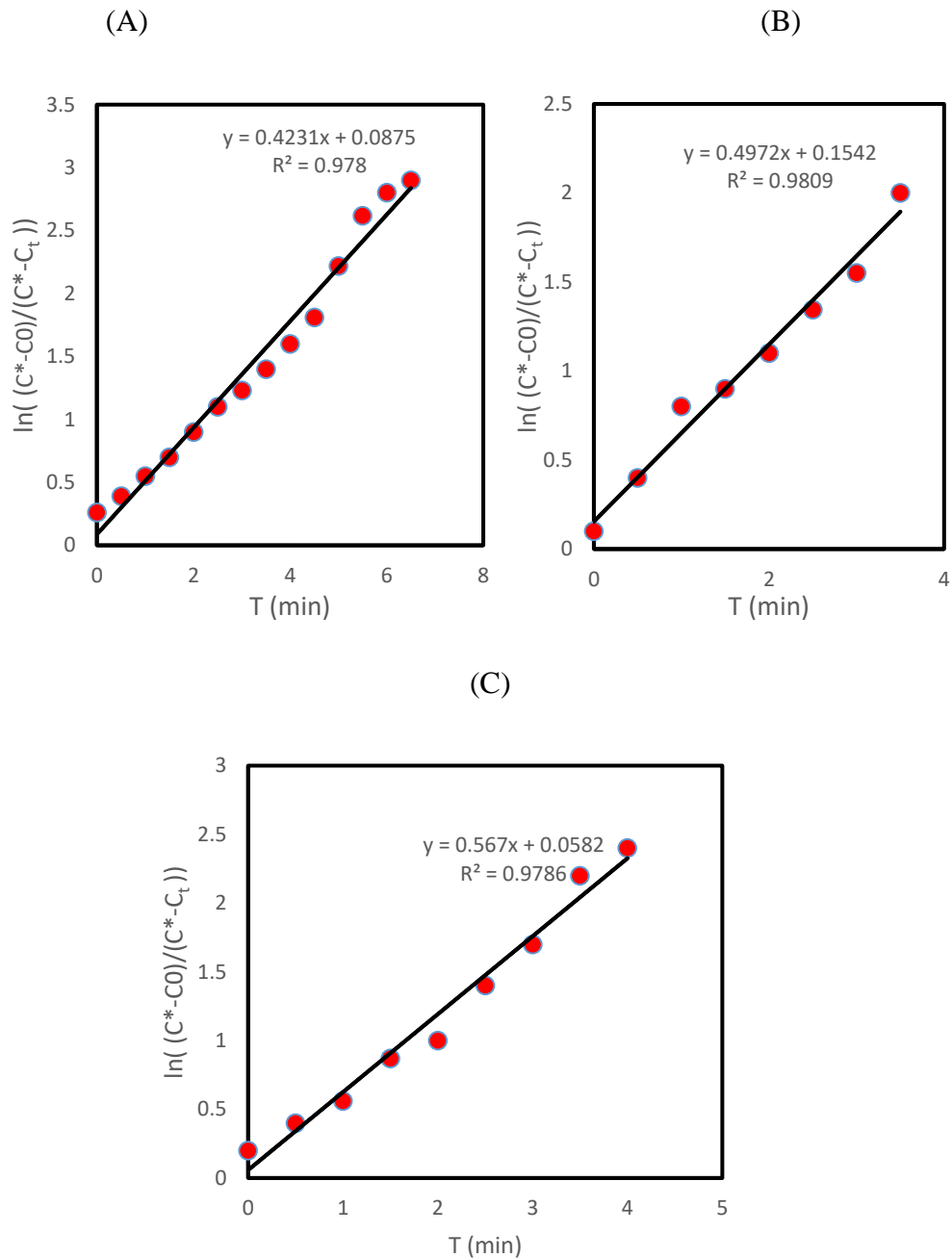


Figure 9.6: Mass transfer rate against time at different flowrates. Rate of oxygen transfer increased directly with the increase in flowrate (Q). (A) $Q = 0.1$ L/min ; $K_L a = 25.2$ hr⁻¹. (B) $Q = 0.3$ L/min ; $K_L a = 29.4$ hr⁻¹. (C) $Q = 0.5$ L/min; $K_L a = 33.6$ hr⁻¹.

9.2 Biomass concentration

Figure 9.7(A) presents results of the bacterial growth expressed as an optical density during the propagation stage using various cultivation techniques. Under different cultivation systems, the biomass growth is generated in a different pattern and reached its highest in the shaking flask cultures. On the other hand, the biomass growth in the microbubbles-sparged culture was higher than in the stationary culture, but lower than that in the shaking flask

culture. When oxygen is delivered to the growing cells, the acetaldehyde accumulation increases. The difference in the biomass growth may be attributed to differences in the level of acetaldehyde produced by these cultures when they are grown under various oxygen concentrations. The dissolved oxygen concentration in the shaking flask culture decreased below the proposed critical oxygen concentration (Figure 9.2), and this oxygen limitation reduces the accumulated acetaldehyde. In contrast, the microbubbles-sparged culture was regularly oxygenated by the periodical sparging strategy and thus; the oxygen concentration kept above the critical oxygen concentration, where acetaldehyde preferentially accumulates. Regarding the stationary culture, the oxygen concentration in the culture medium decreased below the critical oxygen concentration after just 40 minutes from the beginning of the inoculation and thus, *Zymomonas* cells spent very short time growing under aerobic conditions before shifting to the anaerobic conditions. Consequently, ethanol preferentially accumulates within the stationary culture with very limited acetaldehyde if it exists at all. Figure 9.7 (B) shows the specific growth rates of this bacterial strain under different cultivation systems. The mutant *Zymomonas* strain showed its highest growth rate, more than 0.5 hr^{-1} , in the shaking flasks system in comparison with other culture systems, when it was grown at 0.3 hr^{-1} and at 0.4 hr^{-1} in stationary and microbubble-sparged cultural systems respectively.

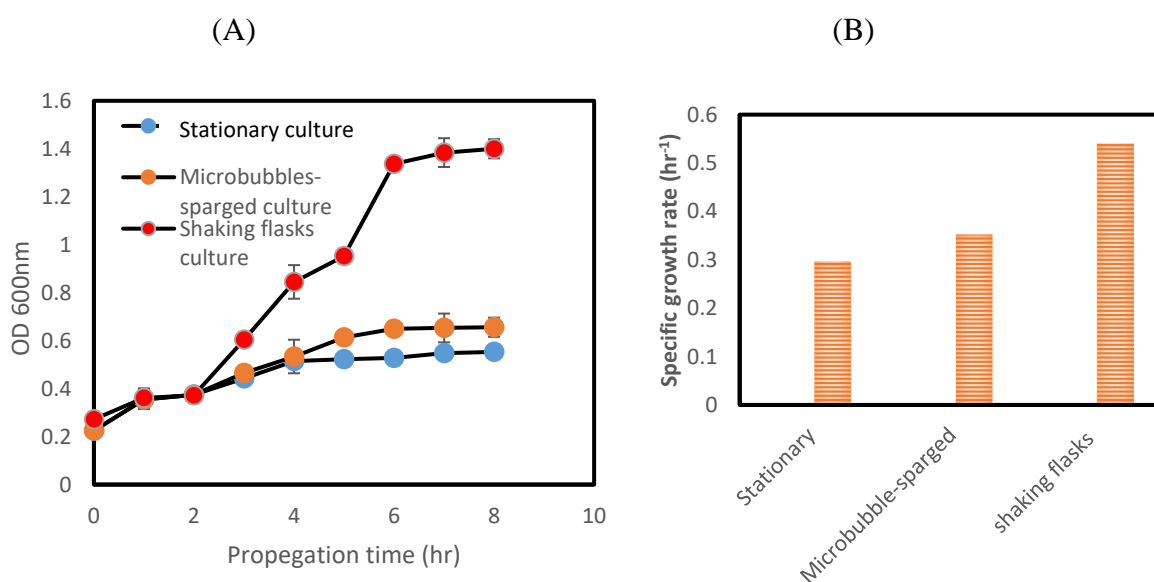


Figure 9.7: (A) The biomass concentration of the mutant strain of *Zymomonas mobilis* against time, where a variation in the growth patterns seen in different cultivation systems. (B) specific growth rates of the mutant strain within various cultivation systems. Error bars depict standard deviation.

The biomass growth of the wild strain of *Zymomonas mobilis* ZM4 was also tested under all three-cultivation systems, stationary, shaking flasks and microbubble-sparged cultural systems (Figure 9.8A).

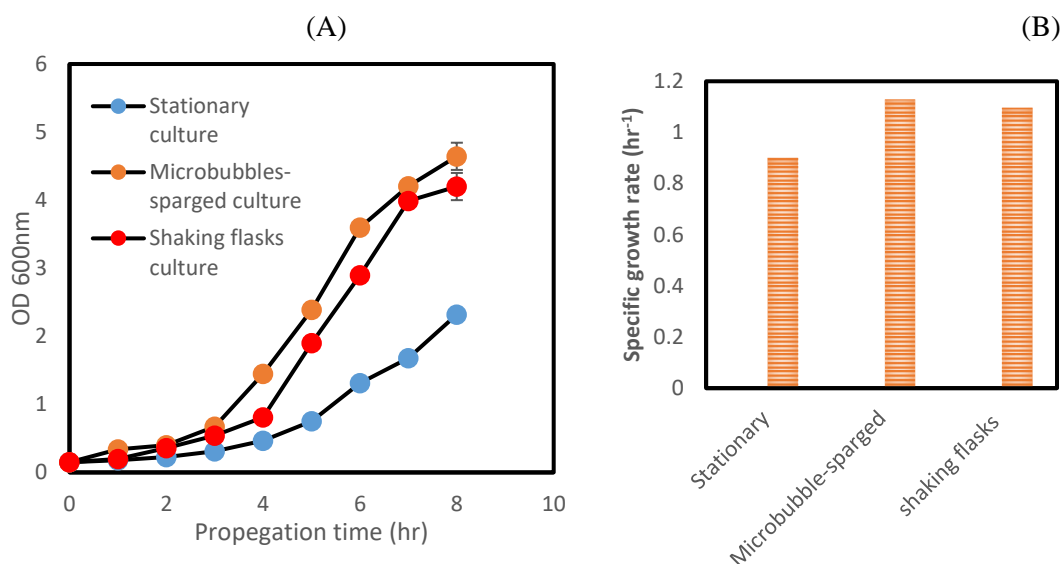


Figure 9.8: (A) The biomass concentration of the wild strain of *Zymomonas mobilis* ZM4 against time, whereby the wild type shows its highest growth in the microbubble-dosed system. (B) Specific growth rates within various cultivation systems. Error bars depict standard deviation.

The wild strain of *Zymomonas* has achieved its highest biomass growth within the microbubble-sparged system, while the lowest biomass growth was occurred in the stationary culture. The biomass growth of the wild strain differs from its counterpart the mutant strain in their growth, and the wild strain was preferentially grown in the microbubble-sparged culture with 733 % more biomass produced with almost double specific growth rate in comparison with the mutant strain (Figure 9.8B). In addition, the shaking flasks culture was also shown high biomass growth, but it was less than the biomass produced in the microbubble-sparged system. The same differences in the growth between the wild and the mutant strains of *Zymomonas mobilis* were reported previously by Wecker and Zall, (1987). In addition, the wild strain produced very limited acetaldehyde under aerobic conditions in comparison with the mutant strain as the latter strain was selected for its decreased alcohol dehydrogenase activity and consequently, an increased amount of acetaldehyde is likely to be accumulated in the culture medium. Therefore, the limited amount of produced acetaldehyde by the wild strain can be readily removed by sparging microbubbles and subsequently, *Zymomonas* cells are unlikely to be inhibited by the

acetaldehyde accumulation. In contrast, the shaking flasks technique provides mixing with inefficient aeration (Figure 9.2).

9.3 Design and simulation of a propagation unit for *Zymomonas mobilis*

To optimise both the operational conditions and the design of the propagation unit, flow and mass transfer models within the propagation unit are studied. An airlift loop bioreactor-based propagation unit was used. Critical design parameters for the propagation unit were considered taking into account the study done by Al-mashhadani et al., (2015). Al-Mashhadani et al., (2015) studied the flow modelling of only one flow rate and the focus was given to study the effect of different bubble sizes without mass transfer modelling. Both flow modelling and mass transfer modelling of the propagation unit, however, are investigated in the current project. 150 μm -air microbubbles were introduced at the bottom of the propagation unit, which operates at 30°C and pH 5.5, at different flowrates, 0.1, 0.3 and 0.5 L/min until reaching the steady state. The liquid circulation (mixing) resulted from the introduction of microbubbles concurrent with the mass transfer achieved by microbubbles to efficiently maintain the oxygen concentration in the cultivation medium above the critical oxygen concentration was fundamentally explored. No antifoam was used in the current study and the used mass transfer coefficient (K_{La}) was measured experimentally in figure 9.6. The configuration of the propagation unit as follows: The radius of microbubble diffuser is 0.025 m. A draft tube is fitted inside the reactor with 0.035 m radius and 0.12 m height and it is based 0.02 m from the bottom of the reactor and 0.02 m from the headspace. The overall height of propagation unit, however, is 0.16 m and 0.0625 m radius. Figure 9.9 shows the 3D configuration of the bespoke propagation unit along with the meshing.

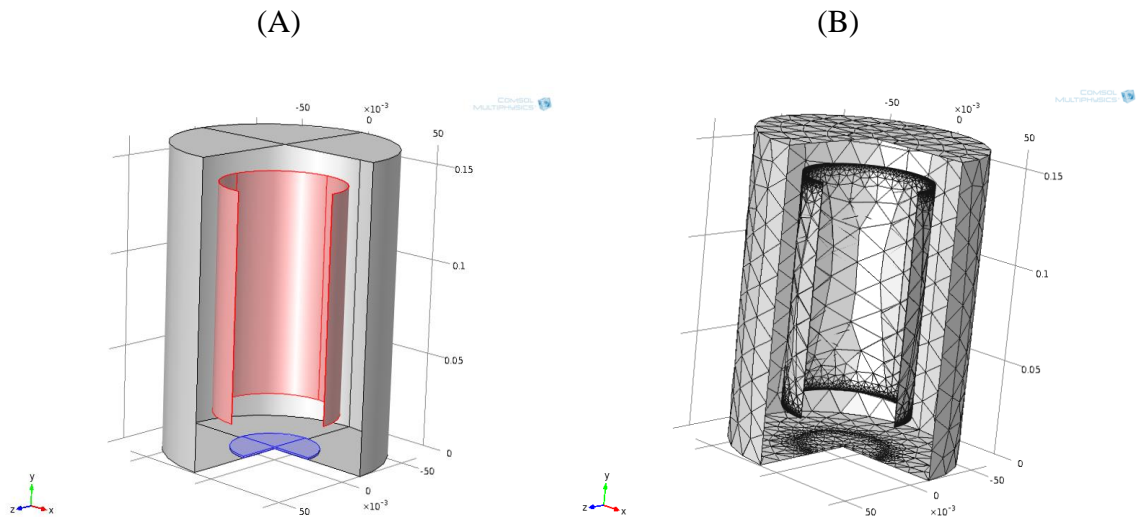


Figure 9.9: Illustration and drawing of the propagation unit. (A) The fully assembled propagation unit. (B) Computational domain and mesh for the investigated propagation unit (Mesh-independent solutions were obtained with 7171 tetrahedral elements).

To streamline the computation, a 2-D model was considered. The axial symmetry of the unit allowed reduction of the computational domain to one fourth of the geometry. Figure 9.10 shows the 2D axisymmetric configuration used in the current study to model the flow and mass transfer of the bespoke propagation unit.

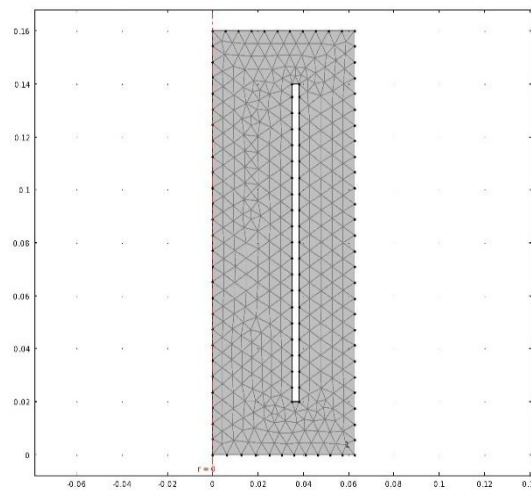


Figure 9.10: 2D axisymmetric domain used along with the meshing of the propagation region within the unit.

9.3.1 Computational modelling

The effect of gas flowrate on the liquid circulation in the propagation unit was investigated using numerical simulations. The experimental results show that using 0.1 L/min flowrate

preferably produces more biomass without the need to add any antifoam. Therefore, the oxygen concentration within the propagation unit using 0.1 L/min flowrate was explored with the mass transfer modelling. These computations provided system and operating parameters most suitable for conducting the propagation of bacteria using the bespoke propagation unit.

9.3.2 Computational geometry

The computational domain consists of the inlet channel, propagation unit chamber, draft tube and a section above the draft tube as shown in Figure 9.10. The main purpose of this simulation is to find out the flow distribution and the distribution of oxygen within the propagation unit, hence all the suitable operating conditions can be used.

9.3.3 Governing equations

Comsol Multiphysics was used to carry out the simulation study on the propagation unit that shown in Figure 9.10. This model was calculated according to following equation:

$$\phi_l \rho_l \frac{\partial u_l}{\partial t} + \phi_l \rho_l u_l \cdot \nabla u_l = -\nabla P + \nabla \cdot [\phi_l \eta_l (\nabla u_l + \nabla u_l^T)] + \phi_l \rho_l g \quad (\text{Eq. 9.1})$$

Where ρ_l is the density of liquid (kg/m^3), ϕ_l is the liquid volume fraction (m^3/m^3), u_l is the velocity of liquid phase (m/s), P is the pressure (Pa), t is the time (sec), η_l is the dynamic viscosity of liquid phase (Pa.s) and g is the gravity (m/s^2).

For low gas concentrations, the liquid holdup coefficient (ϕ_l) is approximately one. Therefore, the change in ϕ_l can be neglected in the conservation equation (Eq. 9.2) (Bired et al., 1960), which simplifies to the common condition for divergence of free velocity fields in incompressible flow (Eq. 9.3):

$$\frac{\partial \phi_l}{\partial t} + \nabla \cdot (\phi_l u_l) = 0 \quad (\text{Eq. 9.2})$$

$$\nabla \cdot u_l = 0 \quad (\text{Eq. 9.3})$$

The momentum transport equation for the gas phase is illustrated as follows:

$$\frac{\partial \rho_g \phi_g}{\partial t} + \nabla \cdot (\phi_g \rho_g u_g) = -m_{gl} \quad (\text{Eq. 9.4})$$

Where ρ_g is the density of gas phase (kg/m^3), ϕ_g is the gas volume fraction (m^3/m^3), u_g is the velocity of gas and $-m_{gl}$ is the mass transfer rate ($\text{kg/m}^3/\text{s}$).

The initial modelling approach was carried out with no mass transfer between gas and liquid phases, to illustrate the fluidic dynamics in isolation. Thus, the $m_{gl} = 0$. Therefore, the continuity equation can be arranged for two phases (e.g. gas and liquid) but without mass-transfer terms as follows:

$$\frac{\partial \rho_g \phi_g}{\partial t} + \nabla \cdot (\phi_g \rho_g u_g) = 0 \quad (\text{Eq. 9.5})$$

The ideal gas law was used to calculate the density of gas (ρ_g):

$$\rho_g = \frac{P M_w}{RT} \quad (\text{Eq. 9.6})$$

Where M_w is the molecular weight of the gas bubble, R is the ideal gas constant (8.314 J/mol/K) and T is the temperature of gas (K).

The gas volume fraction is estimated by the following equation:

$$\phi_g = 1 - \phi_l \quad (\text{Eq. 9.7})$$

The gas velocity can be determined as $u_g = u_l + u_{slip}$, since u_{slip} is the relative velocity between two-phases (gas and liquid).

Pressure-drag balance, which obtained from the slip model, was used to calculate the u_{slip} . The assumption of this model suggests that there is a balance between viscous drag and pressure forces on the gas microbubble:

$$\frac{3Cd}{4d_b} \rho_l |u_{slip}| u_{slip} = -\nabla P \quad (\text{Eq. 9.8})$$

Where Cd is the viscous drag coefficient (dimensionless), d_b is bubble diameter (m), because the microbubble diameter used in the simulation is equal or less than 150 μm , the Hadamard-Rybczynski drag law was used, and hence:

$$Cd = \frac{16}{Re_b} \quad (\text{Eq. 9.9})$$

Where:

$$Re_b = \frac{d_b \rho_l |u_{slip}|}{\eta_l} \quad (\text{Eq. 9.10})$$

Where Re_b is the Reynolds number.

In the second modelling development, the study assumed that there is a mass transfer taken place between two phases; therefore, the dilute species transport model was used for this diluted system using the convective diffusion reaction equation according to following equation:

$$\frac{\partial c_i}{\partial t} + \mathbf{u} \cdot \nabla c_i = \nabla \cdot D_i \nabla c_i + R_i \quad (\text{Eq. 9.11})$$

Where c_i is the concentration of specie I (mol/L), \mathbf{u} is the velocity, D_i is the diffusion coefficient and R_i is the rate of reaction.

9.3.4 Boundary conditions

Since the two-dimensional axial – symmetry simplification was used to model the propagation unit in the current study, the boundary condition at $r=0$ must be zero flux in all dependent variables. On the draft tube and internal airlift and bioreactor walls, there was no slip ($u = 0$) for liquid phase, whilst no gas flux values were used for the gas bubble phase, hence the values of u_l and $n(u_g \phi_g)$ equal to zero. On the other hand, the “gas outlet” and the slip ($n \cdot u = 0$) BCs were used at the top of liquid phase for both liquid and gas phases respectively. The pressure point constraint of the upper right corner equals to zero. On the top of the diffuser, no slip boundary conditions were used for liquid phase and the “gas flux” boundary conditions for the gas phase.

9.3.5 Numerical method

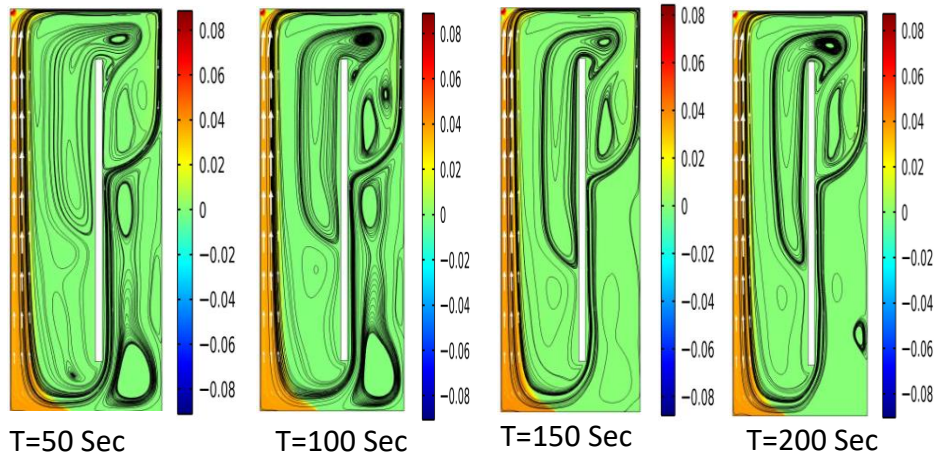
The problem was solved using a commercial finite element code - Comsol Multiphysics™ 5.2. Mesh-independent solutions were obtained with 738 tetrahedral elements and the simulation time for each case was approximately 120 minutes on an Intel Core i5 64-bit 2.7 GHz processor.

9.3.6 Flow modeling of the propagation unit

Figure 9.11 shows the distribution of gas volume fraction and the liquid velocity at different flow rates, 0.1 L/min, 0.3 L/min and 0.5 L/min for 200 seconds after reaching the steady state, and at bubble diameter 150 μm , which was measured experimentally. This time is increasing with decreasing the bubble size, and it reaches to 900 seconds when 50 μm was used (Al-Mashhadani et al., 2015).

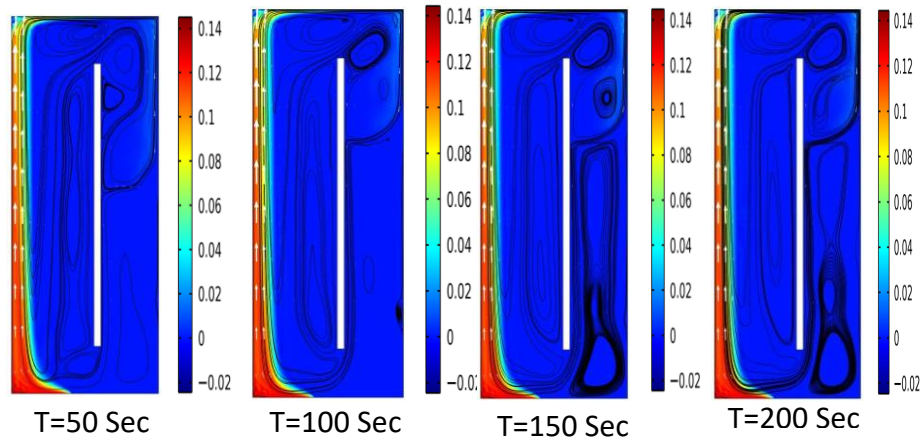
(A)

Surface: Volume fraction, gas phase
Streamline: Velocity field, liquid phase m^2/s
Arrow: Velocity field, liquid phase



(B)

Surface: Volume fraction, gas phase
Streamline: Velocity field, liquid phase m^2/s
Arrow: Velocity field, liquid phase



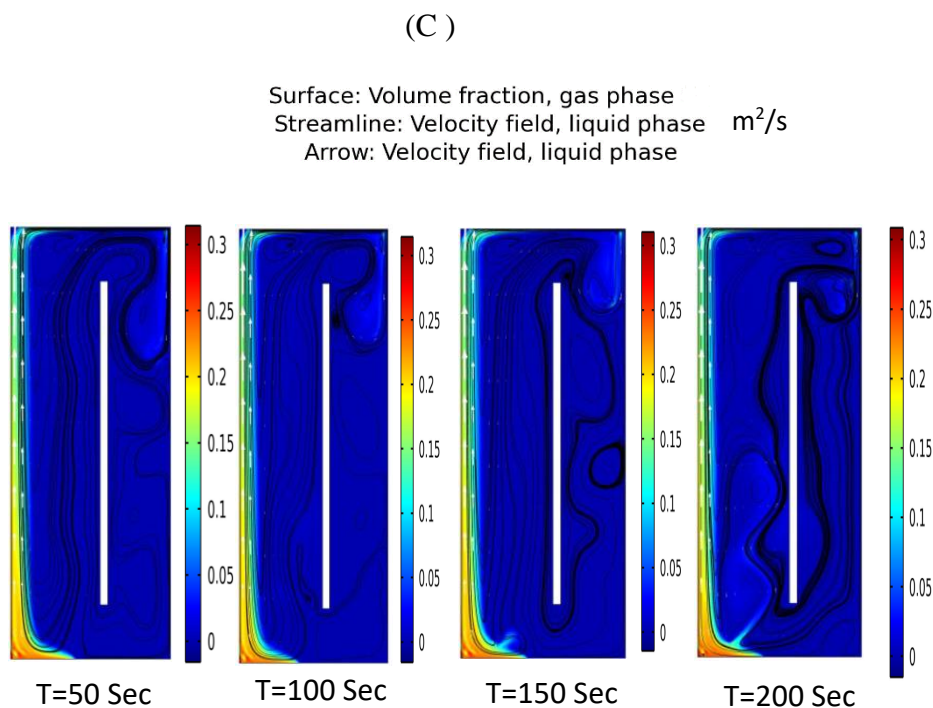


Figure 9.11: Snapshots of gas fraction at different flowrates after steady state with $150 \mu\text{m}$ bubble diameter, where a small fraction of the gas can be seen in the downcomer of the 0.1 L/min flowrate with no eddy currents. (A) At 0.1 L/min (B) At 0.3 L/min (C) At 0.5 L/min .

Apparently, the gas bubbles are not present in the downcomer region for both 0.3 L/min and 0.5 L/min flowrates, while a small fraction of gas bubbles is recirculated in the downcomer of 0.1 L/min sparged reactor (Figure 9.11). Therefore, both mass and heat transfers for 0.3 L/min and 0.5 L/min are restricted to the riser region of the reactor (Figure 9.11), while these transfer phenomena can be taken place in downcomer region for 0.1 L/min flowrate as well as the riser region but to much lesser extent (Figures 9.11 and 12). The downcomer region is equivalent to 44 % of the total working volume of the used reactor, and thus, both mass and heat transfer can happen in both regions, and this helps the system to perform better when 0.1 L/min is used. Liquid circulation in both 0.3 L/min and 0.5 L/min is unable to overcome the tremendous buoyancy of the gas bubbles and thus; it is unable to circulate these bubbles in the downcomer, while it does with 0.1 L/min . The presence of these gas bubbles in the downcomer region allows mass transfer to occur in this region, and gas recirculation as microbubbles in 0.1 L/min flowrate increases the liquid circulation velocity and therefore, it gives the potential for better mixing. As mentioned above, 0.1 L/min is used in the current study to test the biomass productivity of the proposed propagation unit, which is chosen according to the modelling results. The experimental validation of the differences between these flowrates is challenging since the microbial culture overflows from the reactor

when 0.3 L/min and 0.5 L/min flowrates are used. To oppose overflowing, an antifoam agent needs to be added and this can adversely affect the mass transfer within the system as it enhances the bubbles coalescence, giving larger bubbles and vigorous vibration in the reactor (Al-Masry, 1999). Indeed, increasing the flowrate can increase the bubble coalescence (bigger bubbles), which can cause a substantial turbulence and developing eddy currents within the reactor (Kim et al., 2016). This observation can be seen in the snapshots of both 0.3 L/min and 0.5 L/min flowrates (Figure 9.11B and C). This turbulence is increased by increasing the flowrate (Davies et al., 1986), which can stress the microbial cells and encourage them to form biofilms in the reactor (Pereira et al., 2002). These biofilms are three-dimensional aggregations of interacting unicellular microorganisms. It must be noted that the cell concentration is low at the beginning of the propagation stage and thus; the competition between these cells for the nutritional resources is minor. Therefore, single cells have better access to these resources than cells in the aggregates and the cells in the aggregates interior in particular (Kragh et al., 2016). As a result, single cells are fitter than aggregated cells to grow in the propagation unit.

In contrast, the aggregated cells have a fitness advantage over single cells when the competition for resources is high. Consequently, production of single cells in the propagation unit when there is a low competition on the nutritional resources, has a fitness advantage over the aggregated cells, which has a net growth disadvantage because of the limited access of nutrients to the aggregate interior (Kragh et al., 2016).

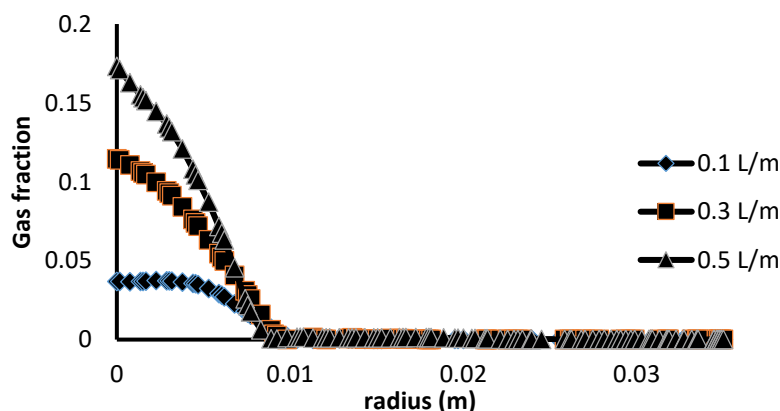


Figure 9.12: The gas fraction in a cross section of riser region at three different flowrates, 0.1, 0.3 and 0.5 L/min, where the gas fraction is proportionate to the air flowrate.

9.3.7 Mass transfer modelling of the proposed propagation unit

From the flow modelling study, it is clear that using 0.1 L/min offers both good mixing and adequate oxygen supply without using antifoam agents, which can affect the performance of

the whole system. Consequently, a mass transfer model was built up using 0.1 L/min flow rate and the mass transfer coefficient (K_{La}), which was measured experimentally in Figure 9.6. Figure 9.13 shows the oxygen concentration profiles in both the riser and downcomer regions during the sparging course for 30 seconds at 0.1 L/min.

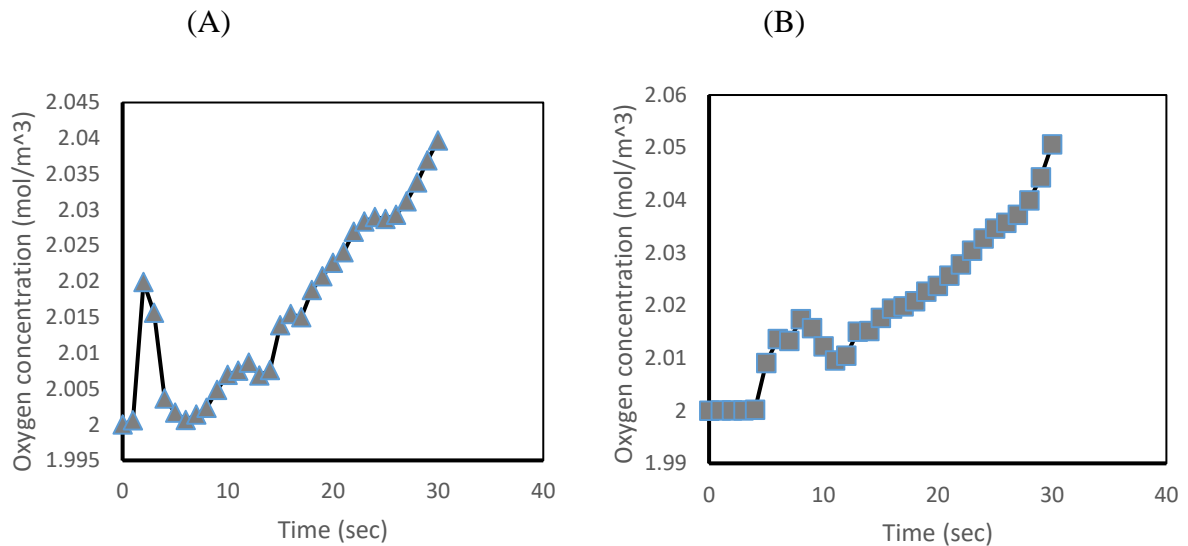


Figure 9.13: Oxygen concentration profiles in the propagation unit at flowrate 0.1 L/min, where is a gradual increase in the oxygen concentration in both regions. (A) in the riser region (B) in the downcomer region.

It can be observed from Figure 9.13 that there is a gradual increase in the oxygen concentration in both riser and downcomer regions during the air sparging. However, the oxygen concentration in the riser concentration was instantly increased at the beginning of the sparging course in comparison with the downcomer region, where the oxygen concentration started to increase after few seconds. These results can be explained by the fact that the mass phenomenon is mainly taken place in the riser region, which represents 56 % of the total working volume of the used propagation unit and to less extent in the downcomer region. Figure 9.14 shows snapshots of oxygen concentration profiles during the sparging course at 0.1 L/min flowrate.

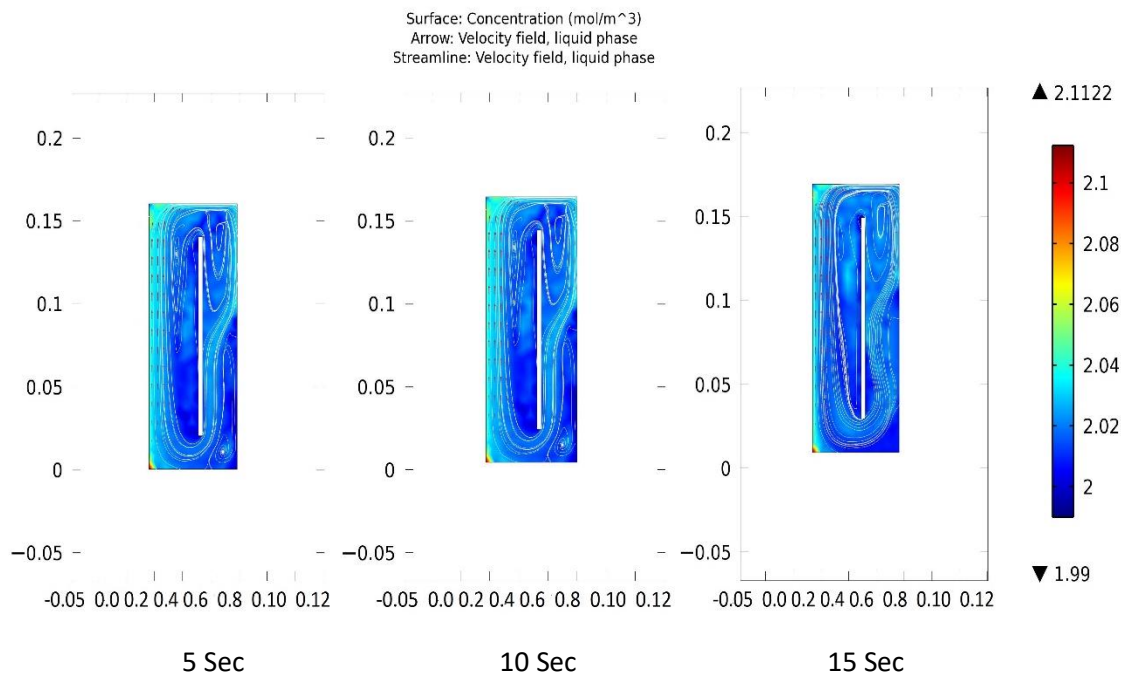


Figure 9.14: Snapshots of oxygen concentration at different times after steady state with 150 μm bubble diameter and 0.1 L/min.

It can be observed from Figure 9.14 that the oxygen concentration is increasing gradually within the propagation unit and the oxygen concentration distributes homogeneously within the whole system. This result is crucial as it ensures that the oxygen concentration in the downcomer region (represents 44 % of the total working volume) and the riser region (represents 56 % of the total working volume) is almost the same. This means that the microbial cells within the propagation unit are exposed to uniform concentrations of oxygen. Certainly, using the current propagation unit avoids the localized oxygen depletion, which might have a significant impact on the physiology of the microbial culture (Konz et al., 1998). On the other hand, exposure to elevated oxygen concentrations may stress the microbial cells as some detrimental products, such as superoxide (O_2^-) and hydrogen peroxide (H_2O_2), can be accumulated as byproducts of the elevated aerobic metabolism (Baez and Shiloach, 2014). These products are toxic to microorganisms since they are more reactive than the molecular oxygen (Imlay, 2013), and they might promote metabolic changes, protein oxidation, DNA oxidation and plasmid replication (Konz et al., 1998). Therefore, providing an adequate oxygen supply is vital to the growth, leading to avoid harmful effects of both high and low oxygen concentrations. Table 9.1 shows a summary of the objectives, predictions and learning outcomes of the modelling approach.

Table 9.1: A summary of the objectives, predictions and learning outcomes of flow and mass modelling developed in the current study

	Objectives	Predictions	Learning outcomes
Flow modelling approach	Choosing the best flow rate to conduct the propagation stage	-Using 0.3 l/min and 0.5 l/min flowrates provide higher liquid velocity than 0.1 l/min	Using 0.1 l/min flowrate can achieve good liquid velocity without the need to add antifoam agents to oppose overflowing.
	Avoiding overflowing	-Both mass and heat transfer are restricted to the riser region but they are also taken place in the downcomer region with 0.1 l/min	With 0.1 l/min flowrate, mass transfer can take place in both riser and downcomer regions and therefore, more biomass can be produced.
	Avoiding dead zones	No dead zones were seen with all flowrates used in the current study.	
	Reduce turbulence in the propagation unit	Neither turbulence nor eddy currents are developed in the propagation unit.	
Mass modelling approach	Study mixing inside the propagation unit.	A good mixing can be achieved using 0.1 l/min	Microbial cells within the propagation unit are exposed to uniform concentration of oxygen and thus, more biomass can be produced.
	Monitoring the oxygen concentration within the unit	Uniform oxygen distribution can be achieved using 0.1 l/min.	

9.4 Effect of the inoculum size on the fermentation process

Initial conditions such as the inoculum size, can determine the productivity of the fermentation process (Webb and Kamat, 1993). Both quality and quantity of the inoculum influences the type and yields of the fermentation process. In this study, the inoculum volume was (10% v/v), to be transferred to the fermentation broth. Using this inoculum volume was based on both experimental observations and the study conducted by Sivamani et al., (2015), who studied the effect of inoculum size on the ethanol production by *Z.mobilis*. According to the Sivamani, et.al (2015) study, the inoculum size was varied from 5 to 15% (v/v) and the ethanol production was altered significantly by increasing the inoculum size, and the best ethanol yield was achieved

by using the 10 % (v/v) inoculum size. Interestingly, using the same inoculum volume does not mean that it has the same bacterial concentration as the bacterial growth tends to be varied with each cultural set due to various reasons such as the state of inoculum culture, the inoculum size of the original culture and other unidentified physiological factors.

All inoculum preparations were conducted according to Saharkhiz et al., (2013), whereby the inoculum of the mutant strain was activated in Glucose standard medium (2% GSM) and then it was allowed growing for 18 hours at 30°C and pH 5.5 under shaking flasks technique. Thereafter, 5-15% (v/v) inoculum sizes were used to inoculate the fermentation medium and the increase in the turbidity was monitored at 600 nm during the experimental duration. Figure 9.15 shows biomass synthesis trends in different experimental sets, which were started at different inoculum concentrations. In general, inoculum size influences both the fermentation time and the fermentation performance. Faster fermentation is observed when high inoculum concentration (15% v/v) was used, when the highest biomass synthesis was noticed after 5 hrs and the bacterial culture then launched the stationary phase (Figure 9.15). The stationary phase can be very long as the carbon source is still present in excess with low concentrations of inhibitory compounds. Ethanol and acetaldehyde are formed directly as end or by-products of the energy generation, and the growth is normally the principal energy requiring process of the microbial cells. Therefore, these products will be formed whenever there is growth within the fermentation process (Doran, 2013). Due to the low biomass synthesis when high inoculum concentration used, low bioproducts (ethanol and acetaldehyde) concentrations were produced in the fermentation medium.

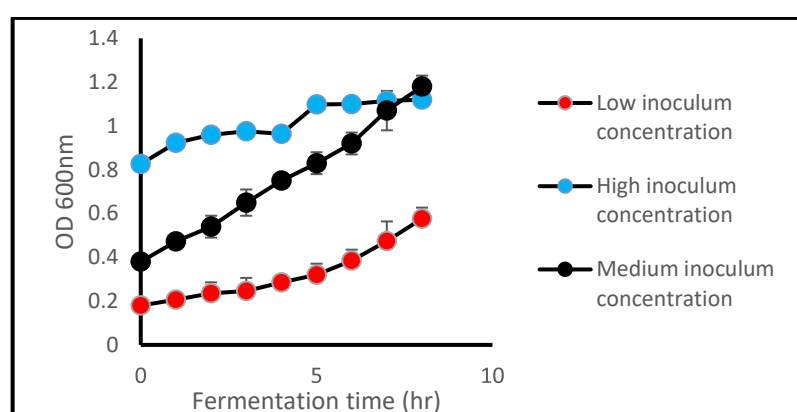


Figure 9.15: Biomass synthesis trends at different inoculum concentrations. Using high inoculum size generated low biomass with limited ethanol, while low and middle inoculum sizes generated elevated concentration of biomass as well as ethanol and acetaldehyde. Error bars depict standard deviations.

Indeed, a trace amount of ethanol was detected in the fermentation broth, while no acetaldehyde was detected in the cultural broth when the high inoculum size used (Figure 9.16).

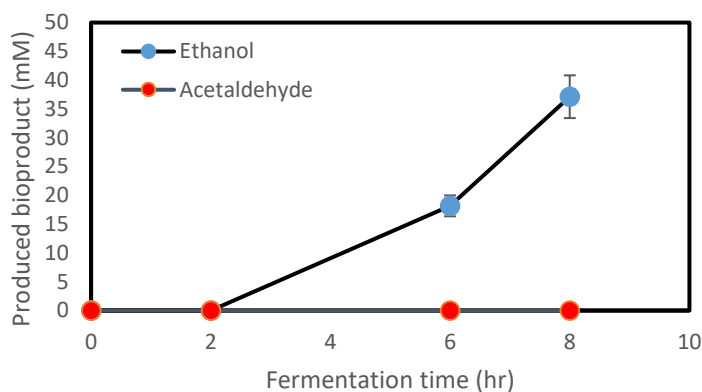


Figure 9.16: Ethanol and acetaldehyde production at high inoculum concentration, whereby it can be seen that only limited amount of ethanol produced in the fermentation broth without acetaldehyde. Error bars depict standard deviations.

In contrast, the biomass synthesis was very slow (Figure 9.15), and it just started launching the exponential phase after 8 hrs when a low inoculum concentration (5% v/v) was used. In addition, the mutant strain did not reach the stationary phase after 8 hrs from the fermentation beginning. This slow growth is combined with low ethanol and acetaldehyde productions. Interestingly, the ethanol concentration was doubled when the low inoculum concentration was used in comparison with the high inoculum concentration, while the acetaldehyde concentration reached 12 mM at hour eighth (Figure 9.17). The reason behind the detection of acetaldehyde after 8 hrs is that this chemical tends to diffuse poorly across the plasma membrane compared to ethanol, leading to its intracellular accumulation as the accumulated intracellular acetaldehyde concentration can build up to several times than the extracellular concentration (Aranda and del Olmo, 2003). A third inoculum concentration (10% v/v) was chosen as a middle choice between the above two concentrations, and the initial inoculum concentration increased to around 0.4 (OD 600), and this is double the used low inoculum concentration and half the used high inoculum concentration. The bacterial culture grown with this inoculum concentration showed an accelerated growth trend without exhibiting Lag or stationary phases during the fermentation time (8 hrs).

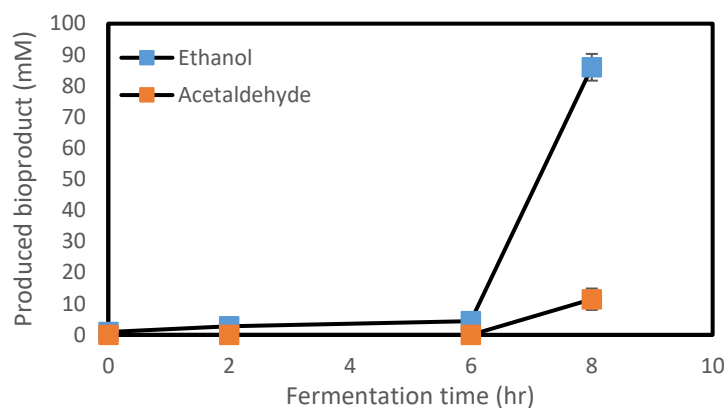


Figure 9.17: Ethanol and acetaldehyde productions at low inoculum concentration. Error bars depict standard deviation.

Both produced ethanol and acetaldehyde were doubled with this culture, but the acetaldehyde production was fluctuated (Figure 9.18). The reason behind this fluctuation is that the strategy used to supply oxygen to the bacterial culture is the periodically sparging strategy, which has been developed during this study and used to grow the mutant strain and to strip out acetaldehyde from the fermentation broth.

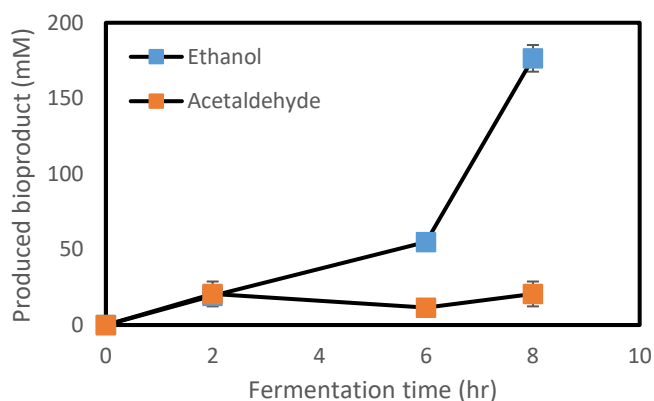


Figure 9.18: Ethanol and acetaldehyde productions at medium inoculum concentration. Error bars depict standard deviation.

The microbial biomass with middle inoculum size (10 v/v) is started to grow almost immediately after the inoculation and it continued to grow, reaching higher concentration than other groups, even the one used high inoculum concentration.

To sum up, the acetaldehyde and ethanol productions are directly related to growing of the microbial cells. Using high inoculum concentration can speed up the fermentation process to reach the stationary phase without acetaldehyde production and with limited ethanol production. On the other hand, low growth trend can be seen in the culture, which inoculated with low inoculum concentration. Preferentially, using the suitable inoculum concentration is

crucial, and it can improve the biomass growth and consequently, acetaldehyde, and ethanol productions can surge.

9.5 Conclusions

Chapter 7 and 8 were tested the performance of wild and mutant strains under aerobic conditions. While the mutant strain shows elevated acetaldehyde and carbon dioxide productions, this strain shows a reduced biomass yield. To enhance the biomass synthesis, various propagation techniques are explored. To compare between different propagation techniques, two conventional growing techniques were investigated with a novel microbubble-based propagation technique. Microbubble-based propagation process is an alternative technique, which can be used to grow bacteria generally, and to grow the bacterial inoculum for bacterial based industries.

Oxygen is a vital factor for the bacterial growth, and its limitation has a severe implication on the microbial growth. While bacteria grown under the traditional cultivation techniques suffer from the oxygen limitation, the microbubble-based technique can keep the aerobic conditions as well as provides a proper mixing. The results show that the dissolved oxygen concentration drops below the critical oxygen concentration after 40, 200 and 30 mins, for stationary, shaking flask and microbubble techniques respectively; however, the last technique can be readily adapted to work periodically, leading to maintaining the oxygen concentration above the critical oxygen concentration throughout the fermentation process. Both oxygen uptake rate and mass transfer coefficient are substantial increased using the microbubbles technology and there were 41-fold and 150-fold increases in the oxygen uptake rate and mass transfer coefficient respectively in the microbubbles-dosed system in comparison with the shaking flask system. Using the periodically sparging strategy can achieve a better mixing during the propagation stage. Regarding the biomass yield, the mutant strain shows an increased biomass generation in shaking flasks technique (around 100 % and 133 %increase) in comparison with other (microbubbles-dosed and stationary respectively) techniques, while the wild strain produces more biomass in the microbubble-based technique (around 50 % and 100 %) than other (shaking flask and stationary respectively) techniques. Importantly, flow and mass transfer models are built and used to design and optimise the designed propagation unit.

Chapter 10

Conclusions and Future Perspective

This chapter presents the main findings and conclusions of this research study and the future perspective for further research works based on the obtained results. The main findings are chapter specific and might be in their respective chapters. Herein, an attempt is made to sum up these findings to address/answer the original research questions.

10.1 General Conclusions

The study was set out to use lignocellulosic biomass as a substrate to obtain the sugary content, which can be fed to the fermentation process. Three main objectives are addressed in the current study, which are using microbubble mediated and microbubble mediated ozonolysis technologies in pretreatment of lignocellulosic biomass (wheat straw) in combination with cellulolytic bacterium *Pseudomonas Putida* KT2440 as a biological pretreatment agent in the first upstream stage of the supply chain. The second objective is to inactivate the pretreatment slurry with carbon dioxide enriched microbubble in the midstream stage and to avoid any overlapping with the next stage. Finally, fermentation integrated with microbubble technology to strip out some bioproducts from the fermentation broth is the third objective and the downstream stage.

The literature review in *Chapter 2* starts with a detailed analysis of lignocellulosic biomass and their chemical and morphological characteristics. Subsequently, a review of the pretreatment techniques showed that four groups of pretreatment approaches exist for lignocellulosic biomass, which mechanical, physiochemical, chemical and biological pretreatment. However, most these methods are energy intensive and use a variety of chemicals, which are toxic, hazardous and corrosive that added more costs to the downstream processes (Dussán et al., 2014). Also, biological methods use commercial enzymes, which are expensive and require keeping optimum and this will add a complexity to any industrial process. From the review, key examples of the pretreatment technologies were outlined such as steam explosion, acid hydrolysis and ozonolysis and subsequently, reviewed in detail. Of key importance however, are the disadvantages mentioned of these pretreatment techniques. Some of the main examples include: high energy consuming, increased pretreatment time, using expensive enzymes combinations and unsuitability for continuous large-scale production (Sukumaran et al., 2005). Owing to these shortcomings, the review revealed an industrial need for alternative techniques as a solution.

Following the pretreatment methodologies, a critical review of the fundamentals of inactivation processes was undertaken, highlighting the relevant and most applied processes. Each inactivation method focused on a different pertinent issue governing the inactivation, which generally underpinned the importance of inactivating and decreasing the number of microbial population. In addition, the processes emphasized the importance of both pressure and temperature and concluded that supercritical carbon dioxide trigs disturbance or damage the balance of the biological system of cells and subsequently, inactivates the microbial cells (Garcia-Gonzalez et al., 2007).

The chapter further presented *Zymomonas mobilis*, as a potent fermentative bacterium. From the review, it was apparent that the success of acetaldehyde production is intrinsically linked with keeping the aerobic conditions, while shifting to anaerobic conditions leads to accumulate more ethanol (Kalnenieks et al., 2000 and Kalnenieks et al., 2006). Acetaldehyde is a substrate for fuels production and its can be separated efficiently from the fermentation broth with low energy consumption. On the other hand, ethanol separation is an energy intensive process and it can account for more than half the energy consumed by the ethanol production process. Thus, the fermentation process needs to be kept aerobic and different techniques can be used to provide oxygen as well as to strip out the acetaldehyde and carbon dioxide from the fermentation medium.

The chapter closes by introducing microbubbles and their general characteristics, which are central to the *in-situ* separation and oxygenation processes. Also, a review of the fundamentals of Airlift Loop Bioreactor (ALB) was undertaken highlighting the relevant and most applied features. A critical review of the fluidic oscillator (an alternative bubble generating device) and its main features was presented with highlighting of the promise of energy efficiency. Particularly, the study highlights the mode of operation and previous applications of the fluidic oscillator and potential of the microbubbles generated by this system to meet the challenges of traditional aeration and separation systems.

The experimental materials and methods were presented in **Chapter3**. The chapter was structured into four key parts. The first section dealt with the pretreatment of wheat straw with microbubble-mediated technology combined with the biological pretreatment. Also, this section reported the characterisation of *Pseudomonas putida* cellulolytic activity. In addition, the first section dealt with exploiting ozonolysis-microbe synergy for biomass processing with more detail about the ozone generating method.

In second section, the methodologies of inactivation combined cell lysis of *Pseudomonas putida* at low pressure were mentioned. The survivor ratio of the treated bacterial population using pure carbon dioxide and carbon dioxide plus additives were calculated. pHs of the bacterial culture during the carbon dioxide sparging course were monitored and used to work out the carbon dioxide concentration.

In third section, the fermentation process with *Zymomonas mobilis* integrated with *in situ* separation using microbubble technology was presented. Both oxygen providing strategies and oxygen consumption rates were explored. Also, glucose consumption and products formation were monitored and subsequently, both the microbubble sparging duration and glucose concentration were manipulated.

In this section, a mutant of *Zymomonas mobilis* was selected using elevating allyl alcohol concentrations. Sparging duration was manipulated to meet the oxygen demand as well as stripping the elevated acetaldehyde concentration out the fermentation broth.

In the fourth section, the attention was drawn towards intensification of the bacterial biomass using various cultivating techniques. A promising new cultivating technique was developed using microbubble technology to enhance the oxygenation and mixing processes during the propagation stage and subsequently, increasing the biomass concentration. Also, another important aspect was the comparison between different cultivating techniques and the steps taken in designing and modelling of both flow and mass transfer of the proposed propagation unit were clearly outlined.

The first experimental results were presented in **Chapter 4**. The chapter explored the exploiting of microbubble-microbe synergy for biomass pretreatment. Sub-100 μm bubbles were largely used in the microbubble-mediated part and thereafter, the treated biomass was used as a substrate to the next biological pretreatment with *Pseudomonas putida*. Sub-100 μm Microbubbles generate free radicals that attacked and disintegrated biomass lignin, making cellulose more accessible for hydrolysis. Further pretreatment with *Pseudomonas putida* enhanced the glucose yield. The synergy between microbubbles and microbes in biomass processing offers some prospective benefits as a pretreatment technique for biofuel production. A new, relatively cheap pre-treatment option that works at ambient temperatures was presented. This chapter is the first part of the upstream stage.

In **Chapter 5**, the study further explored ozonolysis-microbe synergy for biomass pretreatment. Ozone is a strong oxidative agent that reacts with lignin by attacking the carbon-carbon double bonds (Sakai and Uprichard, 1991), while *P. putida* preferentially hydrolyses the exposed

cellulolytic parts of the biomass to simple sugars. Traditionally, the ozonation processes are mass transfer limited with confined interfacial area and this reduces the efficacy of the pretreatment process (Sakai and Uprichard, 1991). However, microbubbles used to introduce ozone to the bulk of liquid and these bubbles have high surface area to volume ratio with higher driving force in terms of mass transfer to the solution. It was found that pH 3 and 8.87 mg/L ozone are fitness conditions to conduct the ozonation process. The pretreatment efficacy increases coincidentally with the ozonation duration and After 24 h of ozonation combined with biological pretreatment, however, 85% of the cellulose in straw was degraded.

The above two chapters concluded that the traditional pretreatment methodologies such as dilute acid hydrolysis (Dussán et al., 2014), are energy intensive and using hazardous chemicals such sulfuric acid at high temperature, while microbubble-mediated and microbubble-mediated ozonolysis are less energy intensive and performed at room temperature and pressure without producing toxic residues that can affect the subsequent fermentation process.

The results of the investigations on the performance of carbon dioxide enriched microbubbles for bacterial inactivation were presented and discussed in **Chapter 6**. Carbon dioxide enriched microbubbles is a technology developed during this study to inactivate combined with cell lysis of *Pseudomonas putida* cells. After biological pretreatment of the lignocellulosic biomass, the pretreatment slurry needs to be inactivated and traditionally, the inactivated processes need high temperature and pressure and these extreme conditions might caramelize the sugary yield from the upstream pretreatment method as well as consuming high energy. Alternatively, carbon dioxide enriched microbubble technology can achieve the inactivation process at room temperature and pressure without compromising on product quality and the total yield. In addition, this technology uses carbon dioxide, which is a by-product from the fermentation process and using it in this midstream stage is advantageous option. While, using carbon dioxide enriched microbubbles achieved around 2-Log reduction in the bacterial population of *Pseudomonas putida* after 1.30 hrs of treatment, addition of ethanol to the inactivation solution enhanced the inactivation process to achieve 3, 2.5 and 3.5-Log reduction for 2 %, 5 % and 10 % (v/v) ethanol respectively. Furthermore, using acetic acid as an additive decreased the survivor ratio of *Pseudomonas cells* to more than 2.5-Log reduction.

In **Chapter 7**, fermentation process of *Zymomonas mobilis* integrated with *in situ* separation using microbubble technology was reported. After feeding the fermentation broth to the fermentation vessel, the fermentation process can be started at 30 °C and pH 5.5. The aim of the

fermentation process is to enhance the production of acetaldehyde preferentially from *Zymomonas mobilis*, while both carbon dioxide and ethanol are also produced during the fermentation process. Wild type strain tends to accumulate ethanol with much less acetaldehyde (Kalnenieks et al., 2000). Conventionally, oxygenation and gas stripping are conducted by inefficient aeration techniques such as air distribution by an in-line cotton filter, which tend to generate millimetre to centimetre-bubbles with limited surface area to volume ratio, leading to inefficacious aeration and products stripping out (Zimmerman et al., 2009). Using microbubble technology, however, can substantially improve both the oxygenation and the stripping processes, leading to provide sufficient oxygen to the bacterial culture and to remove some of the by-products (the inhibitors) from the fermentation broth and that can enhance the microbial growth without compromising with the process yield. The results showed that ethanol yield reached 70 % in the initially sparged group in comparison with 45 % in the periodically sparged group. Acetaldehyde yield achieved about 1 % and 0.5 % in the periodically sparged group and the initially sparged group respectively. Additionally, biomass yield was maximized in the periodically sparged group and reached 110 %, while its yield in the initially sparged group was around 90 %.

In **Chapter 8**, the study explored the fermentation process of a mutant of *Zymomonas mobilis* integrated with *in situ* separation using microbubble technology. The mutant strain (Or adapted strain) of *Zymomonas mobilis* was selected using increasing allyl alcohol concentrations and shown to have higher acetaldehyde productions. Having generated microbubbles and obtained the optimum operating conditions from the previous chapter, the conditions were used for *in situ* separation of acetaldehyde and carbon dioxide from the fermentation broth. However, the sparging duration was extended to 24 mins to strip out the elevated level of acetaldehyde. The result from the selected strain showed that the ethanol yield reached about 20 %, the acetaldehyde yield was built up to 35 % under the periodically sparging group. In contrast, the ethanol yield reached up to 25 % and acetaldehyde yield hit 10 % in the initially sparged group. Regarding the biomass yield, the selected strain flourished in the periodically sparged group and its yield reached almost 50 % in comparison to around 35 % under anaerobic conditions (The initially sparged group). Under the 20 g/L glucose concentration, the selected strain reached almost 30 % of the acetaldehyde yield and more than 15 % of the ethanol yield, while the biomass yields reached 70 % and 50 % for the periodical sparged group and the initially sparged group respectively. Fruitfully, the ethanol to acetaldehyde yields ratio was 1:75 using

40 g/L glucose, while this ratio was switched to 1:1.87 (ethanol to acetaldehyde yields) when 20 g/L glucose was used.

In **Chapter 9**, the study explored the intensification of *Zymomonas* biomass growth using various cultivating techniques. Traditionally, bacterial propagation is achieved using techniques such as stationary culture or shaking flask culture (Sivamani, et al., 2015), and these cultivating techniques are useful if the mixing and oxygen supply are less important than the nutritional requirements and incubation conditions for instance, temperature, pressure etc, as these cultivating techniques suffer from oxygen limitation and thereafter, shifting to a partial anaerobic state and the anaerobic state. Also, there is no convective mixing taken place in the stationary cultivating technique, while sufficient mixing occurs in the shaking flask technique. Microorganisms such as *Zymomonas mobilis*, however, are heavily reliant on the oxygenation conditions (aerobic or anaerobic) in their growth and propagation. Under aerobic conditions, *Zymomonas mobilis* shows an increased growth yield in comparison with the growth yield under anaerobic conditions, and this bacterium is also required to be shaken during the propagation stage to keep a homogeneous cell distribution, and this can encourage microbial growth. The performance of an airlift-loop bioreactor equipped with fluidic oscillator generated microbubbles in bacterial propagation was investigated and discussed in this chapter. Bacterial cells in microbubbles-dosed culture were kept growing under aerobic conditions but similarly, they were kept well mixed.

The chapter closes by conducting a design and simulation study on the proposed propagation unit to show the advantages of having a microbubble-based propagation technique.

10.2 Future works and perspective

Results from this study have shown the advantages of integrating fluidic oscillator driven microbubbles generation in various stages of the current project. Following the findings from this work, there are several areas requiring further investigations, which can be sum up in the following sections:

10.2.1 Lignocellulosic biomass pretreatment

Owing to the fact that this research work was limited to wheat straw, it is recommended for future study, to investigate other lignocellulosic biomass such as agricultural residues (corn stove and bagasse) and herbaceous crops (alfalfa, switchgrass), and also it can be extended to municipal and industrial wastes, to improve our understanding of the system robustness and versatility. It is also important to conduct comprehensive study on the energy consumption

aspect of microbubble-mediated technologies and draw comparisons with traditional pretreatment methods.

Owing to the results obtained from the microbubble-microbe synergetic approach that shown application of microbubbles and *Pseudomonas putida* for the pretreatment of lignocellulosic biomass has improved the hydrolysis of the biomass, showing both physical and chemical changes and the consequent production of glucose. To improve the commercial viability of the pretreatment technique, therefore, further work is necessary for understanding the key physicochemical and biochemical mechanisms underpinning the technique and exploring options to improve glucose yield. One option is to increase the surface area of microbubbles by further decreasing bubble size (Li et al., 2009a) as cellulose is a composite material with the surface structure of 3-5 nm size (George and Sabapathi, 2015). The extent of surface damage can vary depending on the bubble surface charge magnitude, bubble size and particle size and carrier gas (Li et al., 2009b). Dosing charge-laden microbubbles can play a crucial role in the catalysis and cleavage of organic compounds, facilitating the release of sugar from the biomass (Mulakhudair et al., 2016).

The application of microbubble mediated ozonolysis for the higher biomass concentration should be explored in the future works. Also, this study is limited of pretreatment lignocellulosic biomass under acidic and neutral pHs and thus, it is recommended to investigate the ozonation process under alkaline conditions.

The efficacy of the ozonation process depends on the diffusion coefficient of ozone, which is dependent on the gas-liquid contact time and interfacial area (Sakai and Uprichard, 1991). This rate relies, however, on diffusion rate of ozone in an aqueous solution (Sakai and Uprichard, 1991). Traditional ozonation processes are mass transfer limited. To enhance the mass transfer, ozone should be introduced to the bulk of liquid as microbubbles with high surface area to volume ratio (Kuvshinov et al., 2014). The low-rise velocity of microbubbles and high surface to volume ratio can ensure efficient mass transfer (Zimmerman et al., 2009). Microbubbles allow higher driving force in terms of mass transfer in the solution (Zimmerman et al., 2009 and Kuvshinov et al., 2014).

Given the high glucose concentration used in fermentation processes, increasing both the feedstock concentration and capacity is worth exploring. Due to the intensification of fermentation by microbubble-microbe synergy and pretreatment of lignocellulosic feedstocks

by microbubbles, releasing glucose more effectively, there is great potential to exploit these processes industrially.

Investigating the performance of various species of cellulolytic microbes such as fungi, bacteria, yeast and gut cellulolytic organisms would make a valuable contribution to the biological pretreatment method and it might be a good replacement to the commercial enzymes (Behera et al., 2017). Also, insertion of the cellulolytic genes in the commercially valuable microbes such as yeast, would be valuable as the microbial biomass growth is coincidentally produced during the biological pretreatment method (Chang et al., 2012).

10.2.2 Inactivation of the microbial pretreatment agent

Owing to the role played by cellulolytic microbe in the biological pretreatment method, future works should explore to enhance the effectiveness of carbon dioxide enriched microbubbles to inactivate the cellulolytic microbes. Also, it would be interesting to study the inactivation effect on an extended range of microorganisms such as fungi, yeast and algae; however, there are some indications that carbon dioxide enriched microbubbles can disrupt the algal cell membrane and this might help to release lipids for biodiesel production such as the study done by Kamaroddin et al., (2016).

Also, the connection of this process with the previous pretreatment method should be explored to create a simultaneous process for both lignocellulosic biomass pretreatment and inactivation of the cellulolytic pretreatment agent.

10.2.3 Fermentation integrated with *in situ* separation by microbubble technology

Owing to the fact that this research work was limited to wild strain of *Zymomonas mobilis* and a selected mutant, it is recommended for future study, to investigate the acetaldehyde production from genetically modified strains to improve acetaldehyde production. there are several genetic modifications interesting to explore for their acetaldehyde production, which are being explored in collaboration with Prof. Uldis Kalnenieks and Dr. Katherine Pappas as a part of ongoing ERA-IB grant such as:

B- Deletion of Alcohol dehydrogenase gene(s)

The most straightforward way to stop the ethanol accumulation is by a knockout mutation of the alcohol dehydrogenase gene (*adh*), yielding a mutant which preferentially accumulates acetaldehyde and the later product can be stripped out using the microbubble technology.

A- Over expression of NADH dehydrogenase (*ndh*)

Z.mobilis respiratory chain competes with alcohol dehydrogenases as both reactions use reducing equivalents NAD (P) H as a cofactor. Respiratory chain consumption of NAD (P) H

limits the reduction of acetaldehyde to ethanol and thus; more acetaldehyde tends to be accumulated. Owing to the fact that this research work was limited to enhance the oxygenation process and selecting a mutant with decreased or attenuated alcohol dehydrogenase activity in spite of the ethanol yield is still elevated. One way to rerouting the flux of reducing equivalent from alcohol dehydrogenase reaction towards respiration chain is by overexpressing the NADH dehydrogenase (*ndh*) gene in the *Zymomonas mobilis* selected strain and this can accelerate the fermentative catabolism of this bacterium by increasing the glucose consumption rate. Coincidentally, all the accumulated acetaldehyde can be efficiently removed using microbubble technology.

C- Enhance the diffusibility of acetaldehyde through the cytoplasmic membrane

Acetaldehyde tends to diffuse poorly across the plasma membrane compared to ethanol, leading to its intracellular accumulation. This compound is a polar molecule because it has unbonded electrons on the O atom and acetaldehyde is a more polar molecule than ethanol, leading to pass slowly through the hydrophobic core of cell membranes. There are some indications that acetaldehyde changes the fatty acid composition of gram-negative bacteria differently from the changes induced by alcohols including ethanol due to the fact that acetaldehyde is more polar molecules and it would be more restricted to the external parts of the phospholipid bilayers. Acetaldehyde diffusibility can be enhanced using the facilitated diffusion in which acetaldehyde (charged molecule) can be passed through the cytoplasmic membrane without directly interacting with its the interior hydrophobic portions (phospholipid bilayer). This passage is mediated by carrier proteins in a direction determined by the electric potential across the membrane.

Indeed, the intracellularly-accumulated acetaldehyde might reach several folds higher than its level in the fermentation broth and even with the external acetaldehyde stripped out from the fermentation broth, the intracellular accumulated acetaldehyde is still a problematic to the microbial cells.

Ultimately, the aim of an engineering project is continuous large-scale production. Following the results of this study, subsequent works should be carried out on fed-batch and continuous fermentation, and on pilot scale with the aim of scaling up to industrial requirements.

Chapter 11

References

- Abdul-kadhim, A.R. and Jarallah, E. M., (2013) "Screening of Cellulase Activity Produced From *Pseudomonas Fluorescens*". *Journal of Babylon University /Pure and Applied Sciences*, **21(3)**, 849-854.
- Agarwal, A., Ng, W.J. and Liu, Y., (2011) "Principle and applications of microbubble and nanobubble technology for water treatment". *Chemosphere*, **84(9)**, 1175–80.
- Al-Mashhadani, M. K. H., Bandulasena, H. C. H., and Zimmerman, W. B. (2011) "CO₂ mass transfer induced through an airlift loop by a microbubble cloud generated by fluidic oscillation" *Industrial and Engineering Chemistry Research*, **51(4)**, 1864–1877.
- Al-Mashhadani, M., (2013) "*Application of Microbubbles Generated by Fluidic Oscillation in the Anaerobic Digestion Process*". PhD thesis, The University of Sheffield, UK.
- AL-Mashhadani, M.K.H., Wilkinson, S.J. and Zimmerman, W.B., (2015) "Airlift bioreactor for biological applications with microbubble mediated transport processes" *Chemical Engineering Science*, **137**, 243–253.
- Al-Masry, W. A., (1999) "Effects of antifoam and scale-up on operation of bioreactors" *Chemical Engineering and Processing: Process Intensification*, **38(3)**, 197–201.
- Amy, P.S. and Morita, R.Y., (1983) "Starvation-survival patterns of sixteen freshly isolated open-ocean bacteria" *Applied and Environmental Microbiology*, **45(3)**, 1109–1115.
- Andrés-Barrao C, Saas MM, Chappuis ML, Boffa M, Perret X, Ortega Pérez R. and Barja F (2012) "Proteome analysis of *Acetobacter pasteurianus* during acetic acid fermentation" *J Proteomics* , **75**, 1701–1717.
- Anwer, H., Strap, J.L. and Costerton, J.W. (1992) "Establishment of ageing biofilms: possible mechanism of bacterial resistance to antimicrobial therapy" *Antimicrobial Agents and Chemotherapy*, **36**, 1347–1351.
- Aranda, A. and del Olmo, M., (2003) "Response to acetaldehyde stress in the yeast *Saccharomyces cerevisiae* involves a strain-dependent regulation of several ALD genes and is mediated by the general stress response pathway", *Yeast*, **20**, 747–759.
- Aspinall G.O., (1980) *Chemistry of cell wall polysaccharides*. Academic Press, New York.
- Axe, D.D. and Bailey, J.E., (1995) "Transport of lactate and acetate through the energized cytoplasmic membrane of *Escherichia coli*", *Biotechnology and Bioengineering*, **47(1)**, 8–19.
- Baez, A. and Shiloach, J., (2014) "Effect of elevated oxygen concentration on bacteria, yeasts, and cells propagated for production of biological compounds. *Microbial cell factories*, **13(181)**, 1-7.

- Bailey, J. E., and Ollis. D. F., (1986) *Biochemical Engineering Fundamentals*. 2nd . McGraw-Hill Book Company, New York.
- Balat, M., Balat.M., Kırtay, E., and Balat, H., (2009) “Main routes for the thermo-conversion of biomass into fuels and chemicals. Part 1: Pyrolysis systems”. *Energy Conversion and Management*, **50(12)**, 3147–3157.
- Bandyopadhyay, R. B. and Humphrey A. E. (1967) “Dynamic measurement of the volumetric oxygen transfer coefficient in fermentation systems”, *Biotechnology and Bioengineering*, **104(5)**, 841–853.
- Barakat, A. and Rouau, X., (2014) “New dry technology of environmentally friendly biomass refinery: glucose yield and energy efficiency”. *Biotechnology for Biofuels*, **7(138)**, 1-11.
- Bar-Even, A. Flamholz, A., Noor,E. and Milo,R., (2012) “Rethinking glycolysis: on the biochemical logic of metabolic pathways”. *Nature Chemical Biology*, **8(6)**, 509–51.
- Bauer, I., Max, N., FETZNER, S. and LINGENS, F., (1996) “2, 4-Dioxygenases Catalyzing N-Heterocyclic-Ring Cleavage and Formation of Carbon Monoxide” *European Journal of Biochemistry*, **240**, 576–583.
- Beard, D. A. and Qian, H., (2007) “Relationship between thermodynamic driving force and one-way fluxes in reversible processes”. *PloS one*, **2(1)**, 1-4.
- Behera, B.C. Sethi, B.K., Mishra, R.R., Dutta, S.K., Thatoi, H.N., (2017) “Microbial cellulases – Diversity & biotechnology with reference to mangrove environment: A review.” *Journal of Genetic Engineering and Biotechnology*, **15(1)**, 197–210.
- Belaich, J. P., and Senez, J. C. (1965) “Influence of Aeration and of Pantothenate on growth Yields of *Zymomonas*” *Journal of Bacteriology*, **89(5)**, 1195–1200.
- Belghith, H., Ellouz-Chaabouni, S. and Gargouri, A., (2001) “Biostoning of denims by *Penicillium occitanis* (Pol6) cellulases” *Journal of biotechnology*, **89**, 257–262.
- Benaroudj, N., Lee, D.H. and Goldberg, A.L., (2001) “Trehalose Accumulation during Cellular Stress Protects Cells and Cellular Proteins from Damage by Oxygen Radicals”. *Journal of Biological Chemistry*, **276(26)**, 24261–24267.
- Bird, R. B., Stewart W. E., Lightfoot E. N., (1960) ‘Transfer Phenomena’, John Wiley and sons, 2nd, p. 75.
- Boisset, C., Chanzy, H. and Henrissat, B., (1999) “Digestion of crystalline cellulose substrates by the *Clostridium thermocellum* cellulosome: structural and morphological aspects”. *Biochem. J*, **340**, 829–835.
- Bolstad, H., (2003) “*Toxicity of Acetaldehyde with Oxygen Radicals*”, Linus Pauling Institute Patrick, Oregon state university.

- Bononi, I., Balatti, V., Gaeta, S., and Tognon, M. (2008) “Gram-negative bacterial lipopolysaccharide retention by a positively charged new-generation filter” *Applied and Environmental Microbiology*, **74(20)**, 6470–6472.
- Booth, I., (1985) “Regulation of cytoplasmic pH in bacteria”. *Microbiological Reviews*, **49(4)**, 359–378.
- Bossier, P., and Verstraete, W. (1996) “Triggers for microbial aggregation in activated sludge” *Applied Microbiology and Biotechnology*, **45(1-2)**, 1–6.
- Boylan, S. a, Redfield, a R., Brody, M. S., and Price, C. W. (1993) “Stress-induced activation of the sigma B transcription factor of *Bacillus subtilis*” *Journal of Bacteriology*, **175(24)**, 7931–7.
- Bravo, V., Pàez, M.P., El-Hadj, M.A., Reyes, A. and Garcí’a, A.L., (2002) “Hydrolysis of carboxymethylcellulose with mixtures of cellulase and β -1,4-glucosidase”. *Journal of Chemical Technology and Biotechnology*, **77**, 15–20.
- Bredwell, M.D. and Worden, R.M., (1998) “Mass-transfer properties of microbubbles. 1. Experimental studies”, *Biotechnology progress*, **14(1)**, 31–8.
- Bringer, S., Finn, R. and Sahn, H., (1984) “Effect of oxygen on the metabolism of *Zymomonas mobilis*” *Archives of Microbiology*, 376–381.
- Bringer-Meyer, S., and Sahn, H. (1993) “Formation of acetyl-CoA in *Zymomonas mobilis* by a pyruvate dehydrogenase complex” *Archives of Microbiology*, **159(2)**, 197–199.
- Brown, D. G., (2002) “Method and apparatus reducing foaming during fermentation ”, patent, EP 1164185 A2, USA .
- Bule, M., Gao, A.H., Hiscox, B. and Chen, S., (2013) “Structural Modification of Lignin and Characterization of Pretreated Wheat Straw by Ozonation”. *Journal of Agricultural and Food Chemistry*, **61**, 3916–3925.
- Burton, K., (1974) “The enthalpy changes for the reduction of nicotinamide-adenine dinucleotide”, *Biochem. J*, **143**, pp.365–368.
- Cabiscol, E., Tamarit, J., and Ros, J. (2000) “Oxidative stress in bacteria and protein damage by reactive oxygen species” *International Microbiology: The Official Journal of the Spanish Society for Microbiology*, **3(1)**, 3–8.
- Çalik, P., Yilgör, P. and Demir, A.S., (2006) “Influence of controlled-pH and uncontrolled-pH operations on recombinant benzaldehyde lyase production by *Escherichia coli*” *Enzyme and Microbial Technology*, **38(5)**, 617–627.
- Capelo J. L., Diniz, M., Fernandes, L., Galesio, M., Lodeiro, C., Santos, H.M. and Vale, G. (2009) “Overview on modern approaches to speed up protein identification workflows relying on enzymatic cleavage and mass spectrometry-based techniques” *Analytica Chimica Acta*, **650(2)**, 151–159.

- Carroll, J., Slupsky, J. and Mather, A., (1991) "The solubility of carbon dioxide in water at low pressure". *J. Phy. Chem. Ref. Data*, **20(6)**, 1201-1209.
- Cartwright, C.P, Jurosze, J-R., Beavan, M.J., Ruby, F.M.S. De Moraisi, S.M.F., (1986) "Ethanol Dissipates the Proton-motive Force across the Plasma Membrane of *Saccharomyces cerevisiae*" *Microbiology*, **132(2)**, 369–377.
- Cazetta, M.L., Celligoi, M.A.P.C., Buzato, J.B. and Scarmino, I.S., (2007) "Fermentation of molasses by *Zymomonas mobilis*: effects of temperature and sugar concentration on ethanol production". *Bioresource Technology*, **98(15)**, 2824–2828.
- Chang, J.-J., Ho, F-J, Tsai, T-Y, Kel, H-M, Wang, C, H-T., Chen, H-L, Shih, M-C, Huang, C-C and Li, W-H., (2012) "PGASO: A synthetic biology tool for engineering a cellulolytic yeast." *Biotechnology for Biofuels*, **5 (53)**. 1-12.
- Charles, C., (2012) "Should We be concerned about Competition between Food and Fuel? Analysis of biofuel consumption mandates in the European Union and the united States". *Iisd*, 1–8.
- Chatterjee, A., Magee, J. L., and Dey, S. K. (1983) "The Role of Homogeneous Reactions in the radiolysis of Water", *Radiation Research*, **96(1)**, 1–19.
- Chatterjee, A., Magee, J.L. and Dey, S.K., (1983) "The Role of Homogeneous Reactions in the Radiolysis of Water" *Radiation Research*, **96(1)**, 1–19.
- Cherchi, C. and Gu, A. Z. (2011) "Effect of bacterial growth stage on resistance to chlorine disinfection". *water science and technology*, 7–13.
- Chisti, M.Y. and Moo-Young, M., (1987) "Airlift reactors: characteristics applications and design considerations", *Chemical. Engineering comm*, **60**, 195–242.
- Chisti, Y., Wenge, F. and Moo-Young, M., (1995) "Relationship between riser and downcomer gas hold-up in internal-loop airlift reactors without gas-liquid separators". *The Chemical Engineering Journal*, **57**, B7-B13.
- Choorit, W. and Wisarnwan, P., (2007) "Effect of temperature on the anaerobic digestion of palm oil mill effluent" *Electronic Journal of Biotechnology*, **10(3)**, 376–385.
- Chou, Y., Linger, J., Yang, S. and Zhang, M., (2015) "Genetic engineering and improvement of a *Zymomonas mobilis* for arabinose utilization and Its Performance on Pretreated Corn Stover" *Biotechnology & Biomaterials*, **5(2)**, 1-8.
- Chubukov, V. and Sauer, U., (2014) "Environmental dependence of stationary-phase metabolism in *bacillus subtilis* and *Escherichia coli*". *Applied and Environmental Microbiology*, **80(9)**, 2901–2909.
- Commonwealth of Massachusetts, (2015), *Cumulative Exposure to Air Toxics*, Massachusetta, the united states.

- Conway, T., (1992) “The EntnerDoudoroff pathway: history, physiology and molecular biology”. *FEMS Microbiology Reviews*, **103**, 4465–70.
- Cook, G.M. and Russell, J.B., (1994) “Energy-spilling reactions of *Streptococcus bovis* and resistance of its membrane to proton conductance” *Applied and environmental microbiology*, **60(6)**, 1942–8.
- Costerton JW, Cheng K-J, Geesey GG, Ladd TI, Nickel JC, Das- gupta M, Marrie TJ (1987) “Bacterial biofilms in nature and disease” *Annu Rev Microbiol*, **41**,435-464
- Cray, J. A., Stevenson, A., Ball, P., Bankar, S.B., Eleutherio, E.C.A., Ezej, T.C., Singhal, R.S., Thevelein, J.M., Timson, D.J. and Hallsworth, J.E., (2015) “Chaotropicity: a key factor in product tolerance of biofuel-producing microorganisms” *Current opinion in biotechnology*, **33**, 228–259.
- Criegee, R., (1975) “Mechanism of ozonolysis”. *Angew. Chem. Internat. Edit*, **14(11)**, 745–752.
- Crout, D. and Vic, G., (1998) “Glycosidases and glycosyl transferases in glycoside and oligosaccharide synthesis” *Current opinion in chemical biology*, 98-111.
- Cui, L., Liu, Z., Si, C., Hui, L., Kang, N. and Zhao, T., (2012) “Influence of steam explosion pretreatment on the composition and structure of wheat straw”. *Bioresources*, **7(3)**, 4202–4213.
- D’avila, S.G. and Silva, R.S.F., (1970) “Isothermal Vapor-liquid equilibrium data by total pressure Method”, *Journal of Chemical and Engineering Data*, **15(3)**, 421–424.
- Dabhi, B., Vyas, C R. and Shelat, H., (2014) “Use of banana waste for the production of cellulolytic enzymes under solid substrate fermentation using bacterial consortium”. *Int. J. Curr. Microbiol. App. Sci*, **3(1)**, 337–346.
- Darani, K. and Mozafari, M.R., (2010) “Supercritical fluids technology in bioprocess industries: a review”. *Journal of Biochem. Techno*, **2(1)**, 144–152.
- Dashtban, M., Maki, M., Leung, K. T. Mao, C. and Qin, W., (2010) “Cellulase activities in biomass conversion: measurement methods and comparison”, *Critical Reviews in Biotechnology*, 1–8.
- Davies, P.F., Remuzzit, A., Gordon, E. J., Dewey, C. F. and Gimbrone, M. A. (1986) “Turbulent fluid shear stress induces vascular endothelial cell turnover in vitro”. *Proc. Natl. Acad. Sci.*, **83**, 2114–2117.
- Dawes, E. A, Ribbons, D.W. and Large, P.J., (1966) “The route of ethanol formation in *Zymomonas mobilis*”, *The Biochemical journal*, **98(3)**, 795–803.
- De Barros, R.D.R.O., Paredes, R. D., Endo, T., Bon, E. P. D. and Lee, S-H., (2013) “Association of wet disk milling and ozonolysis as pretreatment for enzymatic saccharification of sugarcane bagasse and straw”. *Bioresource Technology*, **136**, 288–294.

- De Souza, L.G.M., Oliveira, S.L.I, Bomura, R.Y and Magali, A.J., (2011) “Detection of bacteriocins in *Zymomonas mobilis* and RAPD fingerprinting of the producer strains” *African Journal of Pharmacy and Pharmacology*, **5(19)**, 2132–2139.
- Deanda, K., Zhang, M., Eddy, C. and Picataggio, S., (1996) “Development of an arabinose-fermenting *Zymomonas mobilis* strain by metabolic pathway engineering”. *Applied and Environmental Microbiology*, **62(12)**, 4465–70.
- Debs-Louka, E., Louka, N., Abraham, G., Chabot, V. and Allaf, K., (1999) “Effect of compressed carbon dioxide on microbial cell viability”. *Applied and Environmental Microbiology*, **65(2)**, 626–631.
- Deguchi, S., Mukai, S.A., Tsudome, M. and Horikoshi, K., (2006) “Facile generation of fullerene nanoparticles by hand grinding”. *Adv. Mater.*, **18**, 729-732.
- Demirbas, A., (2005) “Bioethanol from Cellulosic Materials: A Renewable Motor Fuel from Biomass”. *Energy Sources*, **27(4)**, 327–337.
- Department of Health and Human Services, (2014) *Announcement of Availability of the Report on Carcinogens*, united states.
- Deshpande, V., Keskar, S., Mishra, C. and Rao. M. (1986) “Direct conversion of cellulose/hemicellulose to ethanol by *Neurospora crassa*” *Enzyme and Microbial Technology*, **8(3)**, 149–152.
- Devlin, T. M. (2011) *Textbook of biochemistry: With clinical correlations*. Hoboken,NJ: John Wiley & Sons.
- Díaz-Reinoso, B., Moure, A., DomiÁnguez, H. and ParajoÁ, J.C., (2006) “Supercritical CO₂ extraction and purification of compounds with antioxidant activity”. *Journal of Agricultural and Food Chemistry*, **54**, 2441-2469.
- Dillow, A., Dehghani, F., Hrkach, J.S., Foster, N.R and Langer, R., (1999) “Bacterial inactivation by using near-and supercritical carbon dioxide”. *Proc. Natl. Acad. Sci.*, **96**, 10344–10348.
- Dimarogona, M., Topakas, E. and Christakopoulos, P., (2012) “Cellulose degradation by oxidative enzymes”. *Comput and Indust,Biotechn,J*, **2(3)**, 1-8.
- Doe, U., (2005) “Breaking the biological barriers to cellulosic ethanol: a joint research agenda”. Biomass to Biofuels Workshop, Maryland, 39-56.
- Doran, P. M., (2013) *Bioprocess engineering principles* 2nd ed., Waltham, MA: Academic Press.
- Dos Santos, V. A. P.M., Heim, M., Moore, E.R.B., Strätz, M. and Timmis, K.N., (2004) “Insights into the genomic basis of niche specificity of *Pseudomonas putida* KT2440”. *Environmental Microbiology*, **6(12)**, 1264–86.

- Douka, E., Koukkou, A I., Vartholomatos, G., Frillingos, S., Papamichael, E. M., and Drinas, C. (1999) "A *Zymomonas mobilis* mutant with delayed growth on high glucose concentrations" *Journal of Bacteriology*, **181**(15), 4598–4604.
- Dowson, G.R.M. and Wass, D.F., (2013) "Conversion of Alcohols" Patent, BP Biofuels UK Limited, WO2012004572.
- Drummond, D. and Wilke, C., (2008) "Mistranslation-induced protein misfolding as a dominant constraint on coding-sequence evolution". *Cell*, **134**(2), 341–352.
- Duff, S. and Murray, W., (1996) "Bioconversion of forest products industry waste cellulose to fuel ethanol: a review". *Bioresource Technology*, **55**, 1-33.
- Dussán, K. J., Silva, D. D. V, Moraes, E. J. C., Priscila, V., and Felipe, M. G. A. (2014) "Dilute-acid Hydrolysis of Cellulose to Glucose from Sugarcane Bagasse" *Chemical Engineering Transactions*, **38**, 433–438.
- Eames, M. and Kortemme, T., (2012) "Cost-benefit tradeoffs in engineered lac operons". *Science*, **336**, 911–915.
- Eckert, M., Fleischmann, G., Jira, R. and Golka, K., (2012) "Acetaldehyde". *Ullmann's Encyclopedia of Industrial Chemistry*.
- EPA, Environmental Protection Agency, (1987) *Acetaldehyde*, the united states.
- Erakhrumen, A.A., (2011) "Global Increase in the Consumption of lignocellulosic Biomass as Energy Source: Necessity for Sustained Optimisation of Agroforestry Technologies". *ISRN Renewable Energy*, **2011**, 1–8.
- Eram, M.S. and Ma, K., (2013) "Decarboxylation of pyruvate to acetaldehyde for ethanol production by hyperthermophiles". *Biomolecules*, **3**(3), 578–96.
- Ezeji, T.C., Karcher, P.M., Qureshi, N. and Blaschek, H.P., (2005) "Improving performance of a gas stripping-based recovery system to remove butanol from *Clostridium beijerinckii* fermentation". *Bioprocess and Biosystems Engineering*, **27**(3), 207–14.
- Fagade, O. and Bamigboye, O., (2012) "Effect of cultural conditions on the cellulase activity of bacteria species isolated from degrading corn cob". *Archives of Applied Science Research*, **4**(6), 2540–2545.
- Fakhruddin, A. N.M. and Quilty, B., (2006) "The response of *Pseudomonas putida* CP1 cells to nutritional, chemical and environmental stresses" *World Journal of Microbiology & Biotechnology*, **22**, 507–514.
- Fan, L., Lee, Y. and Beardmore, D., (1980) "Major chemical and physical features of cellulosic materials as substrates for enzymatic hydrolysis", *Advances in Biochemical Engineering*, **11**: 101-117.
- FAO, Food and agriculture organisation of the united nations, (2003) *State of the World's Forests, Rome*.

- Fatemeh, Y., Abbas, S.S., Mohsen, N., Mahdi, P. H.A. and Ebrahim, V-F., (2012) "Mixing studies in Loop Bioreactors for production of biomas from Natural Gas", *Iran. J. Chem. Chem. Eng.*, **31(2)**, 91–101.
- Feigl, F., (1955) "Organic spot test analysis". *Analytical Chemistry*, **27(8)**, 1315–1318.
- Finney, L.A. and O'Halloran, T. V., (2003) "Transition Metal Speciation in the Cell: Insights from the Chemistry of Metal Ion Receptors." *Science*, **300(5621)**, 931–936.
- Flamholz, A., Noor, E., Bar-Even, A., Liebermeister, W. and Milo, R., (2013) "Glycolytic strategy as a trade-off between energy yield and protein cost". *PNAS Early Edition*, **110(24)**, 10039–10044.
- Food Safety Commission, (2005) *Evaluation Results on the Health Risk Assessment of Acetaldehyde as Food Additive*, Japan.
- Forster, R.E., Gros, G., Lim, L., Ono, Y. and Wunder, M. (1998) "The effect of 4,40-diisothiocyanato-stilbene-2,20-disulfonate on CO₂ permeability of the red blood cell membrane" *Proc. Natl. Acad. Sci. USA*, **95**, 15815–15820.
- Fox, C., (2010) "Chemical and thermal characterization of three industrial lignins and their corresponding lignin esters". Master thesis, University of Idaho, Moscow.
- Franklin, F., (1981) "Molecular and functional analysis of the TOL plasmid pWVO from *Pseudomonas putida* and cloning of genes for the entire regulated aromatic ring meta cleavage". *Proc. NatL Acad. Sci. USA*, **78(12)**, 7458–7462.
- Fraser, D., (1951) "Bursting bacteria by release of gas pressure". *Nature*, **167**, 33 – 34.
- Gangola, P. and Rosen, B., (1987) "Maintenance of intracellular calcium in *Escherichia coli*". *Journal of Biological Chemistry*, **262(26)**, 12570–12574.
- García-cubero, M. T., González-benito, G., Indacochea, I., Coca, M., and Bolado, S. (2009) "Effect of ozonolysis pretreatment on enzymatic digestibility of wheat and rye straw" *Bioresource Technology*, **100(4)**, 1608–1613.
- Garcia-Gonzalez, L., Geeraerd, A.H., Spilimbergo, S., Elst, K., Van Ginneken, L., Debevere, J., Van Impe, J.F. and Devlieghere, F., (2007) "High-pressure carbon dioxide inactivation of microorganisms in foods: the past, the present and the future". *International journal of Food Microbiology*, **117**, 1–28.
- Garcia-Ochoa, F. Gomezv, E., Santos, V. E. and Merchuk, J. C., (2010) "Oxygen uptake rate in microbial processes: An overview". *Biochemical Engineering Journal*, **49(3)**, 289–307.
- Garcia-Ochoa, F., Castro, E.G. and Santos, V.E., (2000) "Oxygen transfer and uptake rates during xanthan gum production". *Enzyme and Microbial Technology*, **27(9)**, 680–690.

- Garrett, B. C., Dixon, D. A., Camaioni, D. M., Chipman, D. M., Johnson, M. A., Jonah, C. D. and Zwier, T. S. (2005) "Role of water in electron-initiated processes and radical chemistry: Issues and scientific advances", *Chemical Reviews*, **105**(1), 355–389.
- Gary R. K., (2004) "The concentration dependence of the ΔS term in the Gibbs free energy function: Application to reversible reactions in biochemistry", *Journal of Chemical Education*, **81**(11), 1599-1604.
- George, J. and Sabapathi, S.N., (2015) "Cellulose nanocrystals: Synthesis, functional properties, and applications." *Nanotechnology, Science and Applications*, **8**, 45–54.
- Ghose, T., (1987) "Measurement of cellulase activities". *Pure & Appl. Chem.*, **59**(2), 257-268.
- Ghosh, P., (2009) *Colloid and interface science*. New Delhi, India: PHI Learning.
- Gilna, V.V. and Khaleel, K.M., (2011) "Cellulase enzyme activity of *Aspergillus fumigatus* from mangrove soil on lignocellulosic substrate". *Rec Res Sci Tech.*, **3**(1), 132–134.
- Gírio, F.M., Fonseca, C., Carvalheiro, F., Duarte, L.C., Marques, S., and Bogel-Lukasik, R., (2010) "Hemicelluloses for fuel ethanol: A review". *Bioresource Technology*, **101**, 4775–4800.
- Givskov, M. Eberl, L., Moller, S., Poulsen, L. K. and Molin, S., (1994) "Responses to Nutrient Starvation In *Pseudomonas-Putida* Kt2442 - Analysis Of General Cross-Protection, Cell-Shape, And Macromolecular Content", *J. Bacteriology*, **176**(1), 7–14.
- Giwerzman, B., Jensen, E. T., Høiby, N., Kharazmi, A. and Costerton, J. W. (1991) "Induction of beta-lactamase production in *Pseudomonas aeruginosa* biofilm" *Antimicrobial Agents and Chemotherapy*, **35**(5), 1008–1010.
- Gnansounou, E. and Dauriat, A., (2005) "Ethanol fuel from biomass: A review". *J Sci Ind RES*, **64**, 809–821.
- Gomez, E., Santos, V. E., Alcon, A., Martin, A. B. And Garcia-Ochoa, F., (2006) "Oxygen-uptake and mass-transfer rates on the growth of *Pseudomonas putida* CECT5279: Influence on biodesulfurization (BDS) capability". *Energy and Fuels*, **20**(4), 1565–1571.
- Gould, J., (1985) "Studies on the mechanism of alkaline peroxide delignification of agricultural residues". *Biotechnology and Bioengineering*, **27**, 225-231.
- Gunasekaran, P., Karunakaran, T. and Kasthuribai, M., (1986) "Fermentation pattern of *Zymomonas mobilis* strains on different substrates—a comparative study". *J. Biosci*, **10**(2), 181–186.
- Hacking, A.J., (1986) "Economic aspects of biotechnology". In, Baddiley J, Carey NH, Davidson JF, Higgins IJ & Patter WG (eds.) Cambridge studies on biotechnology, Vol. 3.

- Hadiati, A., Krahn, I., Lindner, S.N. and Wendisch, V.F. (2014) “Engineering of *Corynebacterium glutamicum* for growth and production of L-ornithine, L-lysine, and lycopene from hexuronic acids”. *Bioresources and Bioprocessing*, **1(25)**, 1-10.
- Hainal, A. R., Caparu, A.M, VOLF, I. and POPA, V.I., (2012) “Lignin as a carbon source for the cultivation of some *Rhodotorula* species”. *Cellulose Chem. Technol.*, **46(1-2)**, 87–96.
- Hall, J., Black, W.G., Ferreira, L.M.A., Millward-Sadler, S.J., Ali, B.R.S., Hazlewood, G.P. and Gilbert, H.J., (1995) “The non-catalytic cellulose-binding domain of a novel cellulase from *Pseudomonas fluorescens subsp. cellulosa* is important for the efficient hydrolysis of Avicel”. *Biochem. J.*, **309**, 749–756.
- Hall, M. Bansal, P., Lee, J.H., Reaff, M.J. and Bommarius, A.S., (2010) “Cellulose crystallinity--a key predictor of the enzymatic hydrolysis rate”. *The FEBS journal*, **277**, 1571–1582.
- Hall-Stoodley, L, Costerton, J. W. and Stoodley, P., (2004) “Bacterial biofilms: from the natural environment to infectious diseases” *Nature reviews. Microbiology*, **2(2)**, 95–108.
- Hallsworth, J.E., Heim, S. and Timmis, K.N., (2003) “Chaotropic solutes cause water stress in *Pseudomonas putida*” *Environmental Microbiology*, **5(12)**, 1270–1280.
- Hanotu, J.O., Bandulasena, H.C.H. and Zimmerman, W.B., (2012) “Microflotation performance for algal separation” *Biotechnol. Bioeng.* **109 (7)**, 1663–1673.
- Harley, J.P., (2002) *Laboratory exercises in microbiology*, 5th, The McGraw–Hill Companies.
- Harris, E. L. V. and Angal, S., (1995) *Protein purification methods: a practical approach*, 2nd, Oxford : IRL Press.
- He, Y., Pang, Z., Liu, Y., Li, X. and Wang, K., (2008) “Physicochemical characterization of rice straw pretreated with sodium hydroxide in the solid state for enhancing biogas production”. *Energy and Fuels*, **22**, 2775–2781.
- Heipieper, H. J., Keweloh, H., and Rehm, H. J. (1991) “Influence of phenols on growth and membrane-permeability of free and immobilized *Escherichia coli*” *Applied and Environmental Microbiology*, **57(11)**, 1213–1217.
- Heipieper, H. J., Meulenbeld, G., Oirschot, Q. Van, and Bont, J. De. (1996) “Effect of Environmental Factors on the trans / cis Ratio of Unsaturated Fatty Acids in *Pseudomonas putida* S12”., *Applied and Environmental Microbiology*, **62(8)**, 2773–2777.
- Heipieper, H. J., Weber, F. J., Sikkema, J., Keweloh, H., and De Bont, J. a M. (1994). “Mechanisms of resistance of whole cells to toxic organic solvents. *Trends in Biotechnology*, **12(10)**, 409–415.
- Henrissat, B., Teeri, T. and Warren, R., (1998) “A scheme for designating enzymes that hydrolyse the polysaccharides in the cell walls of plants” *FEBS letters*, **425**, 352–354.

- Henzler, H.-J. and Schedel, M. (1991) "Suitability of the shaking flask for oxygen supply to microbial cultures" *Bioprocess Eng.* **7**, 123–131.
- Hiemenz, P.C. and Rajagopalan, R. (1997) *Principles of colloid and surface chemistry*. New York, NY: Marcel Dekker.
- Hirst, E., (1962) "The chemical structure of the hemicelluloses". *Pure and Appl. Chem.*, **5**, 53-66.
- Hoadley R.B., (2000) *Understanding wood: a craftsman's guide to wood technology*, 2nd, Newtown, CT: Taunton Press.
- Holman, W. L. (1914) "The use of decolorized acid fuchin as an acid indicator in carbohydrate fermentation tests with some remarks on acid production by bacteria" *Oxford University Press*, **15(1)**, 227–233.
- Ho-mu, L., Zhiying, Y. and Li, F., (1993) "Inactivation of *Leuconostoc dextranicum* with carbon dioxide under pressure". *The Chemical Engineering Journal*, **52**, B29–B34.
- Hong, S. and Pyun, Y., (1999) "Inactivation kinetics of *Lactobacillus plantarum* by high pressure carbon dioxide". *Journal of Food Science*, **64(4)**, 728–733.
- Hong, S.I. and Pyun, Y.R., (2001) "Membrane damage and enzyme inactivation of *Lactobacillus plantarum* by high pressure CO₂ treatment". *International Journal of Food Microbiology*, **63**, 19–28.
- Hong, S.I., Park, W.S., and Pyun, Y.R. (1997) "Inactivation of *Lactobacillus* sp. from Kimchi by high-pressure carbon dioxide" *Food. Sci. Technol.* **30**, 681–685.
- Hsu, T., Ladisch, R. and Tsao, G., (1980) 'Alcohol from cellulose'. *Chemtech*.
- Hustoft, H.K., Malerod, H., Wilson, S. R., Reubsaet, L., Lundanes, E. and Greibrokk, T., (2010) "A Critical Review of Trypsin Digestion for LC-MS Based Proteomics" *Integrative Proteomics*, 73–92.
- Hutkins, R. and Nannen, N., (1993) "pH homeostasis in lactic acid bacteria". *J Dairy Sci*, **76**, 2354-2365.
- Ibrahim, A. and El-diwany, A., (2007) "Isolation and identification of new cellulases producing thermophilic bacteria from an Egyptian hot spring and some properties of the crude enzyme". *Aust. J. Basic & Appl. Sci.*, **1(4)**, 473–478.
- Imlay, J. A, (2013) "The molecular mechanisms and physiological consequences of oxidative stress: lessons from a model bacterium" *Nature reviews. Microbiology*, **11(7)**, 443–54.
- Immanuel, G., Dhanusha, R., Prema, R. and Palavesam, A. (2006) "Effect of different growth parameters on endoglucanase enzyme activity by bacteria isolated from coir retting effluents of estuarine environment" *International Journal of Environmental Science and Technology*, **3(1)**, 25–34.

- Ingram, L.O., (1976) "Adaption of membrane lipids to alcohols" *J. Bacteriol.*, **125**, 670-678.
- Ingram, L.O., (1977) "Changes in lipid composition of *Escherichia coli* resulting from growth with organic solvents and with food Additives", *Microbiology* **33**, 1233–1236.
- Ingram, L.O., (1986) "Microbial tolerance to alcohols: role of the cell membrane" *Trends in Biotechnology*, **4(2)**, 40–44.
- Inokuma, K., Liao, J.C., Okamoto, M. and Hanai, T., (2010) "Improvement of isopropanol production by metabolically engineered *Escherichia coli* using gas stripping". *J. Bioscie..Bioeng.*, **110(6)**, 696–701.
- Ioelovich, M. and Morag, E., (2011) "Effect of cellulose structure on enzymatic hydrolysis". *BioResources*, **6(3)**, 2818–2835.
- Isenschmid, A., Marison, I. and Stockar, U. V., (1995) "The influence of pressure and temperature of compressed CO₂ on the survival of yeast cells". *Journal of Biotechnology*, **39**, 229-237.
- Ishikawa, H. and Tanaka, H., (1992) "Effect of ventilation on the production of acetaldehyde by *Zymomonas mobilis*". *J. Ferment. Bioeng.*, **70(1)**, 34-40.
- Janardhnan, S. and Sain, M., (2011) "Isolation of Cellulose Nanofibers: Effect of Biotreatment on Hydrogen Bonding Network in Wood Fibers", *International Journal of Polymer Science*, 1–6.
- Jones, C. and Doelle, H., (1991) "Kinetic control of ethanol production by *Zymomonas mobilis*" *Applied Microbiology and Biotechnology*, **35(1)**, 4–9.
- Jones, R. and Greenfield, P., (1982) "Effect of carbon dioxide on yeast growth and fermentation". *Enzyme Microb. Technol.*, **4**, 210–223.
- Juergensmeyer, M. A., Nelson, E.S. and Juergensmeyer, E.A., (2007) "Shaking alone, without concurrent aeration, affects the growth characteristics of *Escherichia coli*". *Letters in Applied Microbiology*, **45(2)**, 179–183.
- Kalnenieks, U. (2006) "*Physiology of Zymomonas mobilis: Some Unanswered Questions*", *Advances in Microbila Physiology*, 51st ed., Sheffield: Elsevier pp. 73–117.
- Kalnenieks, U., Galinina, N., Toma, M.M. and Poole, R.K., (2000) "Cyanide inhibits respiration yet stimulates aerobic growth of *Zymomonas mobilis*". *Microbiology*, **146**, 1259–1266.
- Kalter, R. J., R. N. Boisvert, E. C. Gabler, L. P., Walker, R. A. Pellerin, A. M. Rao, and Hang, Y. D. (1981) "Ethanol production in southern tier east region of New York": technical and economic feasibility. Final report. ERDA report no. 81-7, 136-144.

- Kamaroddin, M.F., Hanotu, J., Gilmour, J. and Zimmerman, W. (2016) “In-situ disinfection and a new downstream processing scheme from algal harvesting to lipid extraction using ozone-rich microbubbles for biofuel production.” *Algal Research*, **17**, 217–226.
- Kamihira, M., Taniguchi, M., and Kobayashi, T. (1987) “Sterilization of microorganisms with supercritical CO₂”, *Agric. Biol. Chem.* **51**, 407–412.
- Kaneko, H., Hosoya, S., Iiyama, K. and Nakano, J., (1983) “Degradation of lignin with ozone: reactivity of lignin model compounds toward ozone”. *J. Wood. Chem. Technol.*, **3** (4), 399–411.
- Katsamas, G. and Sidiras, D., (2013) “Sugars Production from Wheat Straw Using Maleic Acid”. *Rec. Advan. . Chem. Eng. Biochem. Comput. Chem.*, 23–28.
- Katzen, R. Associates (1979) *Grain Motor Fuel Alcohol Technical and Economic Assessment*.
- Khalilitehrani, M. (2011) “An investigation on modelling and simulation of chilled ammonia process using VOF method”, master thesis, Chalmers University of Technology, Sweden.
- Khan, T. and Mubeen, U., (2012) “Wheat straw: A pragmatic overview”. *Curr. Res. J. Biol. Sci.*, **4**(6), 673–675.
- Khuntia, S., Majumder, S.K. and Ghosh, P., (2012) “Microbubble-aided water and wastewater purification: A review”. *Reviews in Chemical Engineering*”, **28**(4-6), 191–221.
- Kim, B. Y., (2011) “Structures of iron-dependent alcohol dehydrogenase 2 from *Zymomonas mobilis* ZM4 with and without NAD⁺ cofactor.” *Journal of Molecular Biology*, **407**(3), 413–424.
- Kim, J., and Park, W. (2014) “Oxidative stress response in *Pseudomonas putida*” *Applied Microbiology and Biotechnology*, **98**(16), 6933–6946.
- Kim, M., Ho, J. and Hyungmin, L., (2016) “Study of bubble - induced turbulence in upward laminar bubbly pipe flows measured with a two - phase particle image velocimetry” *Experiments in Fluids*, **57**(55), 1-21.
- King, J. and Mabbitt, L., (1982) “Preservation of raw milk by the addition of carbon dioxide”. *J. Dairy. Res.*, **49**, 439–447.
- Klöckner, W. and Büchs, J., (2012) “Advances in shaking technologies” *Trends in Biotechnology*, **30**(6), 307–314.
- Kobayashi, F., Ikeura, H., Odake, S. and Hayata, Y., (2014) “Inactivation of *Saccharomyces cerevisiae* by equipment pressurizing at ambient temperature after generating CO₂ microbubbles at lower temperature and pressure”. *LWT - Food Science and Technology* **56**, 543–547.
- Konz, J.O., King, J. and Cooney, C.L., (1998) “Effects of oxygen on recombinant protein expression” *Biotechnology Progress*, **14**(3), 393–409.

- Koolman J, Roehm KH (2005), *Color atlas of Biochemistry*, 2^{ed} ed. thieme stuttgart. New York.
- Kragh, K.N., Hutchison, J. B., Melaugh , G., Rodesney, C., Roberts ,A. E. L., Irie, Y., Jensen, P., Diggle , S. P., Allen, R. J., Gordon ,V. and Bjarnsholta, T. (2016) “Role of Multicellular Aggregates in biofilm formation” *mBio*, **7(2)**, 1-11.
- Kristensen, J.B., Thygesen, L.G., Felby, C., Jørgensen,H. and Elder, T., (2008) “Cell-wall structural changes in wheat straw pretreated for bioethanol production”. *Biotechnology for Biofuels*, **1**, 1-9.
- Kruis, A. J., Levisson, M., Mars, A. E., Van der Ploeg, Max G-D, Fernando, E., Valeria,K., Servé, W.M., Van d-O, J., Weusthuis, R. A., (2017), “Ethyl acetate production by the elusive alcohol acetyltransferase from yeast.” *Metabolic Engineering*, **41**, 92–101.
- Kumar, P., Barrett, D.M., Delwiche, M. J. and Stroeve, P., (2009) “Methods for pretreatment of lignocellulosic biomass for efficient hydrolysis and biofuel production”. *Ind. Eng. Chem. Res.* **48**, 3713–3729.
- Kumar, S., Kusakabe, K., Raghunathan, K., Fan, L.-S., (1992) “Mechanism of heat transfer in bubbly liquid and liquid–solid systems: injection single bubble”, *AIChE*.
- Kuvshinov, D., Siswanto, A. and Zimmerman, W., (2014) “Microbubbles enhanced synthetic phorbol ester degradation by ozonolysis”. *World Academy of Science, Engineering and Technology*, **8(1)**, 78–81.
- Laureano-Perez, L., Teymouri, F., Alizadeh, H. and DALE, B.E., (2005) “Understanding factors that limit enzymatic hydrolysis of biomass”. *Applied Biochemistry and Biotechnology*, **121–124**, 1081–1100.
- Lawford, H.G. and Stevnsborg, N. (1986) “Pantothenate limitation does not induce uncoupled growth of *Zymomonas* in chemostat culture.” *Biotechnol. Lett.* **8**, 345–350.
- Lazdunski, A. and Belaich, J.P., (1972) “Uncoupling in bacterial growth: ATP pool variation in *Zymomonas mobilis* cells in relation to different uncoupling conditions of growth”, *J. Gen. Microbiol.*, **70**, 187–197.
- Leão, C. and Van Uden, N., (1984) “Effects of ethanol and other alkanols on passive proton influx in the yeast *Saccharomyces cerevisiae*” *Biochimica et biophysica acta*, **774(1)**, 43–48.
- Lee, J., Jameel, H. and Venditti, R., (2010) “Effect of ozone and autohydrolysis pretreatments on enzymatic digestibility of coastal Bermuda grass”. *Bioresources*, **5(1)**, 1084–1101.
- Lejeune, A., Dartois, V. and Colson, C., (1988) “Characterization and expression in *Escherichia coli* of an endoglucanase gene of *Pseudomonas fluorescens subsp.*”, *Biochimica et Biophysica Acta*, **950**, 204–214.
- Lemos, M., Teixeira, J.A., Domingues, M.R.M., Mota, M. and Gama, F.M., (2003) “The enhancement of the cellulolytic activity of cellobiohydrolase I and endoglucanase by the

- addition of cellulose binding domains derived from *Trichoderma reesei*". *Enzyme and Microbial Technology*, **32**, 35–40.
- Lendenmann, U.R.S., Snozzi, Mario and Egli, T., (1996) "Kinetics of the simultaneous utilization of sugar mixtures by *Escherichia coli* in continuous culture" *Applied and Environmental microbiology* , **62(5)**, 1493–1499.
- Li, P. and Tsuge, H., (2006) "Ozone transfer in a new gas-induced contactor with microbubbles" *Journal of Chemical Engineering of Japan*, **39(11)**, 1213–1220.
- Li, P., Takahashi, M. and Chiba, K., (2009a) "Degradation of phenol by the collapse of microbubbles". *Chemosphere*, 75, pp.1371–1375.
- Li, P., Takahashi, M. and Chiba, K., (2009b) "Enhanced free-radical generation by shrinking microbubbles using a copper catalyst". *Chemosphere*, **77**, 1157–1160.
- Li, X. Z., Webb, J. S., Kjelleberg, S., and Rosche, B. (2006) "Enhanced benzaldehyde tolerance in *Zymomonas mobilis* biofilms and the potential of biofilm applications in fine-chemical production" *Applied and Environmental Microbiology*, **72(2)**, 1639–1644.
- Limayem, A. and Ricke, S.C., (2012) "Lignocellulosic biomass for bioethanol production: Current perspectives, potential issues and future prospects". *Progress in Energy and Combustion Science*, **38**, 449–467.
- Lin, H. and Chen, L., (1994) *Method for recovery of intracellular material by disruption of microbial cells with carbon dioxide under pressure*, West Lafayette, Ind., 5,306,637,.
- Lin, H., Yang, Z. and Chen, L. (1993) "Inactivation of *leuconostoc dextranicum* with carbon dioxide under pressure". *Chem. Eng. J.*, **52**, B29-B34.
- Lin, H., Yang, Z. and Chen, L., (1992) "Inactivation of *Saccharomyces cerevisiae* by supercritical and subcritical carbon dioxide". *Biotechnol. prog.*, **8**, 458–461.
- Lower, S.S.K., (1999) "Carbonate equilibria in natural waters". Simon Fraser University, Chem 1(Environmental Chemistry), 1–26.
- Lynd, L.R., Weimer, P.J., van Zyl, W.H. and Pretorius, I.S, (2002) "Microbial Cellulose utilization: Fundamentals and Biotechnology". *Microbiology and Molecular Biology Reviews*, **66(3)**, 506–577.
- MacDonald, R. G. and Franklin, J. N. (1969) *Pulp and paper manufacture: The pulping of wood*, 2nd, McGraw-Hill Book Company, New York, **1**.
- Maiorella, B.L., Blanch, H.W. and Wilke, C.R. (1984) "Feed component inhibition in ethanolic fermentation by *Saccharomyces cerevisiae*", *Biotechnol Bioeng* ,**26**,1155–1166.
- Makarov, A.A., Dorofeev, A.G. and Panikov, N.S., (1998) "Cell shape and size of starving microorganisms as determined by computer image analysis", *Microbiology*, **67(3)**, 264–270.

- Mansure, J.J.C., Panek, A. D., Crowe, L.M. and Crowe, J.H., (1994) “Trehalose inhibits ethanol effects on intact yeast cells and liposomes” *Biochimica et Biophysica Acta - Biomembranes*, **1191**(2), 309–316.
- Marcos, M., (2013) “Optimization of the enzymatic hydrolysis conditions of steam-exploded wheat straw for maximum glucose and xylose recovery”, *J. Chem.Biotechn.* **15**(6), 875–881.
- Markwardt, L. and Wilson, T., (1935) “*Strength and related properties of woods grown in the United States*”, Technical Bulletin, N0.479.
- Martin, D. S. (1932) “Oxygen Consumption of *Escherichia Coli* During the Lag and Logarithmic Phases of Growth”. *The Journal of general physiology*, **15**(6), 691–708.
- Mastroeni, M.F., Gurgel, P.V., Silveira, M.M., De Mancilha, I.M. and Jonas, R., (2003) “The influence of oxygen supply on the production of acetaldehyde by *Zymomonas mobilis*”. *Braz. J. Chem. Eng.* **20**(2), 87–93.
- McFeters, G. A., Egli, T., Wilberg, E., Alder, a., Schneider Suozzi, R. M., and Giger, W. (1990) “Activity and adaptation of nitrilotriacetate (NTA)-degrading bacteria: Field and laboratory studies”, *Water Research*, **24**(7), 875–881.
- McKendry, P., (2002) “Energy production from biomass (part 1): overview of biomass”. *Bioresource Technology*, **83**, 37–46.
- McNeil, B. and Harvey, L., (2008) *Practical fermentation technology*, John Wiley and Sons Ltd.
- Mejia, R., Gomez-Eichelmann, M., C. and Fernandez, M. S. (1999) “fatty acids profile of *Escherichia coli* during the heat shock response”. *Biochemistry and Molecular Biology International*, **47**, 835–844.
- Merchuk, J. and Siegel, M., (1988) “Air-lift reactors in chemical and biological technology”. *J. Chem. Tech. Biotechnol.* **41**, 105–120.
- Merlin, C., Masters, M., McAteer, S. and Coulson, A. (2003) “Why is carbonic anhydrase essential to *Escherichia coli*?”, *J. Bacteriol.* **185**, 6415–6424.
- Miller, G. L. (1959) “Use of Dinitrosalicylic acid reagent for determination of reducing sugar” *Analytical Chemistry*, **31**(3), 426–428.
- Millero, F.J., Graham, T.B., Huang, F., Bustos-Serrano, H. and Pierrot, D., (2006) “Dissociation constants of carbonic acid in seawater as a function of salinity and temperature”. *Marine Chemistry*, **100**, 80–94.
- Mills, G.A. and Urey, H.C. (1940) “The kinetics of isotopic exchange between carbon dioxide, bicarbonate ion, carbonate ion and water” *J. Am. Chem. Soc.* **62**, 1019–1026.

- Mingjia, Z., Rongxin, SU., Wei, QI., Ruoyu , DU., Zhimin , HE., (2011) “Enzymatic hydrolysis of cellulose with different crystallinities studied by Means of Sec-Malls”, *Chinese Journal of Chemical Engineering*, **19(5)**, pp.773–778.
- Mokomele, T., Callanan, L. and Clarke, K., (2011) “Ethanol production from xylose and glucose by *Zymomonas mobilis* for the development of a membrane bioreactor”. *crses.sun.ac.za*.
- Montenecourt, B.S. (1985) “*Zymomonas*, a unique genus of bacteria”, *Biotechnol. Ser.* **6**, 261–289. Benjamin Cummings, Menlo Park, CA.
- Moon, J. H., Lee, H. J., Park, S. Y., Song, J. M., Park, M. Y., Park, H. M., Sun, J., Park, J. H.,
- Moo-Young, M. and Blanch, H., (1981) *Design of biochemical reactors mass transfer criteria for simple and complex systems*, Advances in biochemical engineering, 11, 1-69.
- Mrozik, A., Piotrowska-Seget, Z. and Łabuzek, S., (2004) “Cytoplasmatic bacterial membrane responses to environmental perturbations” *Polish Journal of Environmental Studies*, **13(5)**, 487–494.
- Mueller, R.F., (1996) “Bacterial transport and colonitation in low nutrien environments”. *Per g a m o n*, *Pergmona*, **30(406)**, 2681–2690.
- Mulakhudair, A. R., Hanotu, J. and Zimmerman, W., (2016.) “Exploiting ozonolysis-microbe synergy for biomass processing: lignocellulosic biomass pretreatment”, *Biomass and Bioenergy*, **93**, 1–21.
- Müller, V., (2001) “Bacterial Fermentation”. *Encyclopaedia of Life Science*, 1-7.
- Mussatto, S. and Teixeira, J., (2010) “Lignocellulose as raw material in fermentation processes”. *Current Research, Technology and Education Topics in Applied Microbiology and Microbial Biotechnology*, 897–907.
- Nadeem, M.T., (2009) *Production, Purification and Characterization of Carboxymethyl Cellulase For Food Applications*. PhD thesis, University of agricultur, Faisalabad.
- Nair, P., (1995) “Currently practised sterilization methods-some inadvertent consequences”. *J Biomater Appl.*, **10**, 121-135.
- Narang, A. and Pilyugin, S.S., (2007) “Bacterial gene regulation in diauxic and non-diauxic growth”. *Journal of Theoretical Biology*, **244**, 326–348.
- Neale, A., Scopes, R. Kelly, J. M. and Wettenhall, R. E.H., (1986) “The two alcohol dehydrogenases of *Zymomonas mobilis*”. *European Journal of Biochem.*, **124**, 119–124.
- Nelson, L., Lehninger, A., D. L., and Cox, M. M. (2008) *Lehninger principles of biochemistry*, New York, Worth Publishers.

- Neramittagapong, A., Attaphaiboon, W. and Neramittagapong, S., (2008) “Acetaldehyde production from ethanol over Ni-based catalysts”. *Chiang Mai J Sci*, **35(1)**, 171–177.
- Neveling, U.T.E., Klasen, R., Bringer-Meyer and Sahm, H., (1998) “Purification of the Pyruvate Dehydrogenase Multienzyme Complex of *Zymomonas mobilis* and Identification and Sequence Analysis of the Corresponding Genes. *J. Bacterio*, **180(6)**, 1540–1548.
- Nipkow, A., Sonnleitner, B. and Fiechter, A., (1985) “Effect of carbon dioxide on growth of *Zymomonas mobilis* in continuous culture” *Microbe Wiki*, **21**, 287–291.
- Noor, E., Bar-Even, A., Flamholz, A., Lubling, Y., Davidi, D. and Milo, R., (2012) “An integrated open framework for thermodynamics of reactions that combines accuracy and coverage”. *Bioinformatics*, **28(15)**, 2037–2044.
- Noordmans, J., Wit, P. J., VanderMei, H. C., and Busscher, H. J. (1997) “Detachment of polystyrene particles from collector surfaces by surface tension forces induced by air-bubble passage through a parallel plate flow chamber” *Journal of Adhesion Science and Technology*, *11*(January), 957–969.
- Novitsky, J. A. And Morita, R.Y., (1976) “Morphological characterization of small cells resulting from nutrient starvation of a psychrophilic marine vibrio” *Applied and Environmental Microbiology*, **32(4)**, 617–622.
- Ornston, L. N. and Stanier R. Y.. (1966) “The Conversion of Catechol and Protocatechuate to g-Ketoadipate by *Pseudomonas putida*”, *The Journal of Biological Chemistry*, **241(14)**, 3776–3788.
- Osman, Y.A. and Ingram, L.O., (1985) “Mechanism of ethanol inhibition of fermentation in *Zymomonas mobilis* CP4”. *Journal of Bacteriology*, **164(1)**, 173–180.
- Oulé, M.,Tano, K., Bernier, A-M and Arul, J., (2006) “*Escherichia coli* inactivation mechanism by pressurized CO₂”, *Can. J. Microbiol.*, **52**, 1208–1217.
- Pappas, K.M., Galani, I. and Typas, M. A, (1997) “Transposon mutagenesis and strain construction in *Zymomonas mobilis*” *Journal of applied microbiology*, **82(3)**, 379–388.
- Park, S., Baker, J., Himmel, M. E, Parilla, P.A. and Johnson, D.K., (2010) “Cellulose crystallinity index: measurement techniques and their impact on interpreting cellulase performance”, *Biotechnology for Biofuels*, **3**, 1–10.
- Park, S.E., Chao, M. and Raj, P. A, (2009) “Mechanical properties of surface-charged poly(methyl methacrylate) as denture resins”, *International journal of dentistry*,**2009**, 1-6.
- Park, S.H., Oh, K.H. and Kim, C.K., (2001) “Adaptive and cross-protective responses of *Pseudomonas* sp. DJ-12 to several aromatics and other stress shocks” *Current Microbiology*, **43(3)**, 176–181.

- Parmar, R. and Majumder, S.K., (2013) “Microbubble generation and microbubble-aided transport process intensification—A state-of-the-art report”. *Chemical Engineering and Processing: Process Intensification*, **64**, 79–97.
- Pentjuss, A., Odzina, I., Kostromins, A., Fell, D. A., Stalidzans, E. and Kalnenieks, U. (2013) “Biotechnological potential of respiring *Zymomonas mobilis*: A stoichiometric analysis of its central metabolism”, *Journal of Biotechnology*, **165**(1), 1–10.
- Pereira, M.O., Kuehn, M., Wuertz, S. Neu, T. and Melo, L. F. (2002) “Effect of flow regime on the architecture of a *Pseudomonas fluorescens* biofilm”, *Biotechnology and Bioengineering*, **78**(2), 164–171.
- Pérez, J., Muñoz-Dorado, J., de la Rubia, T. and Martí´nez, J., (2002) “Biodegradation and biological treatments of cellulose, hemicellulose and lignin: an overview”, *Int Microbiol*, **5**, 53–63.
- Perlack, R., Wright, L. and Turhollow, A., (2005) “Biomass as feedstock for a bioenergy and bioproducts industry: the technical feasibility of a billion-ton annual supply”, Report, U.S. Department of Energy and Agriculture.
- Pinches, A. and Pallent, L.J., (1986) “Rate and yield relationships in the production of xanthan gum by batch fermentations using complex and chemically defined growth media”, *Biotechnology and bioengineering*, **28**(10), 1484–96.
- Poulsen, O. and Petersen, L., (1988) “Growth of *Cellulomonas* sp. ATCC 21399 on different polysaccharides as sole carbon source induction of extracellular enzymes” *Applied microbiology and biotechnology*, **29**, 480–484.
- Premnath, V., Harris, W.H., Jasty, M. and Merrill, E.W., (1996) “Gamma sterilization of UHMWPE articular implants: an analysis of the oxidation problem”. *Biomaterials*, **17**, 1741–1753.
- Putnina, A. and Kukle, S., (2012) “Steam Explosion as the pretreatment method of lignocellulosic Biomass”. Material Science. *Textile and Clothing Technology*, **7**, 80–83.
- Qureshi, N. and Blaschek, H., (2001) “Recovery of butanol from fermentation broth by gas stripping”. *Renewable Energy*, **22**, 557–564.
- Ragnar, M., Eriksson, T. and Reitberger, T., (1999) “Radical formation in ozone reactions with lignin and carbohydrate model compounds”, *Holzforschung*, **53**, 292–298.
- Rajoka, M. and Malik, K., (1997) “Cellulase production by *Cellulomonas biazotea* cultured in media containing different cellulosic substrates”, *Bioresource Technology*, **59**, pp.21–27.
- Rakness, K., Gordon, G., Langlais, B., Masschelein, W., Matsumoto, N., Richard, Y., Robson, M. and Somiya, I., (1996) “Guideline for measurement of ozone concentration in the process gas from an ozone generator”. *Ozone Science and Engineering*, **18**, 209–229.

- Ram, L., Kaur, K. and Sharma, S., (2014) “Screening isolation and characterization of Cellulase Producing microorganisms from Soil” *International Journal of Pharmaceutical Science Invention ISSN*, **3(3)**, 2319–6718.
- Rando, R.R., (1974) “Allyl alcohol-induced irreversible inhibition of yeast alcohol dehydrogenase”. *Science*, **23**, 2328–2331.
- Rani, K., Swamy, M. and Seenayya, G., (1997) “Increased ethanol production by metabolic modulation of cellulose fermentation in *Clostridium thermocellum*” *Biotechnology letters*, **19(8)**, 819–823.
- Rayi, N. and Ananthula, V., (2014) “Biodegradation of phenolic wastewater in a bubble column bioreactor with internal draft tube”. *Indian .J. Chem. Technol.*, **21**, 44–48.
- Reyes, L. and Scopes, R. K. (1991) “Membrane-associated ATPase from *Zymomonas mobilis*, purification and characterization”, *BBA*, **1068**, 174–178.
- RFA, Renewable Fuels Association, (2007). *Climate of opportunity*, the united states.
- Riedel, T.E., Berelson, W. M., Nealson, K. H. and Finkel, S. E., (2013) “Oxygen consumption rates of bacteria under nutrient-limited conditions” *Applied and Environmental Microbiology*, **79(16)**, 4921–4931.
- Rogers, P. L., Lee, K. J., Skotnicki, M. L., and Tribe, D. E. (1982) “Ethanol production by *Zymomonas mobilis*” *Vacuum*, 37–84.
- Rogers, P., Lee, K. and Tribe, D., (1979) “Kinetics of alcohol production by *Zymomonas mobilis* at high sugar concentrations”. *Biotechnology Letters*.
- Roman, H.J., (2004) *The degradation of lignocellulose in a chemically and biologically generated sulphidic environment*. PhD thesis, Rhodes University, South Africa.
- Romano, P., Suzzi, G., Turbanti, L. and Polsinelli, M., (1994) “Acetaldehyde production in *Saccharomyces cerevisiae* wine yeasts”, *FEMS Microbiology Letters*, **118**, 213–218.
- Roszak, D.B. and Colwell, R.R., (1987) “Survival strategies of bacteria in the natural environment”, *Microbiological reviews*, **51(3)**, pp.365–379.
- Rubio, F. C., Fernandez, F. G., Perez, J. A., Camacho, F. G., and Grima, E. M., (1999) “Prediction of dissolved oxygen and carbon dioxide concentration profiles in tubular photobioreactors for microalgal culture”. *Biotechnology and Bioengineering*, **62(1)**, 71–86.
- Russell, J.B. and Strobel, H.J., (1990) “ATPase-dependent energy spilling by the ruminal bacterium, *Streptococcus bovis*”, *Archives of Microbiology*, **153**, 378–383.
- Saharkhiz, S., Mazaheri, D. and Shojaosadati, S.A., (2013) “Evaluatation of bioethanol production fro carob pods by *Zymomonas mobilis* and *Saccharomyces cerevisiae* in solid submerged fermentation” *Preparative Biochemistry and Biotechnology*, **43(5)**, pp.415–430.

- Sakai, K., and Uprichard, J. U., (1991) "Ozone degradation of cellulose model compounds" *J. Fat. Agr., Kyushu Univ.*, **36**, 45–53.
- Sanin, S.L., Sanin, F.D. and Bryers, J.D., (2003) "Effect of starvation on the adhesive properties of xenobiotic degrading bacteria" *Process Biochemistry*, **38(6)**, 909–914.
- Sarkar, N. and Aikat, K., (2012) "Alkali pretreatment of rice straw and enhanced cellulase production by a locally isolated fungus *Aspergillus fumigatus* NITDGPKA3". *J. Microbiol. Biotech. Res.*, **2(5)**, 717–726.
- Saxena, R.C., Adhikari, D.K., and Goyal, H.B., (2009) "Biomass-based energy fuel through biochemical routes: A review". *Renewable and Sustainable Energy Reviews*, **13**, 167–178.
- Schell, M. A. (1987) "Purification and Characterization of an Endoglucanase from *Pseudomonas solanacearum*" *Applied and environmental microbiology*, **53(9)**, 2237–2241.
- Schrag, D.P., (2007) "Preparing to capture carbon". *Science*, **315**, 812–813.
- Seo, J-S., Chong, H., Park, H.S., Yoon, K-O., Jung, C., Kim, J.J., Hong, J.H., Kim, H., Kim, J-H., Kil, J-I., Park, C-J., Oh, H-M., Lee, J-S., Jin, S-J., Um, H-W., Lee, H-J., Oh, S-J., Kim, J-Y., Kang, H.J., Lee, S.Y., Lee, K.J. and Kang, H.S., (2005) "The genome sequence of the ethanologenic bacterium *Zymomonas mobilis* ZM4". *Nature Biotechnology*, **23**, 63–68.
- Serizawa, A., Inui, T., Yahiro, T. and Kawara, Z., (2003) "Laminarization of micro-bubble containing milky bubbly flow in a pipe". *3rd European-Japanese Two-Phase Flow Group Meeting*, 21–27.
- Sethi, S., Datta, A., Lal Gupta, B. And Gupta, S. (2013) "Optimization of cellulase production from bacteria isolated from soil" *ISRN Biotechnology*, 1-7.
- Shah, D., Johnston, T.P. and Mitra, A.K., (1998) "Thermodynamic parameters associated with guanidine HCl- and temperature-induced unfolding of *bFGF*", *International Journal of Pharmaceutics*, **169**, 1–14.
- Sharma, P. K., Gibcus, M. J., Van Der Mei, H. C., and Busscher, H. J. (2005) "Influence of fluid shear and microbubbles on bacterial detachment from a surface" *Applied and Environmental Microbiology*, **71(7)**, 3668–3673.
- Sheu, K.-F. R. and BLASS, J. P. (1999) "The α -Ketoglutarate Dehydrogenase Complex" *Annals of the New York Academy of Sciences*, **893**, 61–78.
- Sikkema, J., de Bont, J.A. and Poolman, B., (1995) "Mechanisms of membrane toxicity of hydrocarbons" *Microbiological reviews*, **59(2)**, 201–222.
- Singh, A., Singh, N. and Bishnoi, N., (2009) "Production of cellulases by *Aspergillus heteromorphus* from wheat straw under submerged fermentation". *International Journal of Civil and Environmental Engineering*, **1**, 23–26.

- Singh, D. and Trivedi, R., (2013) "Acid and alkaline pretreatment of lignocellulosic biomass to produce ethanol as biofuel", *Int.J.ChemTech Res*, **5(2)**, 727–734.
- Sivamani, I., Anugraka, S. and Baskar, R., (2015) "Optimization of ethanol production from mixed feedstock of cassava peel and cassava waste by coculture of *Saccharomycopsis fibuligera* NCIM 3161 and *Zymomonas Mobilis* MTCC 92" *Chemical and Bioprocess Engineering Trends and Developments*. 14–24.
- Skoog, West, Holler, Crouch, (2000) "Analytical chemistry: An introduction", Brooks/Cole Cengage learning, USA.
- Slaughter, J. C., (1989) "The effects of carbon dioxide on Yeasts" *Biotechnology Applications in Beverage Production*, Netherland, .49-64.
- Smith, R., (2005) *Cell Technology for Cell Products*, Harrogate, UK: Springer Science and Business Media.
- Sootsuwan, K., Thanonkeo, P., Keeratirakha, N., Thanonkeo, S. Jaisil, P. and Yamada, M. (2013) "Sorbitol required for cell growth and ethanol production by *Zymomonas mobilis* under heat, ethanol, and osmotic stresses" *Biotechnology for biofuels*, **6(1)**, 1-13.
- Souza-Corrêa, J., Ridenti, M., Oliveira, C., Araújo, S.R. and Amorim, J., (2013) "Decomposition of lignin from sugar cane bagasse during ozonation process monitored by optical and mass spectrometries". *The Journal of Physical Chemistry*, **117**, 3110–3119.
- Spilimbergo, S. and Bertucco, A., (2003) "Non-thermal bacterial inactivation with dense CO₂", *Biotechnology and Bioengineering*, **84(6)**, 627–638.
- Spilimbergo, S., Elvassore, N. and Bertucco, A., (2002) "Microbial inactivation by high-pressure". *The Journal of Supercritical Fluids*, **22**, 55–63.
- Sprenger, G.A., (1996) "Carbohydrate metabolism in *Zymomonas mobilis*: A catabolic highway with some scenic routes" *FEMS Microbiology Letters*, **145**, 301–307.
- Stride, E. and Edirisinghe, M., (2008) "Novel microbubble preparation technologies", *Soft Matter*, **4(12)**, 2350.
- Suárez, C.G., Noordmans, J., Van der Mei, H. C. and Busscher, H. J., (1999) "Removal of colloidal particles from quartz collector surfaces as stimulated by the passage of liquid-air interfaces", *Langmuir*, **15(15)**, 5123–5127.
- Sukumaran, R., Singhania, R. R. and Pandey, A. (2005) "Microbial cellulases-production, applications and challenges", *Journal of Scientific and Industrial Research*, **64**, pp.832–844.
- Sun, X.F., Xu, F., Sun, R.C. Fowler,P. and Baird, M. S., (2005) "Characteristics of degraded cellulose obtained from steam-exploded wheat straw". *Carbohydrate Research*, **340**, 97–106.

- Sun, Y. and Cheng, J., (2002) "Hydrolysis of lignocellulosic materials for ethanol production: a review". *Bioresource Technology*, **83**, 1–11.
- Swart, J., Jiang, J. and Ho, P., (2007) "Risk perceptions and GM crops: the case of China", *Taylor Biotechnol*, **3(3)**, 11-28.
- Sweeney, N., Laux, D. and Cohen, P., (1996) "*Escherichia coli* F-18 and *E. coli* K-12 eda mutants do not colonize the streptomycin-treated mouse large intestine". *Infection and Immunity*, **64(9)**, 3504-3511.
- Swings, J., and De Ley, J. (1977) "The biology of *Zymomonas*" *Bacteriological Reviews*, **41(1)**, 1–46.
- Takahashi, M., (2005) "ζ potential of microbubbles in aqueous solutions: electrical properties of the gas-water interface". *J. Phys. Chem. B.*, **109**, 21858–21864.
- Takahashi, M., Chiba, K. and Li, P., (2007) "Free-radical generation from collapsing microbubbles in the absence of a dynamic stimulus". *J. Phys. Chem. B.*, **111**, 1343–1347.
- Tanaka, H., Ishikawa, H., Osuga, K. and Takagi, Y., (1990) "Fermentative ability of *Zymomonas mobilis* under various oxygen supply conditions in batch culture". *J. Fermentation and Biotechnol.*, **69(4)**, 234–239.
- Tekic, M., Šijački, I.M., Tokić, M.S., Kojić, P.S., Petrović, D.L.J., Lukić, N. L.J. and Popovic, S.S., (2014) "Hydrodynamics of a self-agitated draft tube airlift reactor". *Chem. Ind. Chem. Eng. Q.*, **20(1)**, 59–69.
- Terasaka, K., Hirabayashi, A., Nishino, T., Fujioka, S. and Kobayashi, D., (2011) "Development of microbubble aerator for wastewater treatment using aerobic activated sludge". *Chemical Engineering Science*, **66**, 3172–3179.
- Tesař, V. and Bandalusena, H., (2011) "Bistable diverter valve in microfluidics" *Experiments in Fluids*, **50**, 1225–1233.
- Tesař, V., Hung, C. and Zimmerman, W., (2006) "No-moving-part hybrid-synthetic jet actuator". *Sensors and Actuators A: Physical*, **125(2)**, 159-169.
- Teymouri, F., Laureano-Peres, L., Alizadeh, H. and Dale, B.E., (2004) "Ammonia fiber explosion treatment of corn stover". *Human Press Inc.* **113–116**, 951-963.
- Timmis, K., (2002) "*Pseudomonas putida*: a cosmopolitan opportunist par excellence" . *Environmental Microbiology*, **4(12)**, 779–781.
- Todhanakasem, T., Sangsutthiseree, A., Areerat, K., Young, G. M., and Thanonkeo, P. (2014) "Biofilm production by *Zymomonas mobilis* enhances ethanol production and tolerance to toxic inhibitors from rice bran hydrolysate" *New Biotechnology*, **31(5)**, 451–459.
- Trček, J., Jernejc, K. and Matsushita, K., (2007) "The highly tolerant acetic acid bacterium *Gluconacetobacter europaeus* adapts to the presence of acetic acid by changes in lipid

- composition, morphological properties and PQQ-dependent ADH expression”, *Extremophiles*, **11(4)**, 627–635.
- Trček, J., Mira, N.P. and Jarboe, L.R., (2015) “Adaptation and tolerance of bacteria against acetic acid”, *Applied Microbiology and Biotechnology*, **99**, 6215–6229.
- Truong, K. N. and Blackburn, J. W. (1984) “The stripping of organic chemicals in biological treatment processes”, *Environmental progress and sustainable energy*, **3(3)**, 143-152.
- Tu, J., Yang, Z., Hu, C. and Qu, J., (2013) “Characterization and reactivity of biogenic manganese oxides for ciprofloxacin oxidation”. *JES*, **26(5)**, 1154–1161.
- U . S . Department of Energy Biomass Program, (2009). *Major Biomass Pathways*, the united states.
- Valley, G. and Rettger, L.F., (1927) “The influence of carbon dioxide on bacteria” *J. Bacteriol.*, **14(2)**, 101-137.
- Vanbogelen, R. A., Kelley, P. M., and Neidhardt, F. C. (1987) “Differential induction of heat shock, SOS, and oxidation stress regulons and accumulation of nucleotides in *Escherichia coli*” *Journal of Bacteriology*, **169(1)**, 26–32.
- Vardar-Sukan, F., (1998) “Foaming: Consequences, prevention and destruction” *Biotechnology Advances*, **16**, 913–948.
- Veeramallu, U.K. and Agrawal, P. (1986) “The effect of CO₂ ventilation on kinetics and yields of cell-mass and ethanol in batch cultures of *Zymomonas mobilis*” *Biotechnol. Lett.* **8**, 811–816.
- Vidal, P. and Molinier, J., (1988) “Ozonolysis of lignin—Improvement of in vitro digestibility of poplar sawdust”. *Biomass*, **16**, 1–17.
- Viikari, L. and Korhola, M., (1986) “Fructose metabolism in *Zymomonas mobilis*” *Applied Microbiology and Biotechnology*, **24(6)**, 471–476.
- Watanabe, T., Furukawa, S., Hirata, J., Koyama, T., Ogihara, H. and Yamasaki, M., (2003) “Inactivation of *Geobacillus stearothermophilus* spores by high-pressure carbon dioxide treatment”. *Applied and Environmental Microbiology*, **69(12)**, 7124–7129.
- Watson, K. (1990) “Microbial stress proteins” *Adv. Microb. Physiol.* **31**, 184– 223.
- Webb, C. and Kamat, S.P., (1993) “Improving fermentation consistency through better inoculum preparation” *World Journal of Microbiology & Biotechnology*, **9(3)**, pp.308–312.
- Wecker, M.S.A. and Zall, R.R., (1987) “Production of Acetaldehyde by *Zymomonas mobilis*”. *Applied and Environmental Microbiology*, **53(12)**, 2815-2820.
- Wecker, M.S.A., (1987) *The production of acetaldehyde using Zymomonas mobilis*. Master thesis. Cornell University, the united states.

- Wendisch, V. F., De Graaf, A. A., Sahm, H. and Eikmanns, B. J., (2000) “Quantitative determination of metabolic fluxes during co-utilization of two carbon sources: comparative analyses with *Corynebacterium glutamicum* during growth on Acetate and/or Glucose”, *J. Bacteriol.*, **182(11)**, 3088–3096.
- Wesley, D.J., (2015.) “The role of surface wettability on bubble formation in air-water systems” The university of Sheffield, UK.
- White, A., Burns, D. and Christensen, T.W., (2006) “Effective terminal sterilization using supercritical carbon dioxide”, *Journal of Biotechnology*, **123(4)**, 504–15.
- WHO, World Health Organisation, (1999) *IARC monographs on the evaluation of carcinogenic risks to humans*, France.
- Widdel, F., (2010) “Theory and measurement of bacterial growth”, *Di dalam Grundpraktikum Mikrobiologie*, **4**, 1–11.
- Williams, J., (2002) “Keys to bioreactor selections”. *Chemical Engineering Progress*, 34–41.
- Wills, C. and Jörnvall, H. (1979) “The two major isozymes of yeast alcohol dehydrogenase.,” *Eur. J. Biochem*, **99(2)**, 323–331.
- Wills, C., P. Kratofil, D. Londo, and T. Martin, (1981) “Characterization of the two alcohol dehydrogenases of *Zymomonas mobilis*”, *Arch. Biochem. Biophys*, **210**:775-780.
- Windeisen, E., Strobel, C. and Wegener, G., (2007) “Chemical changes during the production of thermo-treated beech wood”, *Wood Sci Technol*, **41**, 523–536.
- Wong, T.S., Schwaneberg, U., Stürmer, R., Hauer, B. and Breuer, M., (2006) “A filter paper-based assay for laboratory evolution of hydrolases and dehydrogenases”, *Combinatorial chemistry and high throughput screening*, **9**, 289–293.
- Worden, R., M. and Marshall D. Bredwell, (1998) “Mass-Transfer Properties of Microbubbles, Analysis Using a Dynamic Model”, *Biotechnology progress*, **14(1)**, 39 – 46.
- Xia, L. and Cen, P., (1999) "Cellulase production by solid state fermentation on lignocellulosic waste from the xylose industry", *Process Biochemistry*, **34**, 909–912.
- Xu, Z. and Yu, J., (2008) “Hydrodynamics and mass transfer in a novel multi-airlifting membrane bioreactor”, *Chemical Engineering Science*, **63**, 1941–1949.
- Xue, C., Zhao, J., Liu, F., Lu, C., Yang, S-T., Bai, F-W., (2013) “Two-stage *in situ* gas stripping for enhanced butanol fermentation and energy-saving product recovery”, *Bioresource Technology*, **135**, pp.396–402.
- Yakubu-Gumery, F., (2010) *Mixing characteristics of draft tube airlift bioreactor using the electrical resistance tomography*. Master thesis, Ryerson University, Canada.

- Yamamoto, H., Horii, F. and Hirai, A., (1996) “*In situ* crystallization of bacterial cellulose II. Influences of different polymeric additives on the formation of celluloses Ia and Ib at the early stage of incubation”, *Cellulose*, **3**, 229–242.
- Yamane, T., Achiha, R., Namioka, T. and Yukumoto, M., (2013) “Bubble stripping in closed system to remove residual methanol from crude biodiesel”, *Eur. J. Lipid Sci. Technol*, **115**, 1183–1192.
- Yang, B., Dai, Z., Ding, S. and Wyman C.E., (2011) “Enzymatic hydrolysis of cellulosic biomass”, *Biofuels*, **2**, 421–450.
- Yasina, M., Bhuttob, A., Bazmi, A.A., and Karim, S., (2010) “Efficient utilization of rice-wheat straw to produce value-added composite products”, *Int. J. Chem. Environ. Eng.*, **1(2)**, 136-143.
- Ying, K., (2013) *Microbubble Driven Airlift Bioreactor for CO₂ Sequestration and Algal Biomass Production*. PhD thesis, The University of Sheffield, UK.
- Ying, K., Gilmour, D.J., Shi, Y. and Zimmerman, W.B., (2013) “Growth Enhancement of *Dunaliella salina* by Microbubble Induced Airlift Loop Bioreactor (ALB)—The Relation between Mass Transfer and Growth Rate”, *Journal of Biomaterials and Nanobiotechnology*, **4**, 1–9.
- Yugay, D., (2011) “Attenuated Total Reflectance Fourier Transform Infrared Spectroscopy”. *Analytical Spectroscopy*, 1–10.
- Zhang, X. and Houk, K.N., (2005) “Acid / Base Catalysis by Pure Water : The Aldol Reaction”, *Journal of Organic Chemistry*, **70(24)**, 9712–9716.
- Zhang, X., Wang, T., Zhou, W., Jia, X. and Wang, H. (2013) “Use of a Tn5-based transposon system to create a cost-effective *Zymomonas mobilis* for ethanol production from lignocelluloses”, *Microbial cell factories*, 12-41.
- Zhang, Y. (2008) *Geochemical kinetics*, Princeton University press, Princeton and oxford.
- Zheng, Y., Pan, Z. and Zhang, R., (2009) “Overview of biomass pretreatment for cellulosic ethanol production”. *Int J Agric and Biol Eng*, **2(3)**, 51–68.
- Zhu, H., Gonzalez, R. and Bobik, T. A., (2011) “Coproduct of acetaldehyde and hydrogen during glucose fermentation by *Escherichia coli*”, *Applied and Environmental Microbiology*, **77(18)**, 6441–50.
- Zikmanis, P., Kruce, R. and Auzina, L., (1999) “Molar growth yields of *Zymomonas mobilis* on glucose after the transition from anaerobic to aerobic continuous growth” *Acta Biotechnologica*, **19(1)**, 69–75.
- Zimmerman, W., Tesar, V., Butler, S. and Bandulasena, H. C. H., (2008) “Microbubble generation”. *Recent Patents on Engineering*, **2(1)**, 1–8.

- Zimmerman, W.B., Hewakandamby, B.N., Tesař, V., Bandulasena, H. C. H. and Omotowa, O.A., (2009) “On the design and simulation of an airlift loop bioreactor with microbubble generation by fluidic oscillation”. *Food and Bioproducts Processing*, **87**, 215–277.
- Zimmermann, W.B., Al-Mashhadani, M. K.H. and Bandulasena, H.C.H., (2013) “Evaporation dynamics of microbubbles”, *Chemical Engineering Science*, **101**, 865–877.

Appendices

Appendix A: Cultural media compositions

M9 broth medium composition

Components	Concentration as a percentage
Sodium Carboxymethyl cellulose (CMC)	1%
Na ₂ HPO ₄	0.12%
K ₂ HPO ₄	0.06%
NaCl	0.01%
NH ₄ Cl	0.02%
MgSO ₄ .7H ₂ O	2 ml of 1M solution
CaCl ₂	1 ml of 1M solution
Water	Distilled water is used to dissolve components and to complete the final volume to 1 litre

Carboxymethyl cellulose Medium (CMC Medium) composition

Components	Concentration as a percentage
Sodium Carboxymethyl cellulose (CMC)	1%
Yeast extract	0.5%
MgSO ₄ .7H ₂ O	0.02%
NH ₄ H ₂ PO ₄	0.02%
Agar (Agar medium)	2%
Water	Distilled water is used to dissolve components and to complete the final volume to 1 litre

Wheat straw Medium (WS Medium) composition

Components	Concentration as a percentage
Wheat straw	1%
Yeast extract	0.5%
MgSO ₄ .7H ₂ O	0.02%
NH ₄ H ₂ PO ₄	0.02%
Agar (Agar medium)	2%
Water	Distilled water is used to dissolve components and to complete the final volume to 1 litre

Lignin Medium (L Medium) composition

Components	Concentration as a percentage
Lignin solution	0.5%
Glucose	0.01%
KH ₂ PO ₂	0.05%
(NH ₄) ₂ SO ₄	0.01%
MgSO ₄ .7H ₂ O	0.05%
Yeast extract	0.05%
Water	Distilled water is used to dissolve components and to complete final volume to 1 litre

4 % sucrose standard medium (4SSM) composition

Components	Concentration as a percentage
Sucrose	4%
Peptone	2%
Yeast extract	1%

Appendices

KH ₂ PO ₄	0.1%
(NH ₄) ₂ SO ₄	0.05%
MgSO ₄ .7H ₂ O	0.05%
Agar (agar medium)	2%
Water	Distilled water is used to dissolve components and to complete the final volume to 1 litre

Acid fuchsin agar composition

Components	Concentration as a percentage
KH ₂ PO ₄	3.18%
Na ₂ HPO ₄ .7H ₂ O	0.88%
Acid fuchsin	0.02%
Agar	2%
Water	Distilled water is used to dissolve components and to complete the final volume to 1 litre

The fermentation medium (FM) composition

Components	Concentration
Glucose (hydrolysate)	4%
Peptone	0.25%
Yeast extract	1%
KH ₂ PO ₄	0.1%
(NH ₄) ₂ SO ₄	0.05%
MgSO ₄ .7H ₂ O	0.05%
Water	Distilled water is used to dissolve components and to complete the final volume to 1 litre. pH will be set to 5.5

Pre-inoculum medium composition

Components	Concentration
Glucose	50 g
Yeast extract	10 g
Water	Distilled water is used to dissolve components and to complete the final volume to 1 litre. pH will be set to 5.5

Second stage inoculum medium composition

Components	Concentration
Glucose	50-150 g
Yeast extract	10 g
(NH ₄) ₂ SO ₄	1 g
MgSO ₄ .7H ₂ O	0.5 g
Sorbitol	1 g (if applicable)
Water	Distilled water is used to dissolve components and to complete the final volume to 1 litre. pH will be set to 5.5

Storage medium composition

Components	Concentration
Glucose	50 g
Yeast extract	5 g
Glycerol	200
Water	Water is used to dissolve components and to complete the final volume to 1 litre. pH will be set to 5.5

- This medium will be kept in a freezer at -20°C.

Appendices

RM medium

Components	Concentration
Glucose	20 g
Yeast extract	10 g
K ₂ HPO ₄	2 g
Agar (if needed)	15.0 g
Water	Distilled water is used to dissolve components and to complete the final volume to 1 litre. pH was set to 6

The synthetic medium (SM) composition

Components	Concentration
Glucose (hydrolysate)	20 and 40 g
NaCl	0.5 g
Na ₂ HPO ₄	0.82 g
KH ₂ PO ₄	0.95 g
Trace elements	1 ml
Metal 44 Solutions	1 ml
Trace elements solution	
Nitrotriactic acid	20 g
MgSO ₄	28.9 g
CaCl ₂	6.67 g
(NH ₄) ₆ MO ₇ .O ₂₄	18.5 g
FeSO ₄	0.198 g
Water	Distilled water is used to dissolve components and to complete the final volume to 1 litre
Metal 44 Solution	
ZnSO ₄ .7H ₂ O	10.95 g
FeSO ₄ .7H ₂ O	5 g
Sodium EDTA	2.5 g
MnSO ₄ .7H ₂ O	1.54 g
CuSO ₄ .5H ₂ O	0.392 g
Co(NO ₃) ₂ .6H ₂ O	0.248 g
Na ₂ B ₄ O ₇ .10H ₂ O	0.177 g
Water	Distilled water is used to dissolve components and to complete the final volume to 1 litre
Calcium Pantothenate,	0.005 g
MgSO ₄	0.12 g
CaCl ₂	0.011 g
NH ₄ Cl	0.534 g
Water	Distilled water is used to dissolve components and to complete the final volume to 1 litre. pH will be set to 5.5

Appendix B: Measurement of ozone concentration using Potassium iodide method

Ozone concentration has been measured according to method, which has been proposed by Rakness et al., (1996).

1- Reagents preparations

- A- Unbuffered KI: dissolve 20 g of KI into 1 litre of distilled water.
- B- Sulfuric acid 2N: Mix 56 ml of concentrated sulfuric acid with 946 ml of distilled water.
- C- Sodium thiosulfate ($\text{Na}_2\text{S}_2\text{O}_3$) 1N: dissolve 250 g of sodium thiosulfate in 1 L of distilled water.
- D- Zinc chorine starch: mix 4 g of soluble starch with a little amount of cold distilled water and then disperse a thin starch paste into 100 ml of water containing 20 g zinc chloride. The solution is boiled till the volume is reduced to 100 ml. Finally, the solution is diluted with distilled water to a total volume of 1 litre and is mixed with 2 g of zinc chloride.
- E- Potassium dichromate ($\text{K}_2\text{Cr}_2\text{O}_7$) 0.1N: dissolve 4.904 g of potassium dichromate in 1 litre of distilled water.
- F- Distilled water: conductivity should be less than 10 micromhos/cm.

2- Methodology

- A- Preparing the standardisation of titrant (0.1N sodium thiosulfate): these reagents, which consist of 150 ml of distilled water, 1 ml of concentrated sulfuric acid, 20 ml of 0.1N of potassium dichromate, and 2 g of KI are mixed together in 250 ml of Erlenmeyer flask for 6 minutes in the dark. Sodium thiosulfate 0.1N is utilised to titrate till the yellow colour is almost disappeared. One millilitre of the starch indicator solution is added and continuous titration until the blue colour is gone. The normality of $\text{Na}_2\text{S}_2\text{O}_3$ titrant = $2 / \text{Na}_2\text{S}_2\text{O}_3$ used.
- B- Fill the 0.1N sodium thiosulfate titrant in 50ml Class A burette.
- C- Fill unbuffered KI (400 ml) in the gas-washing bottle.
- D- Flow bubble of ozone through glass washing bottle at flow rate 1-2 L/min. The better accuracy is obtained when ozone volume is at least 2 litres.
- E- Quickly add 10 ml of the 2N of sulfuric acid after bubbling has stopped.
- F- Transfer the liquid from gas washing bottle to 1 litre of Erlenmeyer flask.
- G- Titrate with 0.1N of sodium thiosulfate till the solution becomes a pale yellow.

H- Add 5 ml of the starch indicator to Erlenmeyer flask and continue titration until the blue colour is gone.

I- Record the used volume of the titrant.

J- Calculate the ozone concentration using:

$$\text{Ozone concentration (mg/l)} = \frac{24XV_tXN_t}{V} \quad (\text{Eq. I})$$

Where V is volume of bubble, V_t is volume of sodium thiosulfate used (ml), and N_t is normality of sodium thiosulfate.

Appendix C: Preparing *Zymomonas mobilis* biomass standard curve

Figure 1 describes the correlation of optical density from absorbance reading at 600 and *Z. mobilis* biomass concentration as dry weight (g/L). The optical density at 600 shows increasing in the turbidity due to increasing of cell number and density.

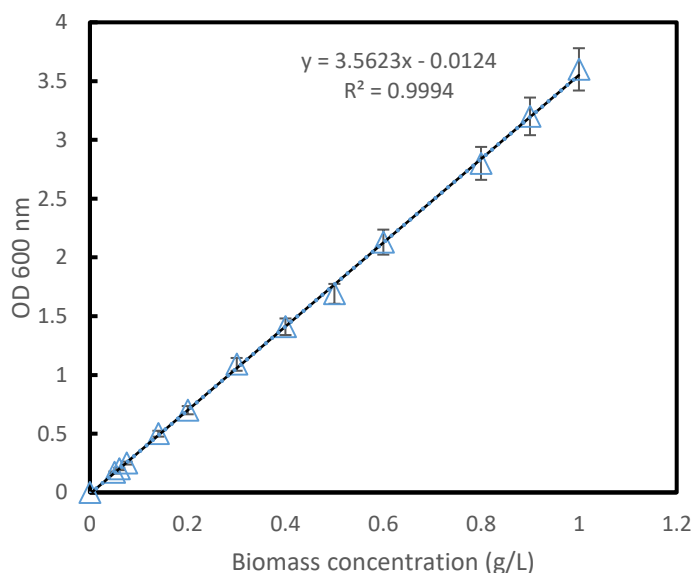


Figure 1: Calibration curve of absorbance against biomass concentration (g/L). Error bars depict standard deviation.

Figure 2 describes the correlation of the number of *Z. mobilis* cell (in CFU/mL) with the value of optical density from absorbance reading at 600. The number of cell is presented as CFU (Colony Forming Unit) which means the number of *Z. mobilis* cell that grows from a single colony.

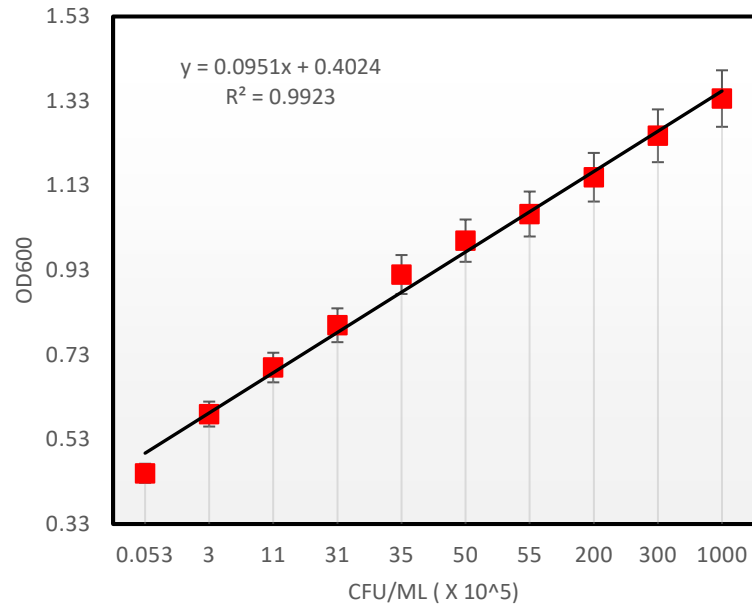


Figure 2: Calibration curve of absorbance against biomass concentration (CFU/ml). Error bars depict standard deviation.

The above two curves were used to work out the concentration of *Zymomonas mobilis* in the fermentation broth as a dry weight as well as CFU/ml.

Appendix D: Preparing glucose standard curve

Figure 3 describes the correlation of optical density from absorbance reading at 575 and glucose concentration (mg/ml). This curve is used to work out the concentration of glucose in the fermentation broth and the dilution was conducted to work out the concentration of glucose higher than 10 mg/ml.

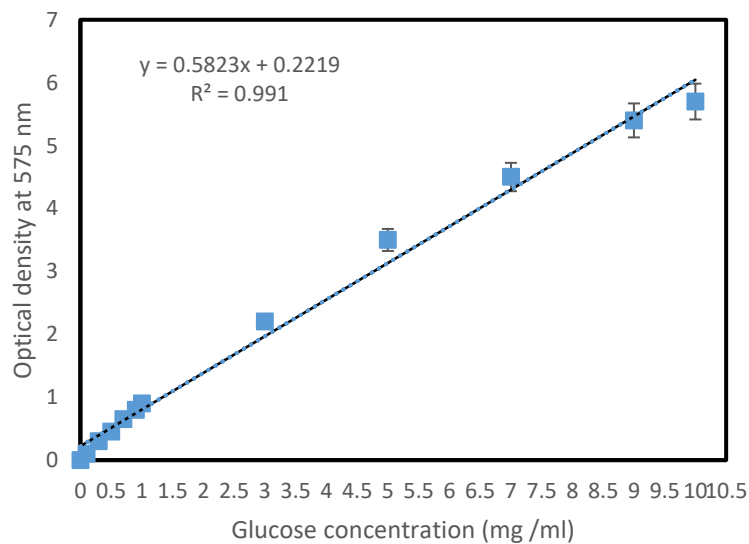


Figure 3: Calibration curve of absorbance against glucose concentration (mg/ml). Error bars depict standard deviation.

Appendix E: Identification of the fermentation products using GC/MS

The fermentation samples were centrifuged to separate the bacterial cells from the supernatant. Refrigerated Centrifuge - Legend RT was set at 5000 rpm for 3 minutes and supernatant (1 µL) was injected via manual injection using a 10 µL syringe (Thermo Scientific) into Gas chromatography (GC) equipped with a GCMS-QP2010 SE sense mass spectrometer (MS) (Shimadzu, UK) chromatograph. The samples were analysed using a DB-1MS capillary column (60 m × 0.25 mm I.D., 0.25-µm film thickness, Hewlett Packard, USA). The GC/MS was running with GCMSsolution, Shimadzu corporation version 4.4 software. The GC/MS method employed for the identifying of liquid products is described in Table 1:

Conditions (GC)	Setting
Injection temperature (°C)	250
Split ratio	50
Carrier flow rate (ml min ⁻¹)	3
Initial column temperature (°C)	40
Isothermal time 1 (min)	2
Ramp rate 1 (°C min ⁻¹)	3
Second temperature (°C)	87
Isothermal time 2 (min)	1
Ramp rate 2 (°C min ⁻¹)	10
Final column temperature (°C)	91
Detector temperature (°C)	250
Conditions (MS)	Setting
Ion source Temp (°C)	200
Interface Temp (°C)	305

The sample was introduced to the injection port of the GC by injecting 1 µL via manual injection using a 10 µL syringe (Thermo Scientific). Each sample was injected three times and the peak areas were averaged. Signal analysis was achieved using GCMSsolution, Shimadzu corporation version 4.4 software based on the library built in the system.

Appendix F: Quantification of acetaldehyde and Ethanol in the fermentation broth and condensates

Acetaldehyde, ethanol and ethyl acetate were analysed with the GC (Shimadzu, UK), equipped with FID detector and connected to a Varian Capillary column: CP-Sil 8 CB, model Agilent J&W (30 m L×0.32 mm ID×0.1 µm active phase thickness), with a maximum working temperature of 400 °C. The GC was running with Chromeleon 7.2 SR4 software. In this GC, the carrier gas was air, and N₂ was used as the make-up gas. A flow rate of 20 ml min⁻¹ of N₂

and 350 ml min⁻¹ of air were used to generate the detector flame. The GC method employed for the analysis of liquid products is described in Table 2:

Conditions	Setting
Injection temperature (°C)	200
Split ratio	150
Carrier flow rate (ml min ⁻¹)	20
Initial column temperature (°C)	35
Isothermal time 1 (min)	2
Ramp rate 1 (°C min ⁻¹)	10
Second temperature (°C)	100
Isothermal time 2 (min)	2
Ramp rate 2 (°C min ⁻¹)	10
Final column temperature (°C)	150
Detector temperature (°C)	250

The sample was introduced to the injection port of the GC by injecting 1 µL via manual injection using a 10 µL syringe (Thermo Scientific). Each sample was injected three times and the peak areas were averaged.

Signal analysis was achieved using Chromeleon 7.2 SR4 software based on a calibration curve built in the system. Figure 4 shows the calibration curve used to calibrate the GC-FID system.

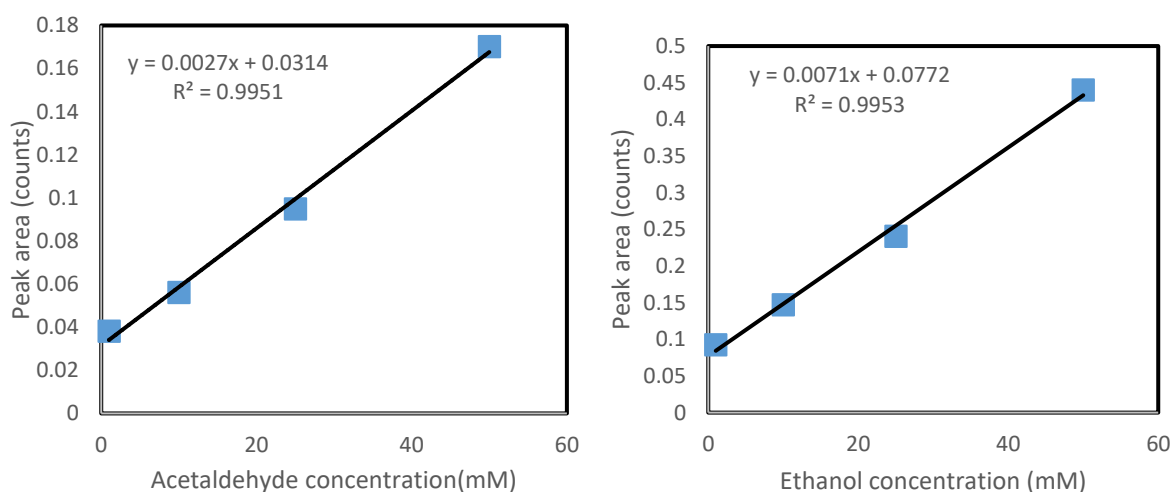


Figure 4: Calibration curve of peak areas (counts) against. (A) Acetaldehyde concentration(mM). (B) Ethanol concentration (mM), used to calculate products concentrations in the fermentation broth.

Appendix G: Quantification of Ethanol in the fermentation broth under anaerobic conditions

The ethanol concentration was analysed with the gas chromatography (Varian CP-3900 gas chromatography, UK), equipped with thermal conductivity detector (TCD) and connected to

glass column (2.08m x 6.0mm x 3.0mm), with a maximum working temperature of 350°C. The GC was running with Varian chromatography workstation version 6.30. In this GC, the carrier gas was N₂ at a flow rate of 20 ml min⁻¹. The GC method employed for the analysis of ethanol under anaerobic conditions is described in Table 2:

Conditions	Setting
Injection temperature (°C)	150
Split ratio	100
Carrier flow rate (ml min ⁻¹)	20
Initial column temperature (°C)	35
Isothermal time 1 (min)	2
Ramp rate 1 (°C min ⁻¹)	10
Second temperature (°C)	100
Isothermal time 2 (min)	2
Ramp rate 2 (°C min ⁻¹)	10
Final column temperature (°C)	170
Detector temperature (°C)	180

The sample was introduced to the injection port of the GC by injecting 0.5 µL via manual injection using a 10 µL syringe (Thermo Scientific). Each sample was injected three times and the peak areas were averaged. Figure 5 shows the calibration curve used to calibrate the GC-TCD system.

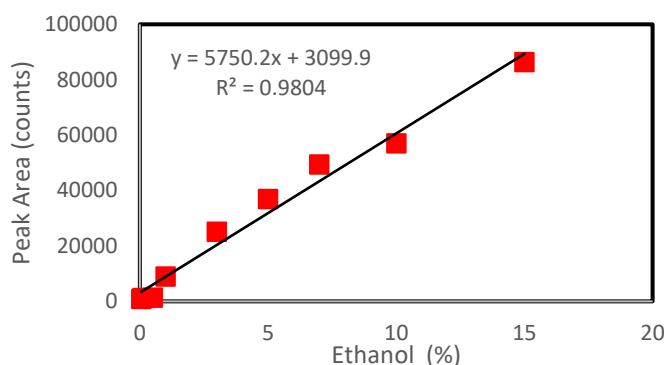


Figure 5: Calibration curve of peak areas (counts) against ethanol concentration (%) used to calculate the ethanol concentration in the fermentation broth under anaerobic conditions.

Appendix H: LC-MS/MS Analysis

To identify the cellulolytic proteins separated on SDS-PAGE by Liquid chromatograph -mass spectrometry (MS)/ mass spectrometry, proteins bands ranged from 20-100 kDa (black-labelled in figure 4.7) on the SDS-PAGE of wheat straw were chosen. After several washes with ultra-high purity H₂O, bands were excised with a clean scalpel and transferred into LoBind Tubes (Eppendorf). Samples were reduced, by 10mM dithiothreitol at 56°C for 1 hour, and alkylated,

by 55 mM iodoacetamide for 30 min at room temperature in the dark, before in-gel tryptic (Sigma-Aldrich) digestion in a final concentration of 50mM ammonium bicarbonate pH 8 at 37°C for 16 hours, with a total of 0.4ug of trypsin in a final volume of 70 ul. Peptides were then collected / eluted by rounds of incubation with 100% acetonitrile, then 0.5% formic acid at 37°C for 15 minutes before being vacuum dried and subsequently being solubilized in Switchoss Solution (0.1% formic acid, 3% Acetonitrile).

40% of the material was injected, using a Dionex Ultimate 3000 uHPLC, onto a PepMap100 C18 2cm x75µm I.D. trap column (Thermo Fisher Scientific) at 5µL/min in 0.1% formic acid, 2% acetonitrile and 35°C in the column oven and 6°C in the autosampler. The sample was separated, over a 35-minute gradient of increasing acetonitrile from 2.4% up to 72%, in 0.1% formic acid, using a 15cm PepMap100 C18 analytical column (2µm particle size, 100Å pore size 75µm I.D) (ThermoFisher Scientific) at 250nL/min and 35°C.

The mass spectrometer analyser used was the electron transfer dissociation (ETD) enabled ThermoFisher-Scientific Orbitrap Elite, equipped with an NanoSpray Flex Ion ESI source (ThermoFisher Scientific). Nanospray ionization was carried out at 1.8kV, with the ion transfer capillary at 250°C, and S-lens setting of 60%. MS1 spectra were acquired at a resolving power of 60,000 with an automatic gain control (AGC) target value of 1x10⁶ ions by the Orbitrap detector, with a range of 350-2000 m/z. Following MS1 analysis the top 20 most abundant precursors were selected for data dependant activation (MS2 analysis) using collision induced dissociation (CID), with a 10ms activation time, and an AGC setting of 10,000 ions in the dual cell linear ion trap on normal scan rate resolution. Precursor ions of single charge were rejected, and a 30 second dynamic exclusion window setting was used after a single occurrence of an ion. Lock mass was enabled, scanning for the 445.120030 ion.

The resulting spectra were searched with SequestHTt (ThermoFisher Scientific) against a *Pseudomonas Putida* KT2440.fasta database (obtained from Uniprot), and a decoy database, within the Proteome Discoverer 1.4 software package (ThermoFisher Scientific). Full trypsin enzymatic specificity was required with up to 2 missed cleavages permitted. Instrument was set to ESI-TRAP. A mass tolerance of 5ppm was used for precursors and 0.2Da for fragment ions. Carbamidomethylation of cysteine (+57.021Da) was specified as a fixed modification. N terminal acetylation (+42.011Da) and oxidation of methionine (+15.995Da) were specified as a variable modification. Peptide-spectral match validation was carried out using the Target Decoy PSM validator node, within Proteome Discoverer 1.4. False discovery rates were set at

1% (strict) and 5% (relaxed) were used to distribute the confidence indicators for the peptide spectral matches. Proteins required a minimum of two peptides with a 95% confidence interval or above in order to be reported.